STRUCTURE OF SOME NEUTRON-DEFICIENT XENON ISOTOPES

by

© Kamilia Sofia

A thesis submitted to the Faculty of Graduate Studies and Research in partial fulfillment of the requirement for the Degree of Doctor of Philosophy.

Foster Radiation Laboratory
McGill University, Montreal
Quebec, Canada

March 1982

ABSTRACT

The level structure of neutron-deficient ^{121}Xe, ^{123}Xe and ^{124}Xe was studied. These levels were populated in the β-decay of ^{121}Cs, ^{123}Cs and ^{124}Cs respectively, which were produced by the proton bombardment of isotopically enriched ^{124}Xe gas targets. Using γ-and β-spectroscopy techniques the level structures of these isotopes were obtained.

High-spin levels of ^{122}Xe and ^{124}Xe populated in the $(\alpha,4n\gamma)$ reaction on enriched tellurium targets, were investigated. Gamma-ray-multiplicity filter, and angular distribution measurements have been carried out. The observation of the backbending of the ground band, and of the two-quasi-particle high-spin bands in $^{122,124}Xe$, is the first in xenon nuclei. These bands were interpreted in the framework of the rotation-alignment picture.

A theoretical interpretation of $^{116-130}Xe$ nuclei was performed using the Interacting Boson Approximation. Also the levels in ^{121}Xe were interpreted using the Interacting Boson-Fermion Model.

RÉSUMÉ

La disposition des niveaux des noyaux déficients en neutrons ^{121}Xe, ^{123}Xe et ^{124}Xe a été étudié. Les niveaux ont été peuplés par la décroissance β de, respectivement, ^{121}Cs, ^{123}Cs et ^{124}Cs, qui fûrent produits par bombardement avec des protons de cibles gazeuses enrichies en ^{124}Xe. A l'aide des techniques de spectroscopie β et γ, les états des niveaux de ces isotopes ont été obtenus.

Les niveaux de haut spin de ^{122}Xe et ^{124}Xe peuplés à l'aide de la réaction $(\alpha,4n\gamma)$ sur des cibles de tellurium enrichi, ont été étudiés. Des mesures de distribution angulaire ainsi que l'usage des techniques de filtres de multiplicité γ et de neutrons ont été exécutées. Pour la première fois une courbure en arrière de la bande fondamentale, ainsi que les deux bandes à haut spin de quasi-particules de $^{122,124}Xe$ ont été observées dans des noyaux de xénon. Le modèle d'alignement rotationnel a servi de cadre pour l'interprétation de ces bandes.

Le modèle "Interacting Boson Approximation" a été utilisé pour une étude théorique des noyaux pairs $^{116\text{-}130}Xe$. Le ^{121}Xe a été interpreté à l'aide du modèle "Interacting Boson Fermion".

ACKNOWLEDGEMENTS

I would like to express my sincere thanks to my research director, Dr. J.E. Crawford for his guidance and encouragement. His valuable time spent in executing the experiments and in assisting in the completion of this thesis is gratefully acknowledged.

Thanks are due to Dr. J.E. Kitching for his assistance in the in-beam experiments and for many illuminating discussions.

Thanks are also in order for Dr. B.N. Subba Rao and Dr. B.J. Varley for their assistance and useful guidance in conducting this work. Thanks are due to my fellow students who contributed their time and effort in watching over some of the experiments. I would also like to thank Mr. I. Kennedy for his help with the Interacting Boson Approximation computer code.

Personal thanks go to my husband for his patience and continuous encouragement throughout the course of this work.

The professional and technical staff of the Foster Radiation Laboratory are to be thanked for their expert assistance.

I am grateful to Mrs. J. Hay for her excellent typing.

The financial assistance provided by the Laboratory on behalf of the Natural Sciences and Engineering Research Council of Canada is gratefully acknowledged.

TABLE OF CONTENTS

LIST OF FIGURES

Figure		Page
17	Gamma multiplicity spectrum ...	50
18	The gamma-multiplicity filter gating spectrum obtained in one-, two-, and four-fold coincidences ...	52
19	The neutron-multplicity set-up ...	54
20	Circiut diagram of the neutron-multiplicity filter ...	56
21	Gamma spectrum obtained in zero-, one-, two- and three-fold coincidence in the neutron multiplicity filter measurement ...	58
22	^{124}Cs $\gamma - \gamma$ spectrum recorded with the 18% Ge(Li) detector ...	64
23	Time decay of ^{124}Cs ...	68
24	$\gamma - \gamma$, background subtracted coincidence spectra of ^{124}Cs for gates shown ...	69
25	Decay scheme of ^{124}Cs. Transition intensities shown are per 100 decays of the 354 keV transition ...	71
26	Time decay of the 511 keV annihilation quantum ...	72
27	^{123}Cs γ-ray spectrum ...	77
28	Time decay of ^{123}Cs activity ...	79
29	$\gamma - \gamma$ background subtracted coincidence spectra of ^{123}Cs ...	81
30	Low energy γ-spectra in coincidence with (a) 511 keV annihilation quanta (b) 261.9 keV γ-ray ...	83
31	Fermi-Kurie plot of ^{123}Cs positron spectrum in coincidence with the 596.4 keV γ-ray ...	87
32	Decay scheme of ^{123}Cs. ...	89

Figure Page

Figure		Page

Figure		Page

Figure		Page
74	Comparison of the experimental and theoretical level schemes of ^{122}Xe ...	178
75	Comparison of the experimental and theoretical level schemes of ^{124}Xe ...	179
76	Backbending plot for the ground-state band of ^{122}Xe ...	181
77	Backbending plot for the ground-state band of ^{124}Xe ...	182
78	The intersection of the ground band of ^{122}Xe with the two-quasiparticle band ...	184
79	The intersection of the ground band of ^{124}Xe with the two--quasiparticle band ...	185
80	The angular momentum as a function of the rotational frequency for ^{122}Xe yrast and side-bands and the $h_{11/2}$, $d_{3/2}$ decoupled bands in ^{121}Xe ...	188
81	The angular momentum as a function of the rotational frequency for ^{124}Xe yrast and side-bands and the $h_{11/2}$, $d_{3/2}$ decoupled bands in ^{125}Xe ...	189
82	Comparison of the theoretical and experimental spectrum of ^{121}Xe ...	194
83	Systematics of positive parity low-lying levels in odd-A xenon nuclei ...	197

LIST OF TABLES

CHAPTER I - INTRODUCTION

The change in nuclear shape with varying mass number in the periodic table has been a well-known phenomenon since Bohr (1952) proposed his collective model. Nuclear deformation is generally observed between shell closures; the change from spherical shape at the closed shell to a deformed one is gradual, and nuclei that fall in between are called transitional nuclei. These nuclei usually show a change from a nearly vibrational structure to one with some similarities to a rotational band structure and such sequences are found in the mass-70 region with $N \gtrsim Z$, the mass-100 region ($Z < 50$, $N > 50$), the mass-120 region ($Z > 50$, $50 < N < 82$) and also in the mass-190 nuclei (Simms et al. 1980). The shape of the nucleus is described by the shape parameters β and γ, where β is a measure of the total deformation of the nucleus and γ is a measure of the deviation of the shape from axial symmetry. Transitional nuclei in the $Z > 50$, $50 < N < 82$ region are believed to be "soft" against γ deformation: therefore one expect to find oblate, prolate and triaxial shapes. Various theoretical models were used to interpret nuclei in this region. Microscopic calculations, for example, were carried out for these nuclei (Rohozinski et al. 1974, Dobaczewski et al. 1977) assuming their γ- softness. Another approach in interpreting these nuclei was to describe them as rotors (Habs et al. 1974, Stephens 1975, Toki and Faessler 1975, Meyer-ter-Vehn 1975). Also several theoretical studies (Kumar and Baranger 1964, Arseniev et al. 1969, de Takacsy and Das Gupta 1976) have been made to find out whether nuclei in this region have prolate or oblate deformation. The last study concluded that prolate shapes are favoured over oblate shapes for the Ba isotopes of mass 126-132. Evidence for prolate shapes was also obtained from the study of $^{125-133}$La nuclei.

It is obvious that detailed experimental information is essential if we are to understand the nature of such transitional regions. Very useful information can be obtained from beta-decay techniques. The Q_β measurements, for example, provide data on masses of nuclei far from stability. This information is eventually used to test mass formulas. Such studies have been carried out for the neutron-deficient rubidium and cesium isotopes (D'Auria et al. 1976, Westguard et al. 1975).

The beta decay populates only low lying levels whose structure provides a good test of the validity of any model. The study of low-lying levels over a chain of isotopes can, for instance, predict the change in the Fermi level as the neutron number changes. In some cases beta decay studies can also provide information on high-spin states as well. These states are usually populated in the β decay of high-spin isomers in the parent nuclei.

During the past few years, there have been many experimental studies on nuclei in all of the transitional regions mentioned earlier. Nuclei in the $50 < N, Z < 82$ regions have been the subject of many investigations ever since nuclei with $Z > 54$, $N < 78$ were proposed as a new region of deformation by Sheline et al (1961). Systematic investigations of nuclear spins and moments for cesium isotopes was carried out by Ekstrom et al. (1977), and the information obtained has been very useful as a test of different models. A study of isomeric states in Xe, Ba and Ce was also carried out by Conlon and Elwyn (1970); this serves as a useful tool in obtaining information on shape changes. Isotope shift and Coulomb excitation studies of even-even stable Te, Xe and Ba nuclei (Fischer et al. 1974) have demonstrated that the deformation parameter is about $|\beta| \leq 0.1$ at N = 80 and increases with decreasing neutron number to $|\beta| = 0.22$ at N = 68. The high-spin levels in $^{116-122}Xe$ were observed in the β-decay of high spin isomers in the cesium nuclei (Batsch et al. 1976, Genevey-Rivier et al. 1977). In this study information on low-lying levels were also obtained from the decay of the low spin ground state of the parent nuclei. The heavy xenon isotopes of ^{126}Xe, ^{128}Xe were also studied recently (Pathak et al. 1976, Droste et al. 1976). Information on heavy odd-A xenon isotopes is also available (Jha et al. 1972, Gelletly et al. 1976).

However little detailed information has been available on the very light xenon isotopes. It therefore appeared attractive to carry out further investigations on these nuclei. In order to obtain more information on the low-lying levels of these nuclei, an investigation of levels in $^{121,123,124}Xe$ was carried out in the present work via the decay of the cesium parent nuclei by employing beta and gamma spectroscopy techniques.

Of interest also is the behaviour of transitional nuclei at high angular momentum. The study of high-spin states was initiated by Morinaga and Gugelot (1963). Information on high-spin states is obtained from studies of (HI,xn) reactions, where HI refers to heavy ions, with $A \geq 4$. With projectile energies moderately above the Coulomb barrier, the compound nucleus cross-section normally dominates the total cross-section for reactions with medium-heavy target nuclei (Johnson and Szymanski 1973). A compound nucleus thus created is left in highly excited states, and its subsequent decay is independent of its formation. Such a decay is described by the statistical model of nuclear reactions (Blatt and Weisskopf 1952). In this case the compound nucleus will first lose energy by evaporation of neutrons, protons, and α particles, and will then lose both energy and angular momentum through the emission of γ radiation. Spectroscopic studies show that much of the energy and angular momentum loss proceeds by a cascade along the yrast line (states having the lowest energy for a given spin value). However the initial de-excitation in general occurs in the region between the yrast line, and a line lying above it by about the separation energy of one neutron (Diamond and Stephens 1980). Two types of γ-rays occur: those that cool the nucleus toward the yrast line, called "statistical", and those that are parallel to the yrast line and remove the angular momentum, called "yrast-like". The competition between the two types depends on the level density and the degree of collectivity which produces enhanced yrast-like transitions. The statistical transitions are unresolved and produce a continuum which is characteristic of in-beam singles spectra and which often interferes with the analysis of yrast-like transitions that are usually resolved up to a reasonably high spin of the deexciting level. Until very recently, most studies of (HI, xn) reactions have concentrated on the detection and the analysis of the yrast-like, resolved, γ-rays. The in-beam techniques normally used are the excitation function studies, γ-transition intensity measurements, and $\gamma - \gamma$ coincidence measurements which give the strongest support for the assignment of γ-rays and the construction of level schemes. Information about the multipolarities of the emitted γ-rays are obtained from the measurement of the γ-ray yield at various angles relative to the incoming beam (angular distribution). The γ-multiplicity filter and the neutron multiplicity filter techniques employed in the present work [III(B)] also constitute very powerful tools in the construction of level schemes.

These methods as well as other in-beam spectroscopy techniques outlined above were employed by using the in-beam spectroscopy set-up at McGill (Chapter II), which is fairly new. The author contributed to the construction and development of this facility.

Though the high-spin study with the use of in-beam spectroscopic techniques has a relatively short history, heavy ion in-beam experiments performed in the last few years have revealed a wealth of spectroscopic information which has stimulated considerable interest in the effort to understand the nature of high-spin states. This interest was spurred on by the discovery of Johnson et al. (1971) and (1972) of the backbending phenomenon, where the name refers to the unusual s-shape of the plot of the nuclear moment of inertia (J) versus the square of the rotational frequency $(\hbar\omega)^2$ of the ground state rotational band of even-even nuclei. The efforts in investigating this phenomenon have been summarized by Sorensen (1973), Johnson and Szymanski (1973), and Sayer et al. (1975). Recently backbending has been observed in $^{126,128}Ba$ and $^{128,130}Ce$ isotopes (Flaum et al. 1974, Ward et al. 1975) to occur around spin 10^+. The present observation of this anomaly in the structure of the ground state band (Chapter IV) is the first to be reported for the xenon isotopes. The backbending phenomenon has been explained by the Coriolis alignment model of Stephens and Simon (1972) as the result of the crossing of the ground band and a decoupled two-quasiparticle band.

The bands observed in deformed nuclei show certain characteristic features, and a number of band classifications have been made. For symmetry reasons, in doubly-even deformed nuclei the angular momentum of the ground state rotational band follows the sequence: $0^+, 2^+, 4^+, 6^+, \ldots$ Those bands are characterized by strongly enhanced E2 transitions between successive members of the band. In these nuclei electric quadrupole vibrational states occur at higher excitation energies (Nathan 1957), and associated with these states rotational bands are found, each of which is characterized by the quantum number K, which represents the projection of the total angular momentum along the symmetry axis. A β vibration is one which preserves axial symmetry. These vibrations have no angular momentum about the symmetry axis (K = 0) and the associated beta band will contain 0^+, 2^+, 4^+,... states. A γ vibration, which causes a departure from axial symmetry, has K = 2, and the states of the associated band will be 2^+, 3^+, 4^+,...; such a sequence is known as the γ-band.

The low-lying even-parity levels of even-even transitional nuclei have been classified into quasi-ground (0^+_g, 2^+_1, 4^+_1, 6^+_1,...), quasi-γ (2^+_2, 3^+, 4^+_2, 5^+, 6^+_2, 7^+) and quasi-β (0^+_2, 2^+_3, 4^+_3) bands (Sakai 1967). These quasi-bands tend gradually to the corresponding rotational bands in the deformed region (Sakai and Rester 1977). The experimental criteria for calling a nucleus "transitional" are the deviation from the J(J+1) energy spacing rule in the ground band, a sharp increase in the $B(E2; 0^+ \rightarrow 2^+)$ value, a sharp decrease in the energy E_{2^+}, with the additional requirement that the β and γ-bands must be low-lying (Kumar 1970). The neutron deficient even-even xenon nuclei show clear quasi-rotational ground state bands (Genevey-Rivier et al. 1977, Kusakari et al. 1975, Goettig et al. 1981) in which the ratio $r = E(4^+_1)/E(2^+_1)$ of the energies of the lowest 4^+ and 2^+ states is 2.5 - 2.1 between ^{122}Xe and ^{130}Xe; this indicates that these nuclei are far from the rotational limit where r = 3.3 (Davydov and Rostovsky 1959).

It is highly desirable to obtain information on the non-yrast level properties of transitional nuclei since these provide a sensitive test of various nuclear models. Information is available on the quasi-ground bands and on the quasi-γ bands in xenon nuclei. However no information has been available on the non-yrast levels in these nuclei. The present in-beam spectroscopy study reports on these non-yrast levels in $^{122,124}Xe$ and confirms as well the information on the quasi-ground and quasi-γ bands in these nuclei. Throughout the present work the quasi-ground, γ-, and β bands are referred to for convenience as simply ground, γ- and β-bands.

Recently, high spin states of odd-xenon isotopes have been extensively studied (Gizon and Gizon 1978 , Helppi et al. 1979, Helppi et al. 1981, Barci et al. 1981, Luukko et al. 1981). These studies have indicated the existence of two kinds of bands in the level structure. The first are called decoupled bands, with $\Delta J = 2$ type cascades which are interpreted as arising from a rotationally aligned quasi-particle coupled to the even-even core; the second are $\Delta J = 1$ type negative parity bands that originate from the coupling of an $h_{11/2}$ quasi-neutron hole to the core. Both types of bands agree with the predictions of the rotation-alignment model of Stephens (1975), which states that for slightly deformed odd-A nuclei at high spin, (i.e. with increasing Coriolis force) the extra particle tends to decouple from the core and align its angular momentum along the axis of rotation. It has been pointed out (Grosse et al. 1973) that if a particular rotation-aligned particle prevents the occurrence of backbending in the odd-mass nuclei, it is likely that this particle is involved in the backbending in the adjacent doubly-even nucleus. The backbending and the side-bands observed in $^{122,124}Xe$ in the present work are explained in terms of the Coriolis alignment model of Stephens and Simon, using the adjacent odd-mass xenon isotopes [V(A)].

The experimental beta decay techniques as well as the in-beam spectroscopy techniques are presented in Chapter III, and in Chapter II a description of the instrumentation is given. The results of the beta decay study as well as the in-beam study are presented in Chapter IV.

Recently the Interacting Boson Approximation Model (Iachello and Arima 1974, Arima and Iachello 1975, 1976a, Otsuka et al. 1978) has had considerable success in describing low-lying collective states in even-even nuclei except those at, or adjacent to closed shells. These states are generated as states of a system of N bosons where bosons are interpreted as pairs of nucleons coupled to angular momentum J = 0 (s- boson) and J = 2 (d- boson) (Arima et al. 1977). In the present work, the energy levels of the quasi-bands of even-even xenon isotopes from 116-130 were fitted using the IBA model (Chapter V). The IBA model has been extended to fit odd-mass nuclei [The Interacting Boson-Fermion Model (IBFM)]. In this model the odd-A nucleus is treated as a system of interacting bosons and fermions. This model has been used in fitting low-lying levels in heavy xenon and barium isotopes (Cunningham 1981) as well as high spin band structures in the lighter xenon isotopes (Cunningham 1981). In the present work the low-lying levels of ^{121}Xe were fitted using the Interacting Boson Fermion Model (IBFM). Fitting the low-lying level structure accurately is considered to be a severe test of the model.

Finally a summary and conclusion of the present work as well as an outline of contributions to original knowledge are presented in Chapter VI.

CHAPTER II - INSTRUMENTATION

A. DECAY STUDIES

i. Targets

The target material of a 100% pure xenon gas, consisted of the following percentage isotopic abundances: ^{124}Xe(40.5), ^{126}Xe(9.7), ^{128}Xe(12.5), ^{129}Xe(34.9), ^{130}Xe(1.0), ^{131}Xe(1.1), ^{132}Xe(0.3), ^{134}Xe and ^{136}Xe(<0.1). Since we were using gas targets, the target material had to be encapsulated in a container made of a non-porous material. Hence, the target container (Fig. 1a) has been made out of beryllium. The container wall was made very thin ($\sim \frac{1}{4}$ mm thick) in order to minimize absorption or scattering of the proton beam by the wall. However the target container has to be strong enough to resist breakage. Beryllium serves both purposes. It also produces little background, since when bombarded by protons it does not produce short-lived γ-activity and it has only a very short-lived positron activity (∿ 800 milliseconds). A high grade of beryllium (99.88% pure) was used as the target container material because it has a very low content of BeO, minimizing as much as possible activities produced from oxygen bombardment by protons.

The target container was mounted on a target holder (Fig. 1). The target holder was made out of Delrin, a strong light plastic material that can be accelerated easily to high speeds, and can withstand impacts during the course of delivery in and out of the cyclotron. Delrin also produces very little background.

ii. Gas Filling Procedure

The target container was filled with the enriched gas using the filling system shown in Fig. 2. The filler and buffer volumes were first pumped

Figure 1

(a) Target Container

(b) Target Holder System

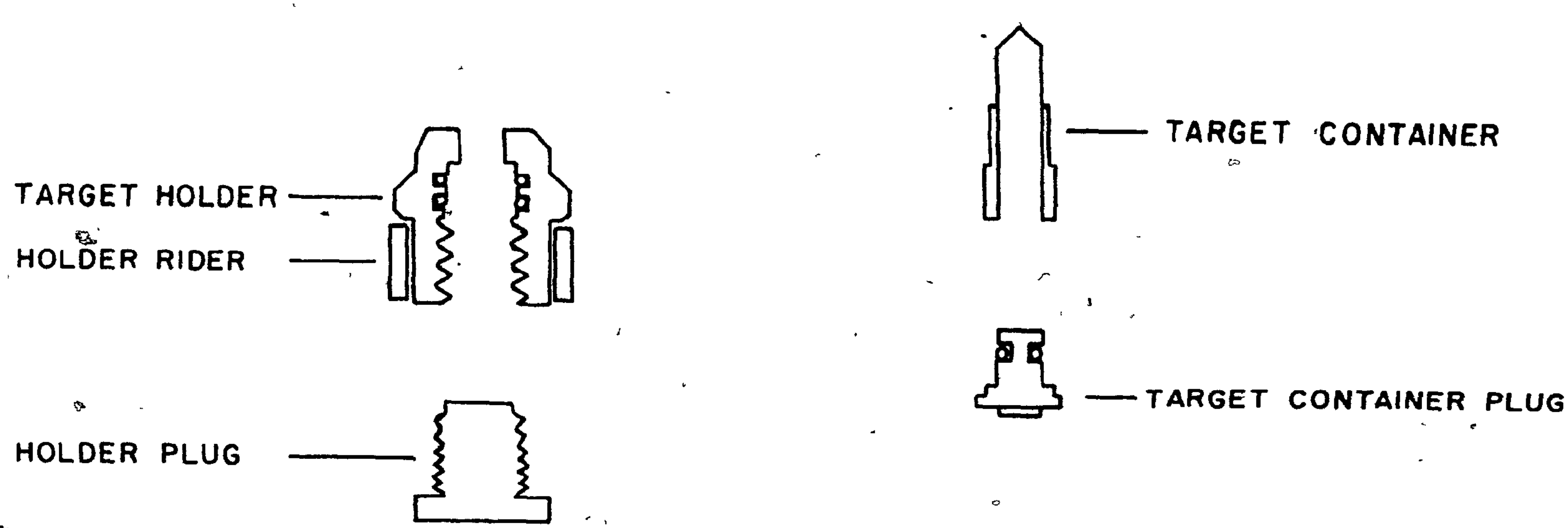

TARGET HOLDER
HOLDER RIDER
HOLDER PLUG
TARGET CONTAINER
TARGET CONTAINER PLUG

out. After evacuation the system was sealed from the pump. Then valves 2 and 3 were closed, the gas supply valve was opened and the gas was allowed to expand to the primary buffer volume. Valve-1 was then closed and the gas was allowed to flow to the buffer volume. This procedure was repeated in order to increase the gas pressure in the buffer volume. This pressure P_1 was then recorded. The filler valve was then opened and the filler cold finger was submerged in liquid nitrogen until the pressure transducer on the buffer showed vacuum, indicating that all the gas had been frozen inside the cold finger. The filler valve was then closed and the cold finger was removed from the liquid nitrogen. After a period of time the gas evaporated, and the line between the cold finger and the filler was closed by lifting the lower part of the filler by means of a setscrew. By pushing the filler piston up, the gas was compressed inside the beryllium container and sealed with the container plug. The lower part of the filler was then pulled down and the filler valve was opened. The buffer cold finger was then immersed in nitrogen, in order to retrieve all the gas not sealed in the container. After all the gas was frozen on the inner surface of the cold finger the filler valve was closed. The cold finger was allowed to warm, permitting the gas to evaporate in the buffer volume, and the pressure transducer reading P_2 was recorded.

The amount of gas transferred into the container, and also the efficiency of the transfer were calculated using the buffer pressure readings P_1 and P_2. The gas pressure inside the target container was about 1.5 atmospheres, and the efficiency of the transfer obtained was 85%. This represents the percentage of the amount of gas that was compressed in the container relative to the amount of gas allowed into the filling system. This improvement was obtained by minimizing the deadspace in the filler

Figure 2

Gas Filling System

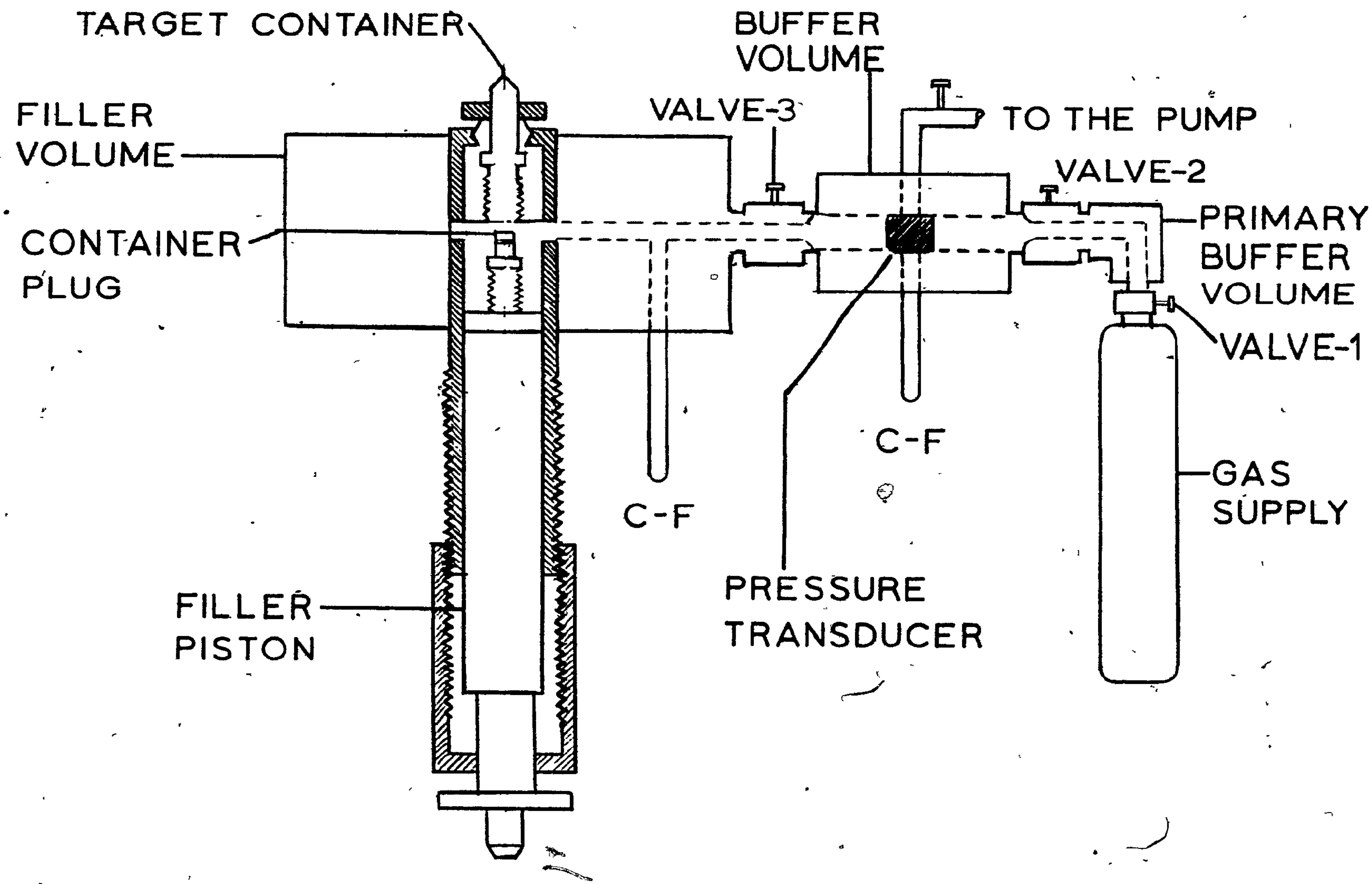
TARGET CONTAINER
BUFFER VOLUME
FILLER VOLUME
VALVE-3
TO THE PUMP
VALVE-2
CONTAINER PLUG
PRIMARY BUFFER VOLUME
VALVE-1
C-F
C-F
C-F
GAS SUPPLY
PRESSURE TRANSDUCER
FILLER PISTON

volume, and also by increasing the volume of the lower part of the filler. High transfer efficiency is most important, since only a very small amount (25 cm^3) of the very expensive separated ^{124}Xe isotope was available. A reasonably high pressure in the container is desirable to obtain a moderate effective target thickness. Also, several targets were needed in order to reduce radioactive build up.

The testing and improvement of the filling system were carried out using natural xenon gas. For more mechanical details of the filling system the reader is referred to Bavaria (1975).

iii. Rapid Transport System

A rapid pneumatic transport system (Bavaria 1975) has been used to bombard the xenon-filled bullets. The bullet is first mounted in the 9-m delivery tube of a system which is isolated from the cyclotron vacuum by a closed shutter on the probe head. The bullet is then blown down by gas pressure to the probe head, which is located at the desired radius (and bombarding energy) inside the cyclotron. The O-ring on the target holder makes a seal with the probe head inner surface, and the area between the shutter and the holder O-ring is pumped out. When a good vacuum is achieved, the shutter is opened and the target is exposed to the cyclotron vacuum. The cyclotron is then triggered to start the bombardment for a predetermined period of time. When the bombardment is over, the shutter is closed and the bullet is blown back to the counting position. The system will then reset awaiting another bombardment. The whole procedure is carried out in an automatic cycle.

B. IN-BEAM STUDIES

i. Alpha Beam

A radial extraction ion source is used to inject particles into the median plane of the cyclotron. This reduces the beam's radial oscillation substantially and thus improves the external beam extraction efficiency. The extraction efficiency for alpha particles with the vertical ion source previously used was about 1%, while with the radial ion source it is about 8%. A diagram of this radial ion source is shown in Fig. 3. It is a Penning-type, where the helium gas is fed through a hole on top of the cathode which is mounted on a copper base (for good thermal conductivity) that is cooled with water. A +5 kV pulse is applied to the anode while the entire source is biased at about +3 kV with respect to ground. The helium ions form a plasma inside the ion source, created by a discharge between the anode and the cathode when the electrode system is exposed to the cyclotron magnetic field; these ions exit through a vertical slit in the anode wall. The efficiency of this ion source is affected by its inclination and relative position with respect to the main and dummy cyclotron dees.

The extracted $^{4}He^{++}$ beam has an energy of 100 MeV, and an intensity of about 40 electrical nanoamperes. The synchrocyclotron has a pulse rate of 500 PPS with external beam bursts about 20 μs long which are modulated by a radio-frequency microstructure. The pulsed beam is, however, poorly suited to in-beam gamma ray studies. When a Ge(Li) detector is exposed to a huge flash of gamma rays during the beam bursts, pileup of pulses occurs causing low useful count rates and poor spectral resolution. High current transients can also damage the detector amplifier (Morinaga and Yamazaki 1976). To overcome these problems, a beam stretcher was designed by Mr. L. Nikkinen

Figure 3

Radial Extraction Ion Source

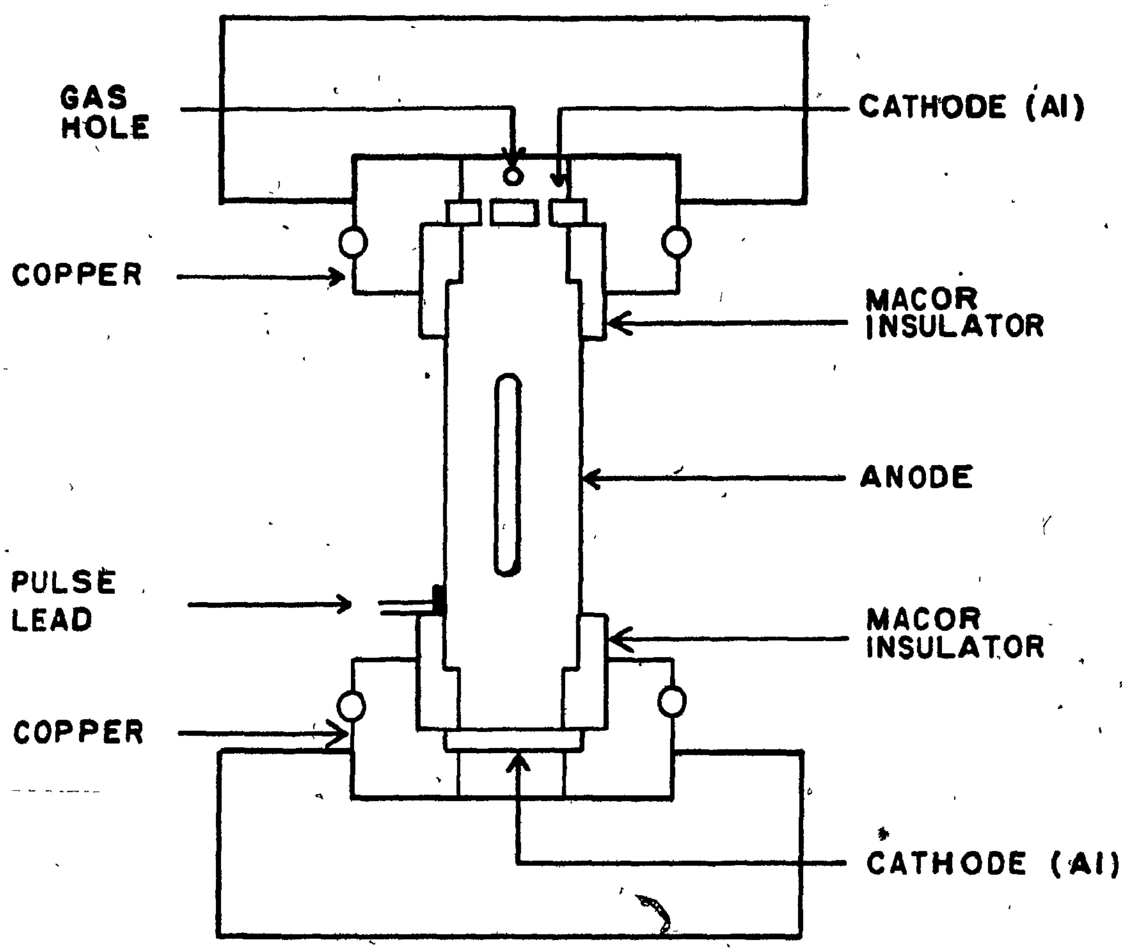
GAS HOLE
CATHODE (Al)
COPPER
MACOR INSULATOR
ANODE
PULSE LEAD
MACOR INSULATOR
COPPER
CATHODE (Al)

of this laboratory (Tacik 1980). This system randomizes the extraction of the beam so that it resembles a continuous one. The monitoring and adjustment of the stretcher were carried out by means of a NaI detector that was placed close the beam path. Fig. 4 shows the radio-frequency (RF) envelope, the ion pulse and the monitoring detector's signal, produced by scattering of the stretched beam from a screen placed in its path. The stretcher is capable of producing macroscopic duty cycles close to 100%. The intensity of the stretched beam is about 10 to 15% of that of the pulsed beam.

The ^4He beam energy was varied by means of beryllium beam degrader discs of selected thickness that were introduced into the beam path at a point where the beam comes to a focus. The loss in energy of the beam in passing through the degrading material is a function of the incoming beam energy and the degrader thickness. The alpha beam energy (Fig. 5) was calculated using stopping power tables (Barkas and Berger 1964). The statistical nature of the slowing down process causes a significant energy spread in the degraded beam. The energy spread in the beam due to the degrader and the target thickness in a typical experiment is estimated to be approximately 5 MeV.

ii. External Beam Alignment

A passive sextupole magnet is used at the exit of the magnetic extraction channel. This corrects for second order distortions in the emittance of the extracted beam. Hence, the beam is focused to a reasonable size in the middle vault by using the 2" quadrupole magnet in the cyclotron vault. The beam is then guided to the external beam hall by means of the 30° and 45° magnet systems (Fig. 6) and is refocused by a pair of quadrupoles, after it passes through the degrader box. In the external beam hall, the switching

Figure 4

Photograph of the radio-frequency oscillator's amplitude envelope, the ion source voltage pulse, and the output of the NaI detector viewing a target being bombarded by a stretched alpha beam.

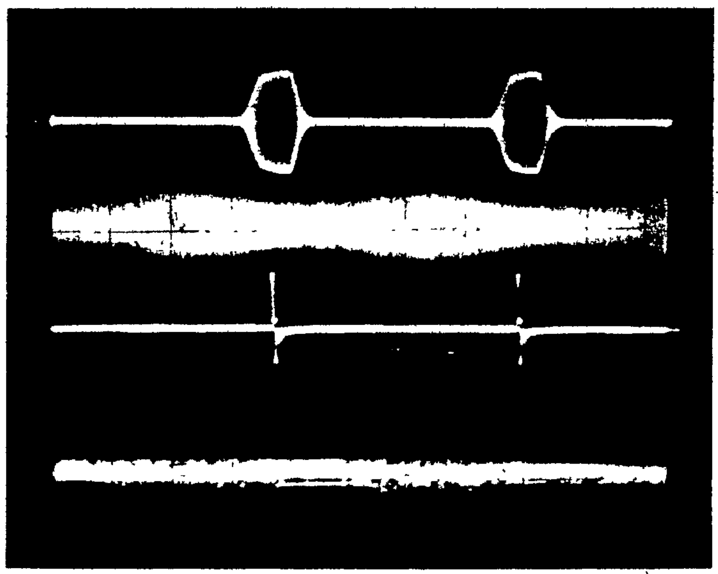

Figure 5

The energy of a degraded alpha beam as a function of the Be degrader thickness.

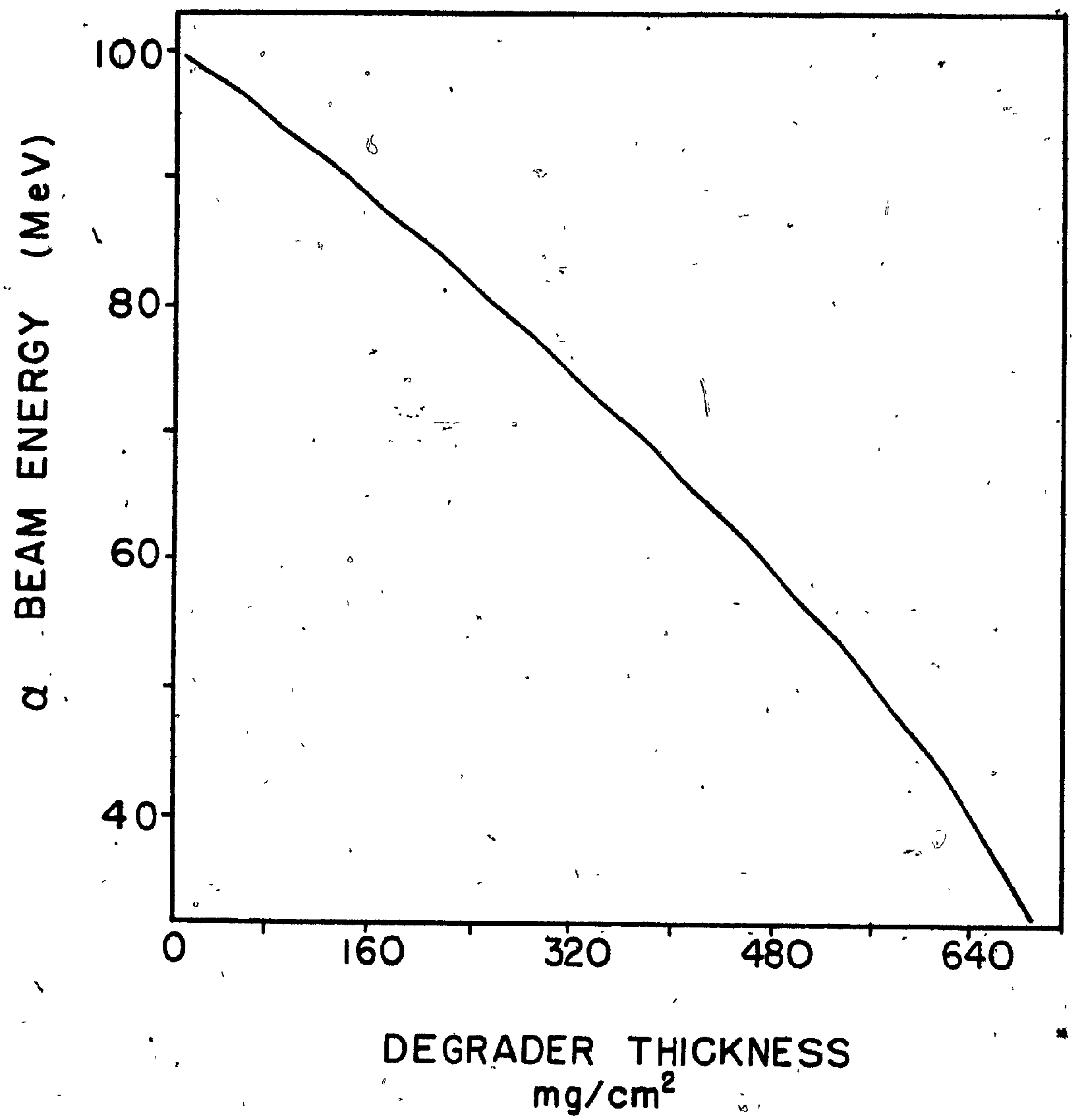

α BEAM ENERGY (MeV)
100
80
60
40
0
160
320
480
640
DEGRADER THICKNESS
mg/cm²

Figure 6

Beam Transport System

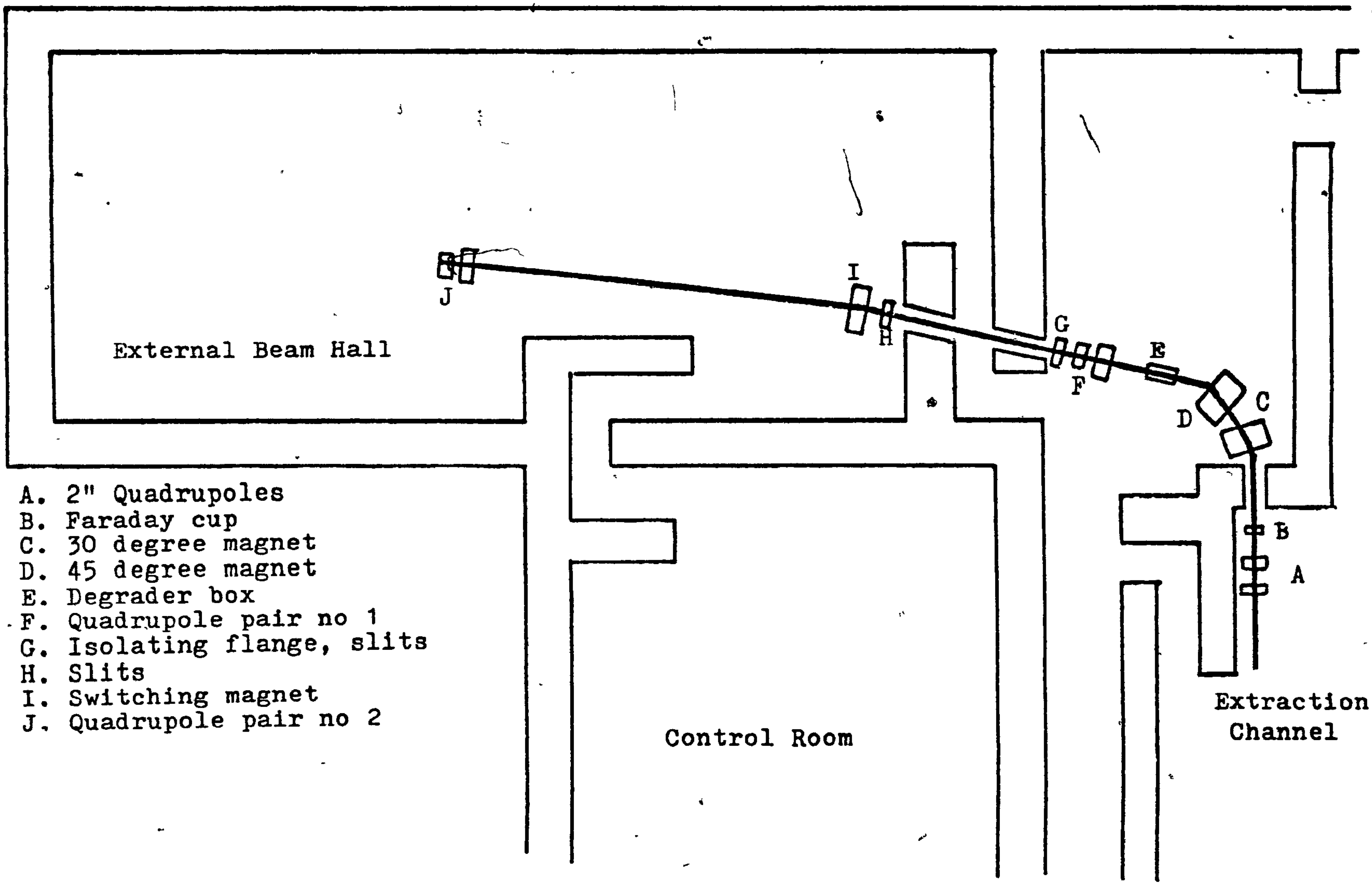

A. 2" Quadrupoles
B. Faraday cup
C. 30 degree magnet
D. 45 degree magnet
E. Degrader box
F. Quadrupole pair no 1
G. Isolating flange, slits
H. Slits
I. Switching magnet
J. Quadrupole pair no 2

magnet is used to direct the beam towards the target, and it is focused to a spot on the target by a second pair of quadrupoles. Experiments were carried out to determine the best target position. Although the transport efficiency of the 100 MeV beam was about 85%, the degraded beam efficiency is lower. This is caused by the scattering of the beam in the degrading material; some beam is lost outright, by scattering, while further losses are caused by the increased divergence of the beam after it passes through the degrader.

To align the beam, a phosphor screen is mounted in the target position. The glow resulting from the beam hitting the phosphor screen is monitored by a video camera. This camera, placed on top of the beam line, looks at the target position through the transparent window in the target chamber, and its picture is transmitted to a video screen in the control room. The magnet power supply settings are then adjusted to focus the beam on the phosphor. The beam spot size on the phosphor can be made as small as 3 mm in diameter.

iii. Targets And Target Chambers

The target material used was 96.5% enriched tellurium-122 for the production of xenon-122 and 92.4% enriched tellurium-124 in the case of xenon-124. The tellurium isotopes were in a pure metallic powdered form. A die mounted in a hydraulic press was used to form the powder into a tablet of about 100 mg/cm^2 thickness. The tablet was then placed on a thin mylar film (350 μg / cm^2), and was glued in place by a thin layer of polystyrene based Q-dope. The mylar film was then attached to the target frame.

The target frame used for the singles measurements and also the angular distribution measurements is shown in Fig. 8. The frame was machined out of aluminum, with an inner radius more than sufficient to clear the beam. For coincidence measurements, a cylindrical copper frame (Fig. 9) was used.

The target chamber for γ-singles and for γ-angular distribution measurements is shown in Fig. 7. The cylindrical shape of the target chamber was chosen to achieve maximum angular displacement of the detectors. The target holder (Fig. 7, 8) was free to rotate around its axis, permitting adjustment of the target angle with the beam. The holder was also free to move in the vertical direction.

The target chamber for the γ-coincidence measurements is shown in Fig. 9. It is a copper tube with a slot milled in the middle. The target frame sits in this slot, which is closed during runs by a plastic window cover. A piece of wire is fixed to the outer surface of the frame, which ensures that the target does not get displaced while the system is being pumped out. An O-ring is placed on both sides of the slot so that a vacuum seal is obtained between the window and the chamber.

iv. <u>In-Beam Experimental Area</u>

The target chamber was placed in the beam line (Fig. 10). An elevated stage was used as the experimental area, with the γ-detectors mounted on two rotating platforms, which were free to rotate around the target chamber. A camera was placed on top of the beam line for beam alignment. It was found that the whole area required shielding against both cyclotron radio-frequency noise pickup and the high ambient neutron background before experiments could be performed. Without shielding, noise from both the synchro-cyclotron's main radio-frequency oscillator and from the beam stretcher oscillator were picked up and amplified by the signal processing system. The whole experimental area including the signal processing system was

Figure 7

Gamma-Ray Singles and Angular

Distribution Target Chamber.

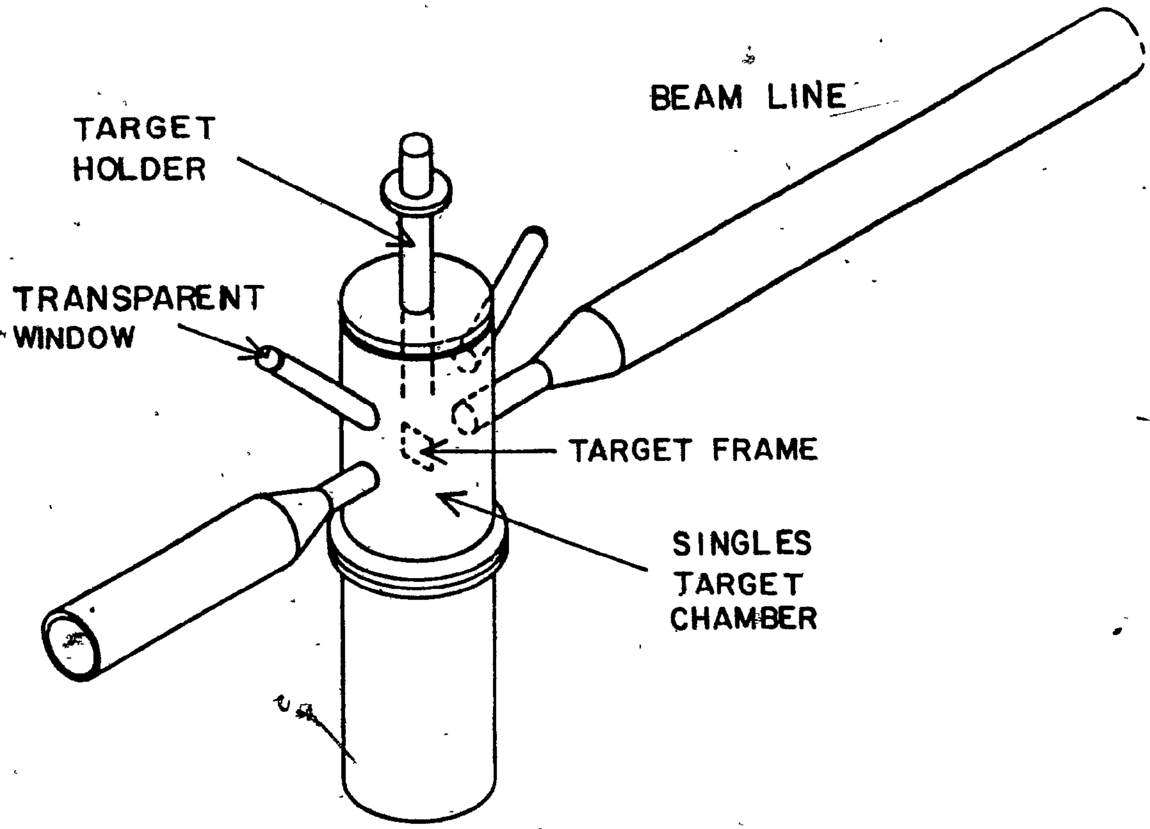
BEAM LINE
TARGET
HOLDER
TRANSPARENT
WINDOW
TARGET FRAME
SINGLES
TARGET
CHAMBER

Figure 8

Target Holder and Target Frame

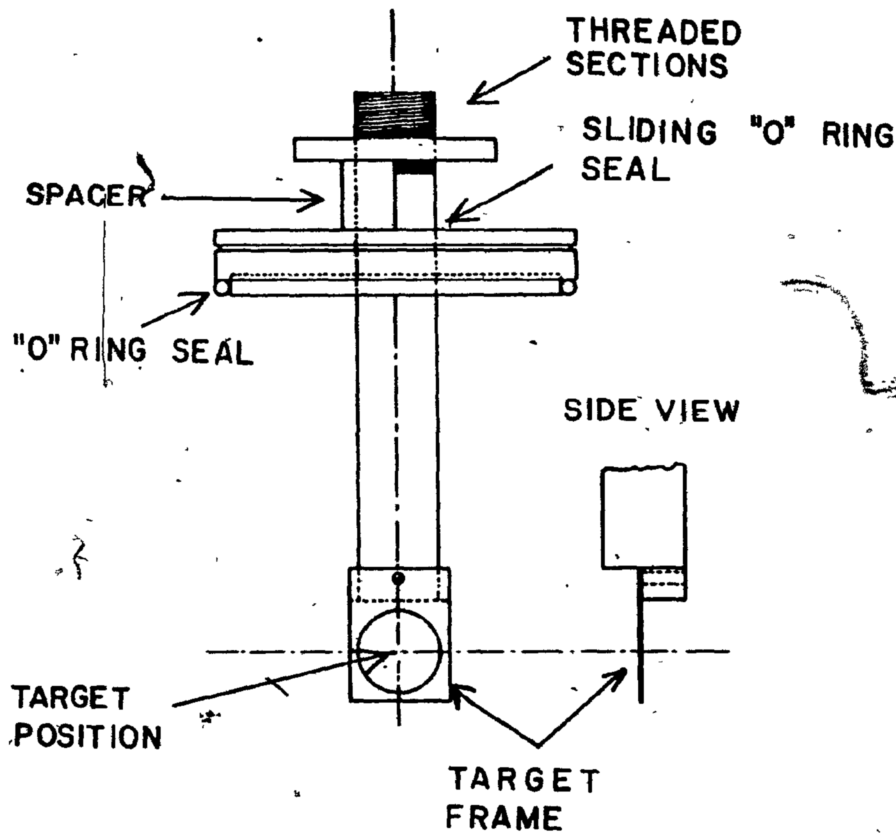
THREADED SECTIONS
SLIDING "O" RING SEAL
SPACER
"O" RING SEAL
SIDE VIEW
TARGET POSITION
TARGET FRAME

<u>Figure 9</u>

$\gamma - \gamma$ Coincidence and Multiple Coincidence Target Chamber and Target Frame.

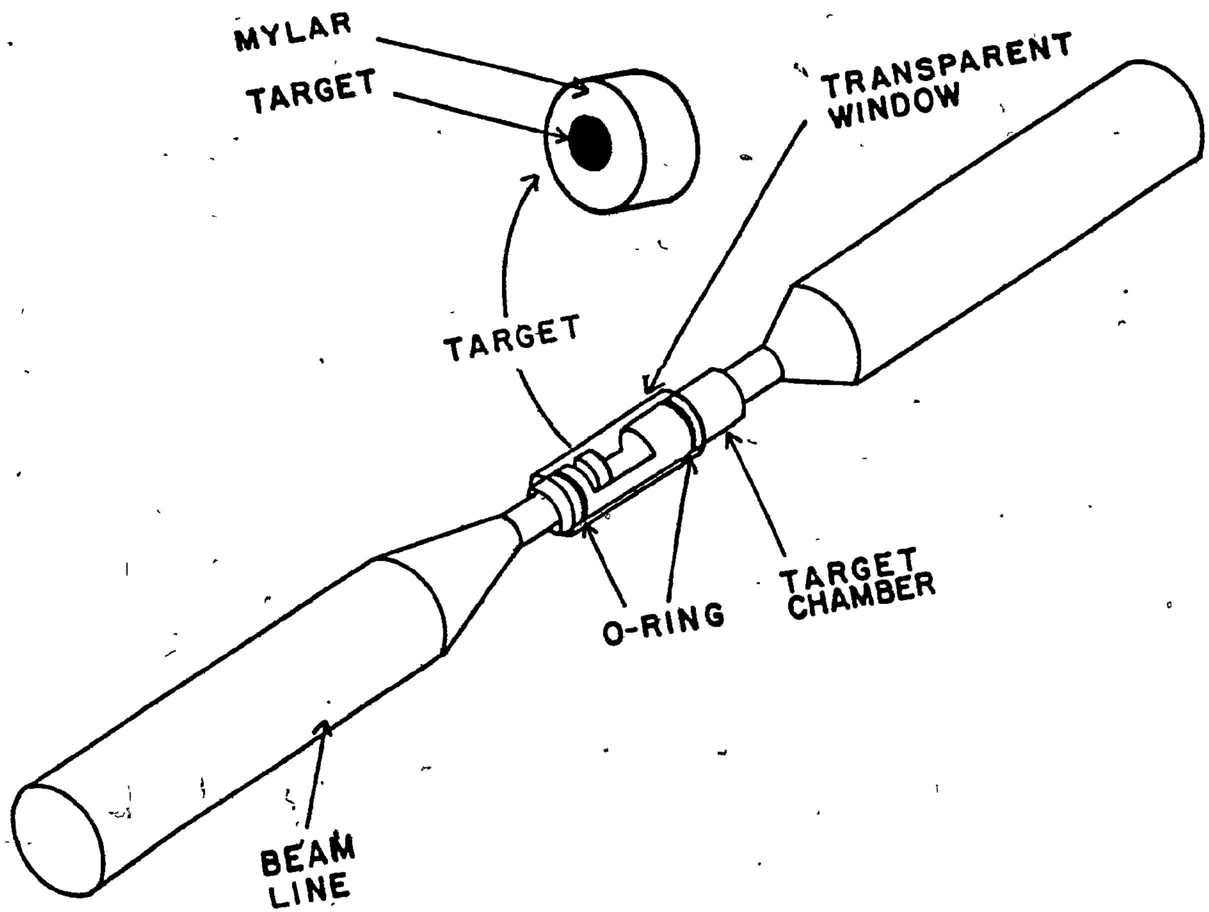
MYLAR
TARGET
TRANSPARENT WINDOW
TARGET
O-RING
TARGET CHAMBER
BEAM LINE

Figure 10

Overview of In-Beam Experimental Area

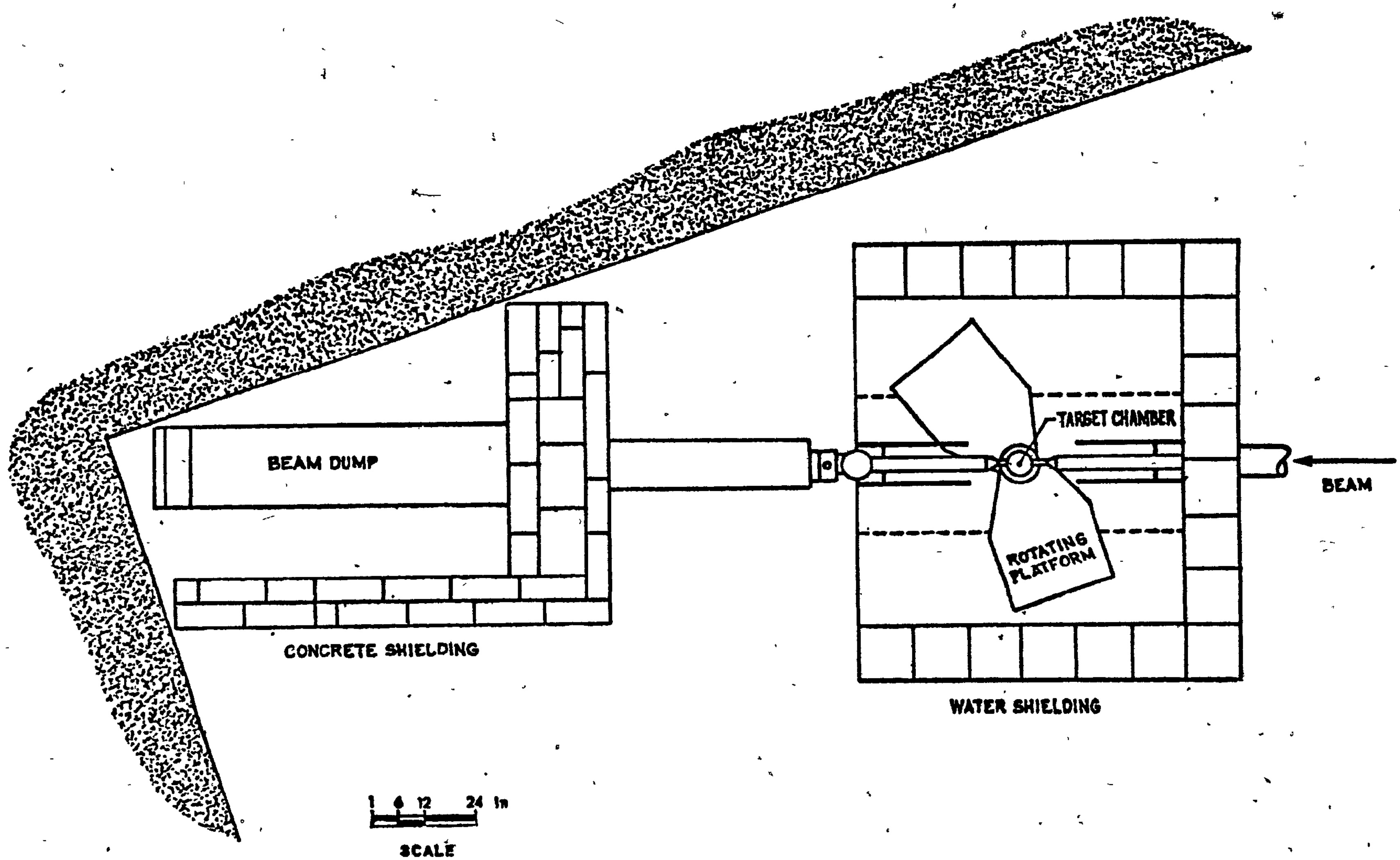
TARGET CHAMBER
BEAM
ROTATING PLATFORM
BEAM DUMP
CONCRETE SHIELDING
WATER SHIELDING
1 6 12 24 in
SCALE

therefore housed in a closed aluminum box (Fig. 10) with dimensions (1.85 m X 1.85 m X 2.0 m). This effectively eliminates nearly all electromagnetic pickup. The electrical ground of the power supply for the electronics system was allowed to float and a capacitor was placed in parallel with the incoming A.C. power line to bypass noise signals which otherwise could enter the shielding box. Since the noise could also be transmitted into the housing via the external beam line, the experimental area was electrically isolated from the beam line by a lucite insulating flange. In order to eliminate the possibility of noise pickup along the signal cables that run between the experimental area and the computer, doubly shielded cables were used.

Although the improved beam emittance somewhat reduced the background in the external beam hall, an unacceptably high neutron background was still produced from the alpha beam's collision with the beryllium degrader. The beam degrader also increased the beam divergence, causing beam scattering into the switching magnet; this produced still higher level fluxes of high energy neutrons. In addition to the deterioration of resolution in the γ spectra, high neutron backgrounds can also damage the detectors themselves (Kraner et al 1968). This problem was cured in part by shielding the beam dump, the degrader area, and also the switching magnet by concrete blocks, sufficiently thick to thermalize the high energy neutrons. In addition, the sides of the aluminum box housing the experimental area were shielded against thermal neutrons by cubic foot-sized containers filled with a mixture of water and boric acid.

CHAPTER III - EXPERIMENTAL TECHNIQUES

A. EXPERIMENTAL TECHNIQUES USED IN DECAY STUDIES

i. Production of Radioactive Samples

Proton bombardments of ^{124}Xe targets produced, ^{124}Cs, ^{123}Cs, and ^{121}Cs via (p,n), (p,2n) and (p,4n) reactions respectively. As mentioned earlier (Chapter II) the gas targets were enclosed in the bullets, which consisted of the target container and the target holder. The bullets were pneumatically transported to the predetermined proton orbit radius of the internal circulating beam of the synchrocyclotron. For the production of ^{124}Cs, the targets were irradiated by 15 MeV protons at 35.6 cm cyclotron radius. To produce ^{123}Cs, and ^{121}Cs, the targets were irradiated by 33 and 52 MeV protons, at 53 and 67.6 cm cyclotron radii, respectively. The targets were bombarded for approximately half the half-life of the isotope to be produced and were blown back to the loading breech following bombardment. The radioactive targets were then carried to the counting area, except for ^{124}Cs, where counting was done directly at the receiving end of the pneumatic probe - this procedure was necessary since the isotope's half-life was short (30 s). Because of the high bombarding energies used and the mixed isotopic composition of the xenon target material, several (p,xn) Cs, (p,pxn) Xe and (p,αxn) I isotopes were produced along with the isotope of interest. Hence, in the case of ^{123}Cs (6 min) and ^{121}Cs (2 min), the activated targets were cooled for approximately 30 seconds. This significantly reduced the shortlived activities of ^{124}Cs (30 sec) and ^{126}Cs (98 sec).

ii. Gamma-Ray Measurement Techniques

Detection of gamma transitions was carried out using three large volume lithium-drifted germanium detectors: 1) an Ortec detector with a 96 cm^3

active volume and a relative efficiency of 18% (relative to a 7.6 X 7.6 cm NaI(Tl) crystal) and an energy resolution of 2.1 keV full width at half maximum (FWHM) at 1.3 MeV; 2) a Princeton Gamma Tech 50 cm^3 detector of 9.7% relative efficiency and an energy resolution of 1.9 keV FWHM at 1.3 MeV; 3) a 15% efficiency hyperpure germanium detector made by Aptec, with a 66 cm^3 active volume, and an energy resolution of 2.2 keV at 1.3 MeV. X-rays and low energy γ-rays in the range of 20 to 200 keV were detected by a .022 cm^3 hyperpure germanium x-ray spectrometer with a resolution of 500 eV at 100 keV.

The efficiencies of these detectors vary with the solid angle exposed to the crystal and with the energy of the transition detected. Fig. 11 shows how the efficiency of the 18% detector varies with energy. The relative efficiency was determined by using a set of standard radioactive sources with known relative intensities. The spectra of ^{154}Eu, ^{133}Ba, ^{56}Co, ^{66}Ga and ^{182}Ta standard sources were obtained individually. These standard sources were placed inside beryllium target containers identical to those housing the xenon gas targets. This produced an efficiency curve which included the effect of the absorption in the beryllium container on the detection efficiency.

The energy pulses from the detector preamplifier were sent to a spectroscopy amplifier for shaping and amplification. The pulses were then fed into a 100 MHZ analog-to-digital converter (ADC), which was interfaced with the PDP-15 computer. The digitized signals can occupy up to 8192 channels. The data were then transferred from the computer memory to be stored on magnetic tape for later analysis. Standard sources were used to calibrate the system to 1 keV per channel for γ-transitions and 0.1 keV per channel for x-rays and low energy γ-rays.

Figure 11

Efficiency calibration for the 18% Ge(Li) detector with the source inside the beryllium target container.

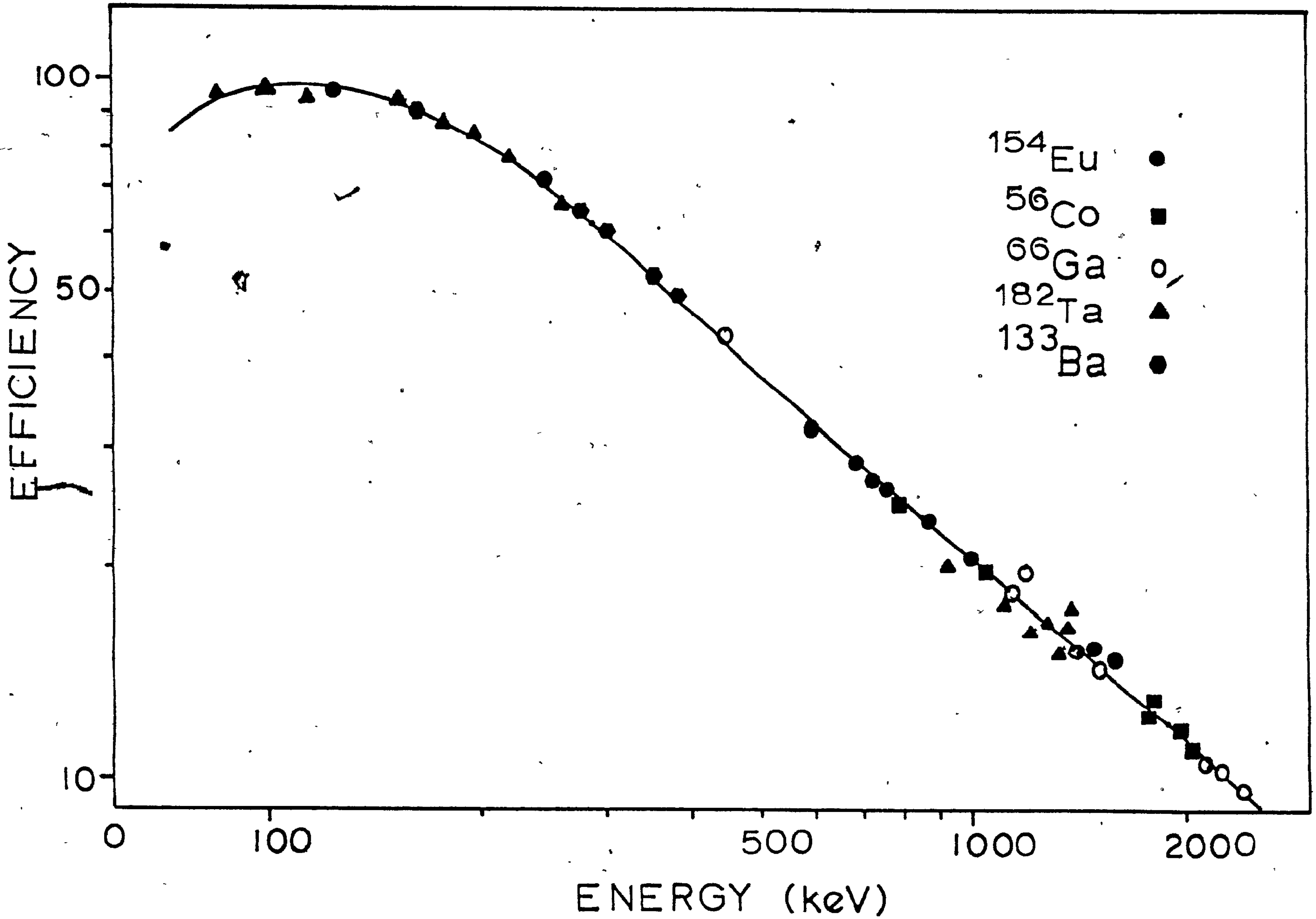
EFFICIENCY
100
50
10
0
100
500
1000
2000
ENERGY (keV)
^{154}Eu
^{56}Co
^{66}Ga
^{182}Ta
^{133}Ba

Gamma transitions were identified mainly on the basis of their half-lives. Lifetime measurements of the decaying nuclei were carried out by means of a multispectrum program on the PDP-15 computer. With this program, successive γ-ray spectra were accumulated for a preset time period, and were then stored in the computer memory. The dead time of the electronic detection system is a function of count rate. Since the count rate of the radioactive nuclei decreases with time, a constant-rate pulser was fed into the detector preamplifier in order to correct for counting losses due to dead time. The pulser voltage was adjusted so that the pulser peak fell at the high energy end of the γ-spectrum. Later, each spectrum was normalized to the intensity of the pulser peak. The multispectrum measurements were carried out using a large volume Ge(Li) detector for intermediate and high energy transitions, and also an x-ray spectrometer for low energies.

Two methods of γ-ray analysis were used. In the first, the spectrum was viewed on the PDP-15 or PDP-11 computer screen, and an analysis routine was used. This routine is linked to the light pen which is coupled to the computer screen. The peak area and centroid were calculated using this routine. This method works fairly well for single, well separated peaks. As mentioned earlier, many isotopes of cesium, xenon and iodine were produced, generating very complicated spectra. For this reason, the computer analysis code "Sampo" (Routti and Prussin 1969, Bavaria 1975) was used on the McGill IBM System. The program fits the peaks with a gaussian curve plus exponential tails, and is capable of analysing closely spaced γ-ray lines and multi-component peaks. Deducing the intensities of different components in a multi-component peak was also done by fitting the time decay of the photopeak to the half-lives of the components, or by accounting for the intensities of known components.

iii. Gamma-Gamma Coincidence Measurements

Once a set of γ-transitions is identified as belonging to the nucleus of interest, a decay scheme can be constructed, if the order of the transitions is known.

Since the life-time of non-isomeric nuclear states for γ-decay is very short compared to the resolving time of Ge(Li) detectors, two gamma rays emitted in cascade are detected simultaneously in coincidence counting experiments by two different detectors. Fig. 12 shows the circuit diagram of the system used for these measurements. In coincidence experiments, the 18% and 10% Ge(Li) detectors were placed nearly 90° relative to each other, with the source at the centre, to avoid 180° coincident events from annihilation quanta. The interscattering between the two detectors was minimized with radiation intercepting graded absorbers. The energy pulses from the detector preamplifiers were first passed through an amplifier and then fed into two analog-to-digital converters (ADC's). The timing outputs of both detectors were sent to timing filter amplifiers (TFA) for shaping and amplification, then passed through constant fraction discriminators (CFD) where the discrimination levels were adjusted to be slightly above the noise level. The two pulses were fed into the "start" and the "stop" inputs of the time-to-amplitude converter (TAC). On the "stop" side the pulse was delayed (≈50 ns) in order to compensate for systematic timing asymmetry. The pulse generated by the (TAC) has an amplitude proportional to the time difference between the "start" and the "stop" pulses. A single channel analyzer was then used to set a window through which only pulses with a certain amplitude, (and hence time difference) can be accepted. The output of the SCA was used to gate the ADC's.

The random concidence rate is proportional to the product of the count

Figure 12

Circuit diagram for $\gamma - \gamma$ coincidence measurement.

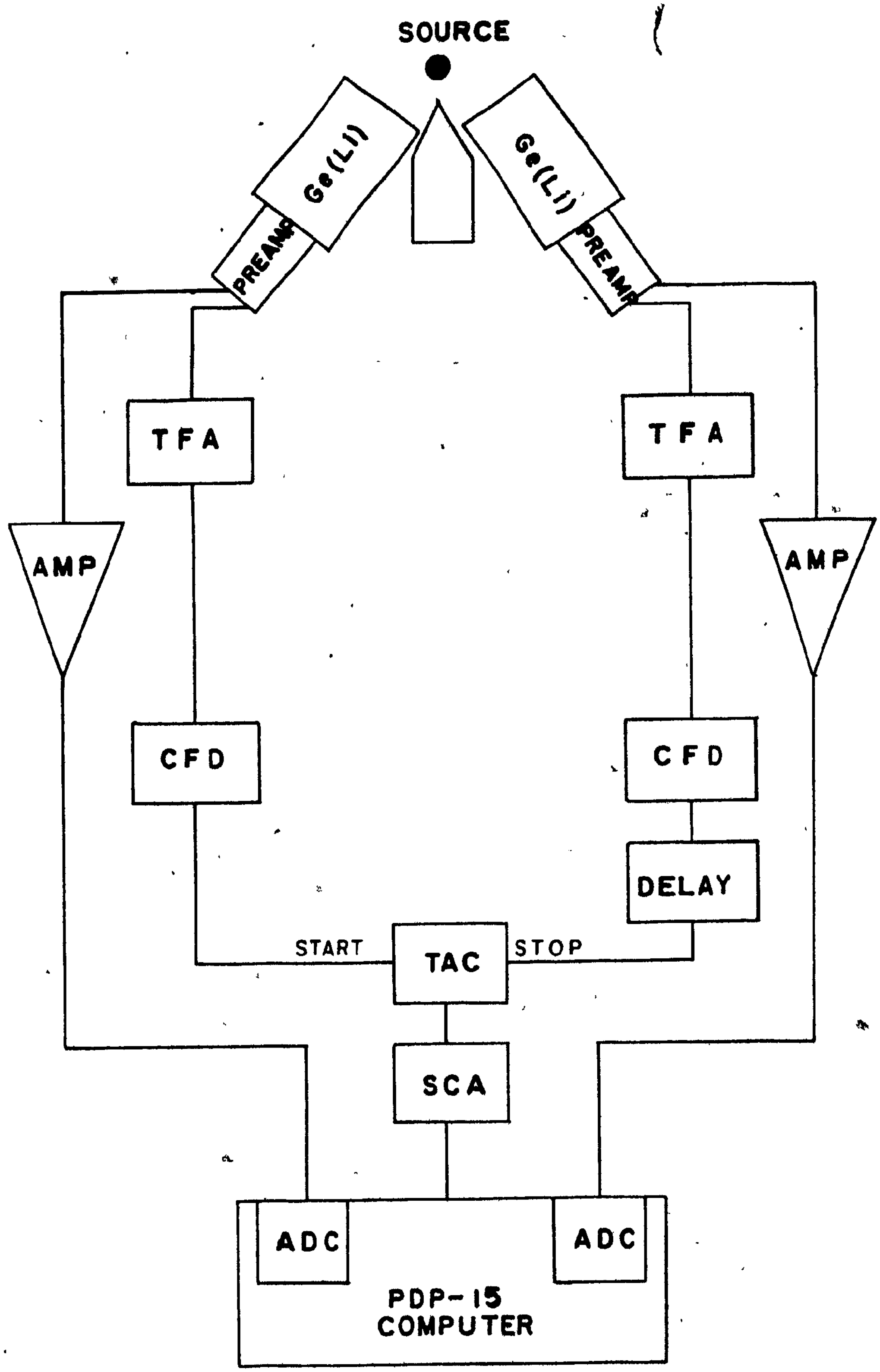
SOURCE
Ge(Li)
PREAMP
Ge(Li)
PREAMP
TFA
TFA
AMP
AMP
CFD
CFD
DELAY
START
TAC
STOP
SCA
ADC
ADC
PDP-15
COMPUTER

rates in both detectors as well as to the resolving time of the coincidence circuit. Therefore the count rates in both detectors were controlled and the resolving time of the system, determined by the window width, was set between 30 and 60 ns.

The data were recorded on magnetic tape event-by-event, and were later analyzed by setting digital gates on the γ-ray peaks of interest in either detector spectrum. The coincident events from the other detector were then recorded as a separate spectrum.

Each γ-peak sits on a background which contains events due to the Compton scattering of higher energy gamma rays. Therefore, when a gate is set on a γ-ray peak the resulting coincident spectrum will contain events in coincidence with the peak of interest as well as with higher energy γ-rays. This was corrected by setting a gate on the background in the region of each peak gate. The two resulting spectra were then compared. Coincidence measurements were also carried out, using the 18% Ge(Li) detector and the hyperpure germanium x-ray spectrometer, to detect coincidences between low and high energy γ-transitions.

iv. Beta End - Point Energy Measurements

Between two neighboring isobars, the one with the larger atomic mass will decay by a beta process to the lighter one. In beta decay by positron emission, the decay energy W_o, which is the energy equivalent to the difference of the two nuclear masses involved, is carried away by a positron and a neutrino. The energy of the emitted positron displays a broad continuous spectrum with a maximum energy E_o, which is called the end-point energy, where E_o is the total kinetic energy of the decay products.

$$E_o = Q_{\beta+} = W_o - m_o c^2$$

$$= {}_{Z+1}M^A c^2 - {}_Z M^A c^2 - 2m_o c^2$$

In an allowed beta decay, in which the positron and the neutrino are both emitted with zero angular momentum with respect to the nucleus, the beta spectrum is predicted to have the shape (Wu and Mosczowski, 1966):

$$N(E)dE = A_o\, W\, F(Z,E)(E_o - E)^2 p\,dE$$

where N(E)dE is the probability of emitting a positron with kinetic energy between E and E+dE, A_o is a constant, F is the Fermi function, W is the total positron energy ($W = E + mc^2$) and p is the positron's momentum.

For a precise determination of the end-point energy E_o, it is conventional to plot the quantity K(E), where:

$$K(E) = \sqrt{N(E)/pWF} = A(E_o - E)$$

This is called the Kurie plot, which should be a straight line intersecting the energy axis at the end-point energy.

After a beta decay, the daughter nucleus is often left in an excited state. Hence, the beta spectrum generated will contain several branches. Therefore, to separate various beta branches, it is desirable to collect beta spectra gated by the detection of subsequent gamma rays. In these measurements of $\beta - \gamma$ coincidences, a vertical superconducting solenoid (Fig. 13), which is kept at liquid helium temperature, was used (Moore et al. 1976). The superconducting solenoid, with 120 amperes current, sets up an axial magnetic field of 4.4 Tesla along its inner bore. The detector used was an intrinsic germanium crystal with a 30 mm^2 surface area and 1 cm

Figure 13

Sectional view of the superconducting solenoid.

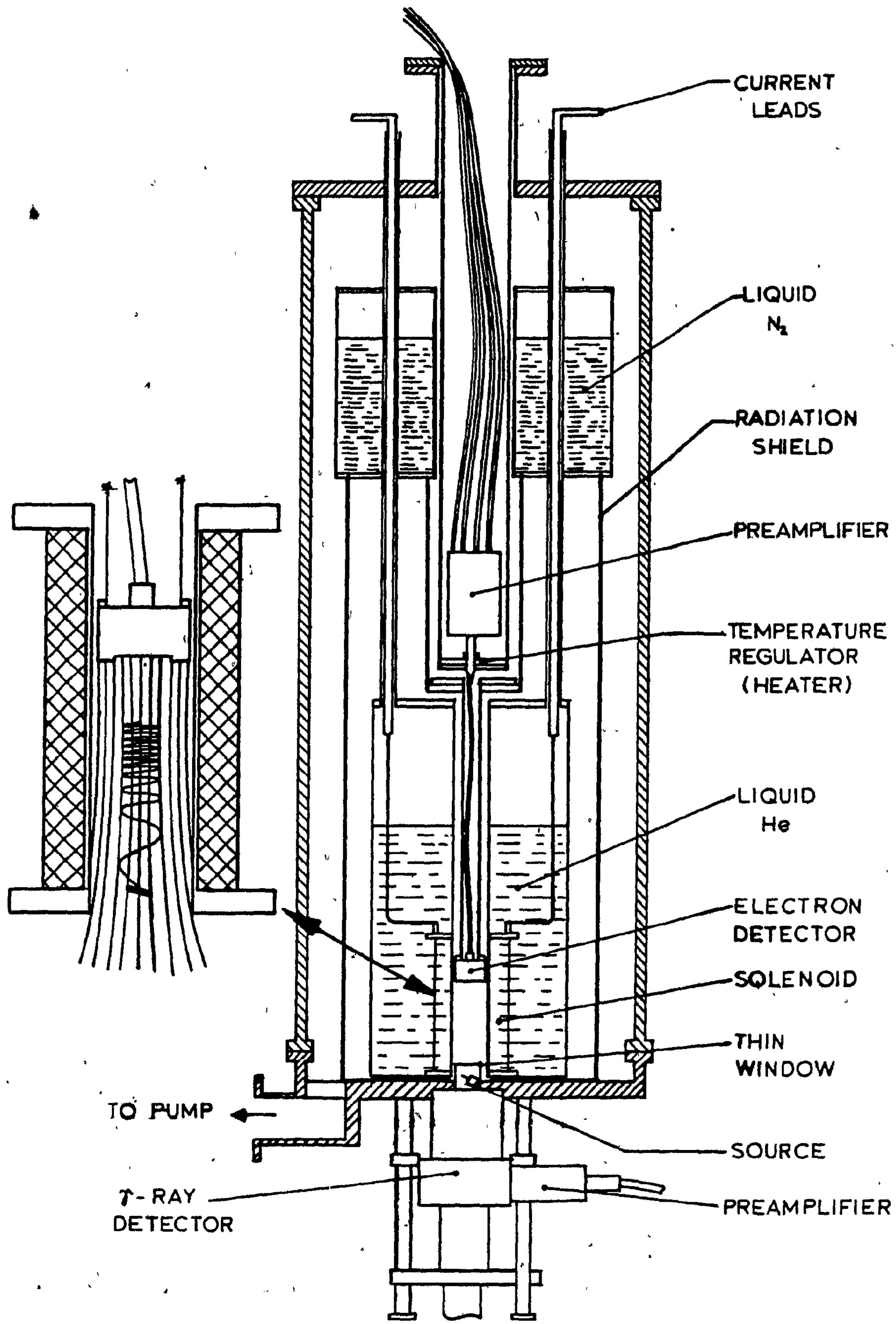
CURRENT
LEADS
LIQUID
N_2
RADIATION
SHIELD
PREAMPLIFIER
TEMPERATURE
REGULATOR
(HEATER)
LIQUID
He
ELECTRON
DETECTOR
SOLENOID
THIN
WINDOW
TO PUMP
SOURCE
γ- RAY
DETECTOR
PREAMPLIFIER

depletion depth. Such a detector has both large energy range and good resolution. In this arrangement, positrons emitted by the source travel in helical orbits along the bore to the detector. Therefore the solid angle for positron detection (23%) is greatly enhanced over the solid angle for gamma ray detection. A vertical 8% Ge(Li) detector, below the source, was used as the γ-ray spectrometer with 2.4 keV FWHM. The coincidence circuit used is similar to that of the two parameter gamma-gamma coincidence arrangement discussed earlier. Pileup effects were eliminated by using a pileup rejector on the preamplifier output. Although the γ-rays are suppressed in the β-spectrum, the strong ones are suitable for calibration. Hence, the β-detector was calibrated using the known γ-rays in the standard sources.

The data were later analyzed by placing a gate on the gamma ray and on the neighbouring background. The distortion in the background-subtracted positron spectrum, caused by backscattering, bremsstrahlung and summing with the annihilation quanta was corrected using the computer code "BETABRAN" (Hetherington 1981). Although this computer code was designed to correct for distortions specifically in electron spectra, the correction for positron spectra should be similar; some added distortion is, however, expected arising from the summing with the annihilation quanta.

Corrections were made for the loss of energy of the positrons in passing through the tip of the beryllium container of the gas target which is about 47 mg/cm^2 thick. Since the stopping power of material for electrons with energies greater than 2 MeV is essentially constant (1 $keV/mg/cm^2$), the beta end-point shift due to the container is estimated to be about 50 keV. The energy loss due to the beta detector's aluminum window (10 mg/cm^2 thick) was also corrected for.

v. Determination of Internal Conversion Coefficients

A nucleus in an excited state usually deexcites to a lower state either by gamma emission or by internal conversion. In the internal conversion process, an orbital electron, which will acquire the available energy, is ejected. In this process the internal conversion coefficient α is defined as the ratio of the probability for emission of a conversion electron λ_c to the probability for emission of a gamma ray λ_γ.

$$\alpha = \lambda_c/\lambda_\gamma$$

Since the probability for emission of a conversion electron is the sum of the probabilities of ejection of K-, L- and M- electrons etc.:

$$\alpha = \alpha_K + \alpha_L + \alpha_M + \ldots\ldots$$

For a given transition energy, the conversion coefficients depend on the type of transition and the multipolarity. The measurements of internal conversion coefficients is, therefore, used to find the order of the multipolarity of the transition and to identify the spins and parities of the nuclear states involved.

The internal conversion coefficients are usually determined by measuring gamma ray and electron transition rates. Internal conversion electron spectra are often measured using a conventional beta ray spectrometer or a solid state silicon detector. The beryllium container of the xenon gas target, 47 mg/cm^2 thick in the tapered end and 140 mg/cm^2 thick on the sides, stops internal conversion electrons with energies $\leq$ 175 keV. Energy loss and straggling persists up to 500 keV resulting in broad lines and large low energy tails. For this reason the common methods of measuring internal conversion coefficients could not be used. Instead, an indirect method of determining the number of K-shell vacancies caused by the ejection of K conversion electrons per unit gamma ray intensity was used.

X-rays in coincidence with any γ ray are due to internal conversion and electron capture. If a gate is placed on the annihilation quantum (511 keV) in a gamma-gamma coincidence experiment, only x-rays that are due to the internal conversion process are present in the resulting spectrum.

After an internal conversion process the atom is left with a vacancy and is therefore in an excited state. Transitions between various atomic states could be carried out by emission of x-rays or by other radiationless processes. The fluorescence yield of an atomic shell is defined as the probability that a vacancy in that shell is filled through a radiative transition (Bambynek et al. 1972). Therefore, for the case of the K-shell of an atom:

$$\omega_K = I_K/n_K$$

where:

ω_K = The fluorescence yield of the K-shell

I_K = Total number of characteristic K x-ray photons emitted from a sample

n_K = The number of primary K-shell vacancies

By correcting for the fluorescence yield of the K-shell and the primary K-shell vacancies, the K-internal electron transition rate could be calculated from the intensity of the observed K x-ray in coincidence with the annihilation quantum. The values of the K x-ray fluorescence yield are tabulated for different elements (Lederer and Shirley 1978).

vi. Angular Correlation Techniques

Gamma rays emitted from a radioactive source are isotropic, since the nuclei are randomly oriented. Gamma rays emitted from nuclei with a preferred direction are anisotropic. The gamma-gamma angular correlation is a method of picking out only those nuclei whose spins lie in a preferred direction.

Nuclei in a state J_i may be observed to decay to a state J which in turn goes to a state J_f, through successive emission of two gamma rays γ_1 and γ_2. The observation of γ_1 in a fixed direction then selects a group of nuclei which has a nonisotropic distribution of spin orientation. Hence, there is a correlation between the direction of γ_2 and that of γ_1.

An angular correlation measurement is carried out by using two detectors which observe gamma rays in coincidence. One of the detectors is held in a fixed position and the other detector is moved about in a plane containing the target. The coincidence rate between γ_1 and γ_2 is then recorded as a function of the angle θ between the two detectors. The shape of the angular correlation observed between γ_1 and γ_2 can be described by the formula:

$$W(\theta) = A_o + A_2' P_2 (\text{Cos}\theta) + A_4' P_4 (\text{Cos}\theta)$$

$$= A_o (1 + A_2 P_2 (\text{Cos}\theta) + A_4 P_4 (\text{Cos}\theta))$$

where

$$A_2 = \frac{A_2'}{A_o} \qquad A_4 = \frac{A_4'}{A_0}$$

$P(\text{Cos}\theta)$ = Legendre polynomial

$W(\theta)d\Omega$ = The probability of finding γ_2 within a solid angle $d\Omega$ at an angle θ from γ_1.

This angular correlation function $W(\theta)$ depends on the angular momenta J_i, J, J_f. Therefore information can be obtained about the spins of nuclear states by observing the angular correlation of successive gamma rays.

This method was used in the present work to determine the position of the first excited 0^+ states in ^{122}Xe and ^{124}Xe. ^{122}Cs was produced by the (P,3n) reaction on ^{124}Xe, using a 45 MeV proton beam. A total of about 2000 samples were used in each experiment. The angular correlation set-up consisted of a fixed 18% Ge(Li) detector and a movable 7.5 cm X 7.5 cm NaI(Tl) detector. The two detectors were kept at fixed distances of 7 cm and 10 cm respectively from the centre of the source. In the case of ^{122}Xe a 15% Ge(Li) detector was used as the movable detector. A coincidence circuit, similar to the one discussed earlier (Sec. iii), was used. The resolving time of the circuit was about 15 ns, and the count rates were kept low in order to keep the random rate at a negligible level.

Normalization of the data at various angles was carried out by accumulating a singles spectrum simultaneously with the coincidence spectrum. In the analysis, gates were set on the movable detector and intensities of the γ rays of interest in the resulting spectrum were normalized and plotted as a function of the angle between the two detectors. The data points were then fitted to the function $W(\theta)$ and the values of A_2 and A_4 thus obtained were compared to the theoretical values.

An additional correction on the experimental values of A_2 and A_4 is required to account for the solid angles subtended by the detectors.

$$A_K = \frac{A_K^{exp}}{Q_K}$$

where Q_K is the solid angle correction factor. The method developed by Krane (1972) was employed in calculating these correction factors.

B. EXPERIMENTAL TECHNIQUES USED IN IN-BEAM STUDIES

i. Production of ^{122}Xe and ^{124}Xe Isotopes

High spin states of ^{122}Xe and ^{124}Xe were populated via (α,4nγ) reactions on ^{122}Te and ^{124}Te respectively. Enriched (96.4%) ^{122}Te, and (92.4%) ^{124}Te targets were bombarded with a ^{4}He stretched beam with a typical intensity of 2-3 nA. The excitation functions were studied at 49, 54, 59, 64, 69 and 76 MeV bombarding energies. The beam energy was varied by introducing different thickness degraders into the beam. Analysis of excitation functions of lines that were assigned to ^{122}Xe and ^{124}Xe in earlier works, indicated that the maximum production for ^{122}Xe and ^{124}Xe is achieved at 54 MeV bombarding energy. The other significant reaction channels observed at this energy were found to be the (α,3n) and (α,2n) reactions. Therefore, in the case of the ^{124}Te target, levels in ^{125}Xe and ^{126}Xe were also populated. It was also found that the (α,p2n) channel is significant in the case of the more neutron deficient target of ^{122}Te. Hence, when the ^{122}Te target was bombarded, ^{124}Xe, ^{123}Xe and ^{123}I were produced along with ^{122}Xe. Levels in some other iodine and tellerium isotopes were weakly populated in both cases. The trends of the excitation functions were found to agree with the theoretically predicted ones. Those were predicted on the basis of fusion evaporation reaction calculations using the computer code ALICE (Blann, 1978).

Because of the complex nature of the gamma-ray spectra, the excitation functions were used as a preliminary study to determine a set of transitions that could possibly belong to the isotope studied. The final identification, however, was mainly based on coincidence results.

Singles spectra were also recorded with and without the beam present. Comparison of the two spectra was used to identify beta-delayed gamma rays.

The multiplicity filter set up which will be discussed in section [B(iii)] of this chapter was a very useful tool in reducing the intensities of gamma rays that were due to radioactive decay of the product nuclei.

ii. On-Line Gamma-Ray Measurement Techniques

The (α,xn) reaction on medium-heavy deformed nuclei leaves the residual nucleus in a highly excited state. These high spin nuclei deexcite by emitting unresolved and discrete gamma rays to the yrast levels. As a result a high background is characteristic of in-beam gamma ray spectra. The gamma measurement techniques are basically similar to the ones discussed earlier in the chapter [A(ii)]. In addition to the 10% and the 18% Ge(Li) detectors, a 16% hyperpure Ge detector made by Aptec, with 2.3 keV resolution at 1.3 MeV, was also used.

The bombardment of Ge(Li) detectors for a long time with neutrons results in damage to the intrinsic region of the Ge(Li) crystal (Kraner et al. 1968). The most pronounced effect is the deterioration of the energy resolution of the detector after it has been irradiated with 10^{10} neutrons/cm^2. In order to avoid radiation damage to the detectors and also to reduce background, the detectors were housed inside the cage which was shielded as described earlier (Chapter II). The detectors were always placed at a backward angle with respect to the beam direction. In addition the crystals were also shielded with layers of Cd, Pb, and Cu. In spite of all these precautions, a few detectors suffered from deteriorating resolution accompanied by a tail on the high energy side of the photopeak. The neutron damage of these detectors might have been caused by their use in a low neutron flux area for long periods of time. At the late stages of this work, an n-type coaxial Ge detector (19% efficiency, and 2.1 keV resolution at 1.3 MeV) having a reverse electrode configuration compared to the conventional one, was used. It was recently found that this type of detector is about 60 times less sensitive to radiation damage (Pehl et al., 1979). While accumulating gamma ray singles the count rates were kept reasonably low, since the detector's resolution is a function of count rate. The shielding layers around the detector crystal block out x-rays, and hence assisted in keeping the count rate reasonably low. Maintaining good resolution was very useful in separating components of multiple peaks.

In order to calibrate the system and determine the relative efficiency of the detectors at different energies, spectra from the standard sources of ^{152}Eu and ^{56}Co were accumulated before and after each experiment. The standard sources were mounted on target holders and placed at the target position in the target chamber.

Gamma ray analyses were carried out using the techniques discussed in the earlier part of the present chapter [A(ii)].

iii. Gamma-Multiplicity Filter

High-spin states populated in the residual nucleus will deexcite to the ground state through a long cascade of gamma rays which is capable of removing the angular momentum of the system. On the other hand beta decay usually feeds low-lying levels. The spectra accumulated in an in-beam experiment contain a considerable number of lines from radioactivity which often interfere with the analysis of the in-beam γ-rays. One way of overcoming this problem, reducing background, and enhancing members of bands that form long cascades is to set up a coincidence system which will only record events when at least three gamma rays are detected simultaneously. Long cascades will thus have a much higher probability of being detected than cascades which contain few gamma rays as is the case with radioactivity. One could even get rid of more radioactivity and reduce the background even further by only accepting events which were detected when more than three gamma rays were detected simultaneously; this procedure will of course reduce the coincidence count rate considerably. Preliminary experiments indicated that the decision of which restriction to place on the recorded events varies from one nucleus to another depending on the spin of the populated levels, the deexcitation process and the relative intensity of the members of a cascade. They also showed that one might even need to place different restrictions on different cascades in the same level scheme. It was therefore decided that the best technique would be to record the multiplicity of each event along with the energy. The multiplicity filter set-up is shown in the photo in Fig. 14. In this measurement 10% and 18% Ge(Li) detectors were used to detect $\gamma-\gamma$ coincidences. Two 5 in X 5 in and four 3 in X 3 in NaI detectors were used to obtain information on the multiplicity of each event recorded as a coincidence by the two Ge(Li) detectors. The two 5 in X 5 in detectors were placed on the top and bottom of the beam line, sandwiching the target chamber, while the 3 in X 3 in ones were placed on the sides looking at the target. The analysis of the data obtained from this measurement indicated that the scattering of gamma rays from one detector to another was causing false multiplicities to be recorded. In order to cure this problem the detectors had to be shielded from each other. Hence, a new γ-multiplicity set-up was designed (Fig. 15). In this arrangement a 16% p-type Ge detector and a 19% n-type Ge detector with resolution 2.3 and 2.1 keV at 1.3 MeV, respectively, were used. The

Figure 14

A photograph of the set-up of the early version of the gamma-multiplicity filter.

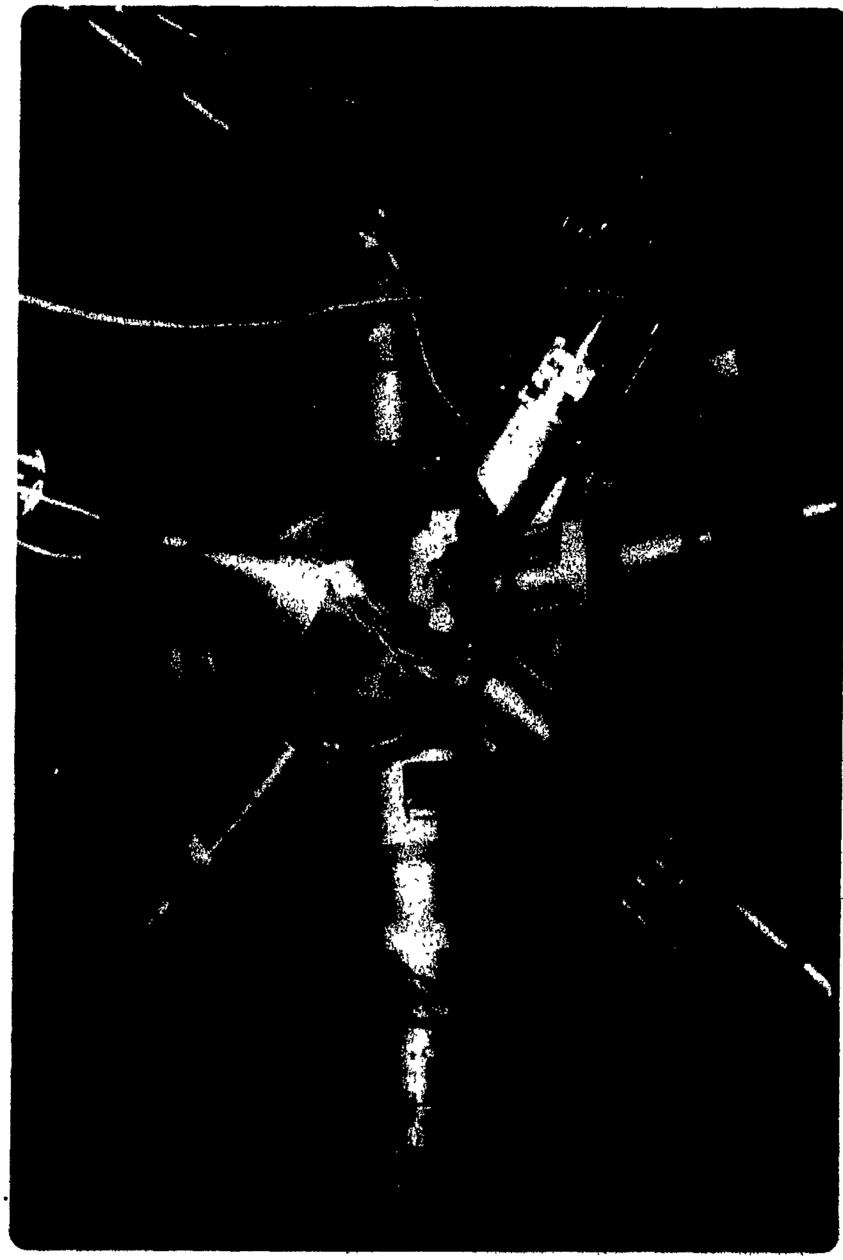

angle between the detectors was kept at 135°. Both detectors were placed at a backward angle to the beam to avoid radiation damage. Six 3 in X 3 in NaI detectors and one 3 in X 3 in BGO detector were used for registration of coincident events. The seven detectors were housed in cavities that were drilled in two hemispheres of lead. These hemispheres were placed facing each other with the beam line and the coincidence target chamber in the middle, centered about the target position. The positions of the cavities were chosen in such a way that the lead would shield the detectors from one another and hence avoid cross-talk. The seven detectors were placed equidistant from the target. The two lead hemispheres were connected together with threaded steel bars so that the size of the gap between them could be adjusted. Layers of Al and Cu absorbers were placed between the NaI detectors (and the BGO) and the lead in order to block lead x-rays. The two Ge crystals were also shielded in the same fashion.

The signal processing circuit is shown in Fig. 16. It contains a gamma-gamma coincidence set up between the two Ge detectors. The arrangement is similar to the circuit discussed earlier [III(A(iii))] except that an ARC (amplitude and rise-time compensated) timing unit is used to do the job of the timing filter amplifier (TFA) and the constant fraction discriminator (CFD) used in the earlier set-up. In order to reject pileup pulses, the SCA output was fed into a linear gate stretcher which was gated in the anti-coincidence mode with the pileup rejector pulses from both amplifiers. The six NaI and the BGO detectors were used only for timing, and provided no information about the energy of the events. Pulses from the seven detectors were first fed into a LeCroy 12 channel amplifier, and then into a LeCroy 8 channel fast discriminator for shaping and amplification. The output pulses were then fed into a LeCroy 16-fold register through some

Figure 15

Diagram of the new gamma-multiplicity filter.

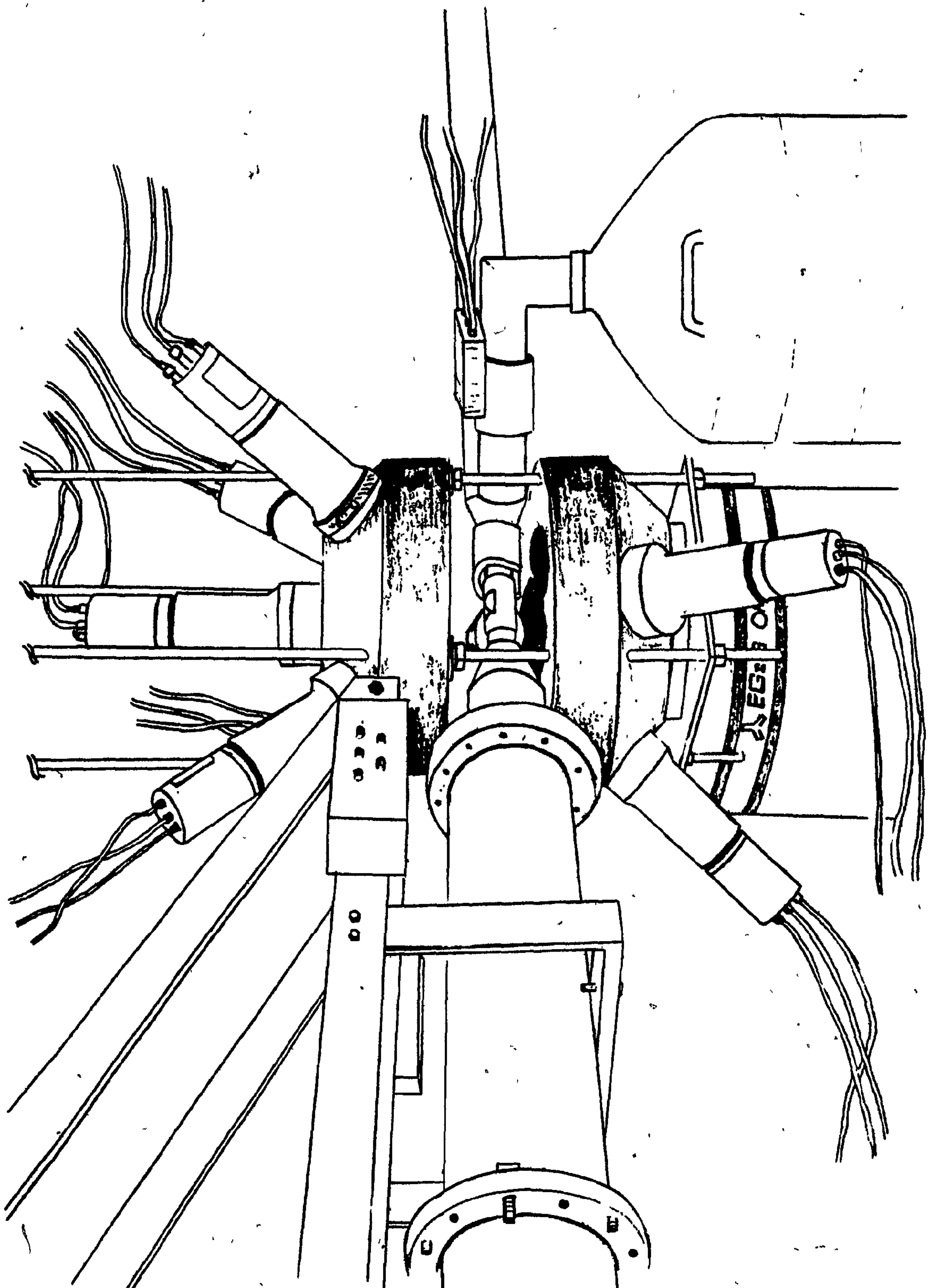

Figure 16

Circuit diagram of the γ-multiplicity filter.

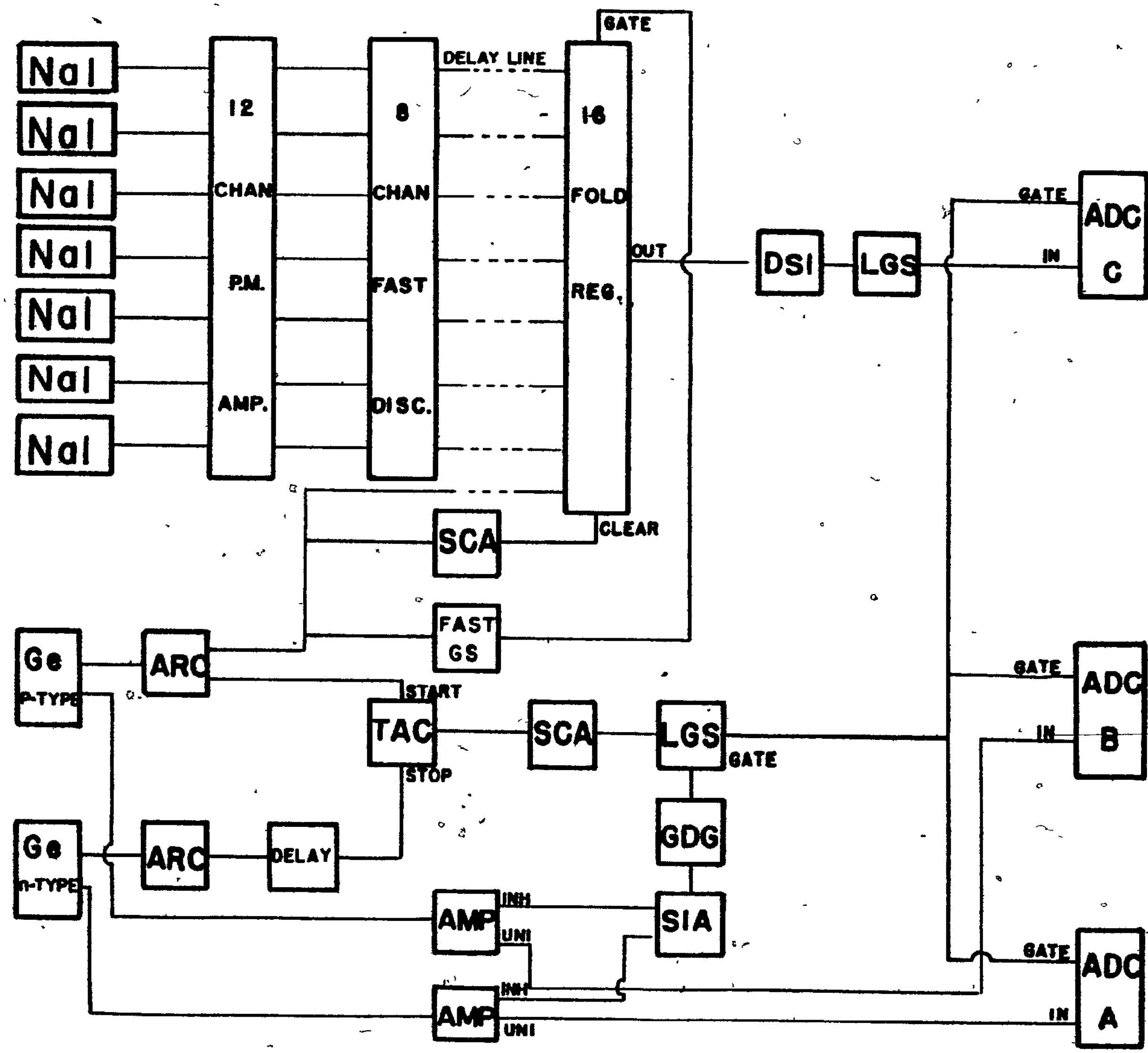

NaI
NaI
NaI
NaI
NaI
NaI
NaI
12 CHAN P.M. AMP.
8 CHAN FAST DISC.
DELAY LINE
GATE
16 FOLD REG.
OUT
CLEAR
SCA
FAST GS
DSI
LGS
GATE
IN
ADC C
Ge P-TYPE
Ge n-TYPE
ARC
ARC
DELAY
START
TAC
STOP
SCA
LGS
GATE
GDG
SIA
AMP
INH
UNI
AMP
INH
UNI
GATE
IN
ADC B
GATE
IN
ADC A

delay lines. The lengths of the delay lines were adjusted to ensure that all signals reached the coincidence register module at the same time. The negative fast timing pulse from the 16% detector was split into four components. One was used in the gamma-gamma set-up, while the second was delayed and used as an input to the register. The third was fed into a fast gate stretcher whose output was adjusted to ≈ 70 ns to gate the register. The last component was delayed about 10 ns from the end of the gate and was used as a clearing pulse for the register, resetting it 10 ns after each gate pulse had terminated. The register would only give an output when one or more gamma rays arrived within the gate period (i.e. at the same time as a gamma ray is detected by the 16% detector). The voltage of the output pulse of the register was proportional to the number of signals arriving simultaneously within the gate. The negative output of the register was then passed through a dual summer and inverter and a linear gate stretcher to obtain a positive pulse with approximately 1 μs width. This pulse was used as the input to the third analog-to-digital converter (ADC). The other two ADC's registered the gamma energy from the two Ge detectors. The gate obtained from the (TAC) on the gamma-gamma side was used to gate the three ADC's. In the third ADC spectrum, the channel number represents the height of the register output (i.e. the number of detectors triggered simultaneously). Since we were triggering the third ADC with the gamma-gamma gate, the multiplicity was recorded for only those events that triggered the two Ge detectors simultaneously. The multiplicity spectrum (Fig. 17) contained eight well-resolved peaks. The first peak represents those events when no NaI (or BGO) were triggered (i.e. simply two gammas in coincidence). The second peak contains events when one NaI

Figure 17

Gamma multiplicity spectrum.

Only seven multiplicity peaks are shown.

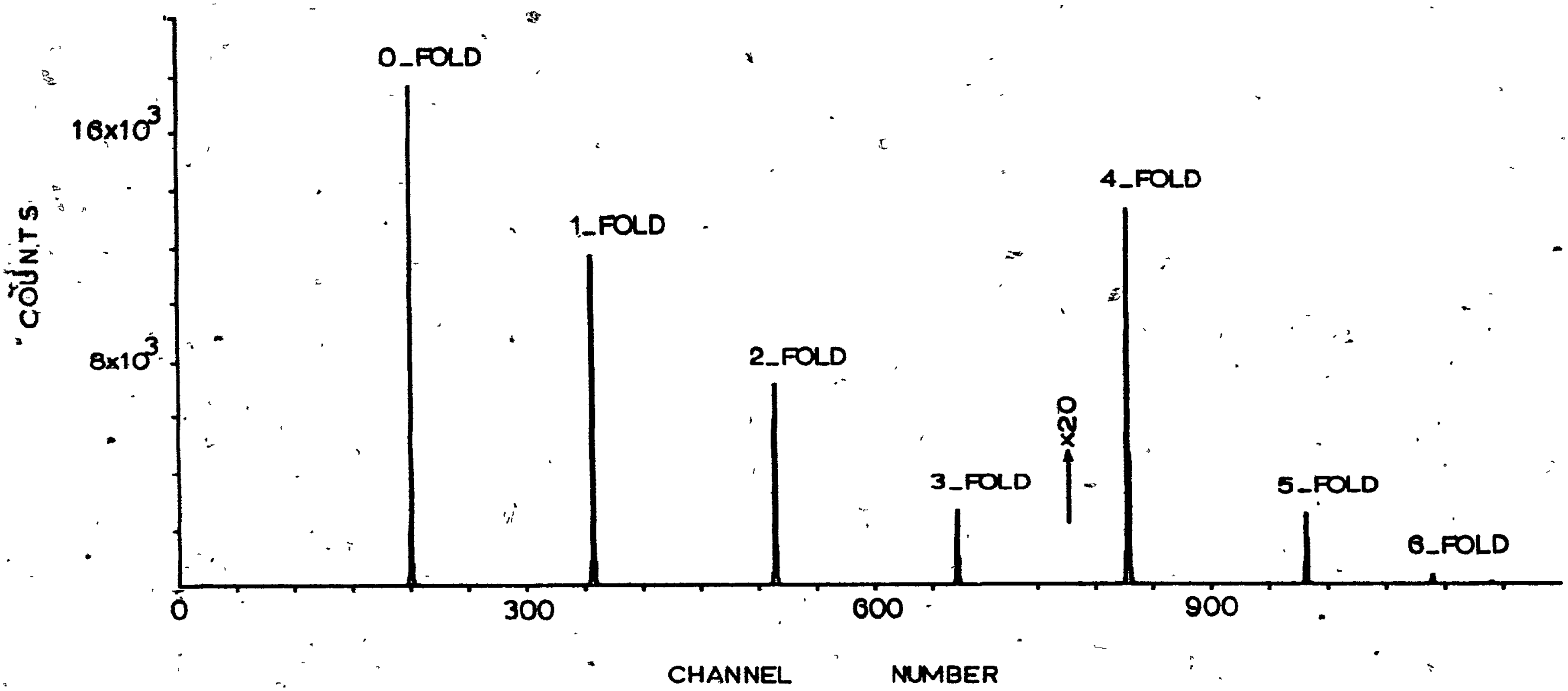
0_FOLD
1_FOLD
2_FOLD
3_FOLD
x20
4_FOLD
5_FOLD
6_FOLD
16x10³
8x10³
COUNTS
0
300
600
900
CHANNEL NUMBER

detector was triggered along with the two Ge detectors. The third peak corresponds to a cascade of four gammas detected by the system, and so on. Although the lead shielding hemispheres could accommodate up to 10 detectors, only seven were used in this measurement. Increasing the number of detectors embedded in the lead shields would increase the solid angle and hence the efficiency of the system.

The data were written on magnetic tape event by event, where each event was written as the energy of γ_1, the energy of γ_2 in coincidence with it, and the multiplicity of the cascade to which γ_1 and γ_2 belong, as seen by the system. The data were later sorted using a special program (XMSRT3) on the PDP-11 computer which was designed for threefold coincidences. The data were analyzed several times by demanding different numbers of NaI (or BGO) detectors in coincidence with the gamma pair in the Ge detectors. Background gates were set along with the photopeak gates on one of the Ge detectors and the resulting spectra were compared. Fig. 18 shows the (gating) total spectrum on the 19% n-type Ge detector obtained with different numbers of gammas in coincidence. It is clear that demanding that one or more γ-rays be detected along with the gamma pair reduces the intensity of lines due to radioactivity along with the general background level and it also enhances the in-beam lines which belong to long γ-cascades. From these spectra one can draw conclusions about the actual multiplicity of the cascade to which a certain gamma ray belongs. This is a very useful tool in constructing level schemes.

In the case of ^{122}Xe and ^{124}Xe, it was found that demanding at least one gamma in addition to the pair in coincidence gave the best results. The multiplicity filter arranged in the fashion described above is a very powerful experimental tool; the data accumulated contain information

Figure 18

The gamma-multiplicity filter gating spectrum obtained in one-, two-, and four-fold coincidences.

R: radioactivity γ-ray

I: in-beam γ-ray

M: high multiplicity in-beam γ-ray

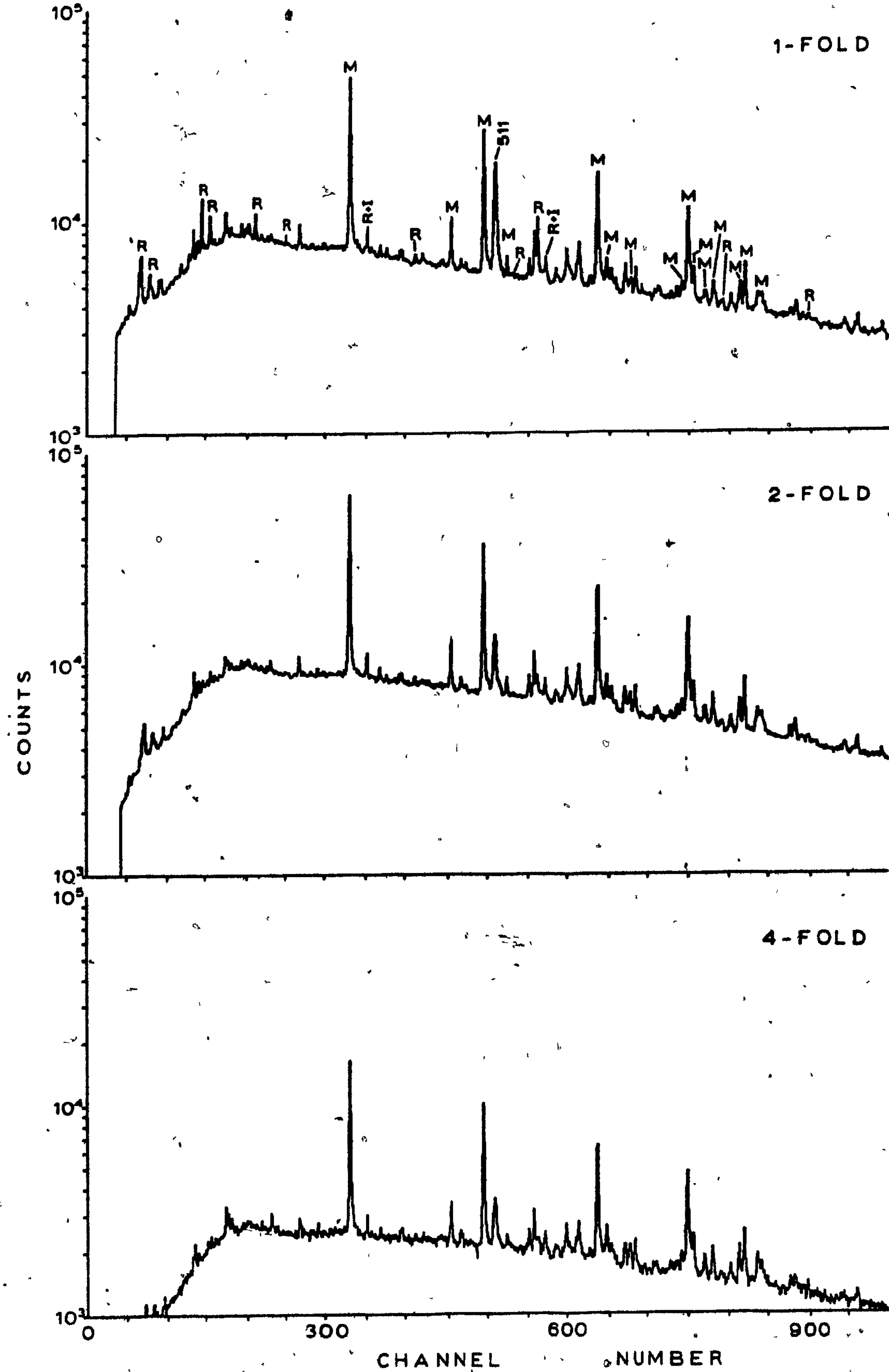
1-FOLD
2-FOLD
4-FOLD
COUNTS
CHANNEL NUMBER
0
300
600
900
M
511
R
R+1

usually obtained from three or more experiments.

iv. Neutron-Multiplicity Filter

The ^{4}He-induced reactions below 25 MeV in medium and light nuclei proceed via the formation of compound nuclei. It has been noted by Sarantites et al. (1978), that above 25 MeV the compound and precompound process compete. At 50 MeV, though, the compound nucleus process dominates and the reaction could proceed via the combination of the two processes; a number of fast neutrons are emitted at the pre-equilibrium stage and later some slow neutrons are evaporated at the equilibrium stage (Sakai et al. 1979, Ejiri et al. 1978). These evaporated neutrons are presumed to have energies corresponding to the nuclear temperature (≃ 1-2 MeV) (Johnson and Szymanski 1973). In the pre-equilibrium process the neutrons are emitted preferably in the forward angle while the neutrons evaporated after the formation of the compound nucleus are isotropic.

A very useful technique of eliminating radioactivity transitions from a singles spectrum is to count the gammas in coincidence with the emitted neutrons. Such an experiment will also enhance transitions that belong to reactions with higher numbers of evaporated neutrons. Transitions that follow an $(\alpha,4n)$ reaction, for example, will have a higher probability of being detected than those following an $(\alpha,3n)$ of $(\alpha,p3n)$ reaction. Demanding two neutrons in coincidence with the gamma detected instead of one further enhances those transitions.

A gamma-neutron multiplicity experiment was therefore carried out. The set-up is shown in Fig. 19. The gammas were detected by the 16% Ge detector. Six liquid scintillators (NE213) detectors on loan from the University of Manchester were used to detect neutrons. Since these neutrons

<u>Figure 19</u>

The neutron-multiplicity setup.

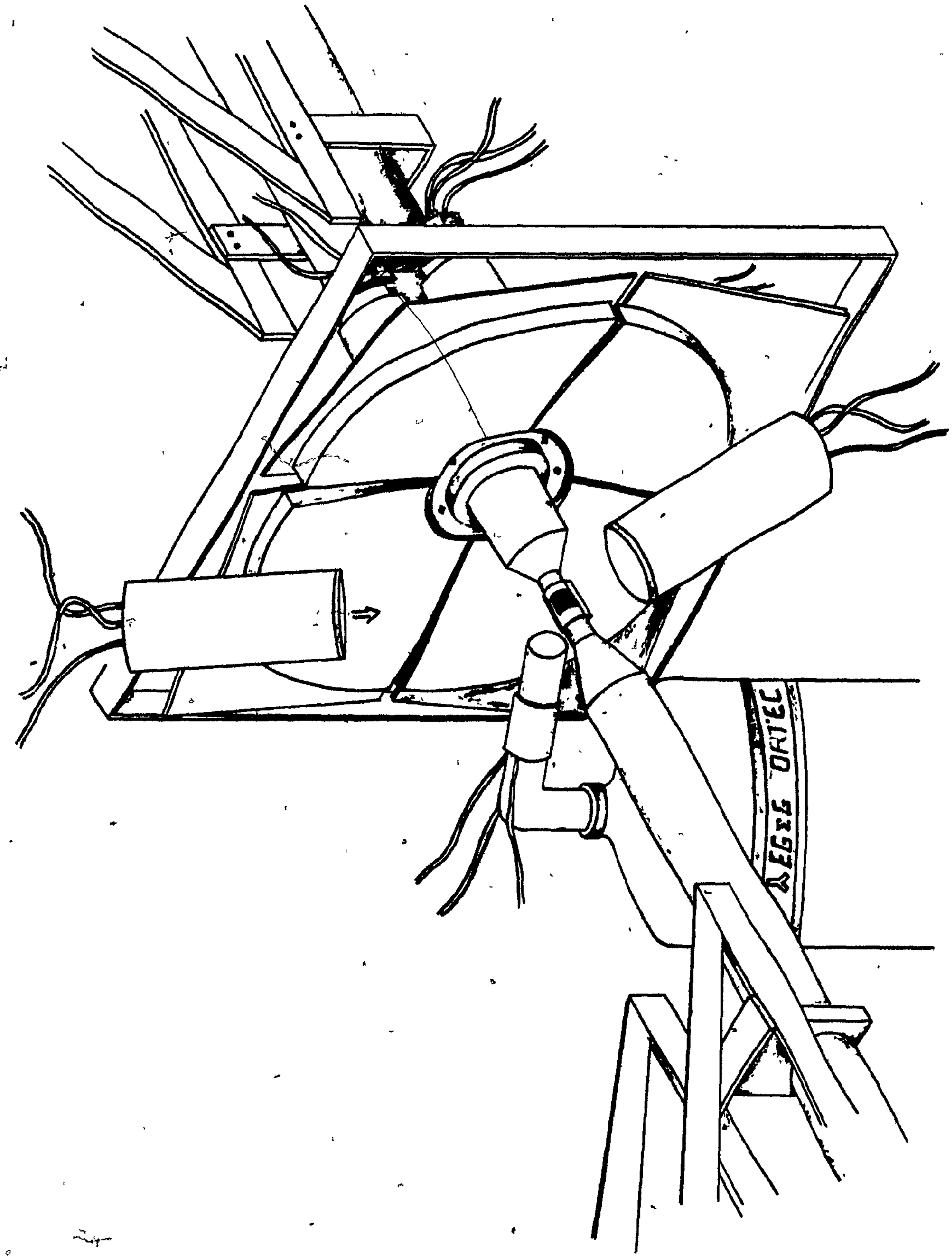

are expected to be emitted preferably in the forward angle, four of these detectors were placed downstream from the target covering an area of 0.5 m^2 around the beam line. Those detectors were about 5 cm thick quadrants, while the other pair had a cylindrical shape and were about 12 cm thick, with 100 cm^2 surface area. The two detectors were placed on opposite sides of the beam pipe, to observe the target at a 90° angle. The aim of the experiment was to accumulate gamma spectra in coincidence with different numbers of neutrons. For this reason the neutron multiplicity of each event was recorded along with its gamma energy. The schematic diagram of the set-up is shown in Fig. 20. The energy output pulse of the Ge detector was first amplified, and then fed into the analog-to-digital converter (ADC). Since gamma rays will also be detected by the liquid scintillators, the pulses from the photomultipliers of these detectors were fed through pulse shape discrimators (P.S.D.) ("Link Systems" Discriminator model 5010) to differentiate between neutron and gamma ray pulses. Such discriminators exploit the different decay times observed in liquid scintillators when irradiated with neutrons and gamma rays. Their principle of operation is based on the comparison of two weighted time integrals of the detector signal over periods of 25 ns and 500 ns. Their output pulses were then delayed to arrive simultaneously. This was done by feeding the pulses into a discriminator, whose output varied from -1v to zero, so that when this was used as an input to a second discriminator (which triggered on the negative slope) the output pulse obtained was delayed by the adjustable width of the first output. These output pulses were then fed through a discriminator and the 16-fold register. The register was gated with a signal derived from the timing output pulse of the preamplifier of the Ge detector. This pulse was also used to reset (clear) the register. It was

Figure 20

Circuit diagram of the neutron-multiplicity filter

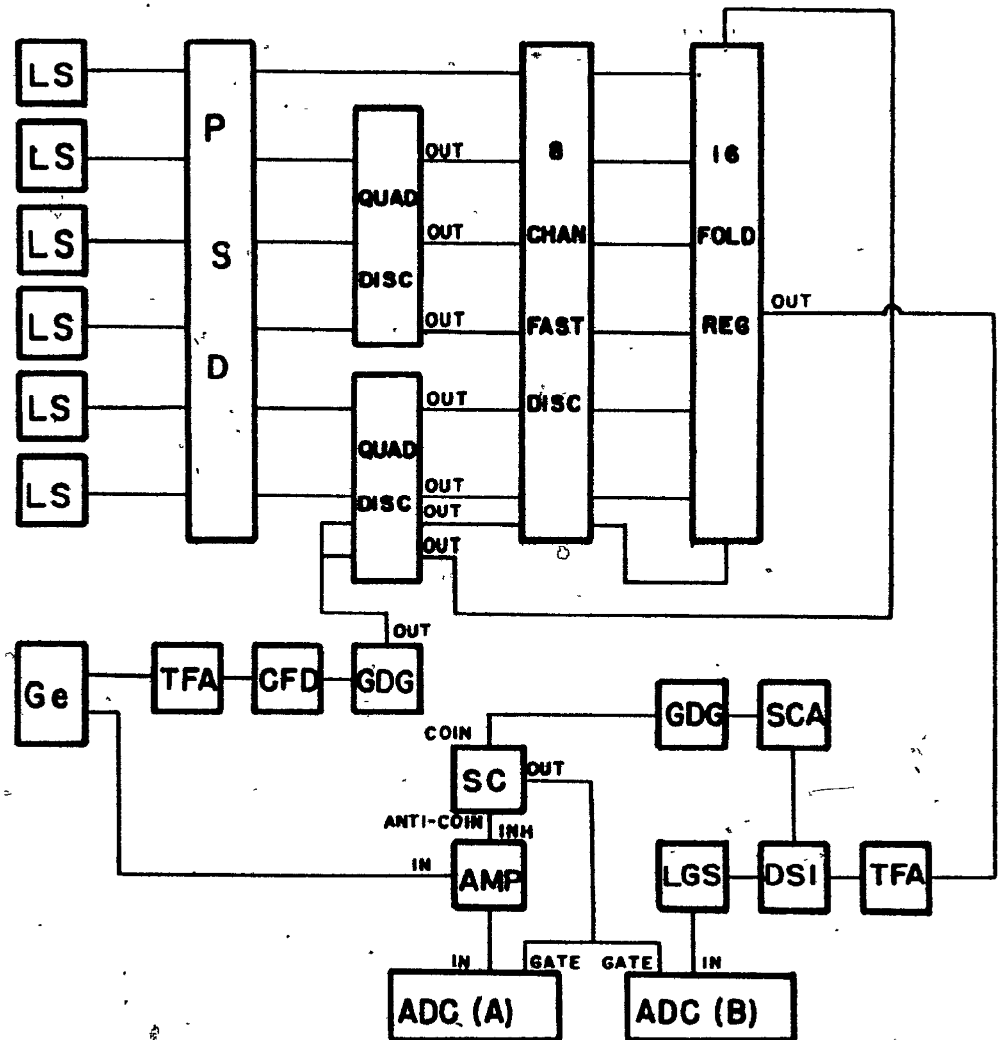
LS
LS
LS
LS
LS
LS
PSD
QUAD DISC
QUAD DISC
OUT
8 CHAN FAST DISC
16 FOLD REG
OUT
Ge
TFA
CFD
GDG
GDG
SCA
COIN
SC
ANTI-COIN
INH
IN
AMP
LGS
DSI
TFA
IN
GATE
GATE
IN
ADC (A)
ADC (B)

delayed so that it would arrive a few nanoseconds after the end of the gate pulse. Gating the register with the Ge pulse ensured that the output of the register was in coincidence with the gammas detected. The register's negative output was amplified, inverted and then fed into a linear gate stretcher which adjusted the pulse's duration to 1 μs, suitable for an input to the ADC gate. The inhibit pulse from the gamma amplifier and the register's inverted and delayed output were fed into a slow coincidence unit, set on anti-coincidence mode, and the output was used to gate the two ADC's. The ADC's could therefore count when the register gave an output excluding pulse pileup. The register output's height was proportional to the number of pulses arriving simultaneously within the gate (i.e. the number of neutrons detected). Since the ADC's were gated with this pulse, only gammas in coincidence with any number of neutrons will be accepted. The second ADC spectrum contained the neutron multiplicity. Since the highest number of neutrons came from the (α,4n) reaction, five peaks appeared in the multiplicity spectrum, with the fifth peak due to random events. The data were sorted on-line during accumulation by setting gates on the neutron multiplicity peaks, and the resulting spectra were then written on DEC tapes. Fig. 21 shows a gamma singles and the gamma spectra obtained in coincidence with one, two and three neutrons. These spectra were obtained from the (α,4nγ) reaction on ^{122}Te. The figure shows clearly the large attenuation of the intensities of the radioactivity gamma rays. The intensities of various gamma rays were then plotted as a function of the number of neutrons in coincidence. The results are discussed in Chapter IV.

Figure 21

Gamma-spectrum obtained in zero-, one-, two- and three- fold coincidence in the neutron-multiplicity filter measurement.

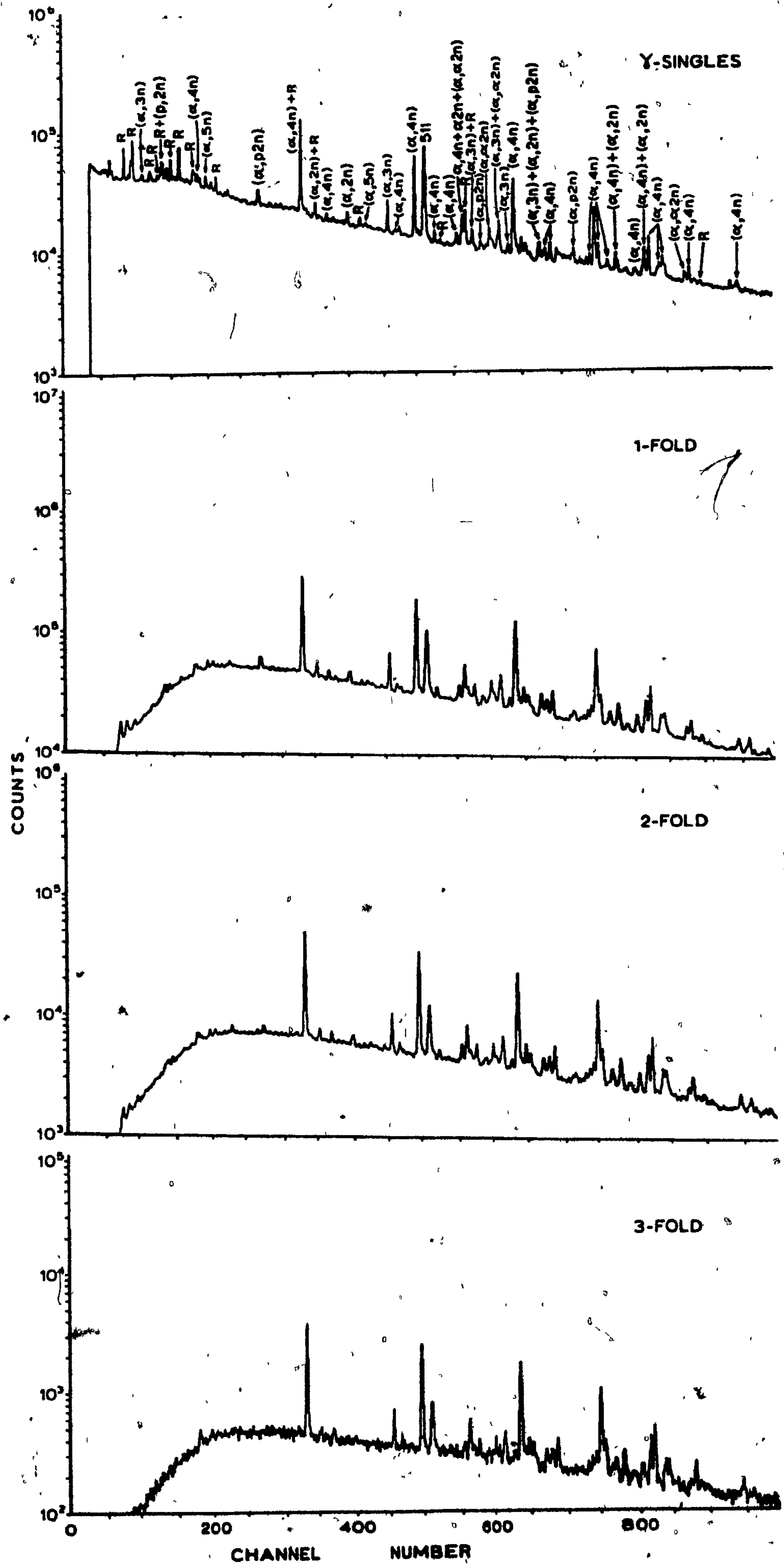

γ-SINGLES
1-FOLD
2-FOLD
3-FOLD
COUNTS
CHANNEL NUMBER
0
200
400
600
800

V. Angular Distribution

As mentioned earlier in this chapter [B(iv)] the $(\alpha,xn\gamma)$ reactions proceed mainly via the formation of the compound nucleus. In the case of an even-even target with spin 0, the spin vector introduced by the alpha particle is well aligned in a direction perpendicular to the beam axis, producing a completely aligned compound state (Diamond 1966, Morinaga and Yamazaki 1976). The spin alignment at the initial stage of the $(\alpha,xn\gamma)$ reaction has, been reported by Ejiri et al. (1965, 1966, 1972), Halpern et al. (1968), and Williamson et al. (1968) to be preserved. The original orientation is retained to a considerable extent by the residual nucleus, since the angular momenta carried away by the evaporated neutrons and early gamma rays are too small to disturb the spin alignment greatly. Because of the alignment the gamma rays emitted from nuclear states display characteristic angular distribution patterns with respect to the beam direction. This angular distribution has the following form:

$$W(\theta) = 1 + A_2 P_2(\cos\theta) + A_4 P_4 (\cos\theta)$$

where: θ is the angle between the incident particle beam direction and the direction of the gamma ray emitted.

P_k = the Legendre polynomial.

Since the alignment of the populated states is partial, the angular distributions are attenuated

$$A_k = \alpha_k A_k^{max}$$

The theoretical coefficients A_k^{max} for complete alignment have been tabulated

(Yamazaki 1967). The attenuation coefficients α_k express the degree of alignment of states in the residual nucleus. The attenuation coefficient is defined as the ratio of the actual statistical tensor to the statistical tensor for complete alignment (Yamazaki 1967). If the evaporated neutrons take out angular momenta at random, then the population of magnetic substates is Gaussian with respect to the beam (i.e. about the m = 0 substate, taking the beam direction as the axis of quantization) with width σ. This was experimentally confirmed by Diamond et al. (1966). It was also experimentally found (Kitching 1981) that for any partially aligned level:

$$\frac{\sigma}{J} \simeq \frac{1.8}{J+0.5}$$

The attenuation coefficients α_k are tabulated versus σ/J (Der Mateosian and Sunyar 1974).

In the present work, angular distribution measurements were carried out using an 18% coaxial Ge(Li) detector fixed at a 90° angle with the beam. A 10% coaxial Ge(Li) detector was placed on a rotating platform 12 cm from the target, which was placed at 45° to the beam direction. Spectra were accumulated with the movable detector placed at 90°, 100°, 110°, 120°, 130° and 140°, with respect to the beam. Later the photopeak intensities were normalized using the corresponding peaks in the fixed detector. In cases where the gamma ray under consideration was very weak, the intensity was normalized to the E2 $2^+ \rightarrow 0^+$ transition intensity in the monitor, in order to reduce the uncertainty in the measurement. The normalized intensities were then fitted by least-squares analysis to the Legendre polynomial expansion. The experimental coefficients A_2^{exp} and A_4^{exp} were then extracted. Because of the finite solid angle subtended by the detector the observed angular distribution is different from that expected with a "point" detector, and has the form:

$$W(\theta) = \sum_k Q_k A_k P_k(\cos\theta)$$

where Q_k is the correction factor, hence:

$$A_k = \frac{A_k^{exp}}{Q_k}$$

where Q_k is a function of the gamma ray energy, source-to-detector distance and the detector dimension (Krane 1972). Due to the large size detector used and the relatively long distance, the finite solid angle corrections were kept small. The corrected coefficients A_k thus extracted were then used to obtain information on the multipolarity of the transitions and hence the spin of different states. This was done by comparing A_k with the tabulated A_k^{max} and $\alpha_k (A_k = \alpha_k A_k^{max})$ for different possible spins that are suggested by the level scheme. Information on the degree of alignment of different states in the residual nucleus was also obtained by empirically determining $\alpha_2 (\alpha_2 = \frac{A_2}{A_2^{max}})$ for established transitions.

CHAPTER IV - EXPERIMENTAL RESULTS

A. RESULTS OF DECAY STUDIES

a) Decay of ^{124}Cs

i. Previous Work

The decay of ^{124}Cs was first reported by Chaumont et al., in 1969. Using the on-line mass-separator technique they measured the half-life of the beta decay of ^{124}Cs to be 26.5 ± 1.5 sec. In 1972, Droste et al. produced ^{124}Cs via the ^{115}In (^{12}C, 3n) reaction. They observed a 354 keV transition which decayed with $T_{1/2}$ = 34 ± 6 sec. The transition was attributed to the decay of ^{124}Cs based on excitation functions. They also produced ^{124}Ba sources via the $^{116}Sn(^{12}C$, 4n) reaction, and studied levels populated in the $^{124}Ba \rightarrow ^{124}Cs \rightarrow ^{124}Xe$ decay chain. Another two transitions of 492 and 847 keV were assigned to the decay of ^{124}Cs and a decay scheme was proposed, with two excited states of energies 354 and 847 keV. Westgaard et al. (1975) measured the total beta decay energy of ^{124}Cs to be Q_{EC} = 5.92 ± 0.46 MeV. This result was obtained from their measured end-point energies for the branches to the first and second excited states in ^{124}Xe.

Using atomic beam magnetic resonance techniques at the ISOLDE isotope separator at CERN, Ekstrom et al.(1977) measured the ground state spin of ^{124}Cs to be I = 1. Even parity was assumed consistent with the cesium ground states from A = 122 up to A = 130.

Following the completion of the present work, a study of the decay of ^{124}Cs by Charvet et al. (1977) was published. Separated ^{124}Cs sources were obtained, following the bombardment of a lanthanum target with 600 MeV protons. These data led to a decay scheme of fourteen excited states.

Subsequently, Droste et al. (1978) published their own findings on the decay of ^{124}Cs, which was produced in the ^{124}Xe (p,n) reaction with Ep ≃ 9.5 MeV. Their group proposed a decay scheme with four excited states, but neither the half-life nor beta end-point energy were measured. The results of both publications will later be compared with those of the present work. A detailed in-beam study was carried out by us, and the results will be presented in part (B) of this chapter. We also performed angular correlation measurements on ^{124}Xe, in order to identify the position of the excited 0^+ states. These results will be presented in section (d) of this chapter.

ii. <u>Gamma Ray Spectroscopy</u>

Levels of ^{124}Xe were populated in the beta decay of ^{124}Cs. Radioactive sources of ^{124}Cs were produced in the (p,n) reaction on ^{124}Xe targets using 15 MeV protons with a bombardment time of 30 sec. The gamma spectrum of the decay of ^{124}Cs was measured, using the 18% Ge(Li) detector (Fig. 22). The γ-rays labelled belong to the decay of ^{124}Cs, while the unlabelled ones mainly arise from the decay of cesium isotopes with mass number 125, 126, 127 and 128. The energies and intensities of gamma rays assigned to the decay of ^{124}Cs are given in table 1. The 492 keV gamma peak is a doublet, produced in the decay of both ^{124}Cs (492.6 keV) and ^{126}Cs (491.2 keV) (Pathak et al. 1976). This was accounted for in the intensity calculation.

The half-life of the ^{124}Cs decay was measured using the multispectrum technique described earlier [IIIA(ii)]. Sixteen consecutive 10 second groups were accumulated. The rapid pneumatic transport system enabled us to start counting only a few seconds after the end of bombardment. The measured half-life is 29.7 ± 0.2 sec. This value was obtained from the time decay of the 354 and the 915 keV gamma rays, shown in Fig. 23.

Figure 22

^{124}Cs γ-ray spectrum recorded with the 18% Ge(Li) detector.

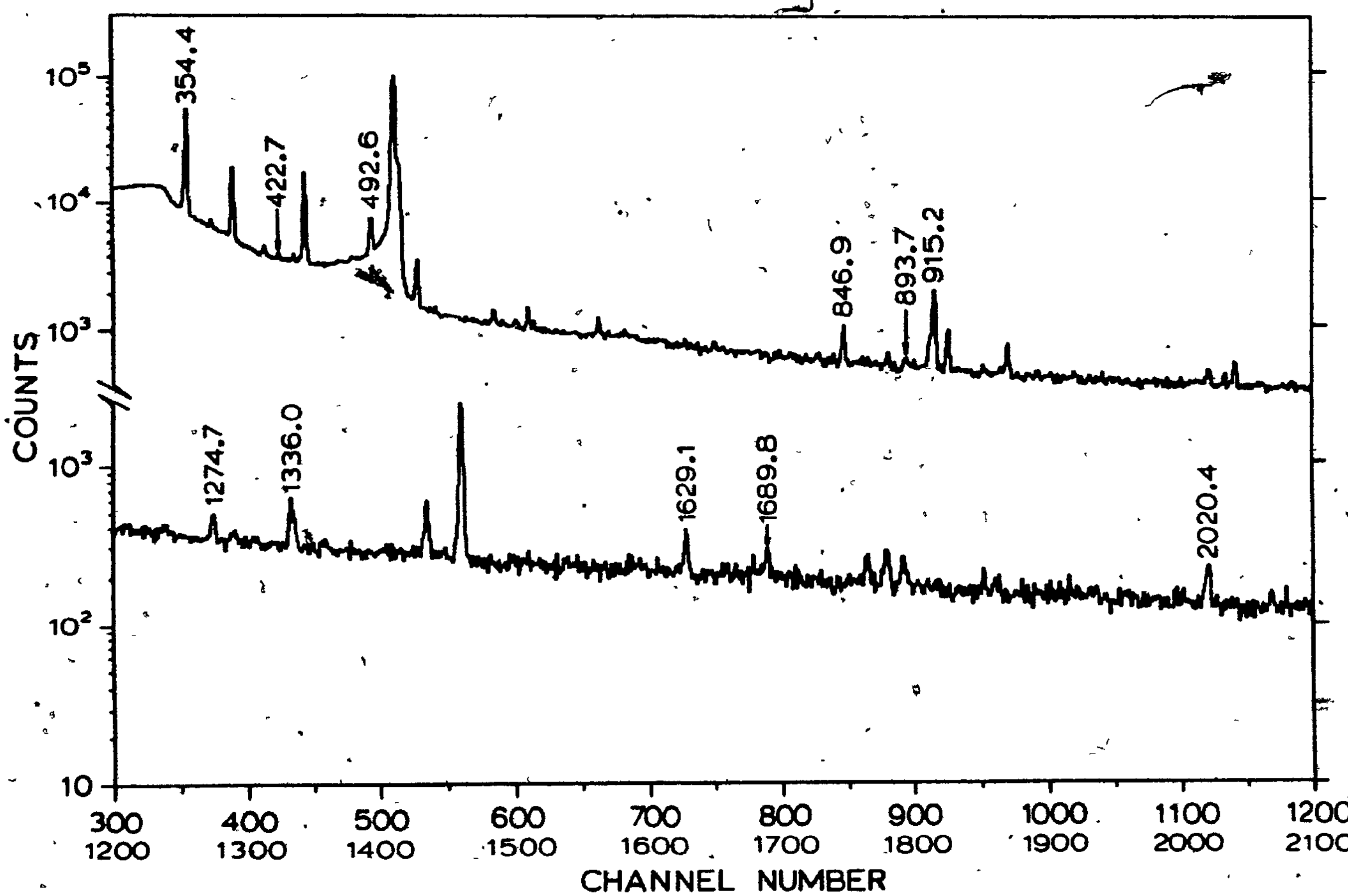

COUNTS
10⁵
10⁴
10³
10³
10²
10
354.4
422.7
492.6
846.9
893.7
915.2
1274.7
1336.0
1629.1
1689.8
2020.4
300 400 500 600 700 800 900 1000 1100 1200
1200 1300 1400 1500 1600 1700 1800 1900 2000 2100
CHANNEL NUMBER

TABLE 1. ^{124}Cs (29.7 ± .2 sec) Gamma-Ray Energy and Intensity

E_γ(keV)	I_γ%
354.4 ± 0.1	100
359.5 ± 0.6	≤ .3
401.2 ± 0.3	0.3 ± 0.1
422.7 ± 0.2	0.9 ± 0.1
492.6 ± 0.1	7.0 ± 0.3
524.5 ± 0.3	0.7 ± 0.2*
846.9 ± 0.2	2.89 ± 0.16
893.7 ± 0.2	0.6 ± 0.1
915.2 ± 0.1	9.7 ± 0.6
1274.7 ± 0.3	1.59 ± 0.12
1336.0 ± 0.3	1.52 ± 0.14
1629.1 ± 0.4	2.13 ± 0.13
1689.8 ± 0.4	1.15 ± 0.13
2020.4 ± 0.4	1.54 ± 0.14

* Intensity deduced from coincidence measurement

In the gamma-gamma time coincidence measurement, two coaxial Ge(Li) detectors, with 10% and 18% efficiencies, were used. The results of this experiment are given in table 2. Fig. 24 shows the background subtracted spectra which were obtained by setting gates on the 354.4, 492.6, 846.9 and the 915.2 keV gamma rays. The two unidentified lines, which appear in the 492.6 keV gate are the 388.6 and the 434 keV γ-rays, in coincidence with the 491.2 keV transition of ^{126}Cs decay (Pathak et al. 1976). The 524 keV γ-ray is identified mainly from the coincidence measurements, since in the singles spectrum it falls between the 526 gamma peak of the ^{125}Cs decay (Jha et al. 1972) and the tail of the 511 annihilation peak.

iii. Decay Scheme and Discussion

The ^{124}Cs decay scheme deduced from the present study is shown in Fig. 25. In order to construct this decay scheme, the measured half-life of $T_{1/2}$ = 29.7 sec, Q_{EC} = 5.92 MeV (Westgaard et al. 1975), coincidence results, and sums and differences of gamma ray energies were used. In the present work a $\beta - \gamma$ measurement was carried out to determine the end-point energy. However, from the beta spectrum obtained in coincidence with the 354 keV transition an inconclusive value of $Q_{EC} = 6.1 \pm 0.5$ MeV was obtained due to poor statistics.

The beta feeding to the ground state of ^{124}Xe was calculated by accounting for the feeding to excited states in the total beta activity due to the decay of ^{124}Cs. The intensity of the positron activity of ^{124}Cs decay was calculated from the multispectrum data accumulated with the copper positron annihilator around the source. The annihilation quantum (511 keV) time decay was then fitted to a mixture of four half-lives (29.7 sec, 45 min, 98.4 sec and 234 sec) representing the half-lives of ^{124}Cs, ^{125}Cs, ^{126}Cs

TABLE 2. ^{124}Cs Gamma-Gamma Coincidence Results

Gate E_γ(keV)	Coincident Gamma Rays, E_γ(keV)
354.4	422.7, 492.6, 524.5, 915.2, 1274.7, 1336.0, [1689.8], 2020.4
492.6	354.4, 422.7
846.9	422.7
915.2	354.4

Figure 23

Time decay of ^{124}Cs.

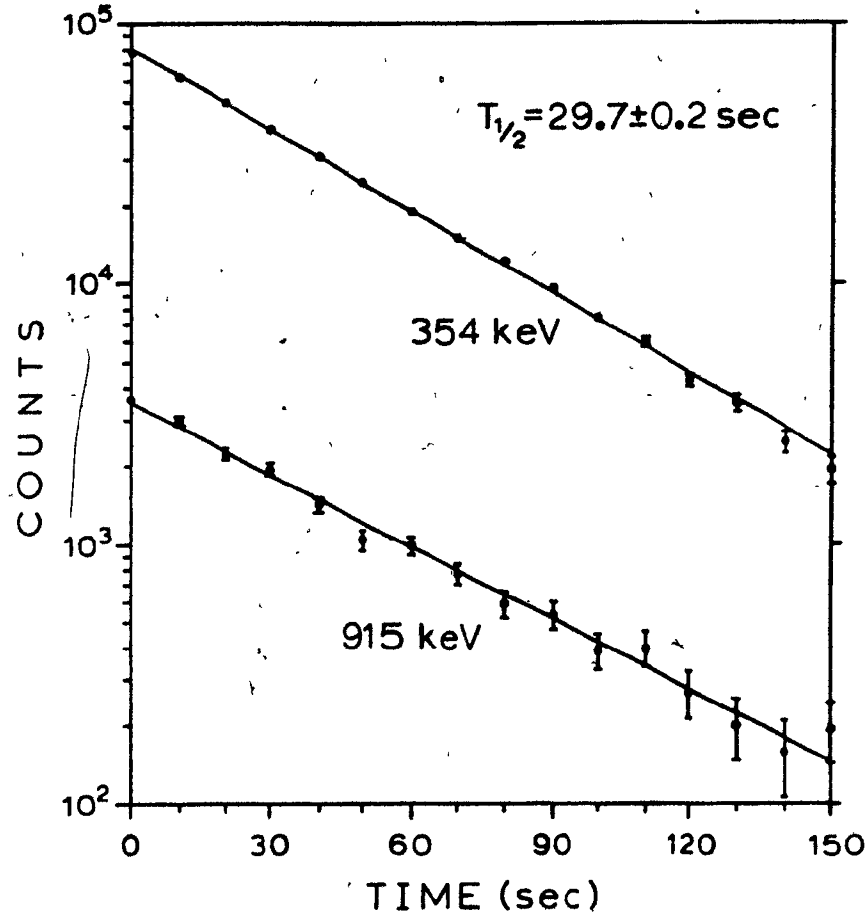
$T_{1/2}$=29.7±0.2 sec
354 keV
915 keV
COUNTS
TIME (sec)
10^5
10^4
10^3
10^2
0
30
60
90
120
150

Figure 24

$\gamma - \gamma$, background subtracted coincidence spectra of ^{124}Cs for gates shown.

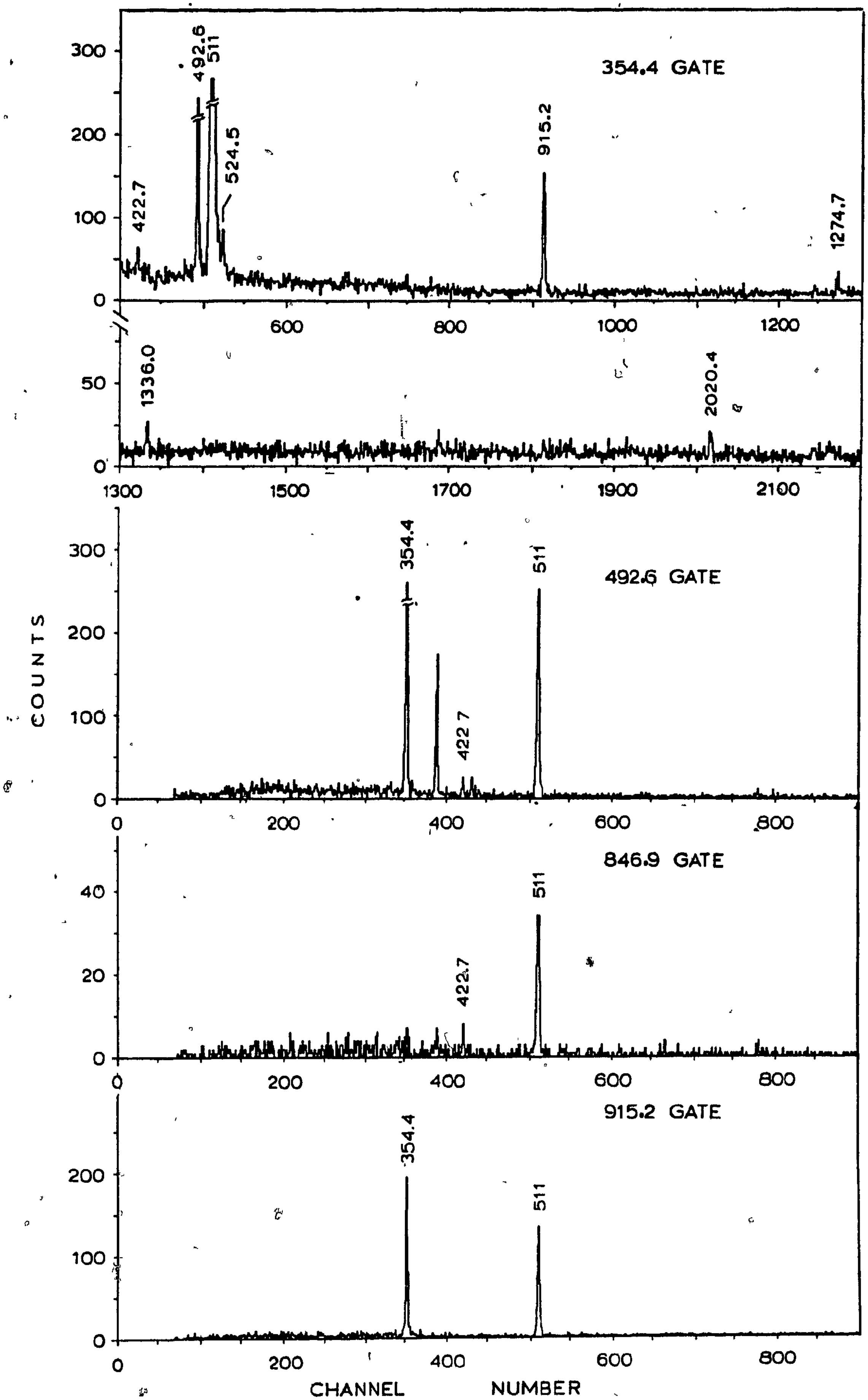
354.4 GATE
492.6
511
524.5
422.7
915.2
1274.7
1336.0
2020.4
492.6 GATE
354.4
511
422 7
846.9 GATE
511
422.7
915.2 GATE
354.4
511
COUNTS
CHANNEL NUMBER

and ^{128}Cs isotopes, respectively (Fig. 26). A correction for both absorption and annihilation-in-flight was then applied (Azuelos et al. 1977). All the gamma rays assigned to the decay of ^{124}Cs on the basis of half-life were placed in the decay scheme. The levels at 354, 846, 878 and 1248 keV were observed earlier in an in-beam study by Kusakari et al. (1975) and were assigned 2_1^+, 2_2^+, 4_1^+ and 3_1^+ spins respectively. In their study, the 846 keV (2_2^+) and (3_1^+) 1248 keV levels were interpreted as members of the quasi-gamma band. The 354 keV level is fed from the ^{124}Cs (1^+) parent by a beta branch of 19.4%, yielding a log ft value of 5.3. This allowed beta transition is therefore consistent with the 2^+ spin assignment. This level and the 878 keV level were confirmed to be the 2_1^+ and 4_1^+ states of the ground state band from our in-beam measurements, as well as the earlier one by Kusakari et al. (1975). The log ft value of 7.1 for the 878 keV level therefore seems low. This could be the result of unobservable gamma transitions feeding that level from higher ones. In the recent study by Charvet et al. (1977) three weak gamma transitions did in fact appear to feed this level; these were not observed in the present work. The β-feeding to the 846 keV level has a log ft of 6.0, suggesting an allowed or first-forbidden transition. The spin assignment $J^\pi = 2^+$ is also consistent with the relative intensities of the deexciting gamma rays of 846.9 and 492.6 keV to the 0^+ ground state and 2_1^+ state. This assignment was also confirmed by our angular correlation results [IV(d)]. The 3^+ spin assignment of the 1248 keV level was made on the basis of the in-beam measurement and from the decay of this level to the 2_1^+ and 2_2^+ states. Although the measured log ft value of 7.1 is low for a 3^+ assignment, this level may also be fed from higher levels through very weak gamma transitions. Since the state at 1269 keV is fed by a beta transition

Figure 25

Decay scheme of ^{124}Cs. Transition intensities shown are per 100 decays of the 354 keV transition.

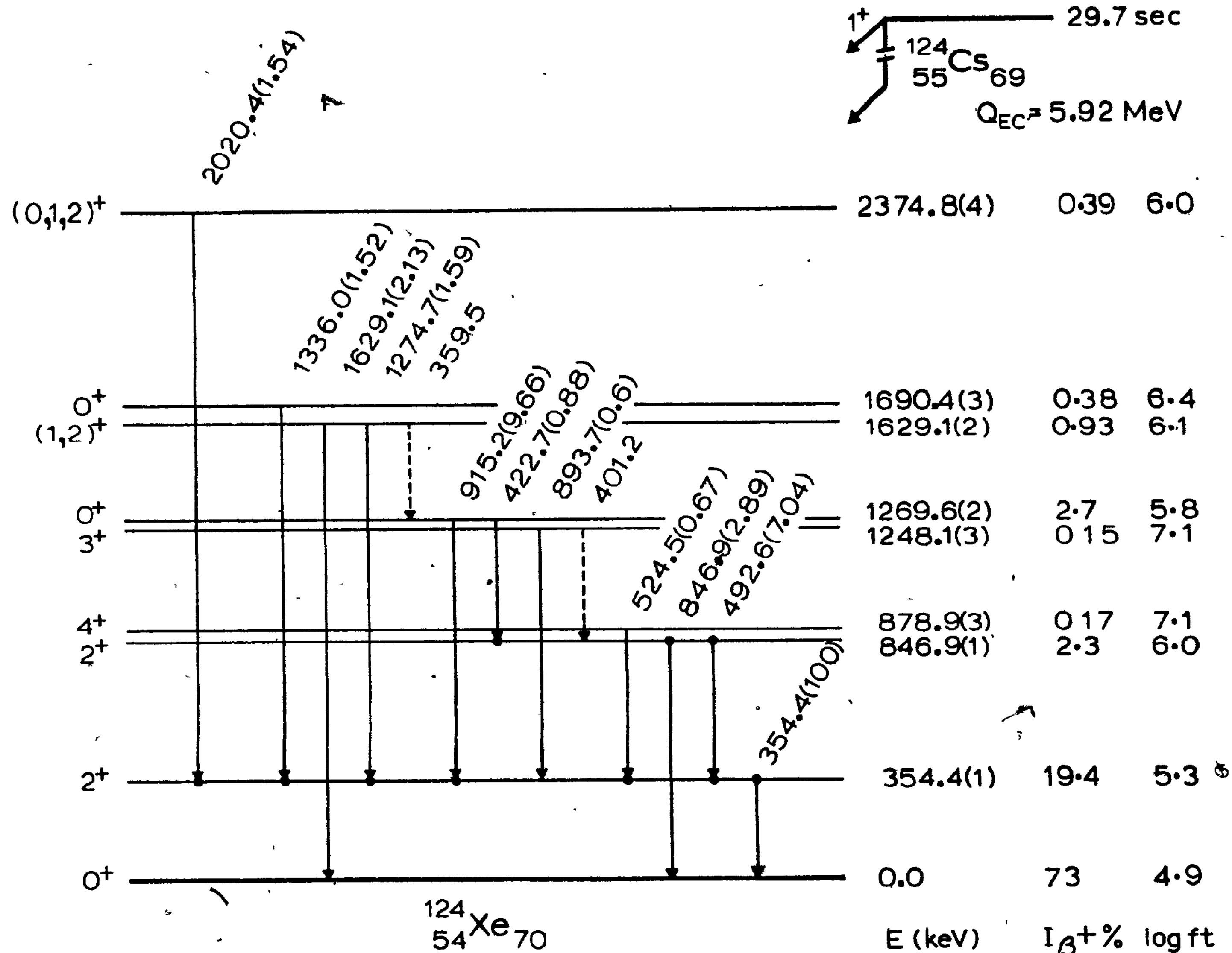

1+
29.7 sec
124 55 Cs 69
QEC = 5.92 MeV
2020.4(1.54)
(0,1,2)+
2374.8(4) 0.39 6.0
1336.0(1.52)
1629.1(2.13)
1274.7(1.59)
359.5
0+
(1,2)+
1690.4(3) 0.38 6.4
1629.1(2) 0.93 6.1
915.2(9.66)
422.7(0.88)
893.7(0.6)
401.2
0+
3+
1269.6(2) 2.7 5.8
1248.1(3) 0 15 7.1
524.5(0.67)
846.9(2.89)
492.6(7.04)
4+
2+
878.9(3) 0 17 7.1
846.9(1) 2.3 6.0
354.4(100)
2+
354.4(1) 19.4 5.3
0+
0.0 73 4.9
124 54 Xe 70
E (keV) Iβ+ % log ft

Figure 26

Time decay of the 511 keV annihilation quantum.

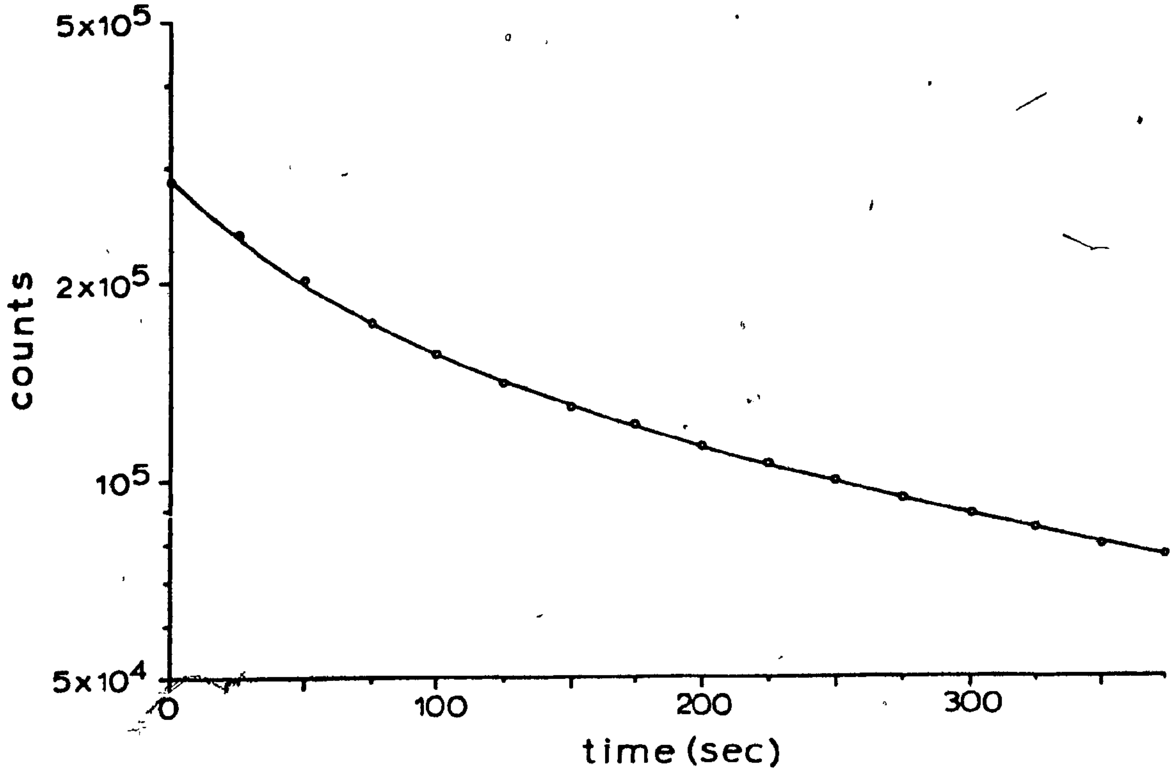
5x10^5
2x10^5
10^5
5x10^4
counts
0
100
200
300
time (sec)

with a log ft of 5.8 from a 1^+ parent, its possible spins are: $(0,1,2)^+$. However the level is strongly connected to 2^+ states with no transition to the 0^+ ground state and was therefore proposed to be the first excited 0^+ state. This assignment was later confirmed on the basis of results of the angular correlation of the 354 - 915 keV transitions. The details of this measurement will be presented in section (d) of this chapter. The level at 1629 keV was assigned $J^\pi = (1,2)^+$ on the basis of its log ft value and the fact that it feeds the 0^+ ground state. The level at 1690.4 KeV has a log ft value of 6.4 and therefore has $(0,1,2)^\pm$ possible spins. However, the 0^+ assignment was confirmed from the angular correlation results of the 354 - 1336 keV cascade [IV(d)]. Hence, the observed 1689.8 keV transition (table 1) could not be depopulating the 1690.4 keV level to the ground state as was later suggested by Droste et al. (1978). Charvet et al. (1977) placed the transition as feeding the (2^+) 846 keV level. In our $\gamma - \gamma$ coincidence measurement we did not observe the 1689.8 keV γ-ray in the 492 keV gate; however it did appear weakly in the 354 keV gate.

b) Decay of ^{123}Cs

i. Previous Work

The decay of ^{123}Cs was first studied in 1966, by D'Auria and Preiss. They produced ^{123}Cs via the decay of its precursor ^{123}Ba, which was obtained through the $^{115}In(^{14}N,6n)$ reaction with a 140 MeV ^{14}N ion beam at the Yale Heavy Ion Accelerator. A 98 keV transition was assigned as the decay of the first excited state. They measured a $T_{1/2} = 5.6 \pm 0.1$ min for the decay of ^{123}Cs, with a positron end-point energy of 2.6 ± 0.4 MeV. This was obtained from a Fermi-Kurie analysis of the beta spectrum, although in that study, branches to the ground state and the 98 KeV level were not clearly separated. The measurements yielded a K-conversion coefficient of the 98 keV transition of 0.8 ± 0.02, and a lifetime of this first excited state $\leq$ 13 nsec. A spin $1/2^+$ for the ground state of ^{123}Xe was assigned in analogy with the ^{125}Xe, ^{127}Xe and ^{129}Xe isotopes, and a spin assignment of $3/2^+$ for the first excited state was made assuming a spin of $1/2^+$ for the ground state of ^{123}Cs in analogy with ^{127}Cs and ^{129}Cs. In 1969, using an on-line mass spectrometer, Chaumont et al. measured the half-life of the ^{123}Cs decay to be 352 ± 3 sec. Later, Kerek et al. (1970) populated levels in ^{123}Xe in the ^{122}Te (α,3n) reaction at a bombarding energy of 43 MeV. They assigned three transitions 83.2, 97.3 and 180.5 keV to ^{123}Xe. Their results indicated that these transitions are composed of a delayed and a weak prompt component. On this basis they reported an isomeric state in ^{123}Xe with a $T_{1/2}$ = 6.3 ± 0.5 μs. No isomeric transition was observed, and hence they concluded that its energy must be so low (<70 keV) that it mostly proceeded via internal conversion. Their proposed decay scheme contained a $3/2^+$ first excited state at 97 keV and a $5/2^+$ excited state at 180 keV. They also proposed a $9/2^-$ isomer (6.3 μs) at an energy <250 keV which decayed to the $5/2^+$ state through an M2 isomeric transition. The $9/2^-$ assignment was made on the basis of systematics, since ^{125}Xe and ^{127}Xe both have $9/2^-$ isomeric state. The half lives of these states, both of which decay by E3 transitions to a $3/2^+$ state, are 60 and 70 sec respectively (Rezanka et al. 1970). These results will be discussed in view of the present work.

An isomer of $T_{1/2}$ = 1.6 ± 0.2 sec in ^{123}Cs was reported by Droste et al. (1972). ^{123}Cs was produced via ^{115}In(^{12}C,4n) and ^{109}Ag(^{18}O,4n) reactions. Two transitions of 63 and 95.3 keV were attributed to the decay of the isomeric level in ^{123}Cs to the ground states.

Mass separated sources of ^{123}Cs were produced at the ISOLDE on-line separator at CERN by Westgaard et al. (1975). They performed $\beta - \gamma$ coincidence experiments and identified seven transitions belonging to the decay of ^{123}Cs. The uncertainty in the gamma ray energies was estimated to be 1 keV, but in fact, some of these energies differed from the present result by 2 - 3 keV. From the β-spectrum in coincidence with the most intense γ-ray they measured a total decay energy of $Q_{EC} = 4.10 \pm 0.31$ MeV, which is in agreement with the result obtained by D'Auria and Preiss (1966). No decay scheme was established.

Ekstrom et al. (1977), using an atomic beam magnetic resonance apparatus connected on-line with the ISOLDE isotope separator, measured the spin of the ground state of ^{123}Cs to be $J = 1/2$.

The present work represents the first detailed study of levels in ^{123}Xe populated in the decay of ^{123}Cs. The results were summarized in a publication (Sofia et al. 1981) which is included in the Appendix. Subsequent to the completion of the present work, a detailed study of the decay of ^{123}Cs was published by Marguier et al. (1981). They produced ^{123}Cs in the La(p,3p 14n) reaction, with 600 MeV bombarding energy, using on-line mass separated sources. They observed the isomeric transitions of 61.7, 64.0, 94.6 keV of ^{123}Cs^{m} decaying to ^{123}Cs^{g} (1.7 sec) and reported no significant direct feeding from the ^{123}Cs^{m} level to states in ^{123}Xe. Their results concerning the isomer in ^{123}Cs are in agreement with those of Droste et al. (1972). Recently Luukko et al., (1981) populated high-spin states of ^{123}Xe in the ^{122}Te (^{3}He, 2n) and ^{123}Te (^{3}He, 3n) reactions with E(^{3}He) = 14 - 27 MeV. Using in-beam γ-ray spectroscopic methods they constructed a level scheme of ^{123}Xe which will be discussed later in connection with the present work.

ii. Gamma Ray Spectroscopy

Levels of ^{123}Xe were populated in the beta decay of ^{123}Cs, which was produced in the $^{124}Xe(p, 2n)$ reaction. The bombarding energy for the optimum production yield for ^{123}Cs was found to be 33 MeV. The γ-ray spectrum of the reaction product was recorded with an x-ray detector [Fig. 27(a)], and Ge(Li) detector. Spectra collected with and without a positron annihilator around the sample are shown in fig. 27b and 27c respectively. This annihilator was a 4.267g/cm^2 copper jacket around the source. The gamma rays associated with the decay of ^{123}Cs are labelled by their energies. The identification of these γ-rays was made on the basis of half-life and threshold production energy. Other gamma rays in the spectrum belong mainly to ^{128}Cs (3.8 min), ^{127}Cs (6.25 hr), ^{125}Cs (45 min) and ^{123}Xe (2 hr) decay. Cooling the activated targets for about half a minute reduced the short-lived activities of ^{124}Cs (30 sec) and ^{126}Cs (98 sec) significantly. The energies and relative intensities of 39 transitions assigned to the decay of ^{123}Cs are given in table 3.

The time decay studies of the gamma rays were carried out using the multispectrum technique explained in [IIIA(ii)]. In these measurements, an x-ray detector as well as a Ge(Li) detector were used, to extract a more precise value for the half lives of low energy transitions, and 30 consecutive groups of 30 seconds were accumulated. An exponential fit to the time decay of the 97.39 keV and the 83.38 keV transitions is shown in Fig. 28. These measurements yielded a half-life of 365 ± 4 sec. To search for a short-lived isomer in ^{123}Cs, we performed a multispectrum experiment by accumulating 10 groups of one second. However no transitions with a half-life of the order of 1 second (as suggested by Droste, (1972)) were observed.

Figure 27

^{123}Cs γ-ray spectrum recorded with:

(a) an x-ray detector.

(b) a Ge(Li) detector with a positron annihilator around the source.

(c) a Ge(Li) detector without the annihilator.

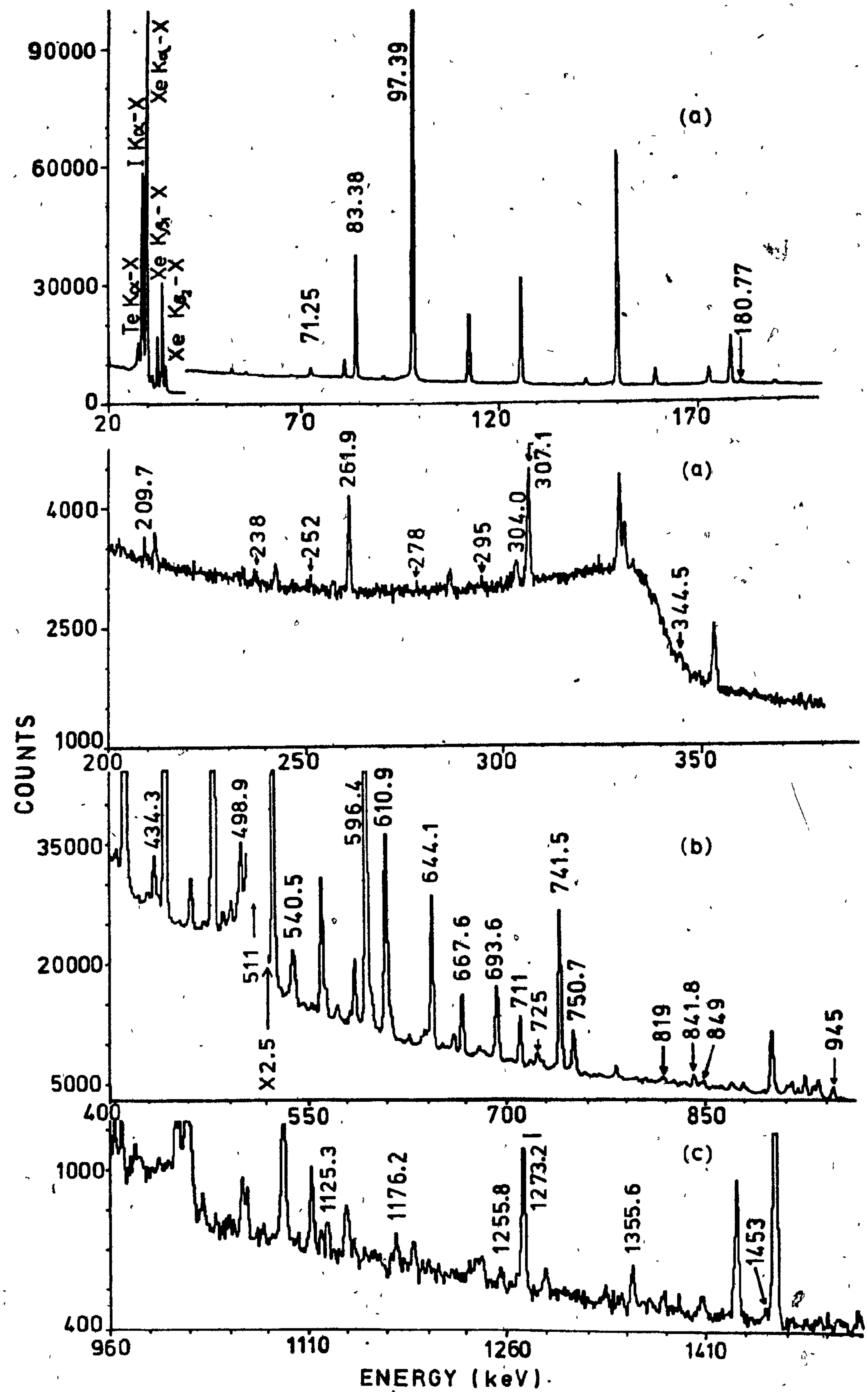

COUNTS
ENERGY (keV)
(a)
Te Kα-X
I Kα-X
Xe Kα-X
Xe Kβ1-X
Xe Kβ2-X
71.25
83.38
97.39
180.77
209.7
238
252
261.9
278
295
304.0
307.1
344.5
(b)
434.3
498.9
511
X2.5
540.5
596.4
610.9
644.1
667.6
693.6
711
725
741.5
750.7
819
841.8
849
945
(c)
1125.3
1176.2
1255.8
1273.2
1355.6
1453

TABLE 3. ^{123}Cs(365 ± 4s) Gamma-Ray Energy and Intensity

E_γ(keV)	I_γ%	E_γ(keV)	I_γ%
71.28 ± .03	1.2 ± .1	596.4 ± .2	57 ± 3
83.38 ± .02	21 ± 1	610.3 ± .2	1.3 ± .4
97.39 ± .03	100	610.9 ± .2	16.7 ± 1.9
180.77 ± .03	3.1 ± .3	644.1 ± .1	15 ± 2
209.7 ± .2	0.7 ± .2	667.6 ± .4	7 ± 1
238.0 ± .5	2.2 ± .6	693.6 ± .4	8 ± 2
252.0 ± .5	2.2 ± .6	711.0 ± .2	4 ± 1
261.9 ± .1	13 ± 1	725.0 ± .5	1.3 ± .3
278.0 ± .5	1.1 ± .4	741.5 ± .1	17 ± 2
294.5 ± .5[a]	1.6 ± .4	750.7 ± .2	4.8 ± .7
304.0 ± .1	5 ± 1	819.0 ± .5	1.2 ± .6
307.1 ± .1	21 ± 1	841.8 ± .2	1.8 ± .5
344.5 ± .5	3.4 ± .9	849.0 ± .5	0.7 ± .4
405.0 ± .5	1.1 ± .2	945.0 ± .3	1.9 ± .5
422.0 ± .5	0.7 ± .3	1125.3 ± .3	3.7 ± .3
430.0 ± .5	0.8 ± .2	1176.2 ± .4	9 ± 4
434.3 ± .2	4.7 ± .7	1255.8 ± .4[a]	1.6 ± .5
498.9 ± .2	6 ± 2	1273.2 ± .2	14 ± 2
511($\gamma^\pm$)	1300 ± 200	1355.6 ± .5	5 ± 2
540.5 ± .5	4 ± 1	1453.0 ± .5	1.1 ± .5

[a]Not placed in the decay scheme

Figure 28

Time decay of ^{123}Cs activity.

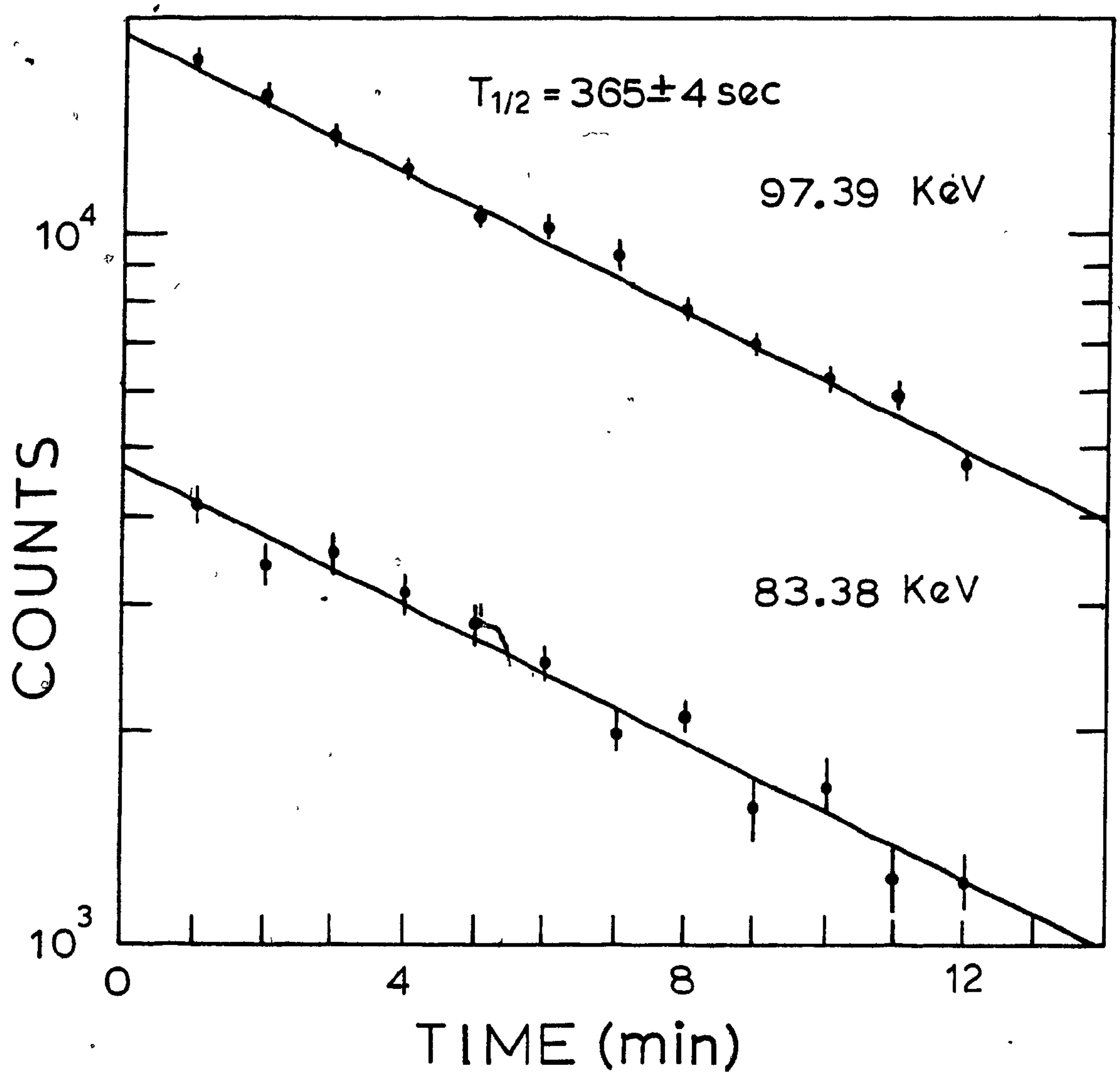

$T_{1/2} = 365 \pm 4$ sec
97.39 KeV
83.38 KeV
COUNTS
10^4
10^3
0
4
8
12
TIME (min)

Gamma-gamma coincidence experiments were performed using either two large volume Ge(Li) detectors or an x-ray detector and a Ge(Li) detector, to observe coincidence relations between low and high energy transitions. Gates were placed on γ-rays as well as on the adjacent Compton background. A sample of coincident γ-ray spectra for a few significant gates is shown in Fig. 29, and the coincidence results are summarized in table 4. Coincidence results require the 610 keV γ-ray peak to be a doublet consisting of 610.3 ± 0.2 and 610.9 keV components, whose relative intensities were deduced to be as given in table 3.

iii. Determination of Internal Conversion Coefficients

The most highly internally converted transitions of interest in the decay of ^{123}Cs, are the 83.38 and the 97.39 keV ones. The indirect $\frac{X}{\gamma}$ ratio method, which was explained earlier [IIIA(V)], was used to determine the value of the K-conversion coefficient for these transitions. The annihilation quantum (511 keV) gate, in the two parameter γ - γ coincidence data, was used to bypass capture x-rays. The resulting x-ray detector spectrum (Fig. 30) shows Xe K_α, $K_{\beta 1}$, and $K_{\beta 2}$ x-rays and the 83 and 97 keV γ-rays. Therefore:

$$I_{83}\ \alpha_K(83) + I_{97}\ \alpha_K(97) = \frac{I_K}{\omega_K}$$

where I_{83}, I_{97} are the intensities of the 83 and the 97 keV γ-rays in the 511 gate

I_K = The intensity of the Xe K x-ray in the same spectrum

ω_K = The K shell fluorescence yield of the Xe atom (≃ 0.889) (Lederer and Shirley 1978).

Figure 29

γ - γ background subtracted coincidence spectra of ^{123}Cs.

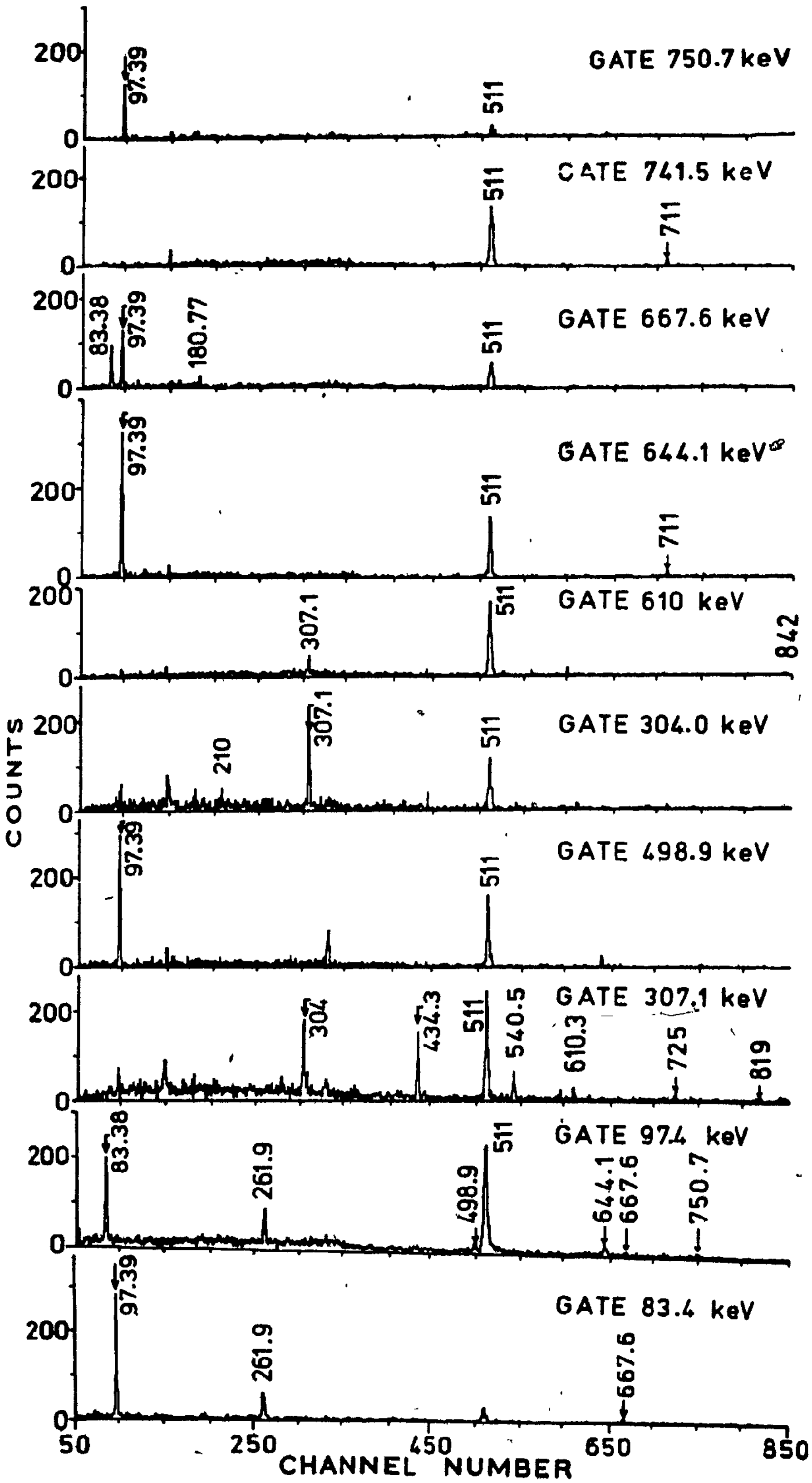
GATE 750.7 keV
97.39
511
GATE 741.5 keV
511
711
GATE 667.6 keV
83.38
97.39
180.77
511
GATE 644.1 keV
97.39
511
711
GATE 610 keV
307.1
511
842
GATE 304.0 keV
210
307.1
511
GATE 498.9 keV
97.39
511
GATE 307.1 keV
304
434.3
511
540.5
610.3
725
819
GATE 97.4 keV
83.38
261.9
498.9
511
644.1
667.6
750.7
GATE 83.4 keV
97.39
261.9
667.6
COUNTS
200
0
50
250
450
650
850
CHANNEL NUMBER

TABLE 4. ^{123}Cs Gamma-Gamma Coincidence Results

Gate E_γ(keV)	Coincident Gamma-Rays, E_γ(keV)
83.38	71.26, 97.39, 261.9, 430.3, 667.6, 945.0
97.39	83.38, 209.7, 261.9, 498.9, 644.1, 667.6, 750.7, 1355.6
261.9	83.38, 97.39, 180.77, 405
304.0	209.7, 307.1
307.1	304, 434.3, 540.5, 610.3, 725, 819
498.9	97.39
610.3) 610.9)	307.1, 841.9
644.1	97.39, 711
667.6	83.38, 97.39, 180.77
741.5	711
750.7	97.39

Figure 30

Low energy γ-spectra in coincidence with:

(a) 511 keV annihilation quanta.

(b) 261.9 keV γ-ray.

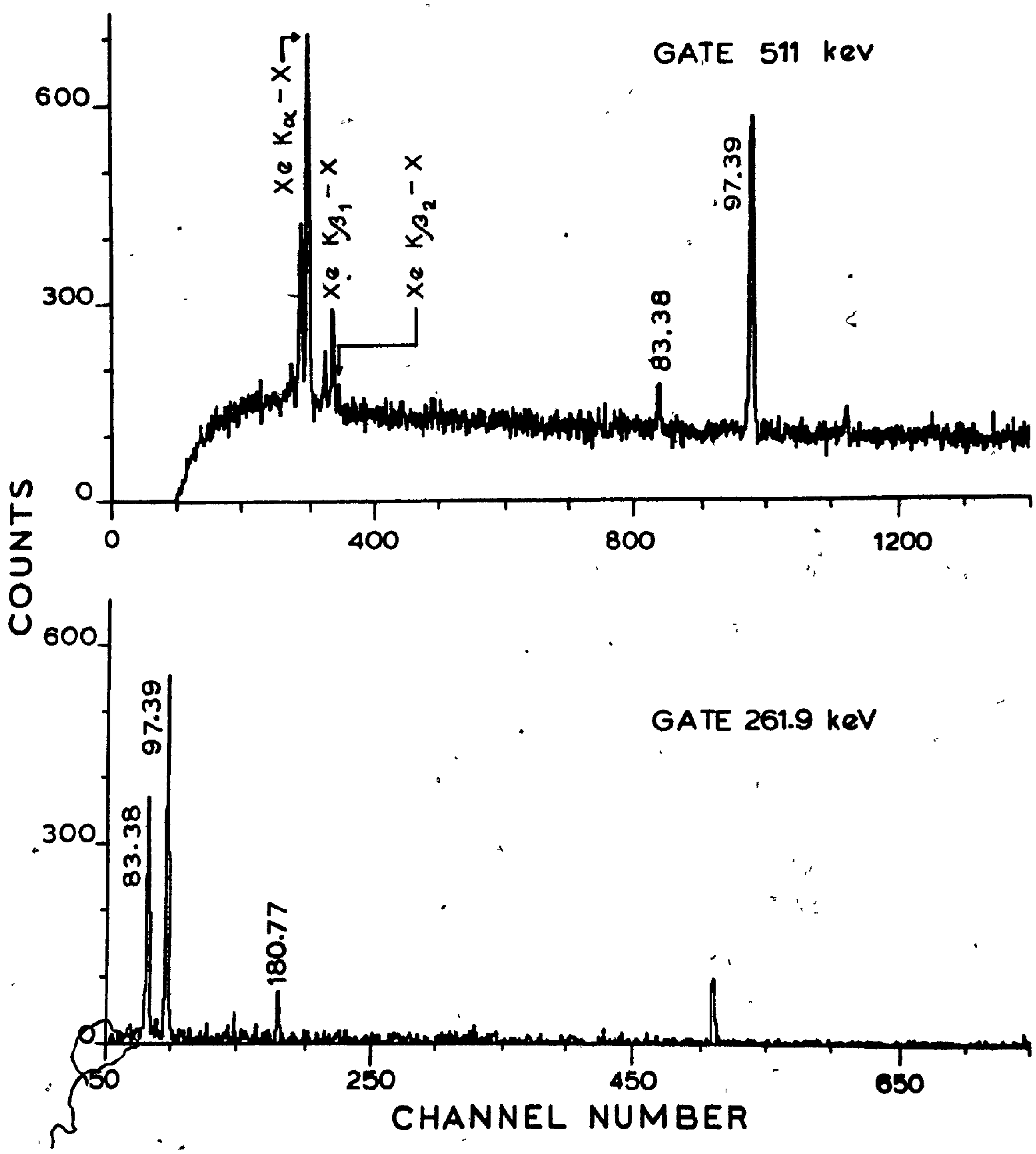

GATE 511 kev
Xe Kα - X
Xe Kβ1 - X
Xe Kβ2 - X
97.39
83.38
600
300
0
400
800
1200
COUNTS
GATE 261.9 keV
97.39
83.38
180.77
600
300
0
150
250
450
650
CHANNEL NUMBER

Therefore:

$$C_1\alpha_K(83) + \alpha_K(97) = \frac{C_2}{\omega_K} \quad \cdots\cdots\cdots \qquad (1)$$

where

$$C_1 = \frac{I_{83}}{I_{97}} = 0.085 \pm 0.005$$

$$C_2 = \frac{I_{\text{[illegible]}}}{I_{97}} = 0.86 \pm 0.02$$

At least one more coincidence relation between the 83 and 97 keV transition is required in order to solve for their α_K's. The 261.9 keV γ gate (Fig. 30) provides this needed relation. In that gate the transition intensity of the 83 and 97 keV transitions should be equal and hence

$$I_{83}\ (1 + \alpha_T(83)) = I_{97}\ (1 + \alpha_T(97))$$

$$I_{83}\ \alpha_K(83)\ \left(\frac{\alpha_T(83)}{\alpha_K(83)}\right) - I_{97}\ \alpha_K(97)\ \left(\frac{\alpha_T(97)}{\alpha_K(97)}\right) = I_{97} - I_{83}$$

From the theoretical values for the internal conversion coefficients (Hager and Seltzer, 1968), it can be shown that if one takes a pure M1 limit (which is very close to what is expected) that the two ratios are equal, even though the α's themselves are different.

$$\frac{\alpha_K(83)}{\alpha_T(83)} = \frac{\alpha_K(97)}{\alpha_T(97)} = R$$

where R is 0.86 in the M1 limit.

$$I_{83}\,\alpha_K(83) - I_{97}\,\alpha_K(97) = R(I_{97} - I_{83})$$

if $C_3 = \dfrac{I_{83}}{I_{97}} = 0.79 \pm 0.03$

then

$$C_3\,\alpha_K(83) - \alpha_K(97) = R(1 - C_3) \tag{2}$$

A contour plot of equations (1) and (2) gives $R = 0.80 \pm 0.01$. Solving the two coincidence relations gives the results: $\alpha_K(83) = 1.3 \pm 0.1$ and $\alpha_K(97) = 0.9 \pm 0.1$. The latter value agrees with the result obtained by D'Auria and Preiss, (1966) within the uncertainty. Comparison of the experimental result with the theoretical α_K's (Hager and Seltzer 1968) of 1.20 (M1) and 2.12 (E2) for the 83.38 keV transition suggests that it has a 90% M1 + 10% E2 multipolarity; a similar comparison for the 97.39 keV transition, where the theoretical α_K's are 0.77 (M1) and 1.32 (E2) suggest 80% M1 + 20% E2 multipolarity.

iv. Beta End-Point Energy Measurement

The decay energy of ^{123}Cs was measured by means of the two parameter $\beta - \gamma$ coincidences described in chapter III. Accumulation of beta and gamma activities started about one and a half minutes after the end of bombardment, in order to reduce the interfering activities of the short-lived isotopes of ^{124,126}Cs (30, 98 sec), and to maintain reasonably low count rates so that pileup and chance coincidences could be minimized. The data analysis was similar to the two parameter gamma-gamma coincidence measurement, using digital gates on the gamma ray peaks as well as on the neighbouring Compton background. The positron spectrum obtained in coincidence with the 596.4 keV γ-ray should contain only one branch, since that level does not seem to be fed through other γ-rays. A Fermi-Kurie plot made of that spectrum after background subtraction (Fig. 31), yields a value of 2.37 ± 0.14 MeV for the end-point energy. From the proposed decay scheme, this end-point energy corresponds to a decay energy of ^{123}Cs of Q_{EC} = 4.0 ± 0.1 MeV. The background subtracted spectrum in coincidence with the 596 keV γ-ray was corrected for the response of the detector which causes distortions of the spectrum due to backscattering, bremsstrahlung, and summing with the annihilation quanta. This correction was carried out using the computer code "BETABRAN" [chapter III A(iv)] and a Q_{EC} of 4.1 ± 0.1 MeV was obtained, which is within the error of the one obtained from the Kurie plot of the unfolded spectrum. This decay energy corresponds to a mass excess of ^{123}Cs of -81.19 ± 0.14 MeV if the mass excess of ^{123}Xe is -85.29 ± 0.1 MeV (Wapstra and Bos 1977). The measured value of the total decay energy is in agreement with the earlier result of Q_{EC} = 4.1 ± 0.3 MeV obtained by Westgaard et al. (1975).

v. Decay Scheme and Discussion

The decay scheme of ^{123}Cs, shown in Fig. 32 was constructed on the basis of sums and differences of gamma ray energies and gamma-gamma coincidence results. The log ft values were calculated using the measured total decay energy of Q_{EC} = 4.0 ± 0.1 MeV and half-life of $T_{1/2}$ = 365 ± 4 sec, and the theoretical electron capture to positron emission ratios (Lederer and Shirley 1978). The transition intensities shown in parentheses are gamma ray intensities per 100 disintegrations of ^{123}Cs. A spin of 1/2 and magnetic moment of μ_I = 1.389 ± 0.016 n.m. was assigned to the ground state of ^{123}Cs by Ekstrom et al. (1977). The ground state of ^{123}Xe has been inferred to be $1/2^+$ since it has an allowed beta decay to a $1/2^+$ level, but no beta

Figure 31

Fermi-Kurie plot of ^{123}Cs positron spectrum in coincidence with the 596.4 keV γ-ray. The solid line is the least-squares fit to data points.

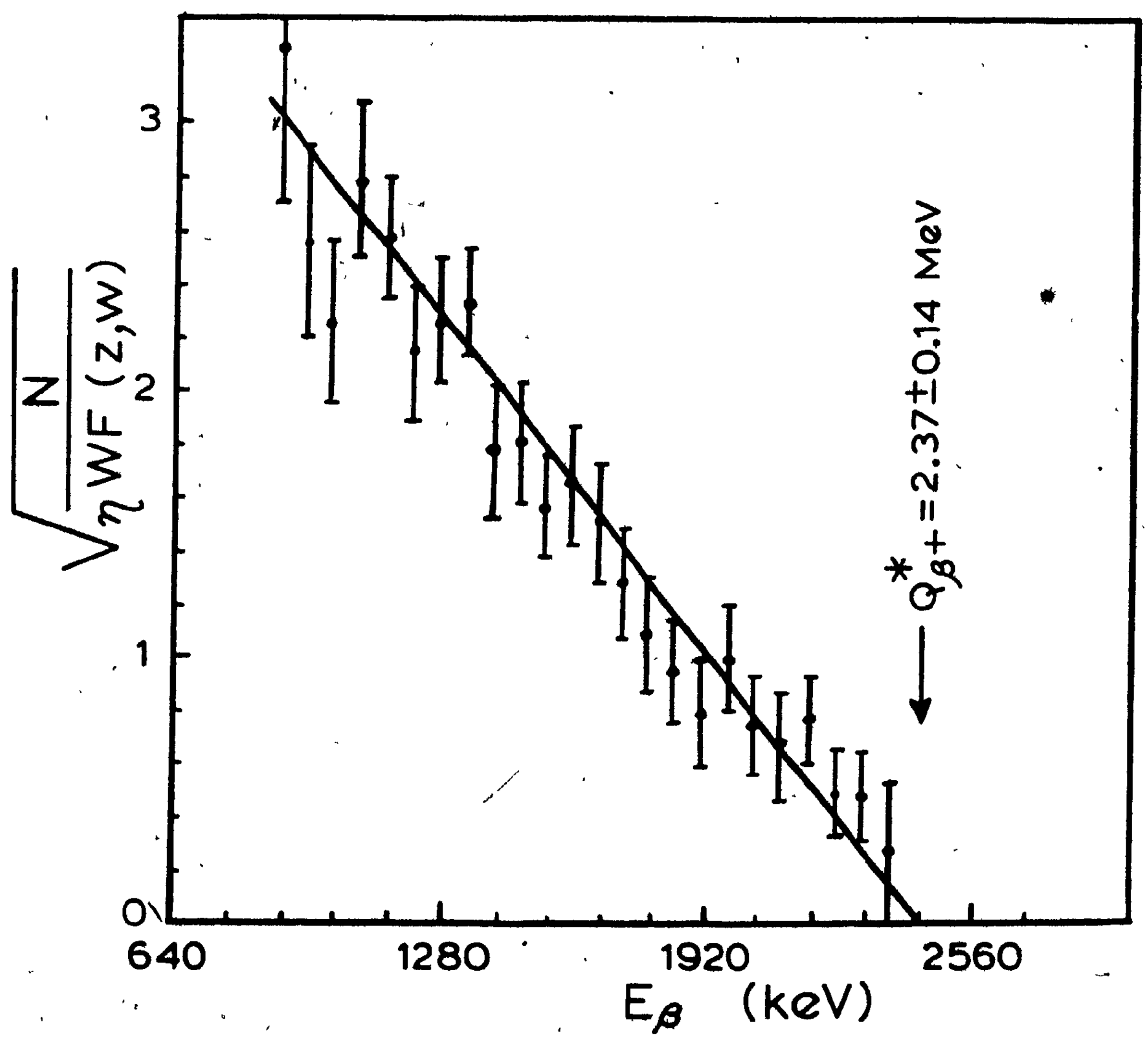

$\sqrt{\frac{N}{\eta WF(z,W)}}$
3
2
1
0
640
1280
1920
2560
E_β (keV)
$Q^*_{\beta^+} = 2.37 \pm 0.14$ MeV

feeding to the $5/2^+$ ground state of ^{123}I (Tamura et al. 1980). The Ge(Li) multispectrum measurement with the positron annihilation jacket in place yielded 6.5 units for total intensity of positrons emitted in the ^{123}Cs decay compared to the intensity of the 97 keV γ-ray (100 units). This was deduced by fitting the decay of the annihilation quantum (511) to a mixture of half-lives representing the different isotopes produced in the reaction (Fig. 33). It was also deduced by accounting for the contribution to the annihilation quantum from isotopes other than ^{123}Cs. These contributions were deduced from the published results of the relative intensities of the annihilation quantum and the prominent γ-ray in the isotope in question. The two procedures agree reasonably well. The positron feeding to the ground state of ^{123}Xe was then calculated by subtracting the amount of positron feeding to the excited states from the total positron intensity of ^{123}Cs decay. The beta feeding to the ground state of ^{123}Xe has a log ft value of 5.2 ± 0.2 which supports the $1/2^+$ assignment (Tamura et al. 1980) of the state. The 97 keV level is fed by an allowed beta transition with a log ft value of 5.8 and is thus assigned a $J = 1/2^+$ or $3/2^+$. The measured K-conversion coefficient of the 97 keV transition of $\alpha_K = 0.9 \pm 0.1$, requiring a multipolarity of 80% MI + 20% E2, supports these spin and parity assignments. The final assignment of $3/2^+$ for this level was made on the basis of systematics of $^{125,127}Cs$ (Jha et al. 1972, Gelletly et al. 1976). The 180 keV level is fed with a log ft value of 6.3 ± 0.1, characteristic of an allowed or first-forbidden beta transition. This level decays to the 97 keV level through the 83 keV transition whose measured α_K requires a 90% MI + 10% E2 multipolarity; it also decays to the $1/2^+$ ground state through the 180 keV transition. The deduced spin of this level is thus

Figure 32

Decay scheme of ^{123}Cs.
Transition intensities shown
are per 100 decays of the parent.

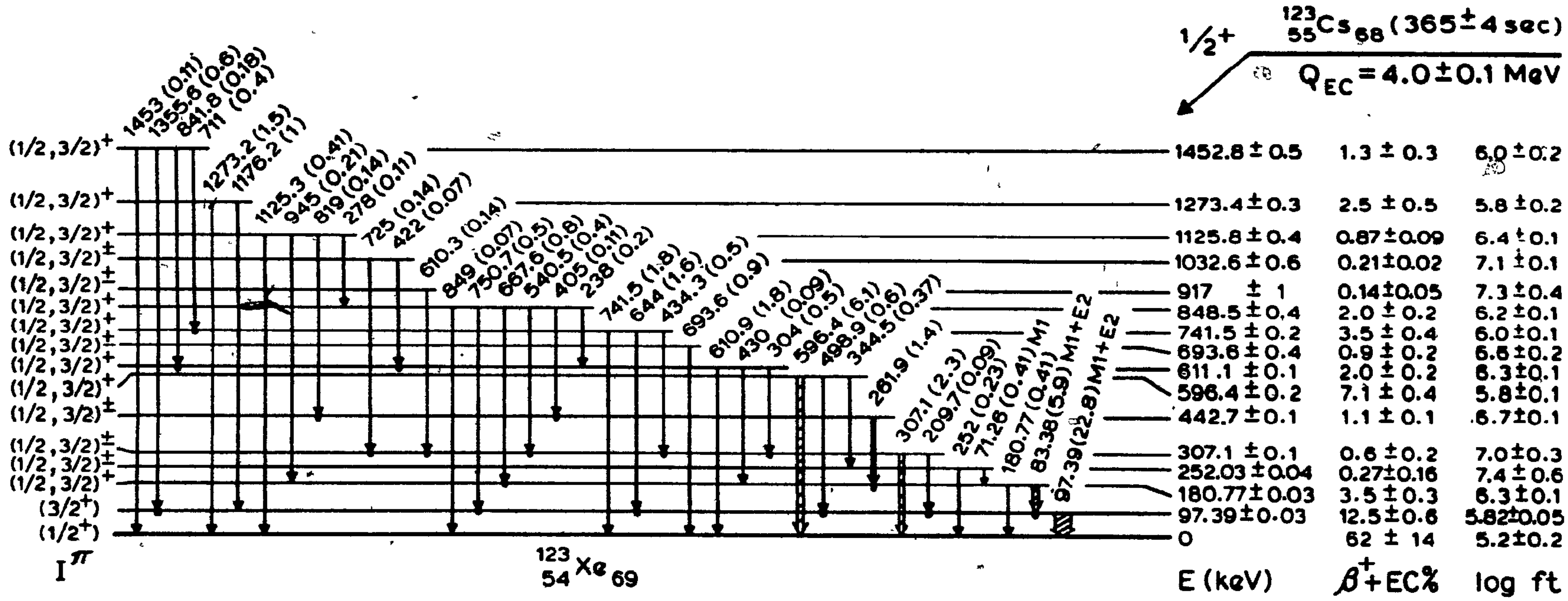

1/2+
$^{123}_{55}Cs_{68}$ (365±4 sec)
Q_{EC}=4.0±0.1 MeV
1453 (0.11)
1355.6 (0.6)
841.8 (0.18)
711 (0.4)
1273.2 (1.5)
1176.2 (1)
1125.3 (0.41)
945 (0.21)
819 (0.14)
278 (0.11)
725 (0.14)
422 (0.07)
610.3 (0.14)
849 (0.07)
750.7 (0.5)
667.6 (0.8)
540.5 (0.4)
405 (0.11)
238 (0.2)
741.5 (1.8)
644 (1.6)
434.3 (0.5)
693.6 (0.9)
610.9 (1.8)
430 (0.09)
304 (0.5)
596.4 (6.1)
498.9 (0.6)
344.5 (0.37)
261.9 (1.4)
307.1 (2.3)
209.7 (0.09)
252 (0.23)
71.26 (0.41) M1
180.77 (0.41)
83.38 (5.9) M1+E2
97.39 (22.8) M1+E2
(1/2,3/2)+
(1/2,3/2)+
(1/2,3/2)+
(1/2,3/2)±
(1/2,3/2)±
(1/2,3/2)+
(1/2,3/2)+
(1/2,3/2)±
(1/2,3/2)+
(1/2,3/2)+
(1/2,3/2)±
(1/2,3/2)±
(1/2,3/2)±
(1/2,3/2)+
(3/2+)
(1/2+)
I^{π}
$^{123}_{54}Xe_{69}$
1452.8 ± 0.5 | 1.3 ± 0.3 | 6.0 ± 0.2
1273.4 ± 0.3 | 2.5 ± 0.5 | 5.8 ± 0.2
1125.8 ± 0.4 | 0.87 ± 0.09 | 6.4 ± 0.1
1032.6 ± 0.6 | 0.21 ± 0.02 | 7.1 ± 0.1
917 ± 1 | 0.14 ± 0.05 | 7.3 ± 0.4
848.5 ± 0.4 | 2.0 ± 0.2 | 6.2 ± 0.1
741.5 ± 0.2 | 3.5 ± 0.4 | 6.0 ± 0.1
693.6 ± 0.4 | 0.9 ± 0.2 | 6.6 ± 0.2
611.1 ± 0.1 | 2.0 ± 0.2 | 6.3 ± 0.1
596.4 ± 0.2 | 7.1 ± 0.4 | 5.8 ± 0.1
442.7 ± 0.1 | 1.1 ± 0.1 | 6.7 ± 0.1
307.1 ± 0.1 | 0.6 ± 0.2 | 7.0 ± 0.3
252.03 ± 0.04 | 0.27 ± 0.16 | 7.4 ± 0.6
180.77 ± 0.03 | 3.5 ± 0.3 | 6.3 ± 0.1
97.39 ± 0.03 | 12.5 ± 0.6 | 5.82 ± 0.05
0 | 62 ± 14 | 5.2 ± 0.2
E (keV) | β⁺+EC% | log ft

$J^{\pi} = 1/2^{+}$ or $3/2^{+}$. As mentioned previously this level had been assigned a $J^{\pi} = 5/2^{+}$ by Kerek et al. (1970), who assumed that it was fed from an (unobserved) $9/2^{-}$ isomer. The 252 keV level has since been considered to be that $9/2^{-}$ isomeric state [Lederer and Shirley 1978, Tamura et al. 1980]. However the present experiment indicates that this J^{π} assignment cannot be correct. The state is fed by a beta transition from the $1/2^{+}$ parent with a log ft of 7.4 ± 0.6. This corresponds with an allowed or first-forbidden transition. Furthermore it decays through the 252 keV gamma ray to the $1/2^{+}$ ground state of ^{123}Xe which likewise forbids a $9/2^{-}$ assignment to that level. The previous observations suggest a spin and parity assignment of $J^{\pi} = 1/2^{+}$ or $3/2^{+}$ for the 252 keV level. Since the states of 596, 741, 1273 and 1452 keV are all fed by an allowed beta transition they were assigned spins and parities of $1/2^{+}$ or $3/2^{+}$. The other levels are fed by an allowed or first-forbidden transition and thus their J^{π} assignments are $1/2^{\pm}$ or $3/2^{\pm}$. In some cases positive parities only were assigned on the basis of deexciting γ-rays. The measured value of the total decay energy corresponds to a mass excess of ^{123}Cs of −81.29 ± 0.14 MeV agreeing well with the previously reported value of −81.19 ± 0.3 MeV (Wapstra and Bos 1977).

The recent in-beam study carried out by Luukko et al. (1981) is in agreement with our conclusion that the isomeric assignment $9/2^{-}$ for the 252 keV level was an error. This conclusion was also reached in the recent ^{123}Cs decay study by Marguier et al. (1981). However the in-beam study assigns a $7/2^{+}$ spin for the 252 keV level based on the fact that a $\Delta J = 1$ band was observed, similar to the $g_{7/2}$ one observed in ^{125}Xe (Helppi et al. 1979). Consequently a spin $5/2^{+}$ was assigned for the 180 keV level. Both of these assignments are implausible. The log ft value of 7.4 ± 0.6 for the

Figure 33

Time decay of the 511 keV
annihilation quantum.

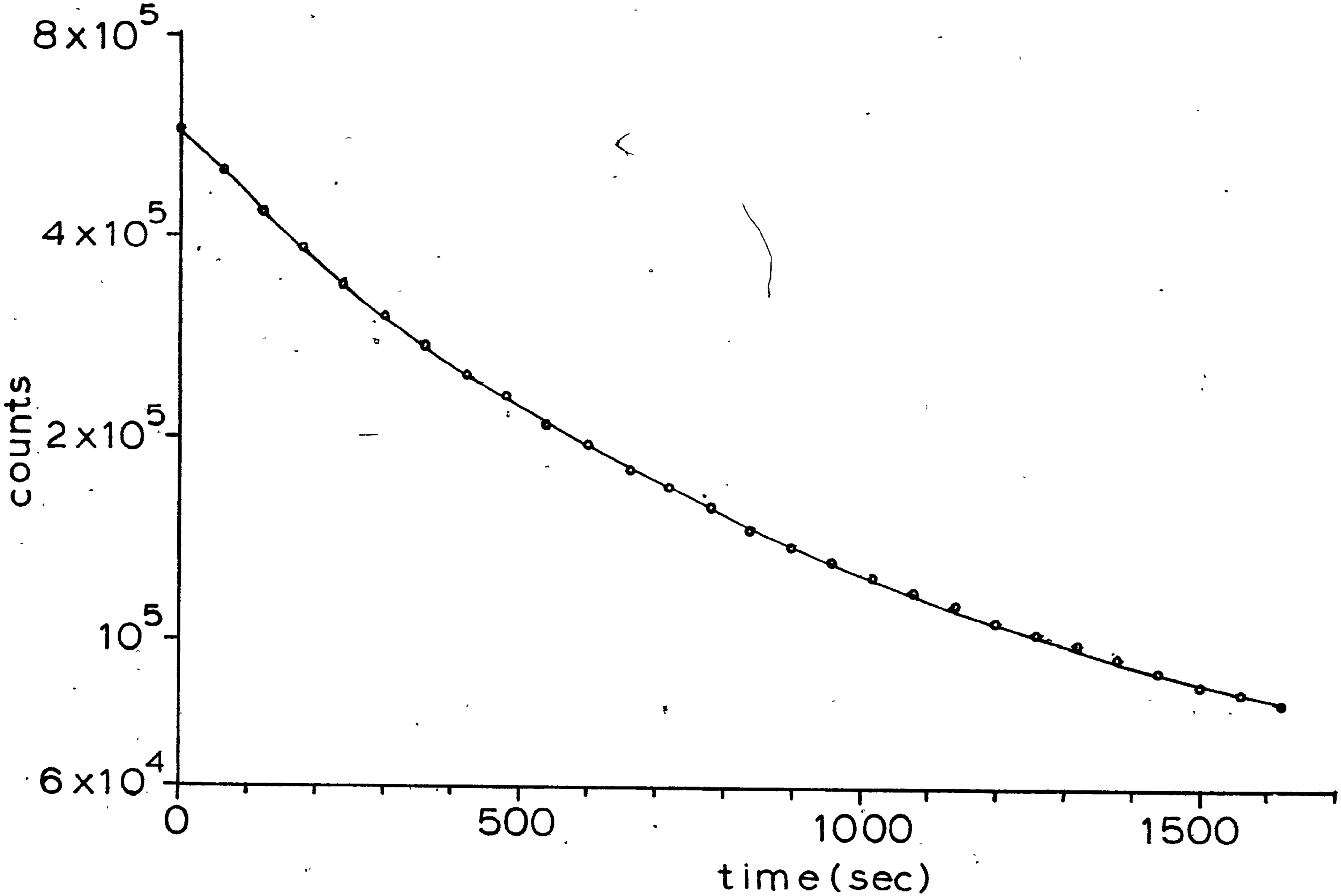
8×10^5
4×10^5
2×10^5
10^5
6×10^4
counts
0
500
1000
1500
time (sec)

252 keV level is not possible for a second-forbidden transition; also the assignment of a spin $5/2^+$ for the 180 keV level is very unlikely since its log ft value is 6.3 ± 0.1. Since the spins of the other levels in the same work were based on the $5/2^+$ and $7/2^+$ assignments of the 180 and 252 keV levels, they are probably in error by one to three spin units. The recent decay study of ^{123}Cs (Marguier et al. 1981) is in agreement with most of the results of the present work. Their tentative decay scheme is very similar to ours, except that they propose levels at 437 and 585 keV which are not included in our decay scheme. Also the levels that we proposed at 917, 1125 and 1273 keV are not seen by them. The only level that may be in doubt is the 917 keV level since only one gamma ray has been observed to deexcite it. In the case of the other two levels, at least two gamma rays have been observed. Their spin assignments of $3/2^+$ for the 97 keV, $(1/2^+)$ or $(3/2^+)$ for the 180 keV level, and $(1/2)^{\pm}$ or $(3/2)^{\pm}$ for the rest of the levels are in agreement with the results of the present work.

c) Decay of $^{121}Cs^{m,g}$

i. Previous Work

In 1966 D'Auria and Preiss reported that cesium samples from the 120 MeV carbon bombardment of ^{113}In targets emitted gamma rays of energies 154, 180 and 195 keV which decayed with 2 - 3 min half-life. They suggested that these gamma rays must belong to the decay of a cesium isotope with mass less than 123 and greater than 118. Their conclusion was based on Q-value calculations. Later Chaumont et al. (1969), using an on-line mass separator measured the half-life of the decay of the beta activity of ^{121}Cs to be 125.6 ± 1.4 sec. Using the ISOLDE on-line isotope separator facility at

CERN, Westgaard et al. (1975) identified further gamma rays belonging to the ^{121}Cs decay; this study confirmed three transitions suggested earlier by D'Auria and Preiss (1966). Their Fermi-Kurie analysis on the beta spectra in coincidence with the most intense γ-rays gave a lower limit on the total decay energy of $Q_{EC} \geq 5.65 \pm 0.49$ MeV. No gamma-gamma coincidence experiments were performed and consequently no decay scheme was proposed.

A hyperfine structure measurement using an atomic beam magnetic resonance apparatus was carried out by Ekstrom et al. (1977). They observed two isomers of ^{121}Cs of similar half-lives having nuclear spins J = 3/2 and J = 9/2.

Recently Chowdhury et al. (1981) studied high-spin states of ^{121}Xe that were populated in the (^{14}N, p2n) reaction on ^{110}Cd. A detailed in-beam study of ^{121}Xe was also carried out by Barci et al. (1981), in which ^{121}Xe levels were populated in the $^{112}Cd(^{12}C, 3n)$ reaction. The connection between the results of both in-beam studies and the present work will be discussed.

The present study establishes the first decay schemes of $^{121}Cs^{g}$ and $^{121}Cs^{m}$. The results have been summarized in a publication (Sofia et al. 1981), a reprint of which is given in the Appendix.

ii. <u>Gamma Ray Spectroscopy</u>

Radioactive sources of ^{121}Cs were produced via the ^{124}Xe (p, 4n) reaction at 52 MeV. Energies and relative intensities of γ-rays were determined from γ-ray spectra obtained using the x-ray detector [Fig. 34(a)] and a large volume Ge detector [Fig. 34(b)]. Gamma ray multispectrum data

Figure 34

^{121}Cs γ-ray spectrum recorded with:

(a) x-ray detector.

(b) Ge(Li) detector.

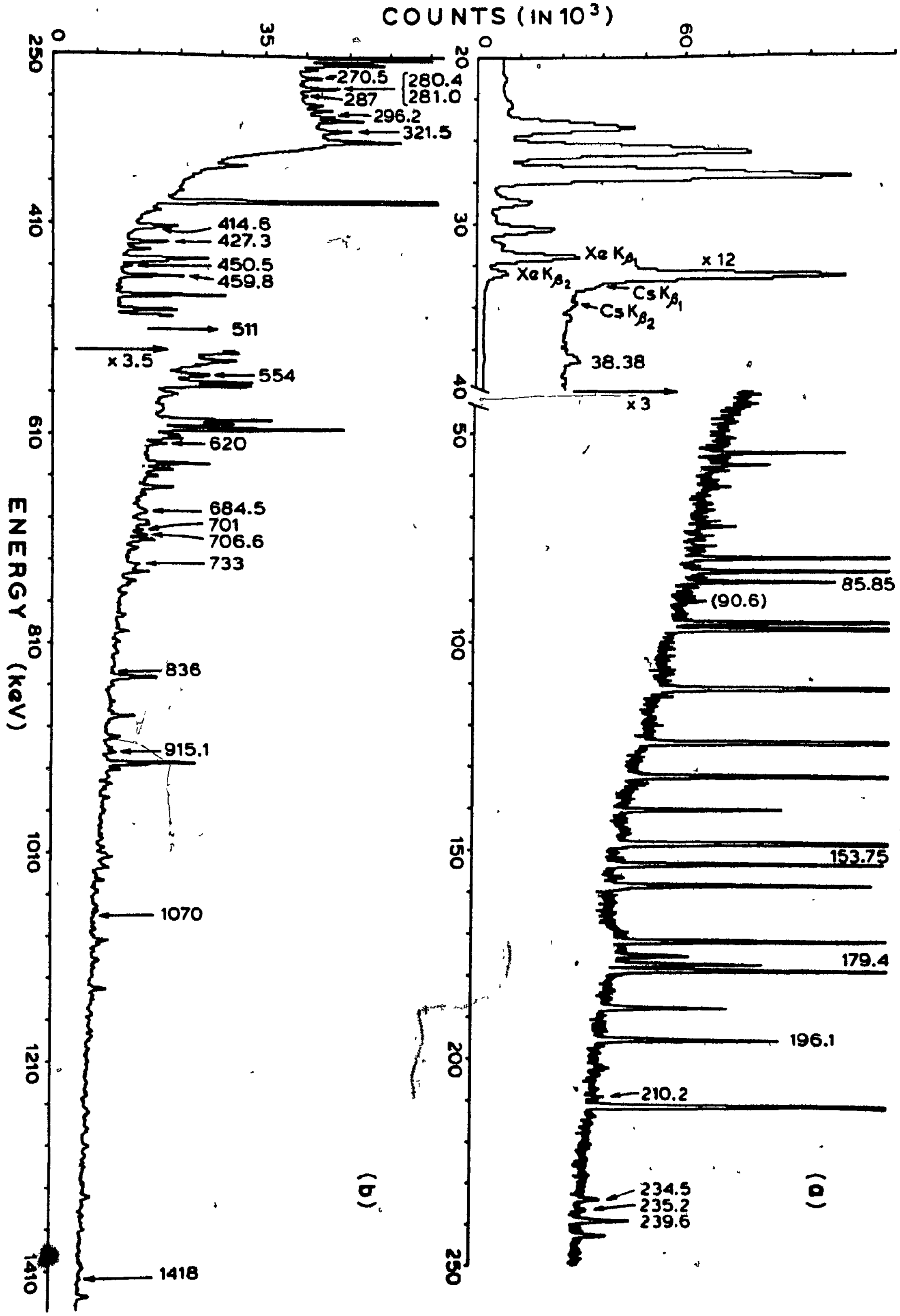
COUNTS (IN 10^3)
ENERGY (keV)
(a)
(b)
Xe K_{β_1}
Xe K_{β_2}
Cs K_{β_1}
Cs K_{β_2}
x 12
x 3
x 3.5
38.38
85.85
(90.6)
153.75
179.4
196.1
210.2
234.5
235.2
239.6
270.5
280.4
281.0
287
296.2
321.5
414.6
427.3
450.5
459.8
511
554
620
684.5
701
706.6
733
836
915.1
1070
1418

obtained with the x-ray detector and with the 15% Ge detector were collected using 10 groups of 30 sec. The results of these measurements suggested the existence of two distinct groups of γ-rays from the ^{121}Cs decay. The group of γ-rays of energies 179.4, 196.1 and 234.5 keV have a 121 ± 3 sec half life (Fig. 35); this group has been reported to belong to the high-spin-band structure of positive ($g_{7/2}$) and negative ($h_{11/2}$) parities of ^{121}Xe by Chowdhury et al. (1981) and Barci et al. (1981). A second group of γ-rays of energies 85.85, 153.75 and 239.6 keV with 136 ± 3 sec half-life (Fig. 35) was also observed, which is associated with a $d_{3/2}$ band structure (Barci et al. 1981). The first group of γ-rays is due to $^{121}Cs^m(9/2^+)$ decay, and the second one is due to $^{121}Cs^g(3/2^+)$ decay. The previous half-life measurement by Chaumont et al. (1969) reported a $T_{1/2}$ = 125.6 ± 1.4 sec for ^{121}Cs without $^{121}Cs^m$ and $^{121}Cs^g$ distinction. The observation of two isomers of ^{121}Cs of almost similar half-lives is in agreement with the findings of the spin measurements carried out by Ekstrom et al. (1977). There are more than 25 other γ-rays with about 2 min half-life identified from multispectrum analysis as belonging to ^{121}Cs decay [Fig. 34(a,b)]. These gamma rays were assigned to either the decay of $^{121}Cs^m(9/2^+)$ or the decay of $^{121}Cs^g(3/2^+)$ on the basis of half-life, coincidence results, and the Ritz combination principle. The energies and intensities of gamma rays belonging to the two separate decay modes are given in tables 5, 6. There are a few other low intensity γ-rays, such as the 90.6 keV γ-ray in Fig. 34(a), which have a half-life of about 2 min, but which could not be definitely placed in either of the decay modes. The unidentified gamma rays in Fig. 34 belong to $^{123-128}Cs$, $^{121,123,125,127}Xe$ and $^{121,123}I$, which are produced in the reaction along with ^{121}Cs. Radioactive sources were cooled for about half a minute

Figure 35

Time decay of two distinct groups of γ-rays of ^{121}Cs with 121 ± 3 and 136 ± 3 sec half-life.

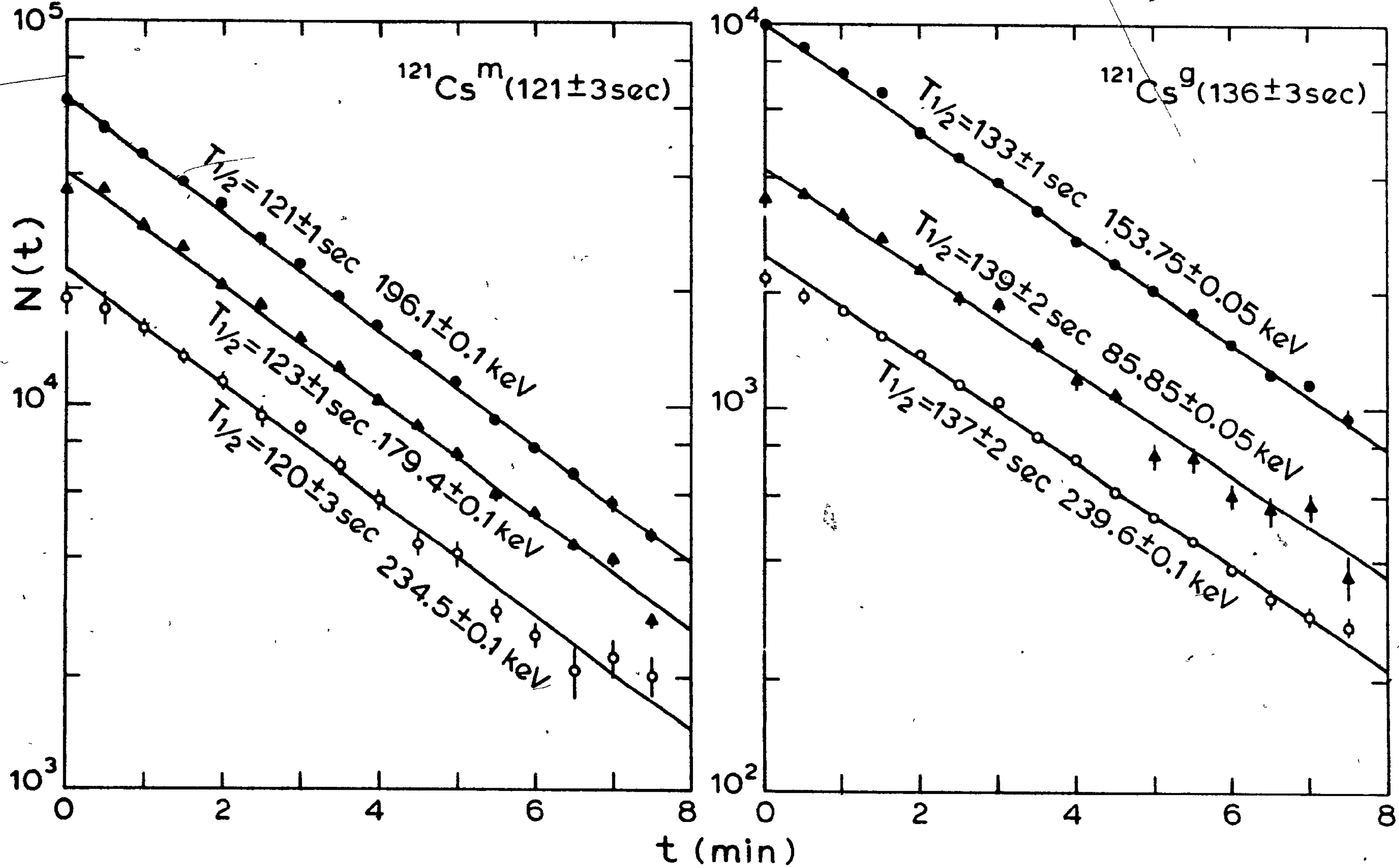

$^{121}Cs^{m}$ (121±3sec)
$T_{1/2}$=121±1sec 196.1±0.1 keV
$T_{1/2}$=123±1sec 179.4±0.1 keV
$T_{1/2}$=120±3sec 234.5±0.1 keV
$^{121}Cs^{g}$ (136±3sec)
$T_{1/2}$=133±1sec 153.75±0.05 keV
$T_{1/2}$=139±2sec 85.85±0.05 keV
$T_{1/2}$=137±2sec 239.6±0.1 keV
N(t)
t (min)

TABLE 5. $^{121}Cs^{m}$(121 ± 3s) Gamma-Ray Energy and Intensity

E_{γ}(keV)	I_{γ}%	E_{γ}(keV)	I_{γ}%
38.38 ± .02	3.8 ± .5	414.6 ± .2	19 ± 5
159.8 ± .3	4 ± 1	427.3 ± .1	39 ± 4
179.4 ± .1	96 ± 5	459.8 ± .1	51 ± 3
196.1 ± .1	100	554.0 ± .2	8 ± 1
234.5 ± .1	20 ± 1	684.5 ± .3	1.9 ± .5
235.2 ± .1	6 ± 1	701.0 ± .5	1.5 ± .5
280.4 ± .5	16 ± 1	706.6 ± .3	3 ± 1
281.0 ± .5	6 ± 1	733 ± 1	2 ± 1
287 ± 1	2 ± 1	1418 ± 1	1.0 ± .5

TABLE 6. $^{121}Cs^{g}$(136 ± 3s) Gamma-Ray Energy and Intensity

E_γ(keV)	I_γ%	E_γ(keV)	I_γ%
38.38 ± .02	0.009 ± .005	296.2 ± .1	10.6 ± .5
85.85 ± .05	11.4 ± .6	321.5 ± .1	10 ± 1
153.7 ± .05	73 ± 2	450.5 ± 5	9 ± 1
179.4 ± .1	10.3 ± .3	563 ± 1	13 ± 2
196.1 ± .1	0.33 ± .16	620.0 ± .5	3 ± 1
210.2 ± .5	10 ± 2	836 ± 1	0.4 ± .2
234.5 ± .1	0.07 ± .04	915.1 ± .2	1.8 ± .8
239.6 ± .1	50 ± 1	1070 ± 1	0.7 ± .4
270.5 ± .5	11.3 ± .3		

in order to reduce activities of ^{124}Cs(30 sec) and ^{126}Cs(98 sec). The production of these undesired isotopes resulted in a very complicated singles spectrum. The identification of γ-rays was done using half-lives, coincidence results and relative intensities of known transitions from published studies of these isotopes.

The existence of a γ decay branch for $^{121}Cs^m$ is confirmed by the observation of Cs $K_{\beta 1}$ and Cs $K_{\beta 2}$ x-rays, of about 2 min half-life [Fig. 34(a)]. The Cs K_β x-ray intensity is 3.0 ± 0.5 times that of the 38.38 keV γ-ray. Based on the Weisskopf estimate, the photon transition probability for an M3 transition is equal to:

$$\lambda = 1.1 \times 10^{1} \quad A^{4/3} E_\gamma^7$$

(Wapstra et al. 1959, Blatt & Weisskopf 1952). The transition probability is defined as:

$$\lambda = \frac{\ln 2}{\tau_{1/2}(1 + \alpha)}$$

(Meszkowski et al. 1965), where the factor (1 + α) accounts for the effect of internal conversion in speeding up transitions. Therefore, an M3 isomeric transition with a half-life of 2 min would be expected to have an energy of about 36 keV and a total internal conversion coefficient of $\alpha_T \simeq 11100$ (Hager and Seltzer 1968). The isomeric γ-ray intensity of 0.0065, relative to the Cs $K_{\beta 1}$ x-ray [Fig. 34(a)] would thus be below the limits of observation.

A two parameter γ - γ coincidence experiment was performed using the 15% Ge and the 18% Ge(Li) detectors. In another γ - γ coincidence experiment, the x-ray detector and the 18% Ge(Li) detector were used. The results of these measurements were obtained by setting digital gates on either the x-ray detector or the large volume detector and are presented in table 7 and Fig. 36. The 38.38 keV and the 196.1 keV were observed in coincidence, and the most intense γ-rays of energies 153.75, 179.4 and 196.1 keV were not observed in coincidence in any pairwise combination.

A γ - γ in-beam coincidence experiment was carried out, to ensure that the 38 keV transition does appear in high-spin band structure, and to determine its internal conversion coefficient. This will be discussed in detail in section (iii). In this experiment, we populated high spin states of ^{121}Xe in the ^{122}Te (5nγ) reaction. The 38 keV transition as well as the 196 keV line were observed. However we did not observe the 69 keV γ-ray (Fig. 37) reported in the ^{121}Xe, in-beam studies of Chowdhury et al. (1981) and Barci et al. (1981). From our data we conclude that if the 69 keV γ-ray does exist it would be very weak, having less than 3% of the intensity of the 38 keV γ-ray.

iii. Determination of Internal Conversion Coefficients

In order to construct a decay scheme for ^{121}Cs, the internal conversion coefficient of the highly converted 38.38 keV transition had to be determined. The spectrum obtained in coincidence with the 196.1 keV γ-ray (Fig. 36) contains the Xe K x-rays and the 38.38 keV γ-ray. This gives, through the X/γ ratio method [IIIA(v)], only an upper limit of α_K<27, because Xe K x-rays arise due to both K conversion and K capture processes. The spectrum in coincidence with the annihilation quantum (511 keV) could not be used to bypass capture x-rays because of the very low intensity of the 38 keV γ-ray. For this reason, and to establish the fact that the 38 keV transition belongs

TABLE 7. $^{121}Cs^{m,g}$ Gamma-Gamma Coincidence Results

GATE E_γ(keV)	Coincident Gamma Rays, E_γ(keV)
38.38	196.1
85.85	153.75, 210.2, 321.5
153.75	85.85, 296, 915
179.4	235.2, 270.5, 280.4, 554
196.1	38.38, 159.9, 281
235.2	179.4
239.6	210.2, 321.5
270.5	179.4
280.4) 281)	179.4, 196.1, 427.3
321.5	85.85
554.0	179.4

Figure 36

$\gamma - \gamma$ background subtracted coincidence spectra of ^{121}Cs.

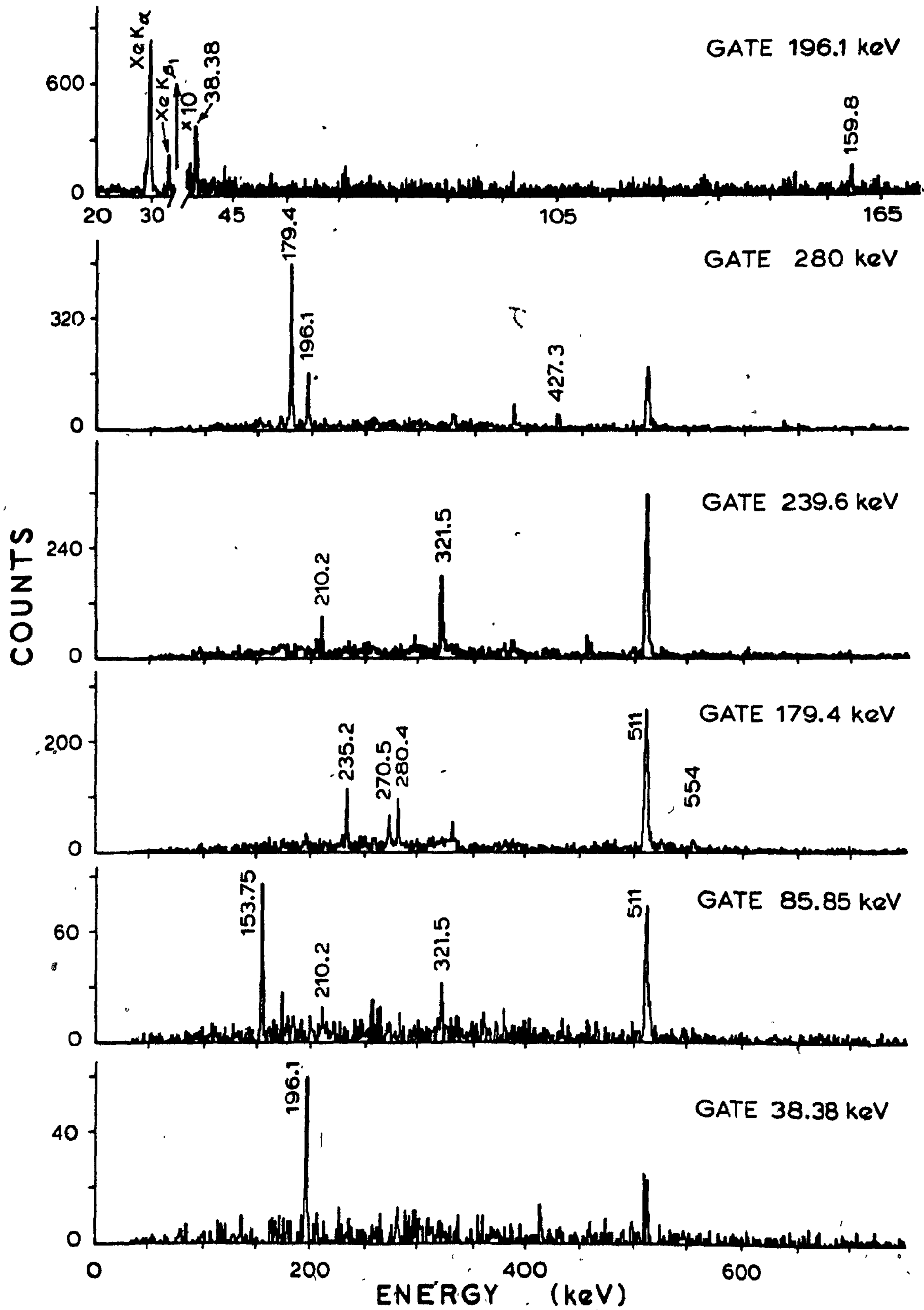

GATE 196.1 keV
Xe Kα
Xe Kβ1
x10
38.38
159.8
600
0
20
30
45
105
165
GATE 280 keV
179.4
196.1
427.3
320
0
GATE 239.6 keV
210.2
321.5
240
0
COUNTS
GATE 179.4 keV
235.2
270.5
280.4
511
554
200
0
GATE 85.85 keV
153.75
210.2
321.5
511
60
0
GATE 38.38 keV
196.1
40
0
0
200
400
600
ENERGY (keV)

to the high-spin band, an auxiliary in-beam two parameter $\gamma - \gamma$ coincidence experiment was performed. In this experiment, ^{121}Xe high-spin levels were populated in the $(\alpha,5n\gamma)$ reaction on isotopically enriched (96.45%) ^{122}Te targets. An x-ray detector and a 16% Ge detector were used. The in-beam excitation does not generate any xenon capture x-rays. The Xe $K_{\beta1}$ and $K_{\beta2}$ x-rays are well resolved in the gating spectrum recorded with the x-ray detector (Fig. 37). These are mainly due to the dominant internal conversion of the 38 keV transition. From the relative intensity of the Xe K_β x-ray and the 38 keV γ-ray, the K conversion coefficient $\alpha_K = 11 \pm 1$ is deduced for this 38 keV transition, using the fluorescence yield (Lederer and Shirley 1978) for the K shell of xenon, $\omega_K = 0.889$, and the K_β x-ray to total K x-ray intensity ratio of 0.155 (Lederer and Shirley 1978). Theoretical α_K values (Hager and Seltzer 1968) for various multipolarities of a 38 keV transition in ^{121}Xe are 2.44(E1), 11.51(M1), 10.4(E2), 263(M2), 18.2(E3) and 1230(M3). From the comparison of the experimental and theoretical α_K's, the 38 keV transition is inferred to be 40% M1 + 60% E2.

iv. <u>Beta End-Point Energy Measurements</u>

The decay energy of ^{121}Cs was measured from the γ-ray multispectra which were obtained with a large volume Ge detector. A positron spectrum following a half-life of 2 min was observed in the 1 to 4 MeV energy range. The region of 3.5 to 4 MeV of this spectrum was free from gamma-ray disturbance. From the multispectrum measurements, carried out with a copper annihilator around the source, it has been established that the $^{121}Cs \rightarrow {}^{121}Xe^g$ positron spectrum (92% of all positrons from ^{121}Cs decay) dominates all other positron components in this energy region. Hence the continuum observed above is considered to be due to the $^{121}Cs^g \rightarrow {}^{121}Xe^g$ positron component. A Fermi-

Figure 37

^{121}Xe in-beam γ - γ coincidence gating spectrum recorded with an x-ray detector. The arrow points to the position of a proposed 69 keV transition.

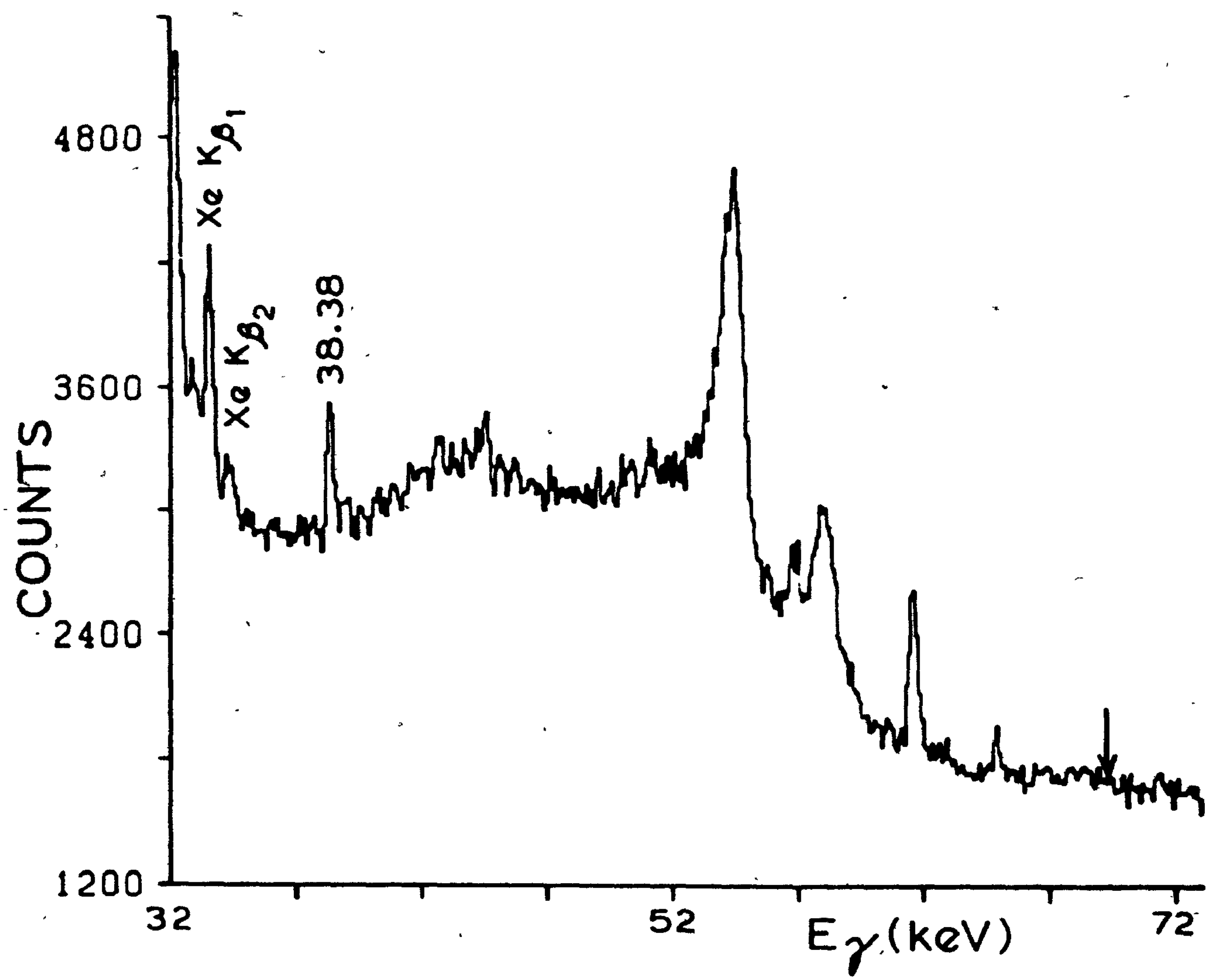

COUNTS
4800
3600
2400
1200
Xe Kβ1
Xe Kβ2
38.38
32
52
72
Eγ (keV)

Kurie analysis of the continuum taken at 2 and 5 min after the end of bombardment is shown in Fig. 38. The weighted mean value of 4.38 ± 0.02 MeV was obtained for the end-point energy. Only the standard deviation from the least squares analysis is quoted. Since the response function of the Ge detector to positrons is not known, no correction for it was made. Therefore the end-point energy value is estimated to have an uncertainty of ≈ 0.2 MeV. The end-point energy obtained corresponds to a decay energy of $^{121}Cs^g$ of $Q_{EC} = 5.4 \pm 0.2$ MeV, in comparison with the previous result of $Q_{EC} \geq 5.65 \pm 0.49$ MeV obtained by Westgaard et al. (1975). If the mass excess of ^{121}Xe is taken as -82.33 ± 0.11 MeV, then the mass excess of $^{121}Cs^g$ is -76.93 ± 0.23 MeV in comparison with the previously reported value of -77.15 MeV (Wapstra and Bos 1977) which was estimated from systematics.

v. Decay Scheme and Discussion

The decay of ^{121}Cs (Fig. 39) was separated into $^{121}Cs^m$ $(9/2^+)$ and $^{121}Cs^g$ $(3/2^+)$ decay schemes [Fig. 39(a,b)] based on the 121 ± 3 and 136 ± 3 sec half-lives, respectively, and using the coincidence results and sums and differences of gamma ray energies. The transition intensities shown are per 100 decays of the parent. The Cs K_β x-ray intensity relative to the 38 keV γ-ray, in the same spectrum, together with the fluorescence yield for Cs ($\omega_K = 0.895$) and K x-ray to K_β x-ray intensity ratio of 5.257 (Lederer and Shirley 1978), require $^{121}Cs^m$ to have $(60 \pm 4)\%$ isomeric transition to $^{121}Cs^g$ and $(40 \pm 4)\%$ positron emission and electron capture to ^{121}Xe. The branching ratio of the capture and positron mode to the isomeric mode has been included in obtaining the log ft values. This branching ratio together with the fact that $^{121}Cs^m$ activity (β + EC) was only 5.7% of $^{121}Cs^g$ suggest

<u>Figure 38</u>

Fermi-Kurie plots of the β spectrum of $^{121}Cs^g \rightarrow {}^{121}Xe^g$ observed at 2 and 5 min. The solid lines are the least squares fit to data points. The end-point energy is the weighted mean of the two results.

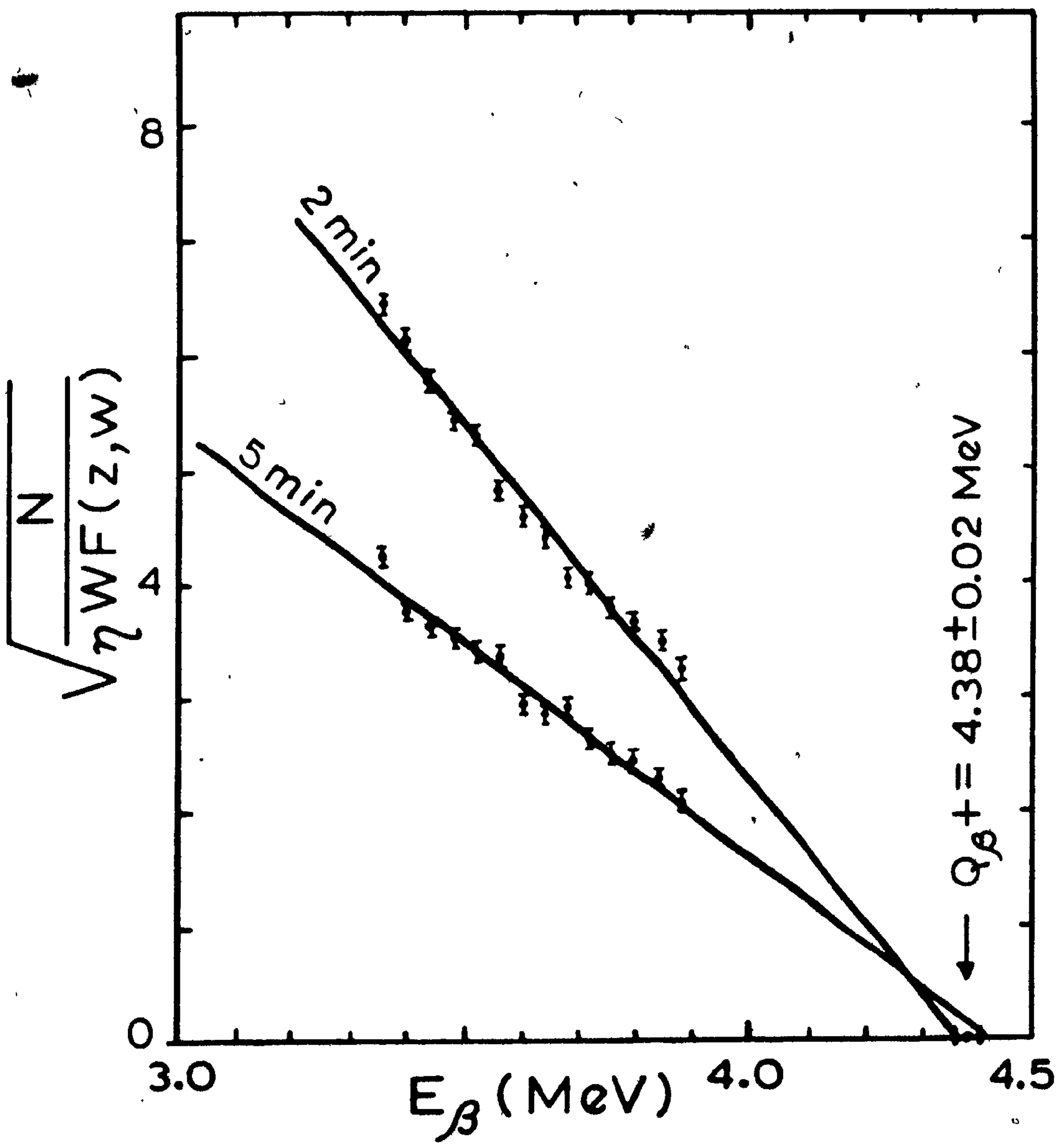

$\sqrt{\frac{N}{\eta WF(z,W)}}$
8
4
0
3.0
4.0
4.5
E_β (MeV)
2 min
5 min
$Q_{\beta^+} = 4.38 \pm 0.02$ MeV

that the ratio of the activation cross-sections of $^{121}Cs^g$ to $^{121}Cs^m$ is $= (\sigma^g_{3/2}/\sigma^m_{9/2}) \simeq 6$.

The intensity of the annihilation quantum, due to all positrons of $^{121}Cs^m + ^{121}Cs^g$, was calculated to be 12360 + 770 units relative to the intensity of the 196.1 keV transition (100 units). This result was obtained from the γ-ray multispectrum data, taken with the positron annihilator. The 2 min component was extracted through least squares analysis (Fig. 40) to overcome contributions from other Cs, Xe and I isotopes which were produced along with ^{121}Cs. The feeding of $^{121}Cs^g$ to $^{121}Xe^g$ was calculated to be 98 ± 7% corresponding to 89% positron branching. There is no observed decay branch to $^{121}Xe^g$ $(5/2^+)$ from $^{121}Cs^m$ $(9/2^+)$ decay.

The ground state of ^{121}Xe has been assigned a $5/2^+$ spin (Münnich et al. 1972) from its beta decay, which feeds $3/2^+$, $5/2^+$ and $7/2^+$ states in ^{121}I, with very little feeding observed to $1/2^+$ and $9/2^+$ states. This assignment is supported by the results of the present work, which indicates that the ground state of ^{121}Xe is fed by a 98% branch from $^{121}Cs^g$ $(3/2^+)$ with a log ft value of 5.20 ± 0.07, appropriate for an allowed beta transition.

The gamma rays of 196.1 and 38.38 keV are in coincidence, but which of them directly feeds the ground state of ^{121}Xe can only be determined by knowing their transition intensities. As mentioned previously, the α_K measured for the 38.38 keV transition implies a 40% M1 and 60% E2 multipolarity. This multipolarity requires a total internal conversion coefficient (ICC) of $\alpha_T = 43$ (Hager and Seltzer 1968) so that although the 38 keV γ-ray has only 3.8 ± 0.5% intensity relative to the 196 keV γ-ray, the 38 KeV total transition intensity is 167% of that of the 196 keV transition. This would imply that the 38 keV transition should be below the 196 keV transition in the cascade. However, it should be noted that the standard deviation of the

Figure 39

Decay scheme of $^{121}Cs^{m,g}$. Transition intensities shown are per 100 decays of parent. The circular insert shows the alternate level ordering reflecting the uncertainity in the intensity of the 38 keV transition.

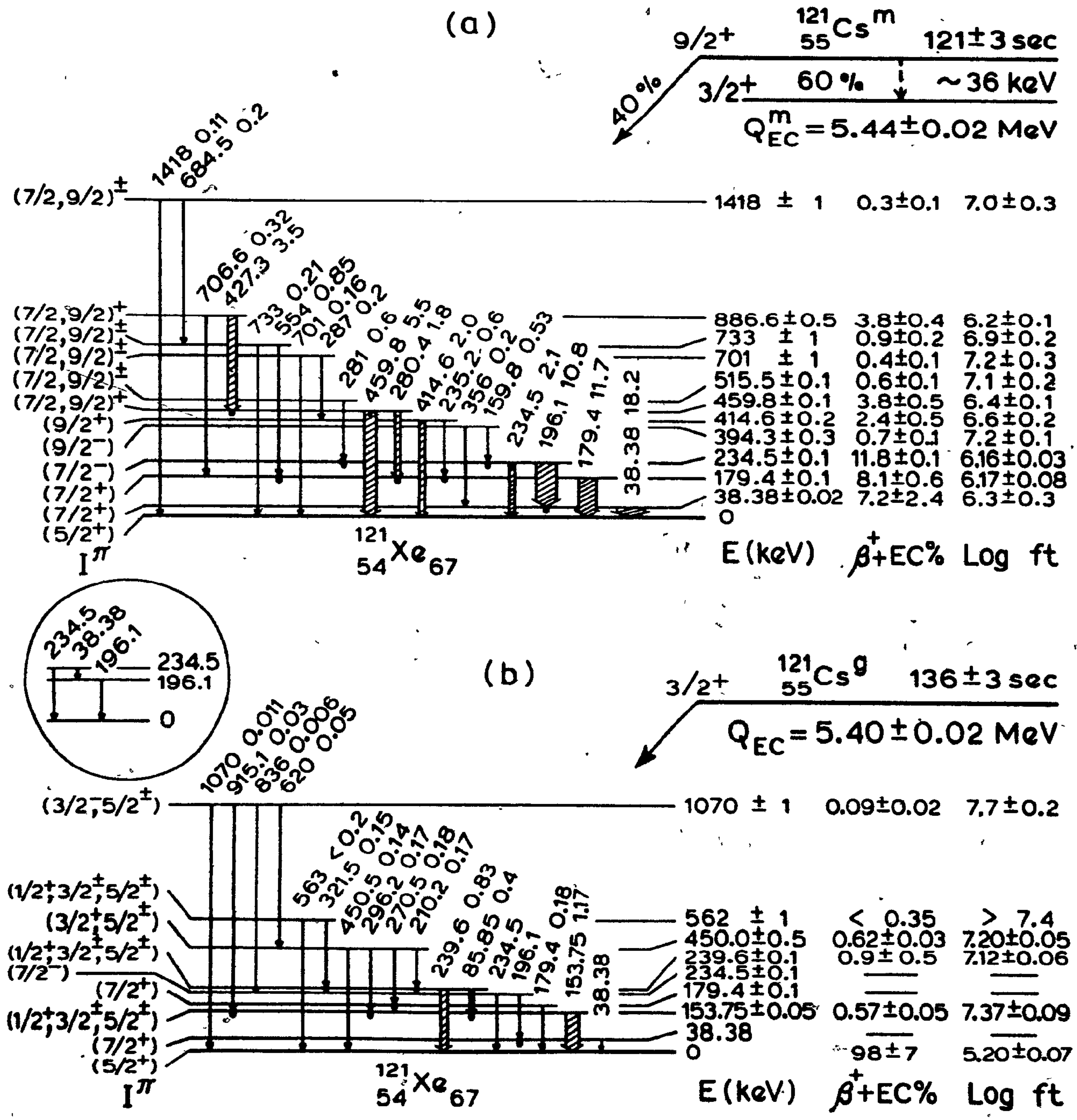

(a)
9/2+
$^{121}_{55}Cs^m$
121 ± 3 sec
40%
3/2+
60%
~36 keV
Q^m_{EC} = 5.44 ± 0.02 MeV
1418 0.11
684.5 0.2
706.6 0.32
427.3 3.5
733 0.21
554 0.85
701 0.16
287 0.2
281 0.6
459.8 5.5
280.4 1.8
414.6 2.0
235.2 0.6
356 0.2
159.8 0.53
234.5 2.1
196.1 10.8
179.4 11.7
38.38 18.2
(7/2,9/2)±
(7/2,9/2)+
(7/2,9/2)±
(7/2,9/2)±
(7/2,9/2)±
(7/2,9/2)+
(9/2+)
(9/2−)
(7/2−)
(7/2+)
(7/2+)
(5/2+)
Iπ
$^{121}_{54}Xe_{67}$
1418 ± 1 0.3±0.1 7.0±0.3
886.6±0.5 3.8±0.4 6.2±0.1
733 ± 1 0.9±0.2 6.9±0.2
701 ± 1 0.4±0.1 7.2±0.3
515.5±0.1 0.6±0.1 7.1±0.2
459.8±0.1 3.8±0.5 6.4±0.1
414.6±0.2 2.4±0.5 6.6±0.2
394.3±0.3 0.7±0.1 7.2±0.1
234.5±0.1 11.8±0.1 6.16±0.03
179.4±0.1 8.1±0.6 6.17±0.08
38.38±0.02 7.2±2.4 6.3±0.3
0
E(keV) β+EC% Log ft
234.5
38.38
196.1
234.5
196.1
0
(b)
3/2+
$^{121}_{55}Cs^g$
136 ± 3 sec
Q_{EC} = 5.40 ± 0.02 MeV
1070 0.011
915.1 0.03
836 0.006
620 0.05
(3/2−,5/2±)
563 <0.2
321.5 0.15
450.5 0.14
296.2 0.17
270.5 0.18
210.2 0.17
239.6 0.83
85.85 0.4
234.5
196.1
179.4 0.18
153.75 1.17
38.38
(1/2±,3/2±,5/2±)
(3/2±,5/2±)
(1/2±,3/2±,5/2±)
(7/2−)
(7/2+)
(1/2±,3/2±,5/2±)
(7/2+)
(5/2+)
Iπ
$^{121}_{54}Xe_{67}$
1070 ± 1 0.09±0.02 7.7±0.2
562 ± 1 < 0.35 > 7.4
450.0±0.5 0.62±0.03 7.20±0.05
239.6±0.1 0.9±0.5 7.12±0.06
234.5±0.1
179.4±0.1
153.75±0.05 0.57±0.05 7.37±0.09
38.38
0 98±7 5.20±0.07
E(keV) β+EC% Log ft

Figure 40

Time decay of the annihilation quantum.

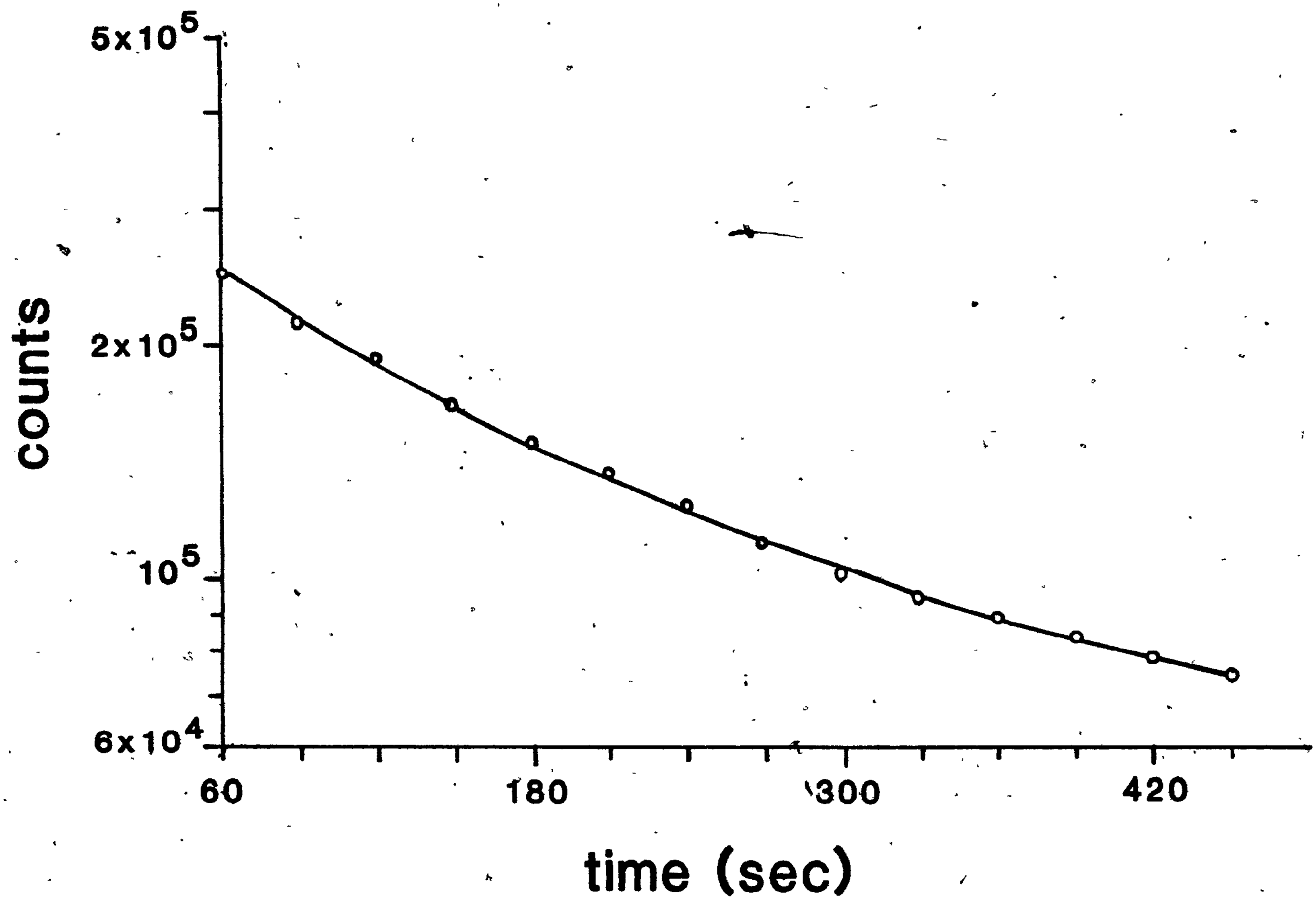

5x10^5
2x10^5
10^5
6x10^4
counts
60
180
300
420
time (sec)

α_K value for the 38 keV transition does not rule out pure M1 or pure E2 multipolarities. Pure E2 multipolarity would require a total ICC of α_T = 62.6, which would make the 38 keV transition intensity 242% of the 196.1 keV transition. This would imply higher feeding and a lower log ft value for the β transition to the 38 keV level. Pure M1 multipolarity, on the other hand, would require a total ICC of α_T = 13.4, so that the 38 keV transition intensity would be 51% that of the 196 keV transition. In this case the 196 keV transition would be below the 38 keV one. Without an extremely precise value of the α_K of the 38 keV transition, no certitude can be associated with the ordering of these transitions. The recent in-beam study of Barci et al. (1981), placed the 38 keV above the 196 keV transition on the basis of coincidence data.

In the decay scheme of ^{121}Cs (121 ± 3 sec) the 38 keV state is fed by a 7.2% positron and electron capture branch with a log ft of 6.3 ± 0.3. This allowed or first-forbidden transition and the multipolarity of 40% M1 + 60% E2 of the 38 keV transition, require the first excited state at 38 keV to be $7/2^+$. The beta transition from the $9/2^+$ parent state to the 234 keV level has a log ft of 6.16 ± 0.03, characteristic of an allowed or first-forbidden transition. The possible spin and parity assignments for the 234 keV level are thus $7/2^\pm$, $9/2^\pm$. In in-beam measurements on 121 Xe Chowdhury et al (1981) and Barci et al (1981) observed a negative parity; thus the 234 and the 196 keV transitions from this level to the $5/2^+$ and $7/2^+$ levels are both of E1 multipolarity. This is consistent with the angular distribution measurement carried out by Chowdhury et al.(1981) which indicated a dipole character for the 196 keV gamma ray. The 234 keV level is thus assigned a spin $J^\pi = 7/2^-$, and is identified as the negative parity bandhead. Chowdhury et al. (1981) assigned a spin $9/2^-$ to this state. The present result of a spin $7/2^-$ for the bandhead agrees with the systematic observation of a negative parity bandhead in odd-Ba nuclei (Gizon and Gizon 1978), with $J^\pi = 11/2^-$ at $N = 77$, $9/2^-$ at $N = 75$, 73 and 71 and $7/2^-$ at $N = 67$. This band head could also possibly be $7/2^-$ at $N = 67$ in Ba and Xe nuclei.

The 179 and 414 keV levels were observed in the positive parity band (Chowdhury et al, 1981) connected by $\Delta J = 1$ transitions. In the present study, the two levels are fed from $^{121}Cs^m$ by allowed or first-forbidden transitions (log ft = 6.17 ± 0.08, 6.6 ± 0.2 respectively). These observations coupled with the fact that the 179.4 keV gamma decays to the $5/2^+$ ground state imply that the 179 and 414 keV levels have $J^\pi = 7/2^+$, $9/2^+$ respectively. Although Chowdhury et al. (1981), assumed that the ground state of ^{121}Xe was the head of a strongly coupled band built on a $g_{7/2}$ neutron hole, the present experiment shows that this cannot be correct. The interpretation of the band structure by Barci et al. (1981) is however, in agreement with the present result; the 179 keV line represents a $7/2^+ \rightarrow 5/2^+$ out-of-band transition. A structure similar to this is seen in $^{117,119}Te$ isotopes with 65 and 67 neutrons (Hagemann et al. 1979). The level at 394 keV is fed by a beta transition with a log ft of 7.2 ± 0.1 and it deexcites to the $(7/2^-)$ 234 keV level through the 159 keV transition and to the $(7/2^+)$ 38 keV level through the 356 keV transition. This level is thus assigned a spin and parity $J^\pi = 7/2^-$ or $9/2^-$. Finally, the levels at 459, 515, 701, 733, 866 and 1418 keV are assigned $7/2^\pm$ or $9/2^\pm$ on the basis of their log ft values.

In the decay scheme of $^{121}Cs^g$ $(3/2^+)$ (Fig. 39) the 153 keV level is fed by an allowed or first-forbidden beta transition (log ft = 7.37 ± 0.09). This level de-excites to the $5/2^+$ ground state through the 153 keV transition with no branching to the $7/2^+$ state of 38 keV; it therefore appears to be a $1/2^+$ state. The 239 keV level was assigned as $1/2^+$ or $3/2^{\pm}$ on the basis of its log ft value (7.12 ± 0.06) and the fact that it deexcites to the 153 keV level, with the crossover transition of 239 KeV to the $5/2^+$ ground state. The spin assignment for the levels at 450, 562 and 1070 keV were made on the basis of log ft values and deexciting γ-rays.

d) The Position of the First Excited 0^+ States in ^{122}Xe and ^{124}Xe

The positions of the first excited 0^+ states in ^{122}Xe and ^{124}Xe have been postulated from beta decay studies on ^{122}Cs and ^{124}Cs isotopes. A level at 1149 keV in ^{122}Xe was thought to be the 0^+ quasi-β state by Genevey-Rivier et al. (1977). In the present work the level at 1269 keV in ^{124}Xe was proposed to be the first excited 0^+ state. These determinations were based on the fact that these levels deexcite to 2_1^+ and 2_2^+ states but not to the 0^+ ground state. The purpose of the present investigation is to confirm these 0^+ assignments by the gamma-gamma angular correlation technique described earlier [IIIA(vi)]. Levels of ^{122}Xe and ^{124}Xe were populated following the decay of ^{122}Cs and ^{124}Cs respectively. ^{124}Cs and ^{122}Cs were produced in the (p,n) and (p,3n) reactions, respectively, by irradiating ^{124}Xe enriched targets with 15 MeV and 45 MeV protons respectively in the fashion described earlier [IIIA(i)]. A total of about 2000 samples was used for each of the experiments. Targets were irradiated for a period of 10 sec and their activities were counted over a period of one minute. For ^{122}Cs decay, coincidence data were accumulated with 90°, 135°, 157° and

180° angles between the two detectors. In the ^{124}Cs experiment an additional angle of 120° was used. The data were sorted by placing a digital gate on one of the gamma-rays in the cascade of interest as well as on the adjacent background. The intensity of the other coincident γ-ray in the cascade in the resulting background-subtracted spectra of the fixed detector was obtained. The normalized intensities were then plotted as a function of the angle subtended by the two detectors. The data points were then fitted using the least squares analysis to the function:

$$W(\theta) = A_o + A_2^{exp} P_2(\cos\theta) + A_4^{exp} P_2(\cos\theta)$$

The values of A_2^{exp}, A_4^{exp} obtained were first corrected for solid angle effects

$$(A_K = \frac{A_K^{exp}}{Q_K})$$

The solid angle correction factors Q_2 and Q_4 were 0.86 and 0.59 respectively. The angular correlation pattern obtained for the 331-818 keV cascade of ^{122}Xe is shown in Fig. 41. Solid lines are the result of a least squares fit of the data points to the function W(θ). For ^{124}Xe, the angular correlation of the 915-354 keV cascade and the 1336-354 keV cascade were studied. The normalized intensities of the 915 and 1336 keV γ-rays in the spectra obtained in coincidence with the 354 keV γ-ray are presented in Fig. 42 and 43 respectively as a function of the angle θ subtended by the two detectors. The correlation of the 492-354 keV cascade for the already known $2^+ \rightarrow 2^+ \rightarrow 0^+$ cascade in ^{124}Xe were also obtained (Fig. 44). The values for the A_2 and A_4 coefficients after correction for solid angles are listed in table 8. The curves for the 818-331 keV cascade of ^{122}Xe and the 915-354 keV,

Figure 41

Angular correlation pattern of the 331 - 818 keV cascade of ^{122}Xe. Solid lines represent least-squares fits to data points.

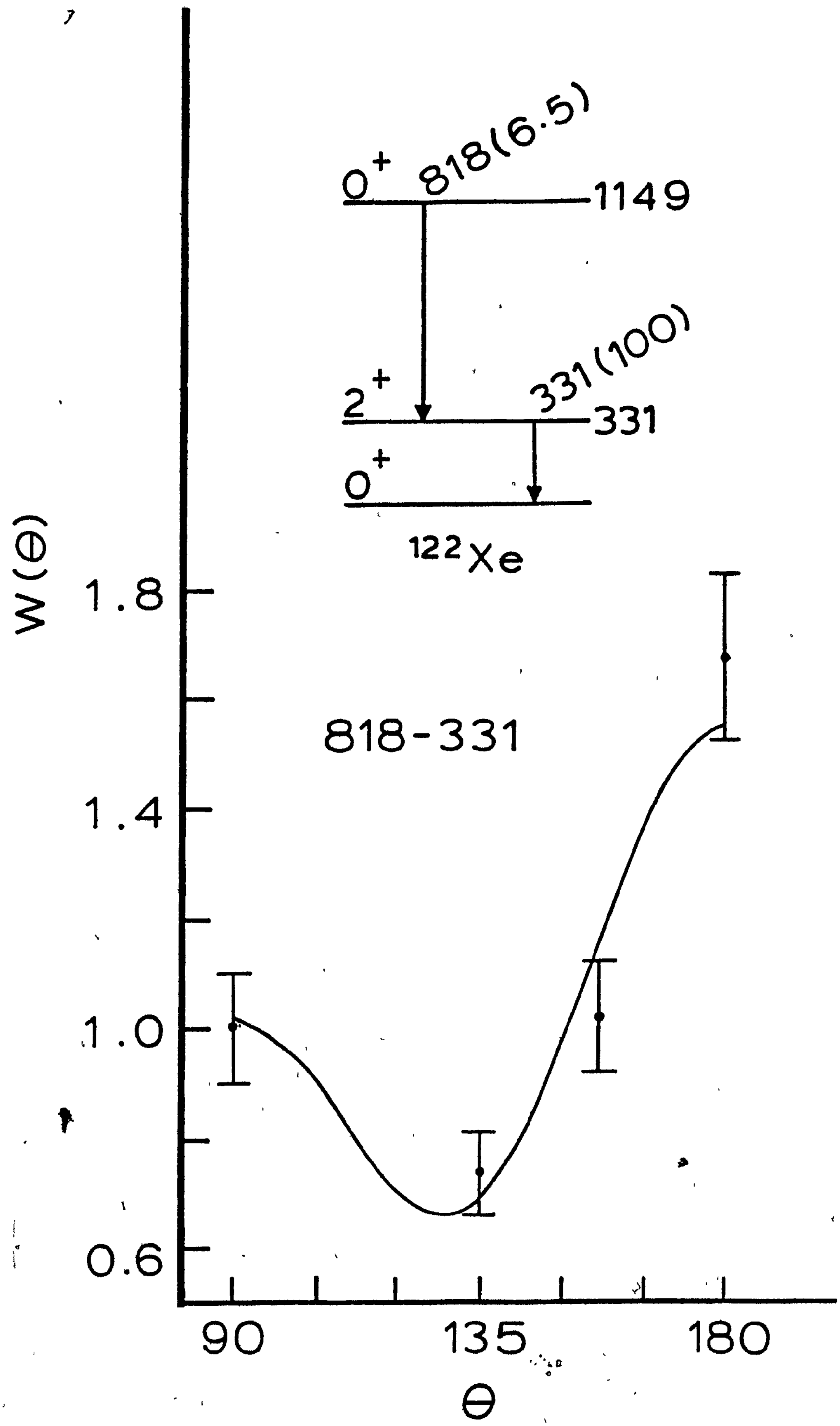

0+ 818(6.5)
1149
2+ 331(100)
331
0+
122Xe
W(Θ)
1.8
1.4
1.0
0.6
818-331
90
135
180
Θ

Figure 42

Angular correlation pattern of the
354 - 915 keV cascade of ^{124}Xe.

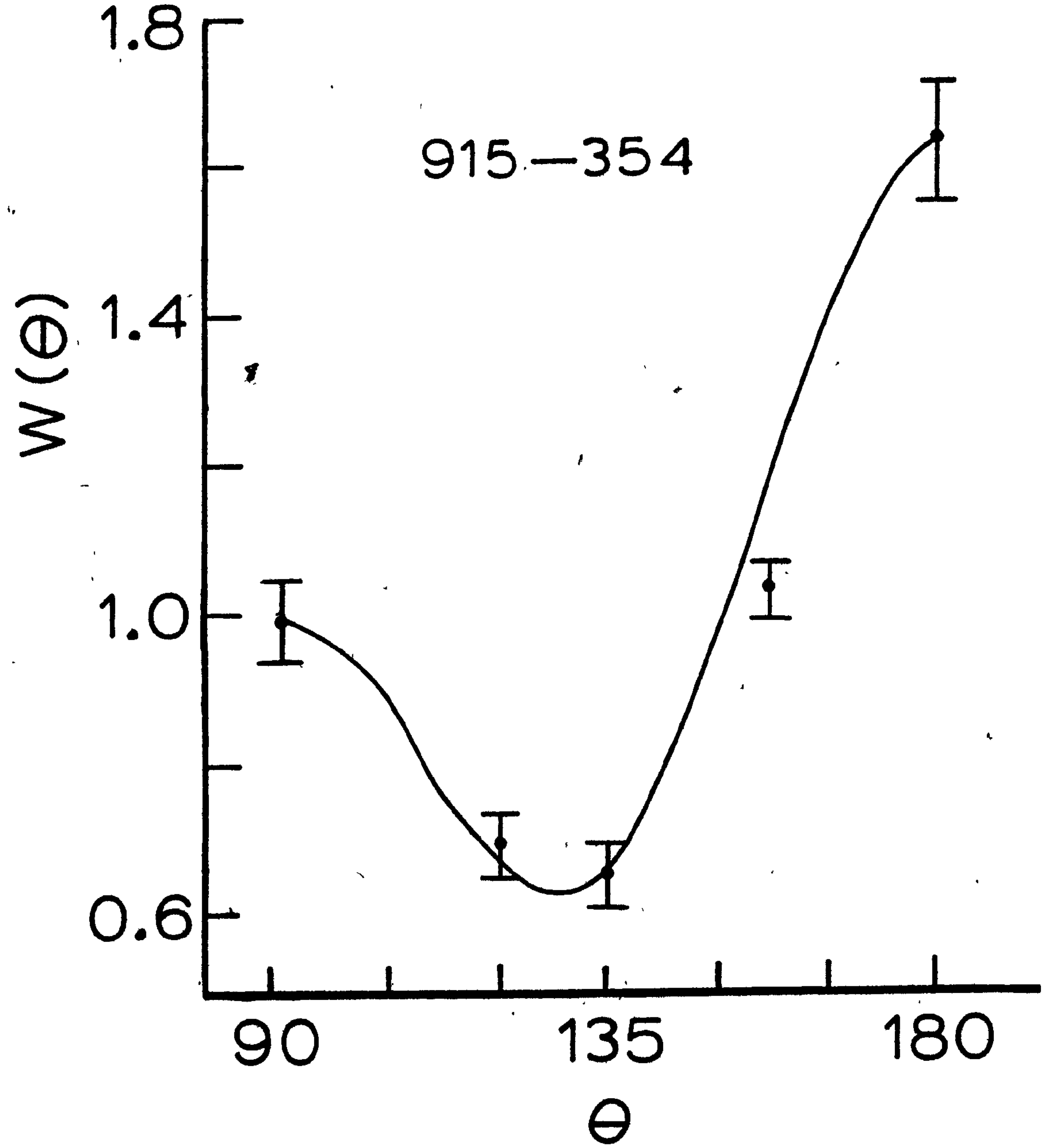

1.8
1.4
1.0
0.6
915—354
W(θ)
90
135
180
θ

Figure 43

Angular correlation pattern of the 354 - 1336 keV cascade of ^{124}Xe.

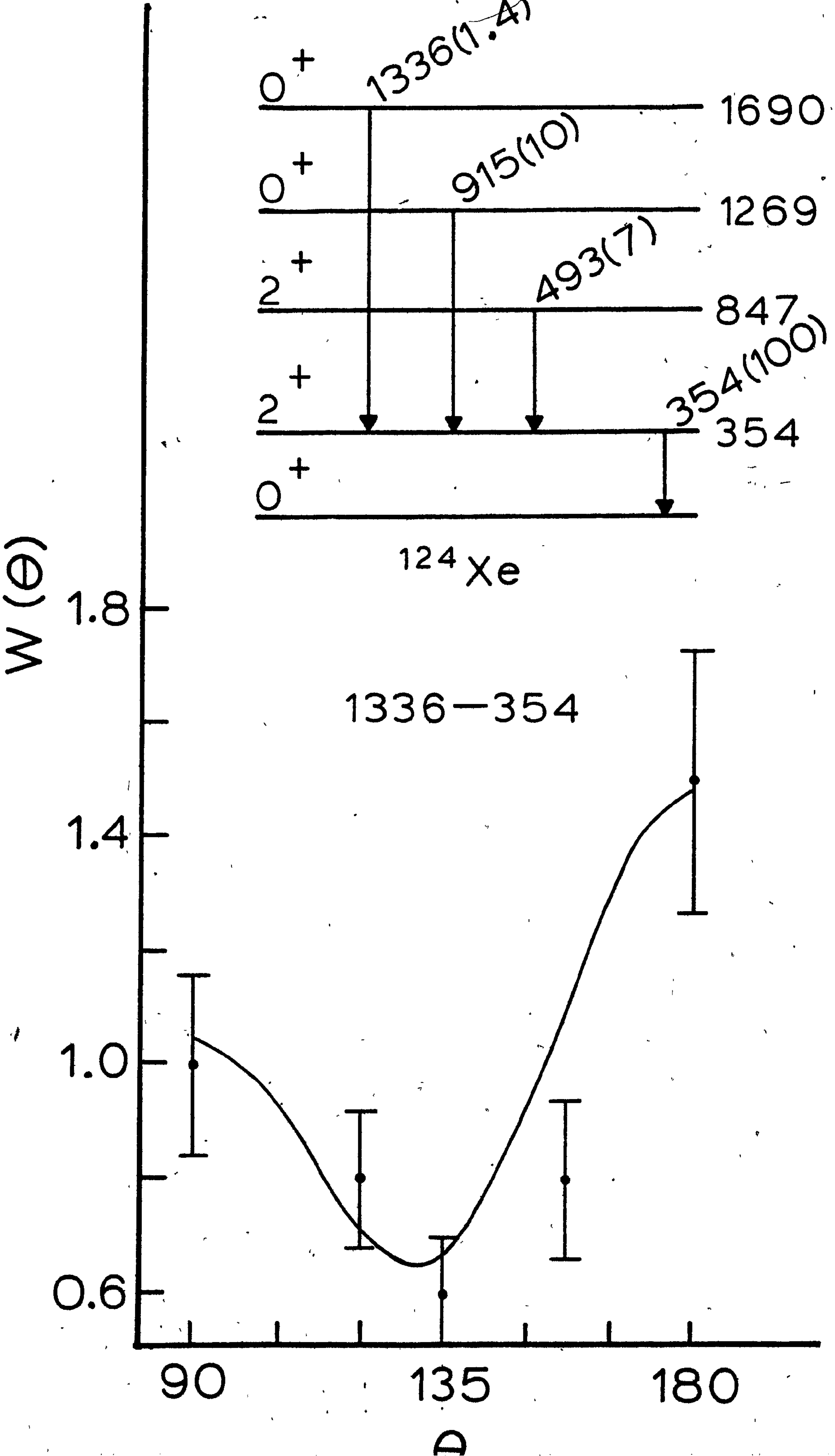

1336(1.4)
915(10)
493(7)
354(100)
0+
0+
2+
2+
0+
1690
1269
847
354
124Xe
W(Θ)
1.8
1.4
1.0
0.6
1336—354
90
135
180
Θ

Figure 44

Angular correlation pattern of the 354 - 493 keV cascade of ^{124}Xe.

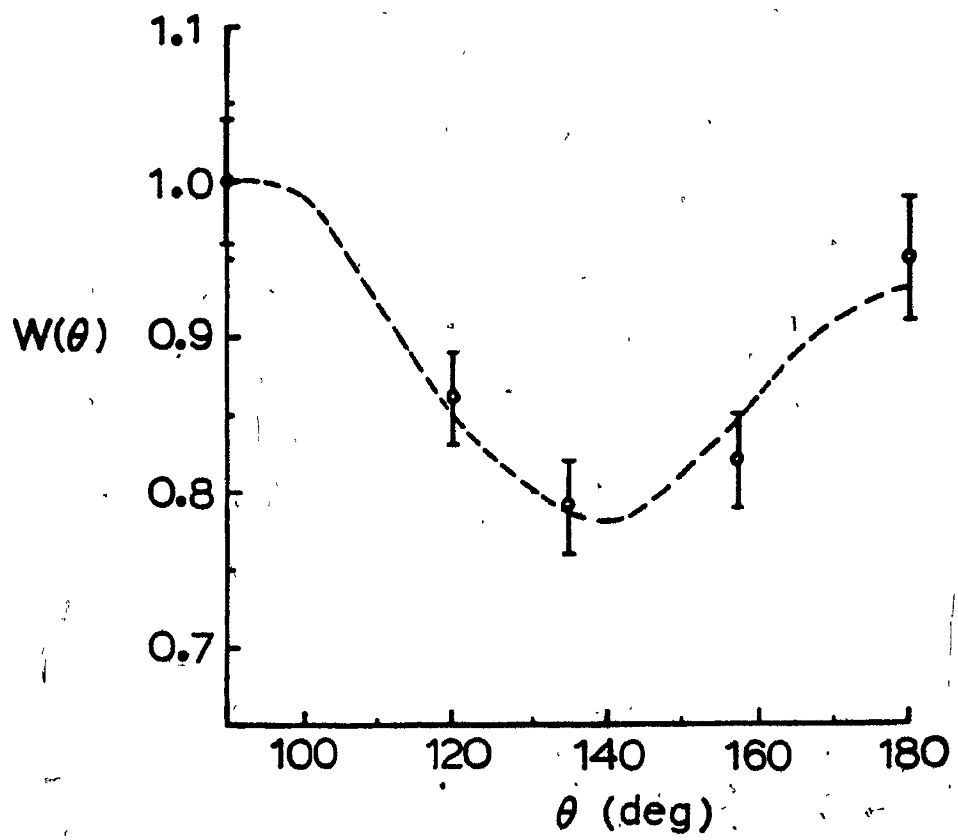

1.1
1.0
W(θ)
0.9
0.8
0.7
100
120
140
160
180
θ (deg)

TABLE 8. Summary of Angular Correlation Measurements in $^{122,124}Xe$

Nucleus	Level (keV)	Cascade γ-ray energies (keV)	A_2	A_4	Spin Sequence
^{122}Xe	1149	818-331	0.2 ± 0.2	1.1 ± 0.4	$0^+-2^+-0^+$
^{124}Xe	847	493-354	-0.16 ± 0.04	0.32 ± 0.05	$2^+-2^+-0^+$ ($\delta = 8\,^{+7}_{-3}$)
	1269	915-354	0.23 ± 0.12	1.14 ± 0.18	$0^+-2^+-0^+$
	1690	1336-354	0.10 ± 0.20	1.0 ± 0.3	$0^+-2^+-0^+$

and 1336-354 keV cascade of ^{124}Xe are characteristic of a $0^+ \rightarrow 2^+ \rightarrow 0^+$ directional correlation pattern. The large A_4 value obtained uniquely implies a zero spin assignment for the level at 1149 keV in ^{122}Xe and 1269 keV and 1690 keV in ^{124}Xe. The experimentally obtained coefficients are in good agreement with the theoretical coefficients for a $0 \rightarrow 2 \rightarrow 0$ cascade: $A_2 = 0.357$, $A_4 = 1.108$ (Taylor et al. 1971).

The 0^+ assignment of the 1149 keV level in ^{122}Xe is in agreement with the predictions of Genevey-Rivier et al.(1977) and that of the 1269 keV level in ^{124}Xe is in agreement with the predictions of the β-decay study of the present work.

Although the error bar is fairly large in the case of the 1336-354 keV cascade, the large A_4 coefficient cannot be explained by other possible spins (1, 2). In the decay study part of this work a transition of 1689 KeV was observed to follow the half-life of ^{124}Cs decay (29.7 sec). In view of the 0^+ assignment for the 1690 keV level, no direct gamma transition to the ground state is possible; our observed 1689 keV transition therefore lies elsewhere in the decay scheme.

The above results are consistent with the features of Xe nuclei previously noted by Kusakari et al.(1975), who pointed out that the first excited 0^+ level is located near the 3_1^+ level and that its position drops as N decreases. The present results have been summarized in a publication, (Singh et al. 1979) which is included in the Appendix.

B. RESULTS OF IN-BEAM STUDY

a) Band Structure in ^{122}Xe

i. Previous Work

The ground state collective band in ^{122}Xe was first observed by Morinaga and Lark in 1965. They populated the levels in ^{122}Xe in the $(\alpha,4n\gamma)$ reaction on ^{122}Te targets using a 52 MeV alpha beam. Members of the ground state band up to the 8^+ state were identified. Since they detected gamma-rays by using NaI(Tl) scintillation counters, the error in the energy determination was large. Also, their γ-ray assignments were based on relative intensities, and $\gamma - \gamma$ coincidence techniques were not employed. In a subsequent study made at Berkeley, Clarkson et al. (1967) produced ^{122}Xe in the $^{115}In(^{10}B, 3n)$ reaction, using the heavy-ion linear accelerator (HILAC). Their results agree with the results of Morinaga and Lark (1965), although the use of lithium-drifted germanium detectors allowed Clarkson et al. (1967) to make a better energy determination. Their spin and parity assignments were based on the energy and observed intensities of the γ-rays. The lifetimes of the levels in the ground-state band in ^{122}Xe were measured by Kutschera et al. (1972) to be of the order of few picoseconds. In the decay study of ^{122}Cs carried out by Genevey-Rivier et al. in 1977, high-spin states were populated in the decay of the high spin isomer of ^{122}Cs (I = 8). A level scheme containing the ground state rotational band up to the 10^+ level and the quasi-gamma band up to the 7^+ level was proposed. Spin and parity assignments were based on values of the measured electron conversion coefficients and decay patterns.

ii. Gamma Ray Spectroscopy

The in-beam singles spectrum recorded with the 10% coaxial Ge(Li) detector is shown in Fig. 45. The labelled gamma rays belong to gamma transitions in ^{122}Xe. The unlabelled γ-rays are mainly gamma transitions between levels of ^{123}Xe, ^{124}Xe and ^{123}I which are produced in the (α,3n), (α,2n) and (α,p2n) reactions respectively, along with the ^{122}Xe of interest. The identification of gamma rays was done on the basis of excitation functions and gamma-gamma coincidence results. The energy calibration was carried out with the beam off, using standard sources of ^{152}Eu and ^{56}Co. The relative intensity measurements were performed at an angle of 125° with the beam in order not to introduce errors due to the P_2 term in the angular distributions. The gamma ray energies and relative intensities are given in table 9. Singles spectra were also recorded with the beam off in order to identify gamma rays following the beta decay of the product nuclei and also to correct for radioactivity contributions in multicomponent gamma lines which were not easy to separate. Gamma singles spectra were analyzed by the computer code SAMPO [IIIA(ii)]. The contribution to the 331 keV line from the decay of ^{123}Xe (330 keV) was accounted for in the intensity calculation. The 815 keV line is a doublet, with a 815.9 keV component of ^{122}Xe and a weak 816.9 keV component of ^{124}Xe. Similarly the contribution to the 838 keV line from the 840.5 keV gamma ray of ^{124}Xe was taken into account. Since the 512 keV gamma ray is buried under the 511 keV annihilation quantum, its intensity was determined from the gamma-gamma coincidence results. The intensity of the 512 keV transition relative to the 843 keV transition which depopulates the same level, is in agreement with the results of the decay study of Genevey-Rivier et al. (1977). The gamma multiplicity filter technique discussed earlier [IIIB(iii)] was very

Figure 45

Spectrum of gamma-rays emitted in the $^{122}Te\ (\alpha,4n\gamma)$ reaction.

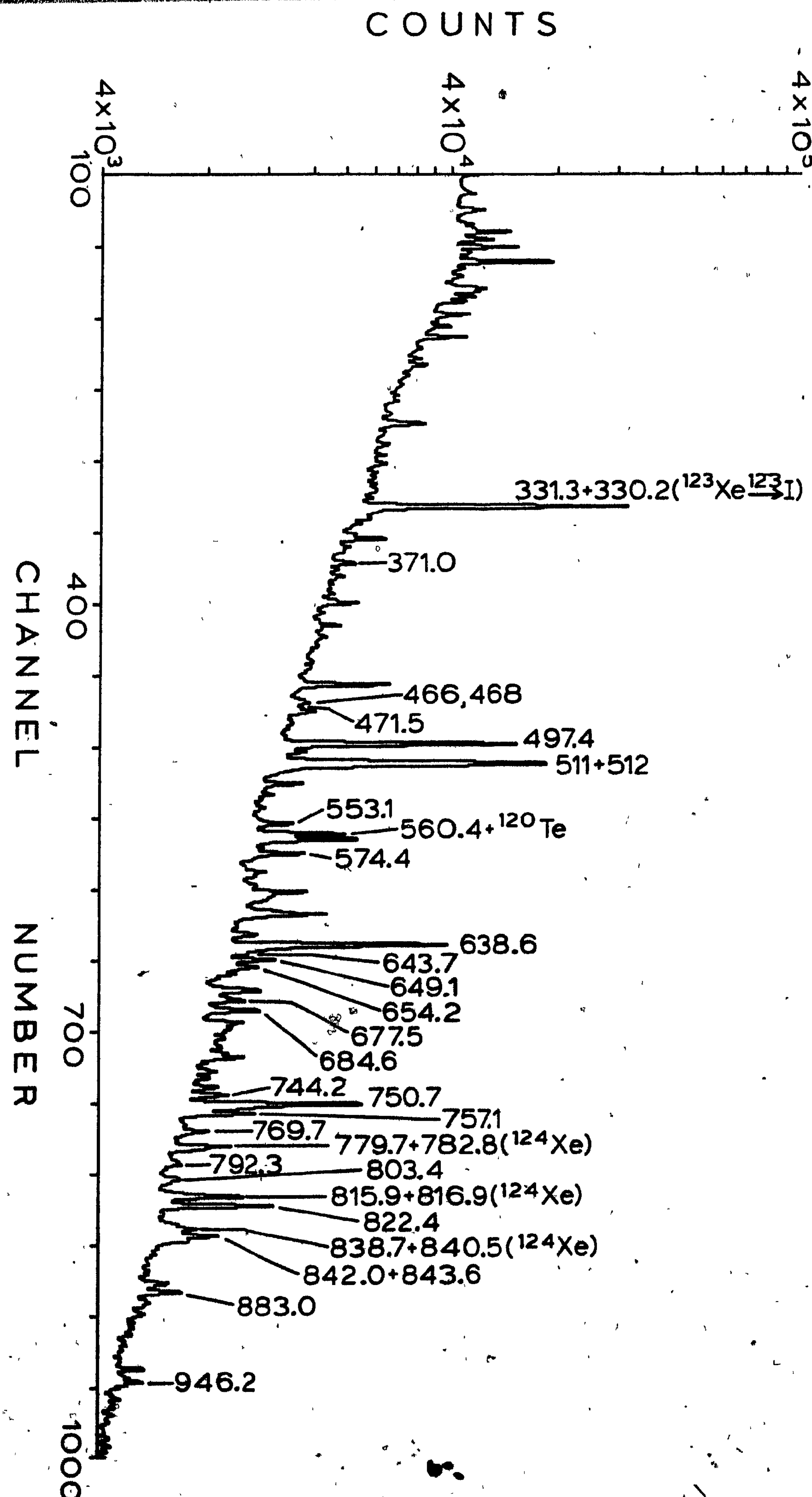

COUNTS
4×10³
4×10⁴
4×10⁵
CHANNEL NUMBER
100
400
700
1000
331.3+330.2(¹²³Xe →¹²³ I)
371.0
466,468
471.5
497.4
511+512
553.1
560.4+¹²⁰Te
574.4
638.6
643.7
649.1
654.2
677.5
684.6
744.2
750.7
757.1
769.7
779.7+782.8(¹²⁴Xe)
792.3
803.4
815.9+816.9(¹²⁴Xe)
822.4
838.7+840.5(¹²⁴Xe)
842.0+843.6
883.0
946.2

TABLE 9. ^{122}Xe Gamma-Ray Energy and Intensity

E_γ(keV)	I_γ	E_γ(keV)	I_γ
331.31 ± .03	100	757.13 ± .04	11.1 ± 0.4
371.0 ± 0.1	3.1 ± 0.3	769.65 ± .03	3.9 ± 0.4
386 ± 0.5	<1*	779.65 ± .04	12.2 ± 0.05
466 ± 0.5	3.0 ± 0.3		
468 ± 0.5	3.0 ± 0.3	792.3 ± 0.3	3.4 ± 0.3
471.5 ± 0.4	2.2 ± 0.2	803.4 ± .2	2.5 ± 0.4
497.35 ± 0.3	86 ± 2.4	815.89 ± .05	9.4 ± 0.4
512* ± 0.4	21 ± 2	822.35 ± .03	20.4 ± 0.7
553.12 ± .05	6.0 ± 0.4	838.7 ± 0.1	4.8 ± 0.4
560.37 ± .04	16 ± 1.0	842 ± 0.5	3.5* ± 1
574.4 ± .06	7.5 ± 0.4	843.6 ± 0.2	8.0 ± 0.5
638.59 ± .03	73 ± 2.4	883.0 ± 0.1	7.3 ± 0.5
643.7 ± 1.0	3 ± 1	946.2 ± 0.1	2.6 ± 0.2
649.07 ± .07	6.8 ± 0.4	993.5 ± 1.0	0.77 ± .15
654.2 ± 0.2	4.8 ± 0.6	1098.1 ± 0.2	6.9 ± 0.5
677.5 ± 0.2	4.3 ± 0.6		
684.57 ± .08	9.1 ± 0.7		
744.19 ± .05	6.2 ± 0.4		
750.68 ± .04	49 ± 1.6		

* intensity obtained from coincidence data.

useful in reducing the radioactivity lines in the coincidence spectra and enhancing members of long cascades. The gamma multiplicity data were recorded on magnetic tape event-by-event along with the multiplicity of each event. The data were then sorted according to multiplicity. Most of the useful results were obtained by analyzing events having a multiplicity of three of more, two recorded by the two Ge detectors and one or more by the six NaI(Tl) or the BGO detector. For some weak gamma rays, only the minimum coincidence requirement of two gamma rays was used in order to gain statistics. The results of the multiplicity filter measurements are summarized in table 10, and Fig. 46, where the background subtracted spectra of some pertinent γ-rays are shown. As can be seen from these spectra, there remains a background which is in real coincidence with the γ-ray gate. This background arises from the γ-rays forming the side-feeding into the rotational states above the gate, which fulfill the coincidence requirement. In the ground band all transitions following the gating transition have constant intensity since the side-feeding into the lower states is not in coincidence with the gating transition.

The neutron-multiplicity filter measurement was carried out using the technique outlined in chapter III [B(iv)]. In these measurements γ-ray spectra, in coincidence with different number of neutrons, were accumulated. The neutron multiplicity of each event was recorded along with the γ-ray energy, and the data were sorted by placing digital gates on different neutron multiplicity peaks. As mentioned earlier, (α,2n), (α,3n) and (α,p2n) reaction channels are also open at the 54 MeV bombarding energy. The neutron multiplicity filter technique proved useful in reducing radioactivity and in differentiating between various reaction channels with different numbers of outgoing neutrons. Fig. 47 shows the intensity of gamma rays

Figure 46

Background subtracted coincidence spectra for ^{122}Xe obtained in the γ-multiplicity filter measurement.

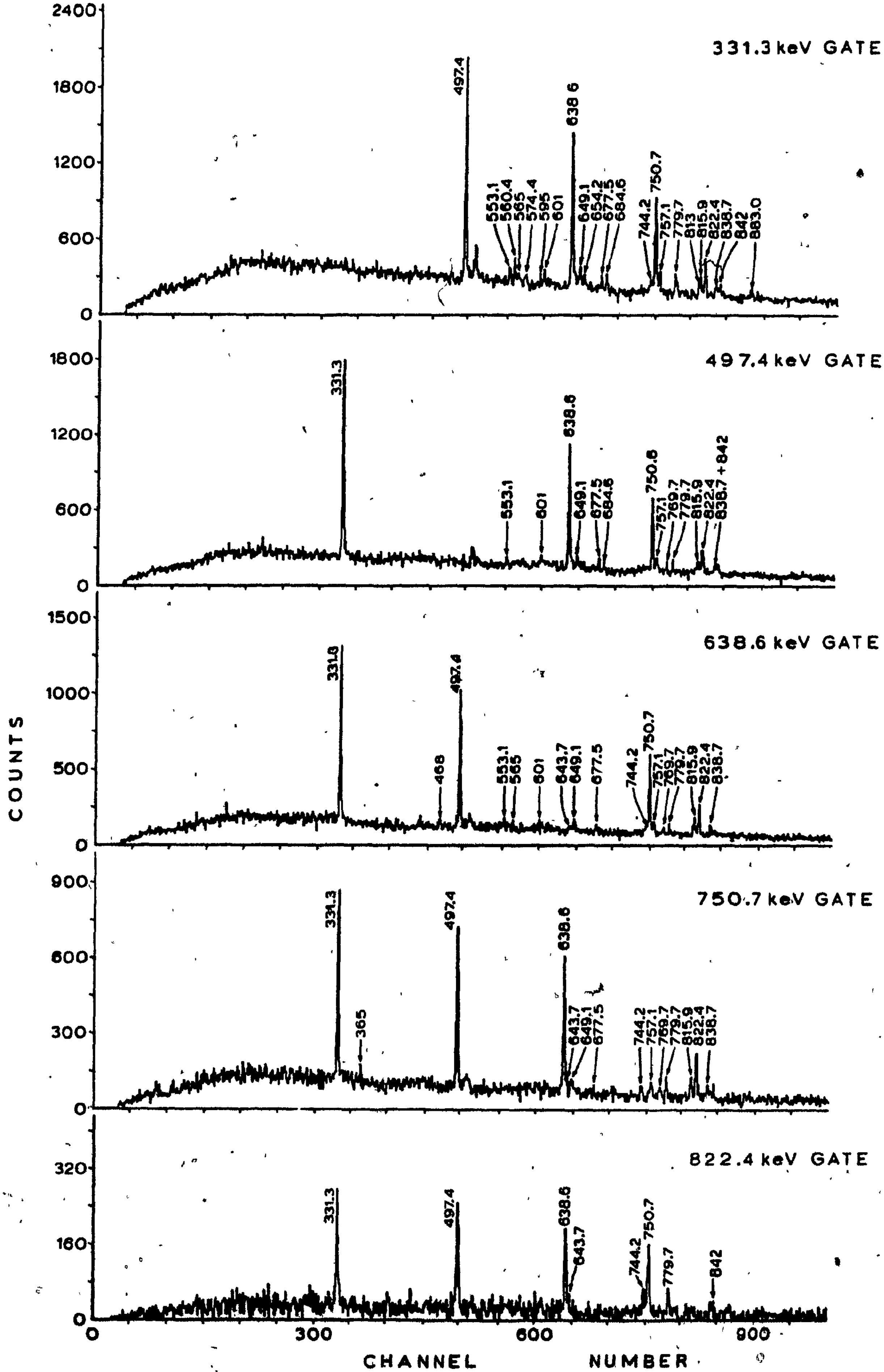
331.3 keV GATE
497.4 keV GATE
638.6 keV GATE
750.7 keV GATE
822.4 keV GATE
COUNTS
CHANNEL NUMBER

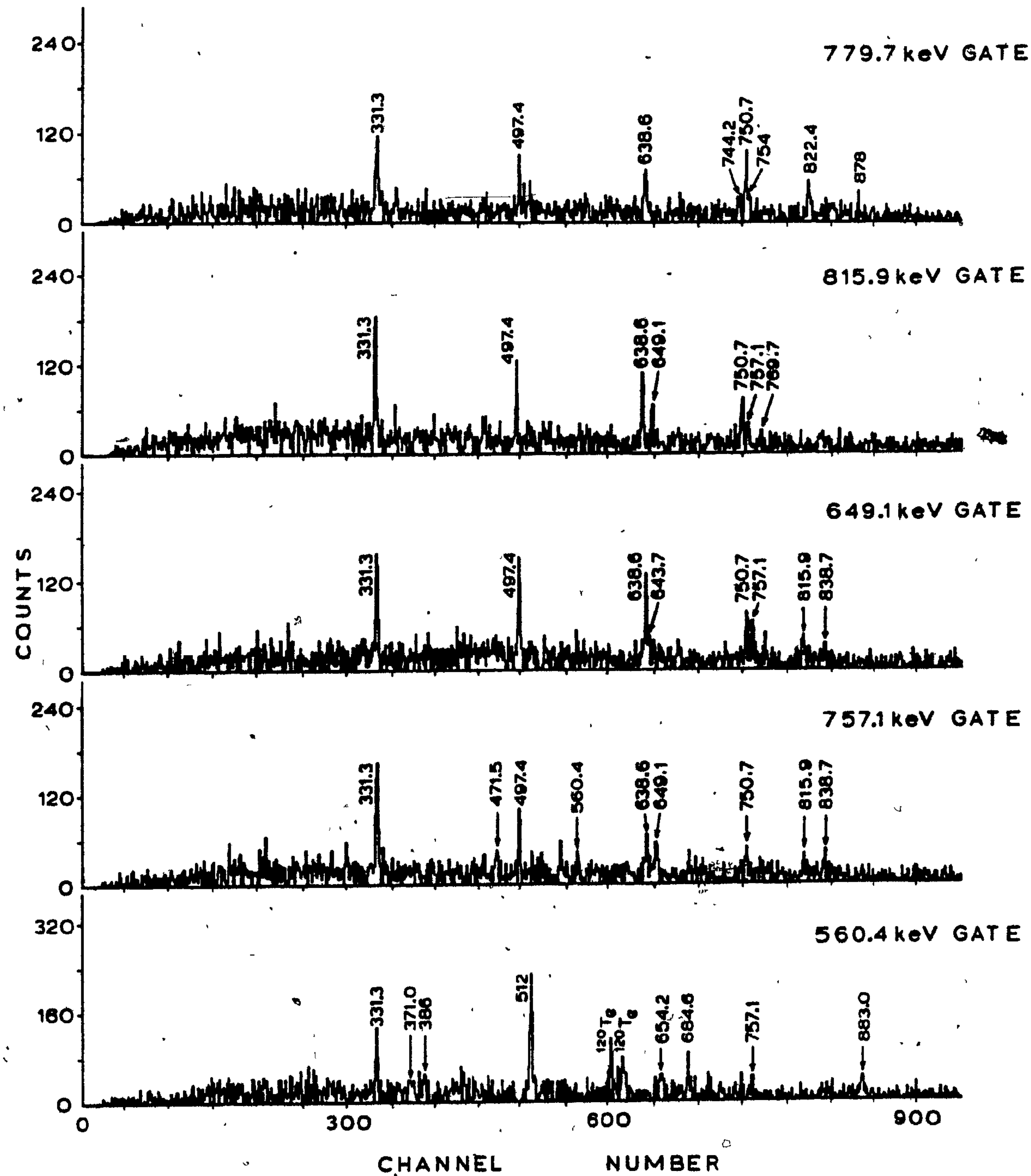
779.7 keV GATE
331.3
497.4
638.6
744.2
750.7
754
822.4
878
815.9 keV GATE
331.3
497.4
638.6
649.1
750.7
757.1
769.7
649.1 keV GATE
331.3
497.4
638.6
643.7
750.7
757.1
815.9
838.7
757.1 keV GATE
331.3
471.5
497.4
560.4
638.6
649.1
750.7
815.9
838.7
560.4 keV GATE
331.3
371.0
386
512
^{120}Te
^{120}Te
654.2
684.6
757.1
883.0
COUNTS
240
120
0
320
160
0
300
600
900
CHANNEL NUMBER

TABLE 10. ^{122}Xe Multiplicity Filter Results

GATE E (keV)	Coincident Gamma Rays, E (keV)
331.3	497.4, 512, 553.1, 560.4, 565, 574.4, 595, 601, 638.6, 643.7, 649.1, 654.2, 677.5, 684.6, 744.2, 750.7, 757.1, 779.7, (813), 815.9, 838.7, 822.4, 842, 883.0, 1026
371.0	331.3, 512, 560.4, 684.6
471.5	497.4, 649.1, 792.3
497.4	(222), 331.3, 553.1, 601, 638.6, 649.1, 677.5, 684.6, 744.2, 750.6, 757.1, 769.7, 779.7, 815.9, 822.4, 838.7, 842, 1098.1
553.1	331.3, (453), (497.4), 512, 638.6, 677.5
560.4	331.3, 371.0, 386, 512, [601], [614], 654.2, 684.6, 684.6, 757.1, (803.4), 883.0, 993.5
574.4	331.3, 454, 497.4, 586, 671
638.6	331.3, 468, 497.4, 553.1, 565, 601, 643.7, 649.1, 677.5, 744.2, 750.7, 757.1, 769.7, 779.7, 815.9, 822.4, 838.7, 842, 1026, 1096.1
643.7	331.3, 497.4, 560.4, 638.6, 750.7, (757.1), 822.4
649.1	331.3, (466), (468), 497.4, 558, 638.6, (643.7), 750.7, 757.1, 815.9, 838.7, (1098.1)
654.2	331.3, 497.4, 512, 560.4, 574.4, 739
677.5	331.3, 497.4, 553.1, 638.6, 741, 750.7
684.6	331.3, 497.4, 560.4, (638.6), 757.1, 883.0, 946.2
744.2	331.3, 497.4, 638.6, 750.7, 779.7, 822.4
750.7	331.3, (365), 497.4, 601, [618], 638.6, 643.7, 649.1, 677.5, 744.2, 757.1, 769.7, 779.7, 815.9, 822.4, 838.7, 920, 1026

TABLE 10. ^{122}Xe Multiplicity Filter Results - (continued)

GATE E (keV)	Coincident Gamma Rays, E (keV)
757.1	331.3, 471.5, 497.4, 560.4, 638.6, 649.1, 684.6, 750.7, 815.9, 838.7, (883.0)
769.7	331.3, 497.4, 638.6, 750.7
779.7	331.3, 497.4, 638.6, 744.2, 750.7, 754, 822.4, 878,
803.4	497.4, 638.6, 752
815.9	331.3, [354], 497.4, 638.6, 649.1, 750.7, 757.1, 769.7, 838.7, 993.5
822.4	331.3, 497.4, 638.6, 643.7, 744.2, 650.7, 757.1, 779.7, (838.7), 842
838.7	331.3, 497.4, 560.4, 638.6, 649.1, 684.6, 750.7, 757.1
842,843	331.3, 497.4, 560.4, 654.2, 638.6, 744.1, 750.7, 779, 822.4
883.6	331.3, 560.4, 684.6
946.2	331.3, 497.4
1098.1	331.3, (497.4), 638.6, 750.7

( ): Uncertain

[ ]: Belongs to another isotope

Figure 47

The intensity of gamma-rays in coincidence with two neutrons relative to that in coincidence with one neutron for different reaction channels.

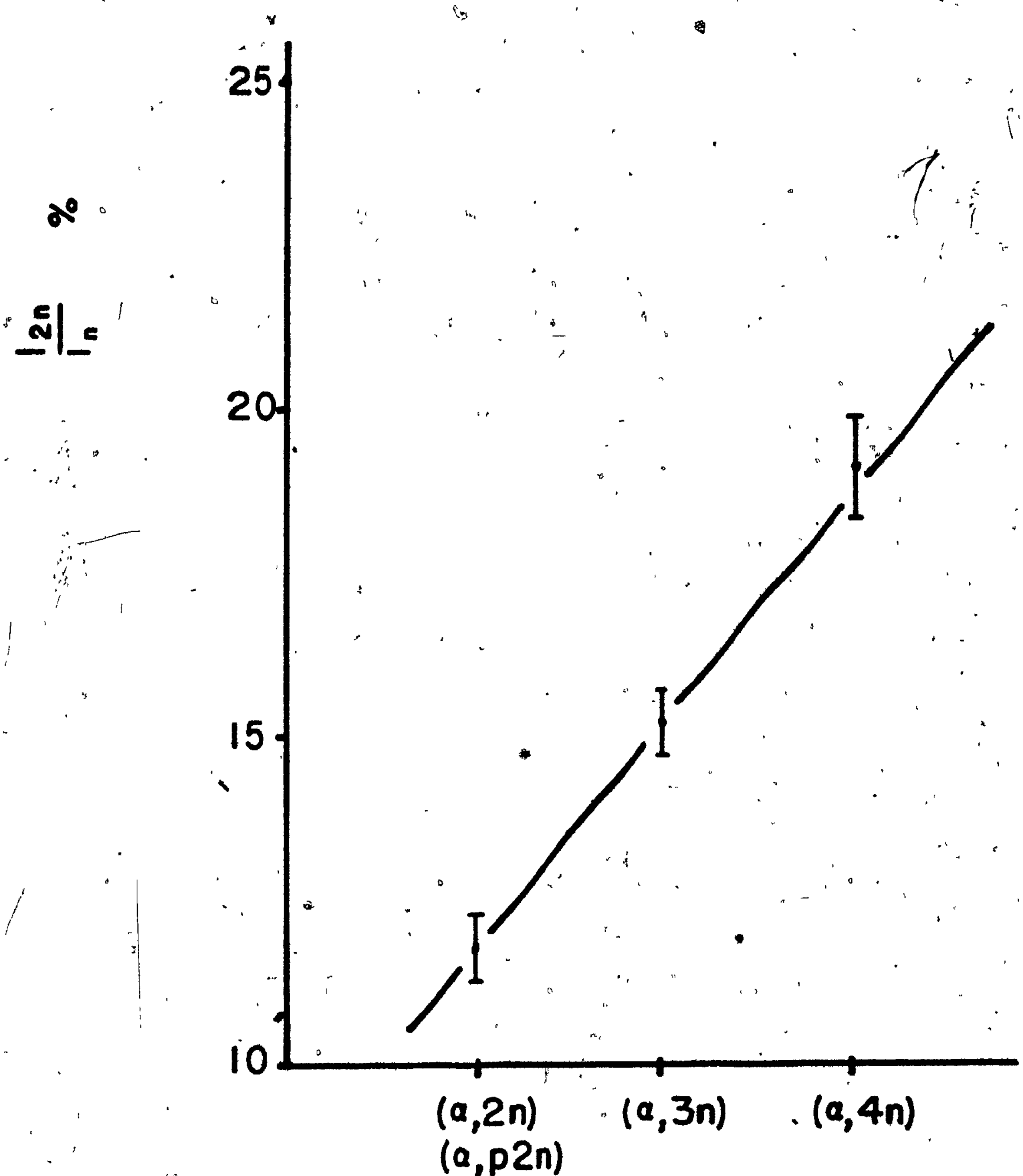
%
$\frac{2n}{n}$
25
20
15
10
(α,2n)
(α,p2n)
(α,3n)
(α,4n)

in coincidence with two neutrons relative to that in coincidence with one neutron for $^{122}Xe(\alpha,4n)$, $^{123}Xe(\alpha,3n)$, $^{124}Xe(\alpha,2n)$ and $^{123}I(\alpha,p2n)$. This relative intensity increases as the number of outgoing neutrons increase Therefore one can easily conclude the type of reaction to which a gamma ray belongs. However the efficiency of the system is low since the γ-ray intensities of γ-rays in coincidence with one neutron are higher than those in coincidence with two neutrons for all reactions. The solid angle covered by the neutron detectors is estimated to be about 25%. The (α,4n) reaction especially should have reached maximum cross-section with two to three neutrons in coincidence. This low efficiency could be the result of several factors: the thickness of the four-quadrant liquid scintilators might have been insufficient to stop all neutrons; a microstructure in the beam could have caused too much pileup; the random rate might have been excessive.

iii. Angular Distribution Results

Gamma-ray spectra of the angular distribution experiment [IIIB(v)] were analyzed and the intensity of the gamma rays as a function of the detector angle were fitted by least squares to the Legendre polynomial [$W(\theta) = A_0 + A_2P_2(\cos\theta) + A_4P_4(\cos\theta)$]. Examples of the results from the angular distribution measurements are shown in FIg. 48 and 49. The A_2 and A_4 values thus obtained (corrected for solid angle effects), are listed in table 11. The correction factors Q_2, Q_4 for the solid angle effect for these measurements were calculated to be 0.984 and 0.946 respectively. These results were interpreted by using the table of Yamazaki (1967) of angular distributions of γ-rays from aligned nuclei following (particle, xn) reactions. As mentioned earlier [IIIB(v)], the experimental A_K

Figure 48

Angular distribution patterns for some gamma-rays emitted in the ^{122}Te $(\alpha,4n\gamma)$ reaction.

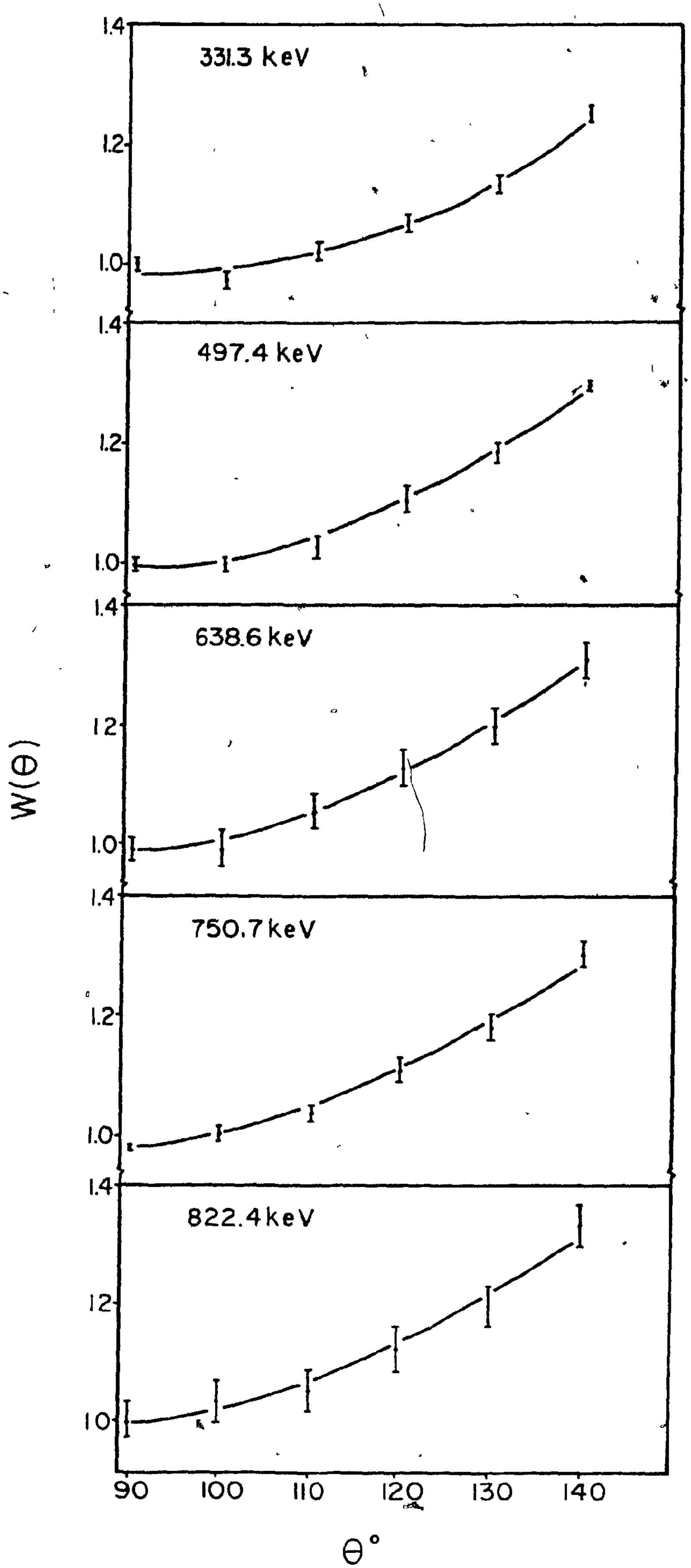

331.3 keV
497.4 keV
638.6 keV
750.7 keV
822.4 keV
1.4
1.2
1.0
W(Θ)
90
100
110
120
130
140
Θ°

Figure 49

Angular distribution patterns for some gamma-rays emitted in the ^{122}Te $(\alpha, 4n\gamma)$ reaction.

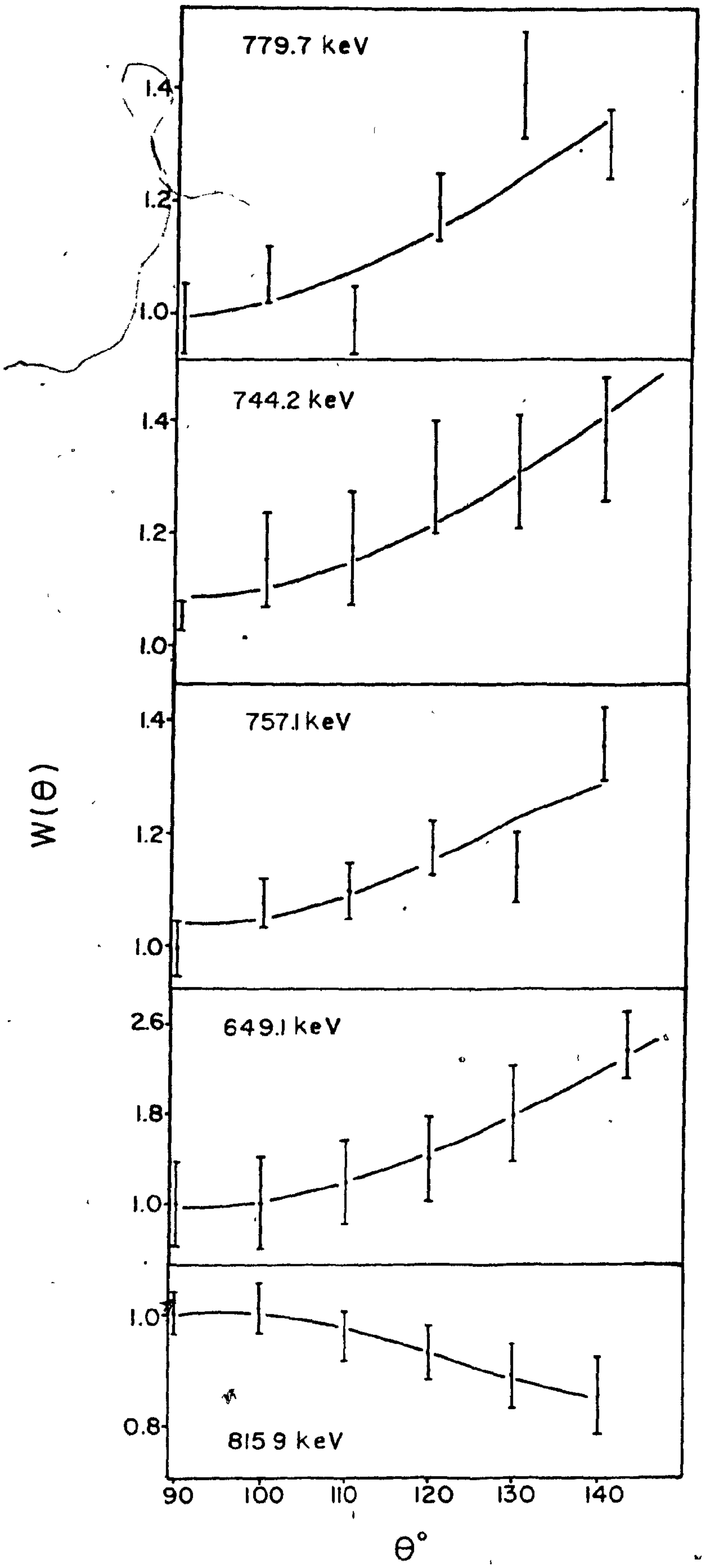

779.7 keV
744.2 keV
757.1 keV
649.1 keV
815.9 keV
W(Θ)
Θ°
1.4
1.2
1.0
2.6
1.8
0.8
90
100
110
120
130
140

TABLE 11.

^{122}Xe Experimental Coefficients A_2 and A_4 and Attenuation Coefficients α_2

E_γ (keV)	A_2	A_4	α_2
331.3	+.35 (4)	+.10 (4)	.48 (5)
497.35	+.39 (4)	+.07 (4)	.75 (7)
560.37	+.40 (6)	+.13 (6)	
638.59	+.38 (8)	+.02 (9)	.83 (17)
649.07	+.59 (25)	+.16 (29)	
654.2	+.35 (17)		
684.57	+.31 (17)	-.01 (18)	
744.19	+.32 (14)		
750.68	+.41 (5)	+.07 (6)	.96 (12)
757.13	+.34 (16)	+.05 (16)	
770	+.30 (15)	-.08 (18)	
779.65	+0.23 (6)		
815.89	+.41 (9)	+.08 (9)	1.00 (20)
822.35	+.43 (10)		
838.7	+.29 (12)	+.18 (15)	
843.6	-0.33 (8)		
1098.1	+.28 (17)	-.07 (20)	

The attenuation coefficients are calculated as the ratio of experimental and theoretical A_2 coefficients.

coefficients are the product of the attenuation coefficient of alignment $\alpha_K(J_i)$ and the theoretical A_K coefficient for complete alignment. The attenuation of the expected anisotropy depends on the spin of the level feeding the transition. In the present measurement, the attenuation coefficients α_2 have been determined experimentally, and the values obtained have been used in making spin assignments. Fig. 50 represents these α_K coefficients as a function of spin. We can conclude from these data that the attenuation is largest for small spin values and approaches unity for high-spin states at the top of the band, in agreement with the calculation of Yamazaki (1967). This decrease in the value of the initial attenuation factor is a natural consequence of the stretched E2 cascade in the ground band (Yamazaki 1967) and is due to the direct "side-feeding" into the rotational levels (Draper and Lieder 1970).

Pure electric quadrupole (E2) transitions have positive A_2 values, while pure dipole transitions have negative A_2 values. The anisotropy pattern of the dipole transition would vary depending on the amount of mixing of other radiations; therefore a positive A_2 value excludes only pure dipole radiation. Transitions with multipoles higher than dipole or electric quadrupole have been assumed to be too slow compared to the spin relaxation time - therefore the attenuation coefficients should be equal to zero and the angular distribution isotropic. The angular distribution measurements carried out for ^{122}Xe indicated patterns characteristic of pure E2 transitions.

iv. Level Scheme and Spin Assignments

The level scheme of ^{122}Xe [Fig. 51] was constructed on the basis of regular spacing of the transition energies, relative intensities of

Figure 50

The attenuation coefficient α_2, for γ-rays deexciting the ground band of ^{122}Xe, as a function of spin.

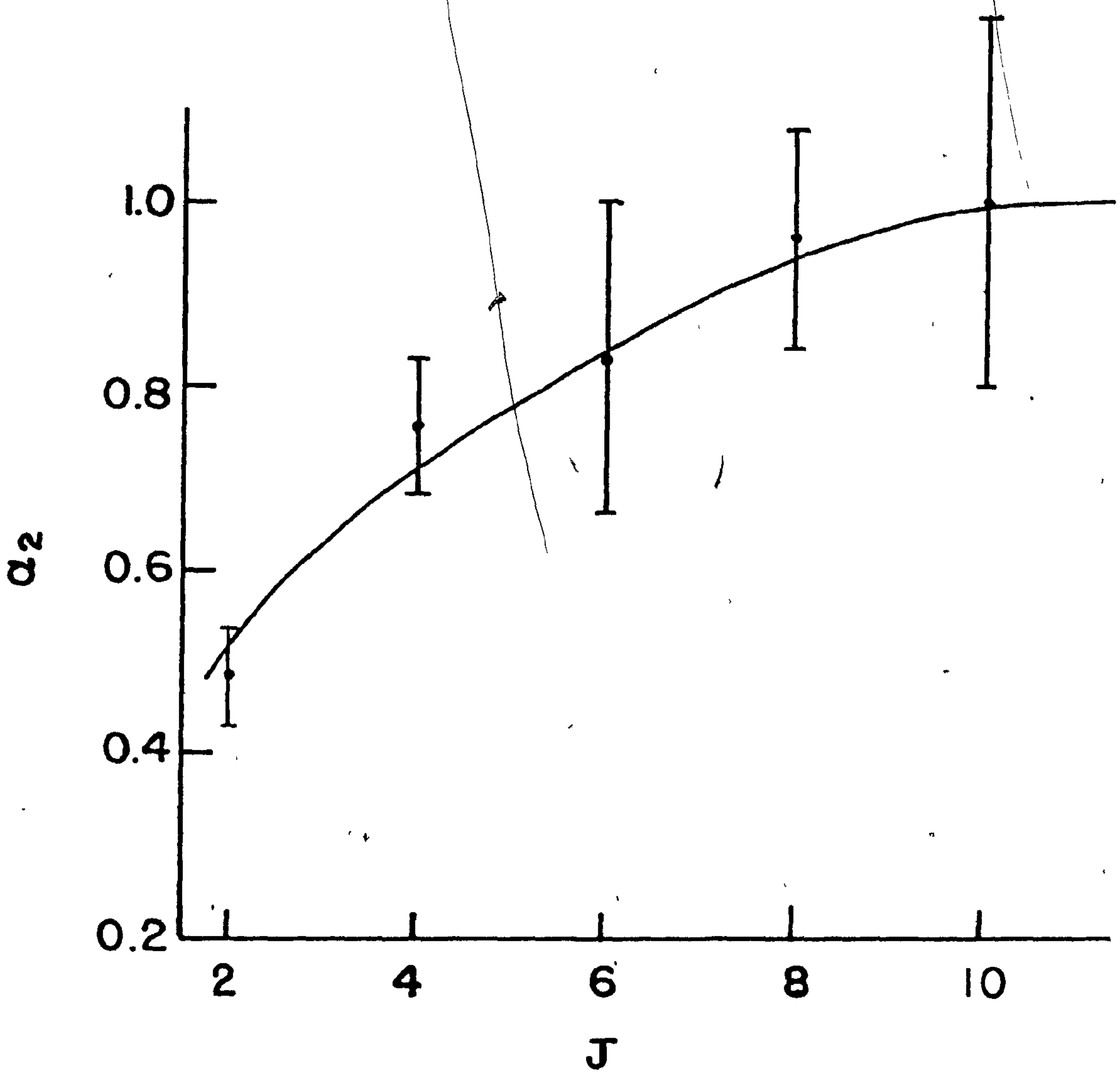
1.0
0.8
0.6
0.4
0.2
a_2
2
4
6
8
10
J

transitions, and from the cascades revealed by the gamma multiplicity filter. Due to side-feeding the intensities of the ground band transitions increase with decreasing spin. This fact has been used to determine the order of the transitions. The spin and parity assignments were based on the angular distribution results and deexciting gamma rays.

Members of the ground band were observed up to a spin of 14^+ (and possibly 16^+) with the backbending occurring at the spin of 10^+, where the transition energy starts to decrease. This is the first backbending to be observed in very neutron-deficient xenon nuclei since earlier studies identified levels only up to those with a spin of 8^+ or 10^+. This is also the first angular distribution measurement to be carried out for ^{122}Xe. The present results on the ground band up to the 2217 keV (8^+) level are consistent with those observed in the in-beam study by Clarkson et al.(1967), and are in agreement with the decay study of ^{122}Cs (Genevey-Rivier et al. 1977). The spacing of the 750.7, 822.4, 779.7 and 744.2 keV transitions varies smoothly and shows a steady decrease in intensity with increasing excitations. The cascade structure of these transitions was revealed by the multiplicity filter results. From coincidence relations, relative yields and the angular distribution coefficients, the levels at 3040, 3819 and 4564 keV are assigned a 10^+, 12^+ and 14^+ spin and parity. The decay study of ^{122}Cs (Genevey-Rivier et al. 1977) assigned an 813.0 keV transition as the $10^+ \rightarrow 8^+$ transition. This assignment is in error since this transition is not observed as the member of high multiplicity transitions in the present in-beam study.

A $\Delta I = 2$ band is seen in coincidence with the 815.9 keV transitions, which has a negative A_2 angular distribution coefficient. Members of this

Figure 51

Level scheme of ^{122}Xe

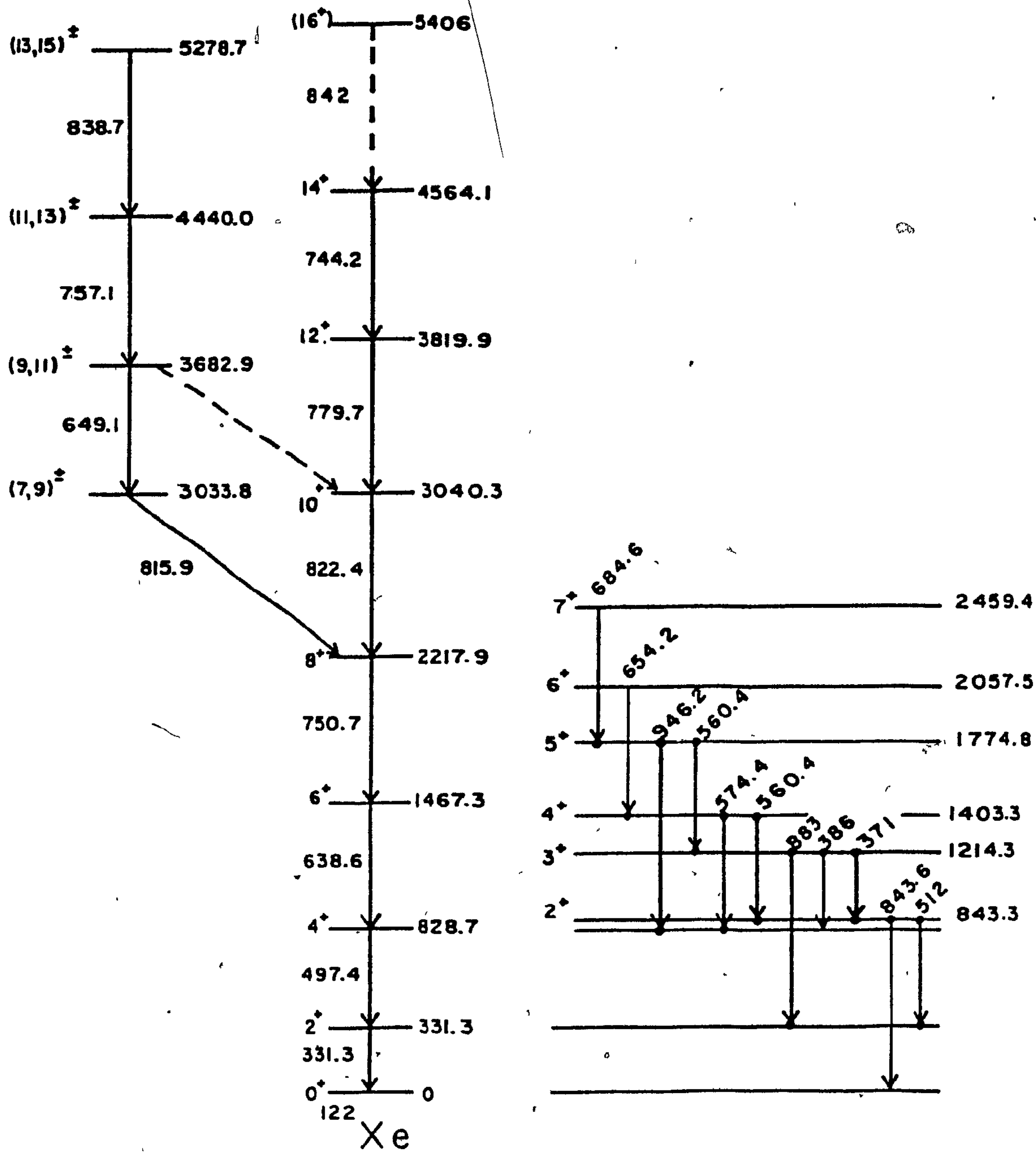
(13,15)±
5278.7
838.7
(11,13)±
4440.0
757.1
(9,11)±
3682.9
649.1
(7,9)±
3033.8
815.9
(16+)
5406
842
14+
4564.1
744.2
12+
3819.9
779.7
10+
3040.3
822.4
8+
2217.9
750.7
6+
1467.3
638.6
4+
828.7
497.4
2+
331.3
331.3
0+
0
7+
684.6
2459.4
6+
654.2
2057.5
5+
946.2
560.4
1774.8
4+
574.4
560.4
1403.3
3+
883
386
371
1214.3
2+
843.6
512
843.3
122Xe

band were found to have high multiplicity in the γ-multiplicity filter measurement. Since the 815.9 keV transition, as well as other members of the band were observed in coincidence with transitions depopulating levels of the ground band up to 8^+, the band head is identified to be the 3033 keV level with $(7,9)^{\pm}$ possible spin. Even though the intensity of the 757 keV transition is higher than that of the 649 keV transition in the singles spectrum, its intensity in the spectra obtained in coincidence with the 750 and 815 keV gamma rays (Fig. 46) is less than that of the 649 keV transition. This supports the order of these transitions in the level scheme.

The present results on the quasi-gamma band are consistent with the finding of the decay study of ^{122}Cs by Genevey-Rivier et al. (1977). In the present work, the 843 keV level assignment of 2_2^+ is consistent with the E2 angular distribution of the 843 keV transition. The assignment of the 512 keV transition as the $2_2^+ \rightarrow 2_1^+$ by the decay study is confirmed in the present in-beam study on the basis of coincidence results. The 1214 keV level is assigned a spin of 3^+ based on the fact that it decays to 2_1^+, 2_2^+ and 4^+ levels. The 4^+ assignment to the 1403 keV level is based on the deexciting gamma-rays and the fact that the 560 keV transition exhibits E2 type angular distribution, while the 574 keV transition to the first 4^+ level is isotropic. The level at 1774 keV feeds 4^+ and 3^+ levels, so its possible spin is 5^+. The 654 and the 684 keV transitions have A_2 values characteristic of E2 transitions. Therefore the levels of 2057 and 2459 keV are assigned 6^+ and 7^+ spins respectively.

b) Band structure in ^{124}Xe

i. Previous Work

In 1965 Morinaga and Lark observed the ground state rotational band in ^{124}Xe by studying the gamma-rays following the (α,4n) reaction on ^{124}Te and reported levels up to the 8^+ state. As in the ^{122}Xe case, their energies had a large uncertainty due to the fact that they used low resolution scintillation counters. No gamma-gamma coincidence measurements were carried out. Later, Bergström et al. in 1969 studied collective levels in ^{124}Xe which they produced in the (α,2n) reaction on enriched ^{122}Te targets. From intensity and angular distribution measurements, they proposed a level scheme up to the 10^+ state and suggested the position of the second excited 2^+ state. Droste et al. in 1972 identified the position of the second excited 2^+ state from the study of ^{124}Cs decay, obtaining a result in disagreement with that of Bergström et al. (1969). The quasi-gamma band in ^{124}Xe was first studied by Kusakari et al. (1975) by means of in-beam γ-ray spectroscopy in the ^{127}I (p,4nγ) ^{124}Xe reaction, where angular distribution and gamma-gamma coincidence measurements were carried out. They proposed a level scheme containing the ground-state rotational band up to 8^+ and the quasi-gamma band up to 5^+. Their 2_2^+ position is in agreement with that of Droste et al. (1972).

ii. Gamma Ray Spectroscopy

The techniques used in the accumulation and the analysis of gamma singles, gamma-gamma coincidence as well as angular distribution measurements are similar to those used in the study of ^{122}Xe which was explained earlier (B(a)). These techniques were also outlined in chapter III.

The singles in-beam spectrum, recorded with the 10% coaxial Ge(Li) detector, is shown in Fig. 52. The labelled gamma rays belong to ^{124}Xe while the other lines in the spectrum are mainly due to ^{125}Xe (α,3n) and ^{126}Xe (α,2n) nuclei produced and to radioactivity. The energies and relative intensities of transitions assigned to ^{124}Xe are presented in table 12. Only 14 of these transitions were identified in the earlier results of Kusakari et al.(1975). The 590 keV line is a doublet comprising a 589.4 and 591.2 keV transition of ^{124}Xe. The two components were separated with the use of the computer code SAMPO [IIIA(ii)] which was used to analyze the gamma ray spectra. The 775 keV line is a mixture of two components of ^{124}Xe and ^{125}Xe. Since the information in the literature about ^{125}Xe was obtained through a different reaction, the relative intensities are likely to differ from those in the present work. Therefore the contribution to the 775 keV line from ^{124}Xe was determined from coincidence results. Similarly the 486 keV line has some contribution from ^{125}Xe; hence its intensity was also obtained from coincidence results.

The gamma multiplicity filter technique [IIIB(iii)] was employed. As with ^{122}Xe, most of the useful results were obtained by analyzing events in which three or more gamma rays were observed in coincidence. Table 13 includes the results of these measurements and Fig. 53 contains the spectra obtained in coincidence with some key gamma transitions.

iii. <u>Angular Distribution Results</u>

The angular distribution measurement analysis for ^{124}Xe were carried out in a fashion similar to that used in the case of ^{122}Xe. The results of these measurements are summarized in table 14 where the A_2 and A_4 coefficients are corrected for limited solid angle. Some of the distribution

Figure 52

Spectrum of gamma-rays emitted in the ^{124}Te $(\alpha,4n\gamma)$ reaction.

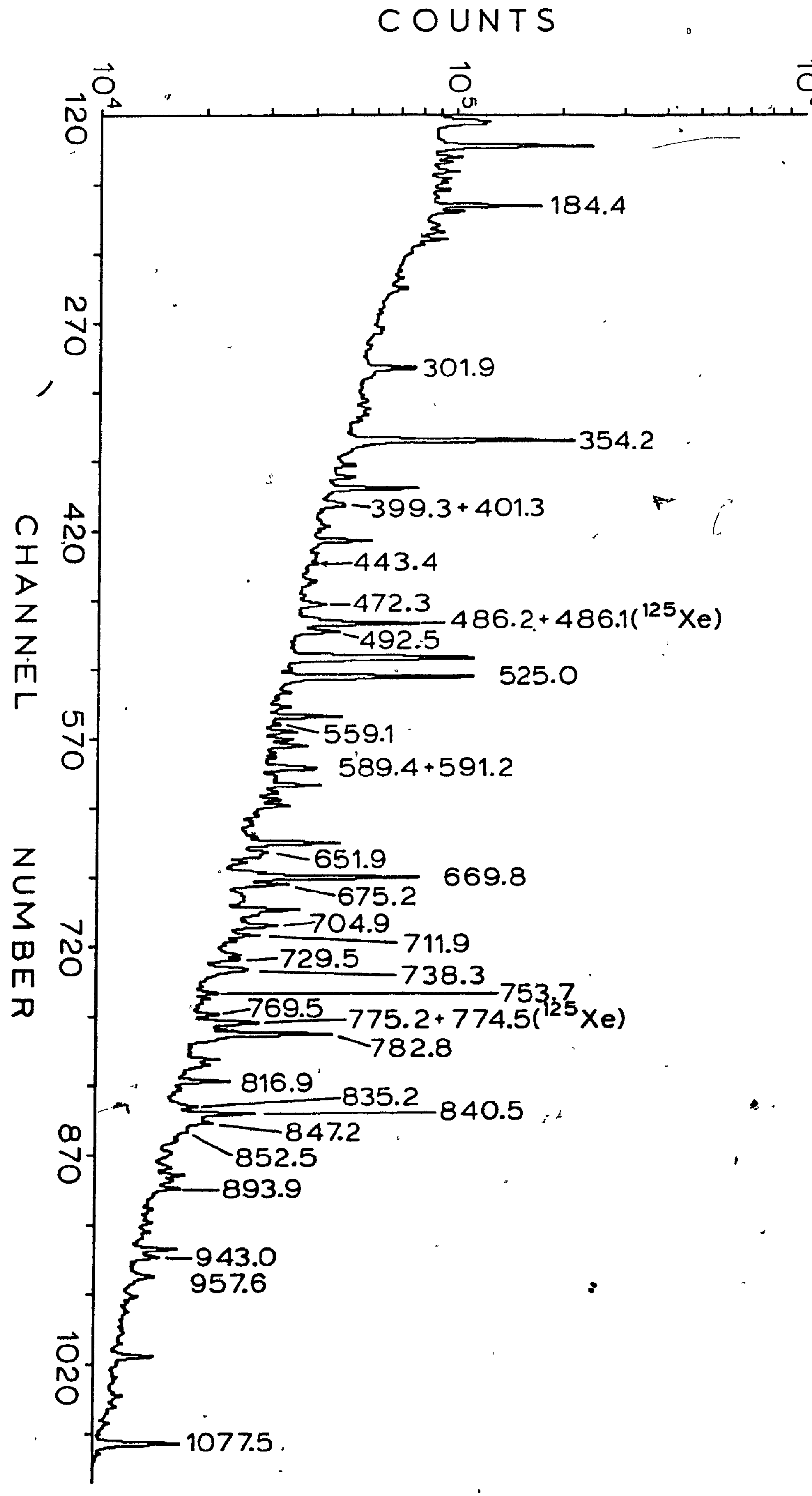

COUNTS
10^4
10^5
10^6
CHANNEL NUMBER
120
270
420
570
720
870
1020
184.4
301.9
354.2
399.3+401.3
443.4
472.3
486.2+486.1(125Xe)
492.5
525.0
559.1
589.4+591.2
651.9
669.8
675.2
704.9
711.9
729.5
738.3
753.7
769.5
775.2+774.5(125Xe)
782.8
816.9
835.2
840.5
847.2
852.5
893.9
943.0
957.6
1077.5

TABLE 12. ^{124}Xe Gamma-Ray Energy and Intensity

E_γ (keV)	I_γ	E_γ (keV)	I_γ
184.44 ± .03	18.5 ± 0.9	711.88 ± .06	7.0 ± 0.3
301.91 ± .02	7.5 ± 0.2	729.48 ± .05	5.9 ± 0.3
354.17 ± .02	100	738.3 ± 0.4	6 ± 2
386.9 ± 0.3	0.5 ± 0.1	753.68 ± .05	5.3 ± 0.3
399.3 ± 0.1	3.3 ± 0.2	769.0 ± .2	4.1 ± 0.5
401.3 ± 0.1	3.7 ± 0.2	775.2* ± .4	6.3 ± .5
443.4 ± 0.1	1.7 ± 0.1	782.84 ± .03	43.0 ± 1.5
472.3 ± 0.1	4.7 ± 0.3	816.93 ± .04	10.6 ± 0.4
486.2* ± 0.5	5 ± 1	835.2* ± .4	4.8 ± 0.3
492.5 ± 0.1	7.7 ± 0.4	840.51 ± .04	18.8 ± 0.7
524.98 ± .03	83 ± 2.4	847.1* ± .4	4.5 ± 0.5
559.1 ± 0.1	2.5 ± 0.3	852.5 ± .2	2.5 ± 0.3
589.4 ± 0.1	6.3 ± 0.7	893.9 ± .1	5.3 ± 0.5
591.2 ± 0.1	8.1 ± 0.7	943.0 ± 0.1	3.8 ± .2
615.88 ± .07	4.7 ± 0.2	957.6 ± 0.3	2.8 ± 0.3
669.8 ± .03	69 ± 2.3	1077.5 ± .05	15.4 ± 0.7
675.15 ± .06	11.2 ± 0.6	1127.97 ± .05	7.2 ± 0.4
704.9 ± 0.1	9.4 ± 0.5		

*Intensity obtained from coincidence results.

TABLE 13. ^{124}Xe Gamma-Ray Energy and Intensity

GATE E_γ(keV)	Coincident Gamma Rays, E_γ(keV)
184.4	301.9, 354.2, 450, 472.3, 525.0, 651.9, 669.8, 675.2, 753.7, 1077.5
301.9	184.4, 354.2, 447, 525.0, 547, 669.8, 675.1, 684, 874, 1031, 1077.5
354.2	184.4, 301.9, 401.3, 472.3, 486.2, 492.5, 525.0, 559.1, 589.4, 591.2, 651.9, 669.8, 675.1, 711.9, 729.5, 738.3, 753.7, 782.8, 803, 816.9, 840.5, 852.5, 893.9, 1077.5, 1128
399.3,401.3	354.2, 559.1, 589.4, 769.0
472.3	354.2, 525.0, 669.8, 675.1, 1128.0
486.2	210, (301.9), 354.2, 525.0, [644], [774], 893.9, 1077.5
492.5	(301.9), 354.2, (382), 401.3, 589.4, 591.2
525.0	184.4, 354.2, 623, 651.9, 669.8, 675.2, 704.9, 711.9, 729.5, 782.8, 803, 816.9, 840.5, 852.5, 1077.5, 1128
589.4,591.2	354.2, 399.3, 401.3, 492.5, 704.9, 738.3, 769.0, 847.1
651.9	354.2, 669.8, 1077.5
669.8	184.4, 301.9, 354.2, 486.2, 525.0, 576, 597, 621, 651.9, 675.1, 711.9, 729.5, 775.2, 782.8, 816.9, 835.2, 840.5, 852.5, 1077.5, 1128
675.1	184.4, 301.9, 354.2, 525.0, 669.8, 704.9, 740, 775.2, 782.8, 816.9, 835.2, (847)
704.9	354.2, (381), 492.5, 559.1, 591.2, 847.1, (957.6)
711.9	354.2, 516, 525.0, 669.8, 729.5, 782.8, 840.5, 852.5
729.5	354.2, 525.0, 588, 669.8, 711.9, 782.8, 840.5, 852.2

TABLE 13. ^{124}Xe Gamma-Ray Energy and Intensity (cont'd)

GATE E_γ(keV)	Coincident Gamma Rays, E_γ(keV)
738.3	354.2, 525.0, 573, 589.4, 847.1
753.7	525.0, 782.8, 1077.5
775.2	354.2, [486], 525.0, [644], 669.8, 675.1, 782.8, 816.9, 835.2 885
782.8	354.2, 525.0, 651.9, 669.8, 675.1, 711.9, 729.5, 775.2, 816.9, 840.5, 869
816.9	354.2, 525.0, 599, 669.8, 675.1, 684, 775.2, 782.8
835.2	354.2, 492.5, 525.0, 558, 669.8, 675.1, 775.2, 782.8, 816.9, 962
840.5	[331], 354.2, 525.0, 669.8, 711.9, 729.5, 769.0, 782.8, 835.2, 852.5, 893.9
847.1	401.3
852.5	354.2, 669.8, 711.9, 729.5, 782.8, 840.5
893.9	354.2, 589.4, 671
943.0	354.2, 525.0, 669.8
957.6	354.2, 525.0
1077.5	184.4, 301.9, 354.2, 486.2, 525.0, 651.9, 669.8, 753.7
1128.0	354.2, 472.3, 525.0, 669.8, 675.1

( ): Uncertain

[ ]: Belongs to another isotope

Figure 53

Background-subtracted coincidence spectra for ^{124}Xe obtained in the γ-multiplicity filter measurement.

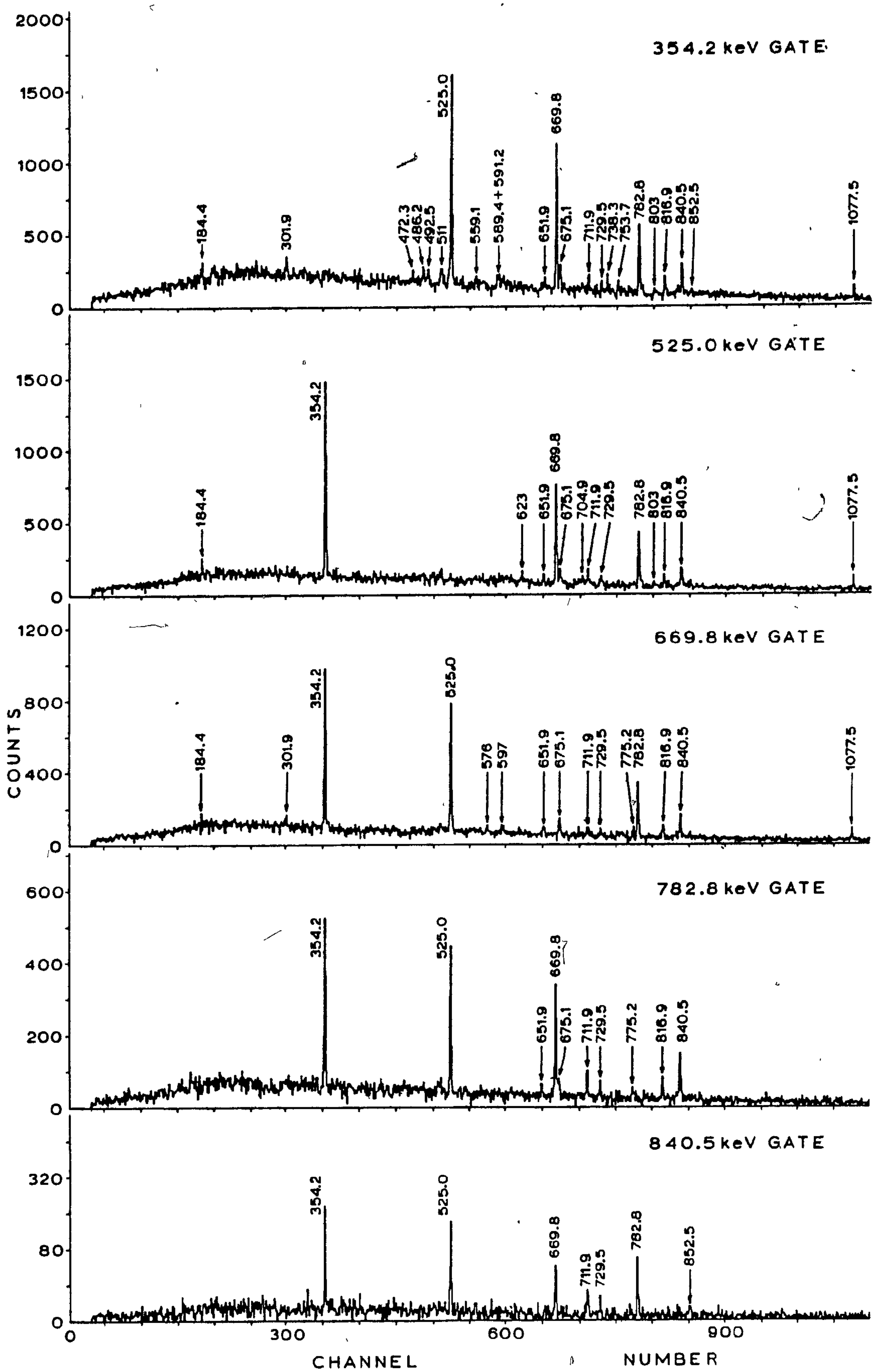

354.2 keV GATE
525.0 keV GATE
669.8 keV GATE
782.8 keV GATE
840.5 keV GATE
COUNTS
CHANNEL NUMBER
184.4
301.9
472.3
486.2
492.5
511
525.0
559.1
589.4+591.2
651.9
669.8
675.1
711.9
729.5
738.3
753.7
782.8
803
816.9
840.5
852.5
1077.5
354.2
623
704.9
576
597
775.2

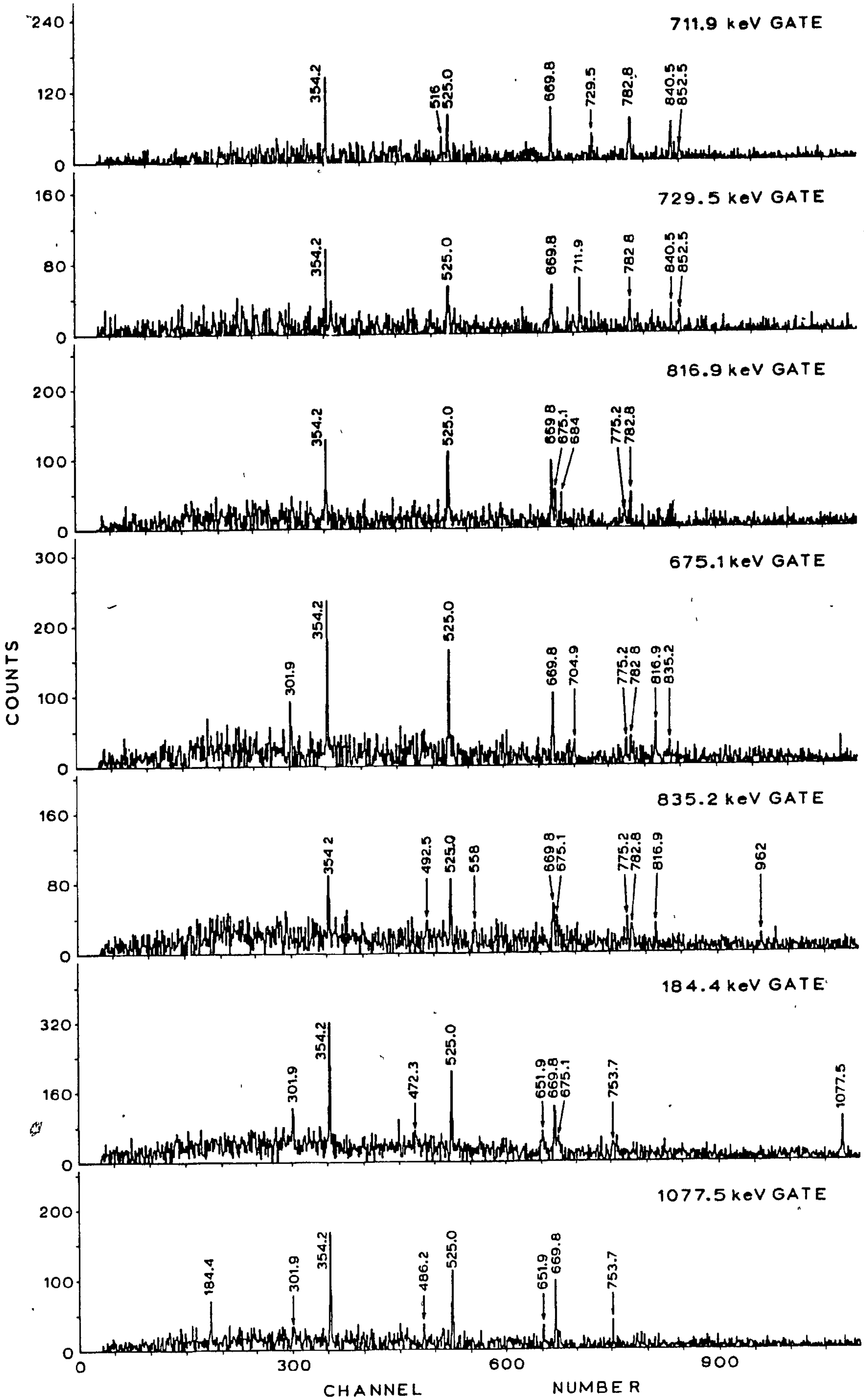
711.9 keV GATE
729.5 keV GATE
816.9 keV GATE
675.1 keV GATE
835.2 keV GATE
184.4 keV GATE
1077.5 keV GATE
COUNTS
CHANNEL NUMBER
354.2
525.0
669.8
301.9
1077.5

TABLE 14. ^{124}Xe Experimental Coefficients A_2 and A_4 and Attenuation Coefficient α_2

E_γ(keV)	A	±	A	±	α_2
184.44	-.30	(8)	-.00	(8)	
301.91	-.80	(15)	-.17	(18)	
354.17	+.21	(3)	-.09	(3)	.29(4)
399.3	-.68	(27)	-.15	(26)	
401.3	+.11	(8)			
524.98	+.27	(5)	-.06	(5)	.53(10)
589.4	+.41	(16)			
651.88	+.48	(12)			
669.8	+.29	(4)	-.15	(4)	.64(9)
675.15	+.51	(17)	+.13	(17)	
704.9	+.49	(8)	+.17	(9)	
711.88	+.35	(9)			
729.48	+.21	(10)			
753.68	+.33	(17)	+.00	(18)	
775.2	+.58	(15)	+.02	(16)	
782.84	+.30	(5)	-.05	(6)	.70(12)
816.93	-.22	(8)	0		
840.51	+.24	(9)	+.02	(10)	.59(23)
894	+.31	(8)			
957.6	+.35	(21)	+.18	(21)	
1077.5	-.26	(8)	-.13	(8)	
1127.97	-.16	(11)			

The attenuation coefficients α_2 are calculated as the ratio of experimental and theoretical A_2 coefficients.

patterns obtained in these measurements are presented in Fig. 54 and 55. The measured α_2 attenuation coefficients are plotted versus the spin of the level feeding the transition (Fig.56). As in the ^{122}Xe case, α_2 increases with the spin of the γ-ray emitting level and approaches a value of unity (complete alignment) for high spin states. However the attenuation in the case of ^{124}Xe is stronger than that of ^{122}Xe (Fig. 50). This could be due to long-lived states partly feeding the transitions. The degree of attenuation along with the A_2 and A_4 experimental and theoretical (Yamazaki 1967) values were used in making spin assignments.

For some weak γ-rays, and for those γ-rays that form part of a multi-component peak and which were not easy to separate, the large error bars on the intensity prevented a spin assignment from the angular distribution study. Most of the transitions observed in ^{124}Xe have distribution patterns characteristic of pure E2 transitions; however there are a few that have negative A_2 value characteristic of dipole transitions.

iv. Level Scheme and Spin Assignments

The proposed level scheme of ^{124}Xe is shown in Fig. 57. This decay scheme was constructed on the same general principles used to construct the level scheme of ^{122}Xe [a(iv)].

The ground state band is observed up to the 14^+ level and possibly the 16^+ level. The backbending occurs at a spin of 10^+ where the transition energies are smaller than those depopulating the next lower I level. The spin-parity assignments of 2^+, 4^+, 6^+ and 8^+ to the 354, 879, 1549 and 2331 keV levels respectively are in agreement with the previous in-beam studies of Bergström et al. (1969) and Kusakari et al. (1975). From the regular spacing of the energies of the 840.3, 711.9 and 729.5 keV transitions,

Figure 54

Angular distribution patterns for some gamma rays of those emitted in the $^{124}Te(\alpha,4n\gamma)$ reaction.

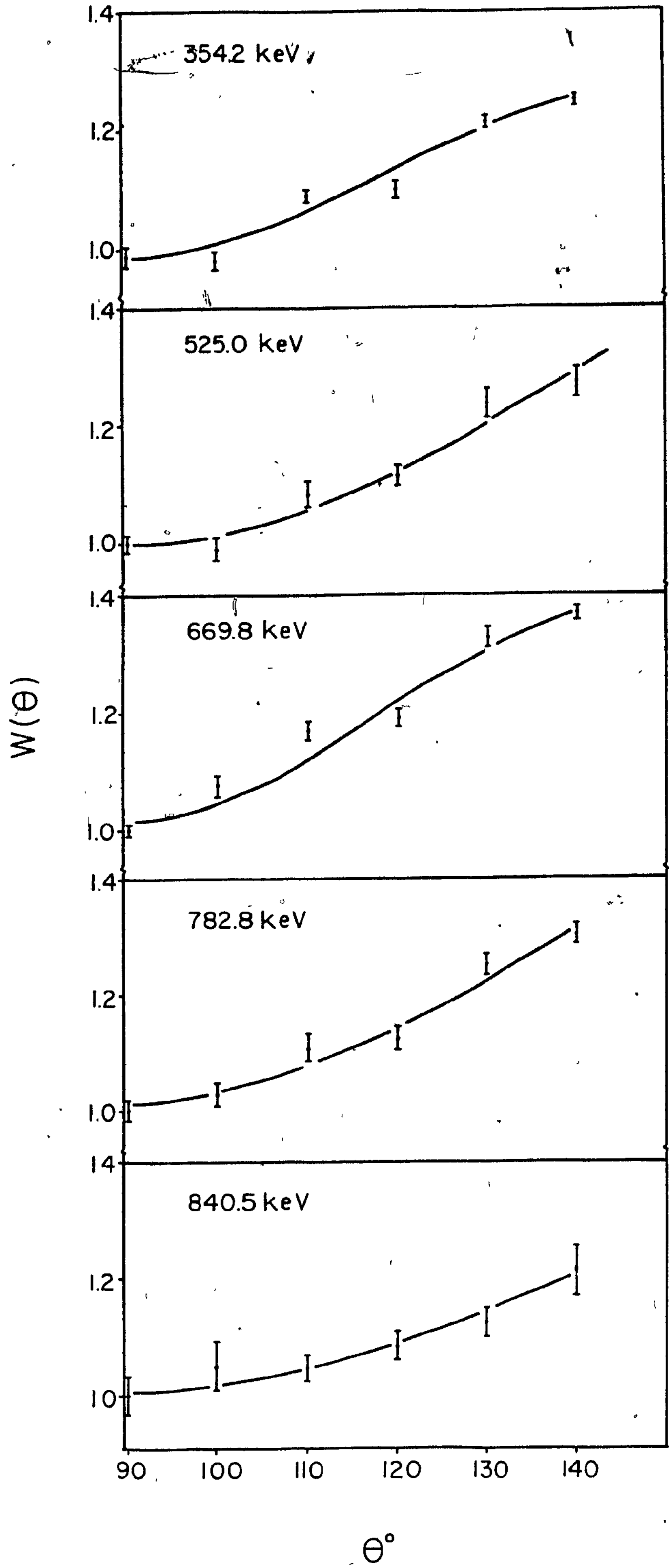
354.2 keV
525.0 keV
669.8 keV
782.8 keV
840.5 keV
1.4
1.2
1.0
W(θ)
90
100
110
120
130
140
θ°

<u>Figure 55</u>

Angular distribution patterns for some gamma rays of those emitted in the $^{124}Te(\alpha,4n\gamma)$ reaction.

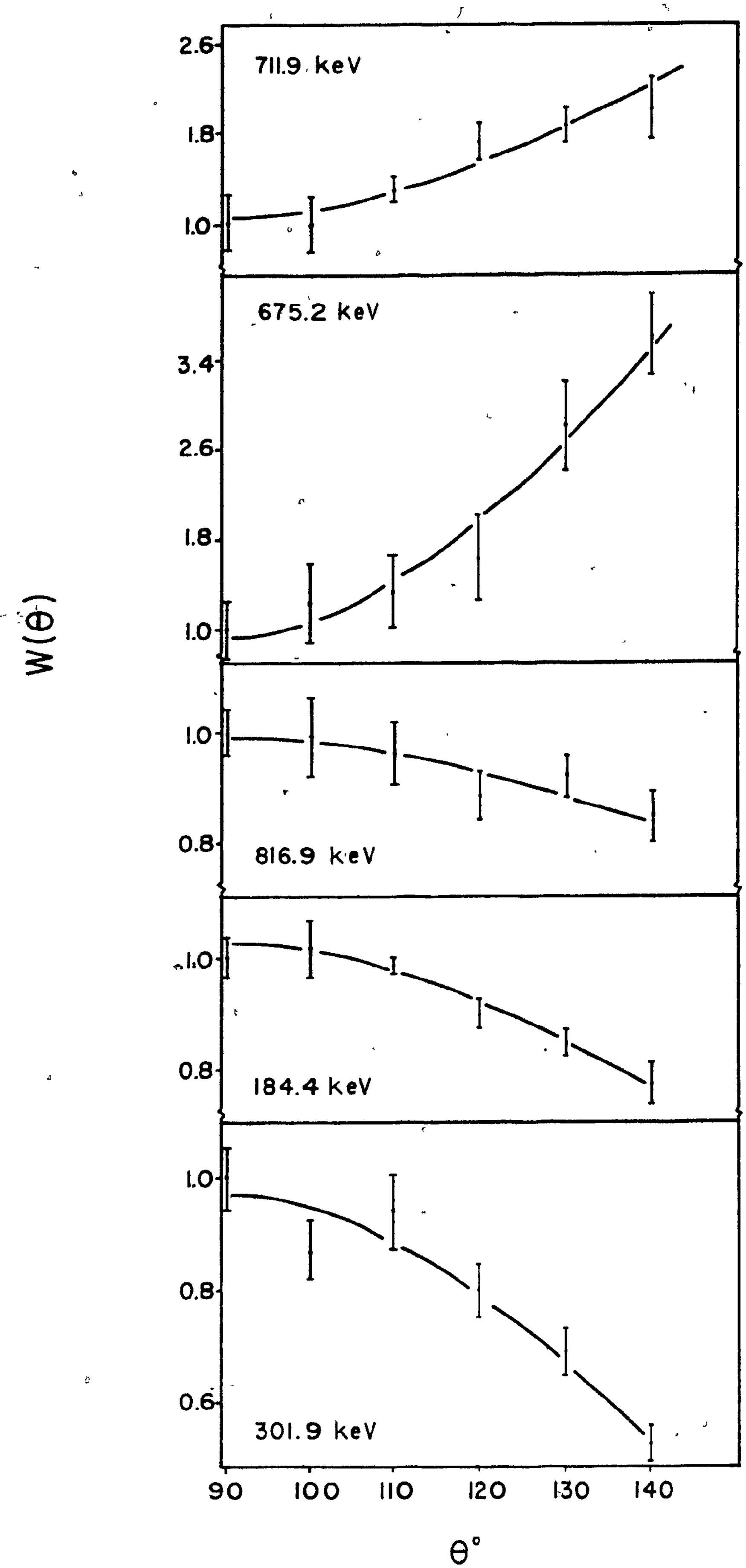
711.9 keV
675.2 keV
816.9 keV
184.4 keV
301.9 keV
W(θ)
θ°
2.6
1.8
1.0
3.4
2.6
1.8
1.0
1.0
0.8
1.0
0.8
1.0
0.8
0.6
90
100
110
120
130
140

Figure 56

The attenuation coefficient α_2, for γ-rays deexciting the ground band of ^{124}Xe, as a function of spin.

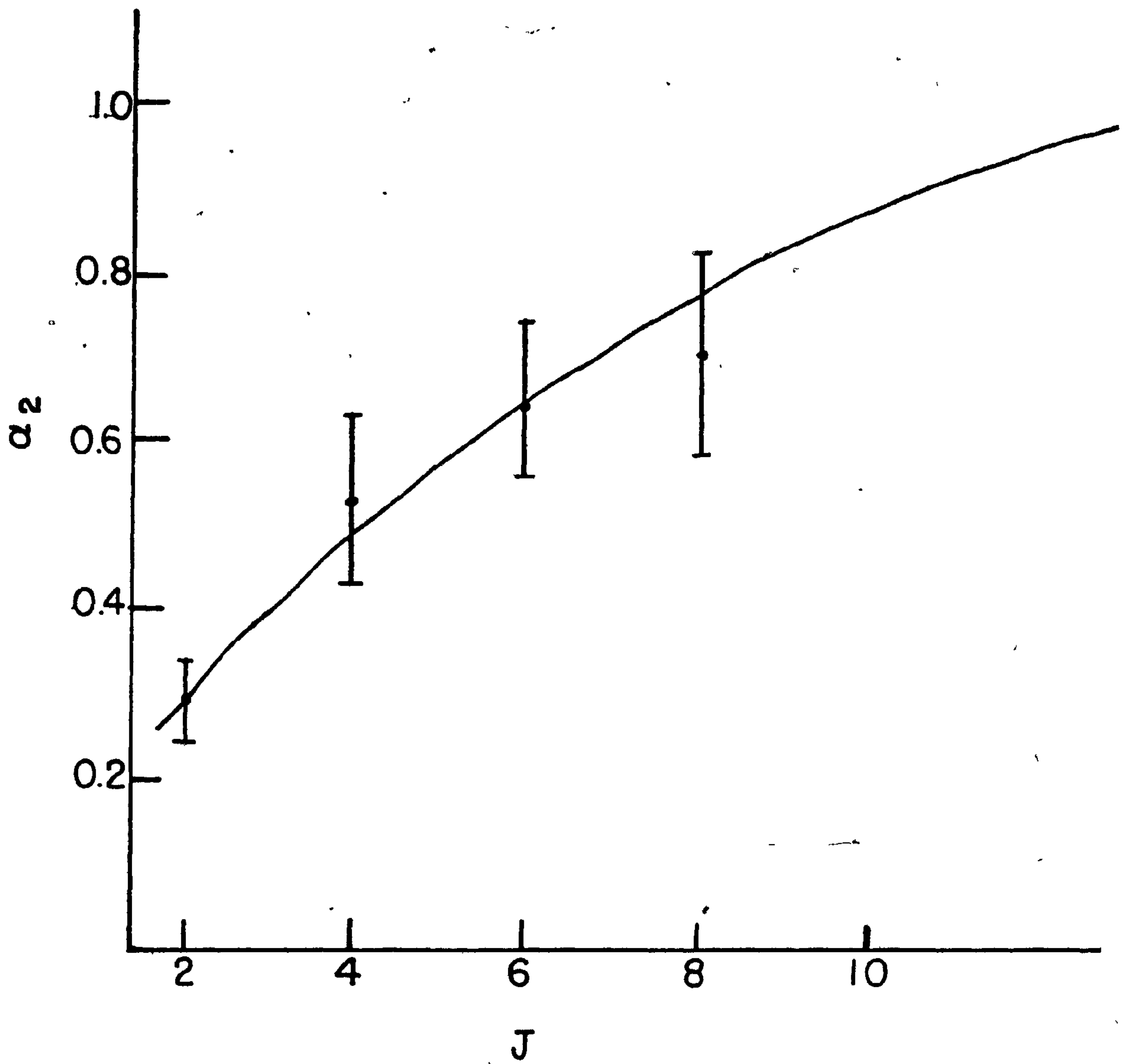

1.0
0.8
0.6
0.4
0.2
a_2
2
4
6
8
10
J

their intensities and the coincidence results as well as multiplicity information, the levels at 3172, 3884 and 4613 keV are assigned a 10^+, 12^+ and 14^+ spin-parity, respectively. This assignment is consistent with the angular distribution results.

A cascade of γ-rays of 675, 775 and 835 keV which were identified in the multiplicity filter measurement as belonging to long cascades, was observed to be in coincidence with the 816.9 keV transition and with transitions between yrast levels up to 8^+. The 816.9 keV transition was also observed in coincidence with those ground band transitions. Both the 675 and 775 keV transitions exhibit E2 - type angular distributions; therefore the cascade is proposed to be a $\Delta I = 2$ band based on the 3148.7 keV state. Since the 816.9 keV transition has a negative A_2 coefficient it is most likely a pure M1 or E1 transition. Therefore the state at 314.8 keV, the sideband head, has a spin of $(7, 9)^{\pm}$.

The gamma band observed in the present work is consistent with that of Kusakari et al. (1975). The angular distribution of the 492 keV transition is isotropic, which confirms the second 2^+ assignment made in the decay study of ^{124}Cs of the present work. The 401 keV line was previously identified as the $2_2^+ \rightarrow 2_1^+$ transition by Bergström et al. (1969). From the coincidence results of both decay and in-beam study and the fact that the 401 keV transition has a positive A_2 value, this assignment is incorrect. The level at 1248 keV is assigned as 3^+ on the basis of its decay to 2_1^+, 2_2^+ and 4_1^+ levels and no feeding to the ground state. This is supported by the positive A_2 values of the 401 keV and the 894 keV transitions which exclude a 3^- assignment. Since the level at 1438 keV decays to 4_1^+ and 2_2^+ levels and the 559 keV transition to the 4_1^+ level is isotropic its spin is proposed to be 4^+. Based on the deexciting gamma rays and the angular

Figure 57

Level Scheme of ^{124}Xe

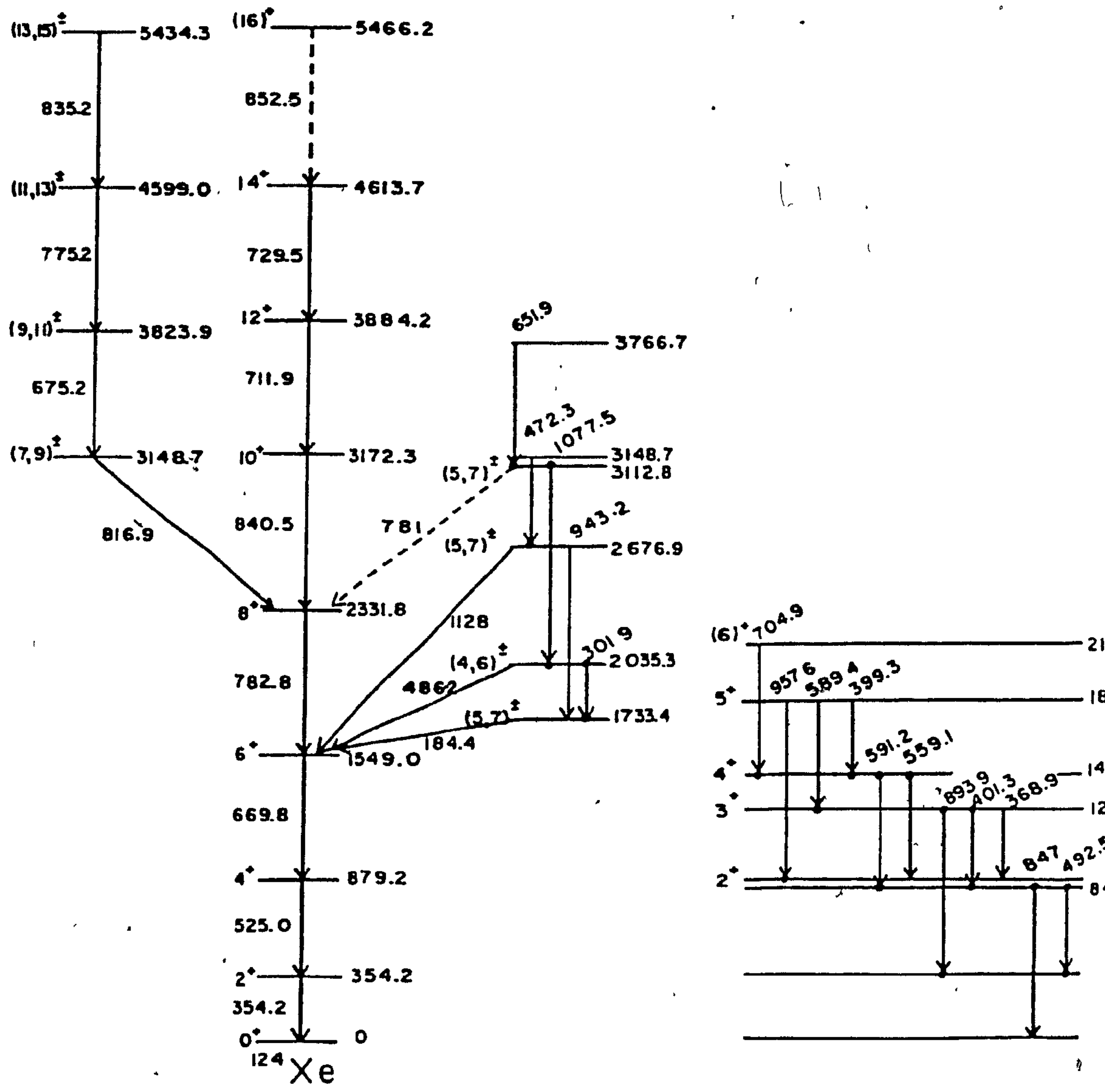

(13,15)± 5434.3
(16)+ 5466.2
835.2
852.5
(11,13)± 4599.0
14+ 4613.7
775.2
729.5
(9,11)± 3823.9
12+ 3884.2
675.2
711.9
651.9
3766.7
472.3
1077.5
(7,9)± 3148.7
10+ 3172.3
(5,7)± 3148.7
3112.8
816.9
840.5
781
(5,7)± 2676.9
943.2
8+ 2331.8
1128
(4,6)± 2035.3
301.9
782.8
486.2
(5,7)± 1733.4
6+ 1549.0
184.4
669.8
4+ 879.2
525.0
2+ 354.2
354.2
0+ 0
124Xe
(6)+ 704.9 2143.0
957.6
589.4
399.3
5+ 1837.4
591.2
559.1
4+ 1438.1
893.9
401.3
368.9
3+ 1248.0
847
492.5
2+ 846.7

distribution of both the 589 and the 957 keV transitions the level at 1837 keV is identified as the 5^+ level of the gamma band.

The 184 keV transition has a negative A_2 value (-0.3 ± 0.077), and feeds a 6^+ level; therefore the 1733 keV level has possible spins of $5^\pm$ or $7^\pm$. The large negative A_2 value of the 301 keV transition ($-0.805 \pm .153$) implies that the transition is of (M1 + E2) multipolarity which restricts the spin of the 2035 keV level to $4^\pm$ if the 1733 keV level has a spin $5^\pm$ and to a $6^\pm$ spin if that level has a $7^\pm$ spin and parity.

CHAPTER V - THEORETICAL DISCUSSION

A. EVEN-A ISOTOPES

a. i. Description of the Interacting Boson Approximation

In the framework of the Interacting Boson Approximation (IBA) the collective nuclear states of even-even nuclei are constructed as states of N bosons. These states are described by symmetric couplings of proton and neutron pairs. These J = 0 and J = 2 pairs are represented by s- and d-bosons respectively, where the boson space is constructed by using boson creation and annihilation operators with L = 0 and L = 2 (Arima et al. 1977):

$$(s^+s)^{(0)},\ (d^+ \times d)^{(0)},\ (d^+ \times d)^{(1)}_{\mu},\ (d^+ \times d)^{(2)}_{\mu},$$

$$(d^+ \times d)^{(3)}_{\mu},\ (d^+s)^{(2)}_{\mu}\ \text{and}\ (s^+d)^{(2)}_{\mu} \qquad (1)$$

The Hamiltonian of the system includes one-boson terms [the scalars in (1)] and two-boson interactions [the scalar products of the operators in (1)] and the total number of bosons N[$= n_s + n_d$] (which is conserved). The operators in (1) are the generators of U(6): therefore the eigenstates are symmetric irreducible representations [N] of SU(6) in the space of s- and d- bosons. The spectrum of the nucleus is defined by the single boson energy difference ($\varepsilon = \varepsilon_d - \varepsilon_s$) and by the two-body matrix elements:

$$\langle d^2L|V|d^2L\rangle\ (L = 0,2,4),\ \langle d^2 0|V|s^2 0\rangle \quad ,$$

$$\langle ds2|V|ds2\rangle,\ \langle ds2|V|d^2 2\rangle,\ \langle s^2 0|V|s^2 0\rangle$$

and by the partition [N] of SU(6) to which it belongs, and the Hamiltonian is given by:

$$H = \varepsilon_s s^+ s + \varepsilon_d \sum_m d_m^+ d_m + \sum_{L=0,2,4} \frac{1}{2}(2L+1)^{1/2} C_L [(d^+d^+)^{(L)} (dd)^{(L)}]^{(0)}$$

$$+\nu_2 [(d^+d^+)^{(2)} (ds)^{(2)} + (s^+d^+)^{(2)} (dd)^{(2)}]^{(0)}$$

$$+ 2^{-1/2} \quad \nu_o [(d^+d^+)^{(0)} (ss)^{(0)} + (s^+s^+)^{(0)} (dd)^{(0)}]^{(0)}$$

$$+ U_2 [(d^+s^+)^{(2)} (ds)^{(2)}]^{(0)} + 1/2 \; U_o [(s^+s^+)^{(0)} (ss)^{(0)}]^{(0)} \qquad (2)$$

With different choices of parameters the Hamiltonians produce both vibrational and rotational spectra.

In the vibrational limit, interactions which change s- bosons into d- bosons are negligible and the system is mostly defined by the single boson energy difference ε. The Hamiltonian is then constructed from operators in (1) that conserve n_d (the number of d- bosons) and n_s (the number of s- bosons) separately (Arima and Iachello 1976a). By eliminating the degrees of freedom of the s- boson, the states in the case are characterized by the number of bosons occupying the L = 2 level (n_d). These states form the basis for the symmetric irreducible representations of the group SU(5) and they are classified by five quantum numbers: the number of d-bosons n_d, the angular momentum L and its third component M, n_β – the number of boson pairs coupled to zero angular momentum ($\nu = n_d - 2n_\beta$) when ν is the boson seniority and n_Δ, the number of boson triplets coupled to zero angular momentum. The Hamiltonian in this limit is written as:

$$H = \varepsilon \sum_m d_m^+ d_m + \sum_L \frac{1}{2} \sqrt{2L+1} \; C_L [(d^+d^+)^{(L)} (dd)^{(L)}]^{(0)} \qquad (3)$$

As the single boson energy difference ε decreases a transition from a vibrational to a rotational spectrum occurs. The Hamiltonian in the rotational limit is constructed from operators which are the generators of U(3). Therefore, the eigenstates are characterized by the irreducible representations of SU(3) in the one-boson space.

ii. Calculation of Collective States of Even-A Xe Isotopes

In the present work we present the results of the calculations of the properties of positive parity collective states in even-even xenon isotopes. In the IBA model, an even-even nucleus with $N_\pi(N_\nu)$ proton (neutron) pairs outside the 50 and 82 closed shells, can be considered as a system of N bosons ($N = N_\pi + N_\nu$). When the major shell contains more protons (neutrons) than proton (neutron) holes, $N_\pi(N_\nu)$ represents the number of proton (neutron) hole pairs. For example ^{116}Xe has $N_\pi = 2$, $N_\nu = 6$ and $N = 8$, while for ^{130}Xe $N_\pi = 2$, $N_\nu = 3$ and $N = 5$. The energies and eigenvectors were calculated with the use of the computer code "PHINT" written by Scholten (1979). The full IBA Hamiltonian (eq. 2) was used, which can be rewritten as:

$$H = \text{HBAR} \times n_d + \sum_{L=0,2,4} \frac{1}{2} \sqrt{2L+1}\, C_L [(d^+d^+)^{(L)} (dd)^{(L)}]^o_o$$

$$+ F[(d^+d^+)^{(2)} (ds)^{(2)} + (s^+d^+)^{(2)} (dd)^{(2)}]^o_o$$

$$+ G[(d^+d^+)^{(0)} (ss)^{(0)} + (s^+s^+)^{(0)} (dd)^{(0)}]^o_o$$

$$+ \frac{\text{CH1}}{2} [(s^+s^+)^{(0)} (ss)^{(0)}]^o_o + \text{CH2} \sqrt{5}\, [(d^+s^+)^{(2)} (ds)^{(2)}]^o_o \qquad (4)$$

where the parameters HBAR ($\equiv \varepsilon = \varepsilon_d - \varepsilon_s$), C_L, F, G, CH1 and CH2 refer to variable names used in the program. In calculating the Hamiltonian the spherical SU(5) basis was used:

$$|\psi> = |[N], n_d, n_\beta, n_\Delta, L_d, L>$$

where

N = total number of bosons = $n_s + n_d$

n_d = number of d- bosons

n_β = number of pairs of d- bosons coupled to L = 0

n_Δ = number of triplets of d- bosons coupled to L = 0

L_d = total angular momentum of d- bosons

L = total angular momentum of the state

For each value of L, the program finds a set of spherical basis states that have a total angular momentum of L, and it then calculates and diagonalizes the Hamiltonian matrix.

The level spacings of the ground band in even-even nuclei can be written as:

$$\Delta E_{exp}(n) = A + B\,n - Cn^2 \qquad n = 0,1,2,\ldots\ldots \tag{5}$$

The variation of the constant, linear, and quadratic terms as a function of the mass number A of the xenon isotopes is shown in Fig. 58, 59 and 60 respectively. For a vibrational nucleus the value of HBAR (the single boson energy difference) is very close to the energy of the first excited 2^+ state and it decreases for nuclei having more rotational spectra. Nuclei in the transitional region could be fitted using the parameter HBAR, C_4 and G. However as the nuclei vary towards rotational-like spectra

Figure 58

Variation of the constant term in ΔE_{exp} as a function of the mass number.

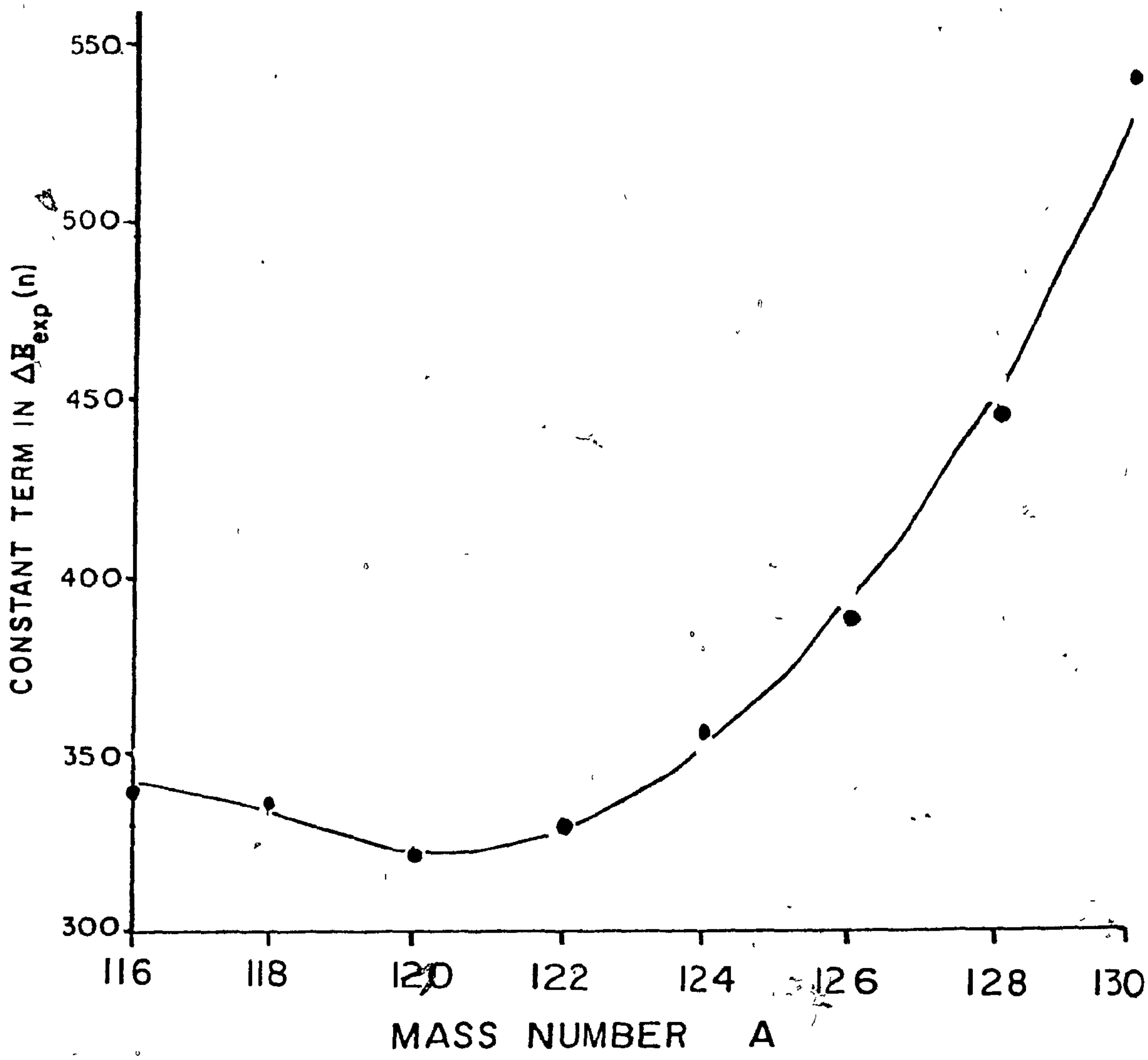
CONSTANT TERM IN ΔB_{exp} (n)
550
500
450
400
350
300
116
118
120
122
124
126
128
130
MASS NUMBER A

Figure 59

Variation of the linear term is ΔE_{exp} as a function of the mass number.

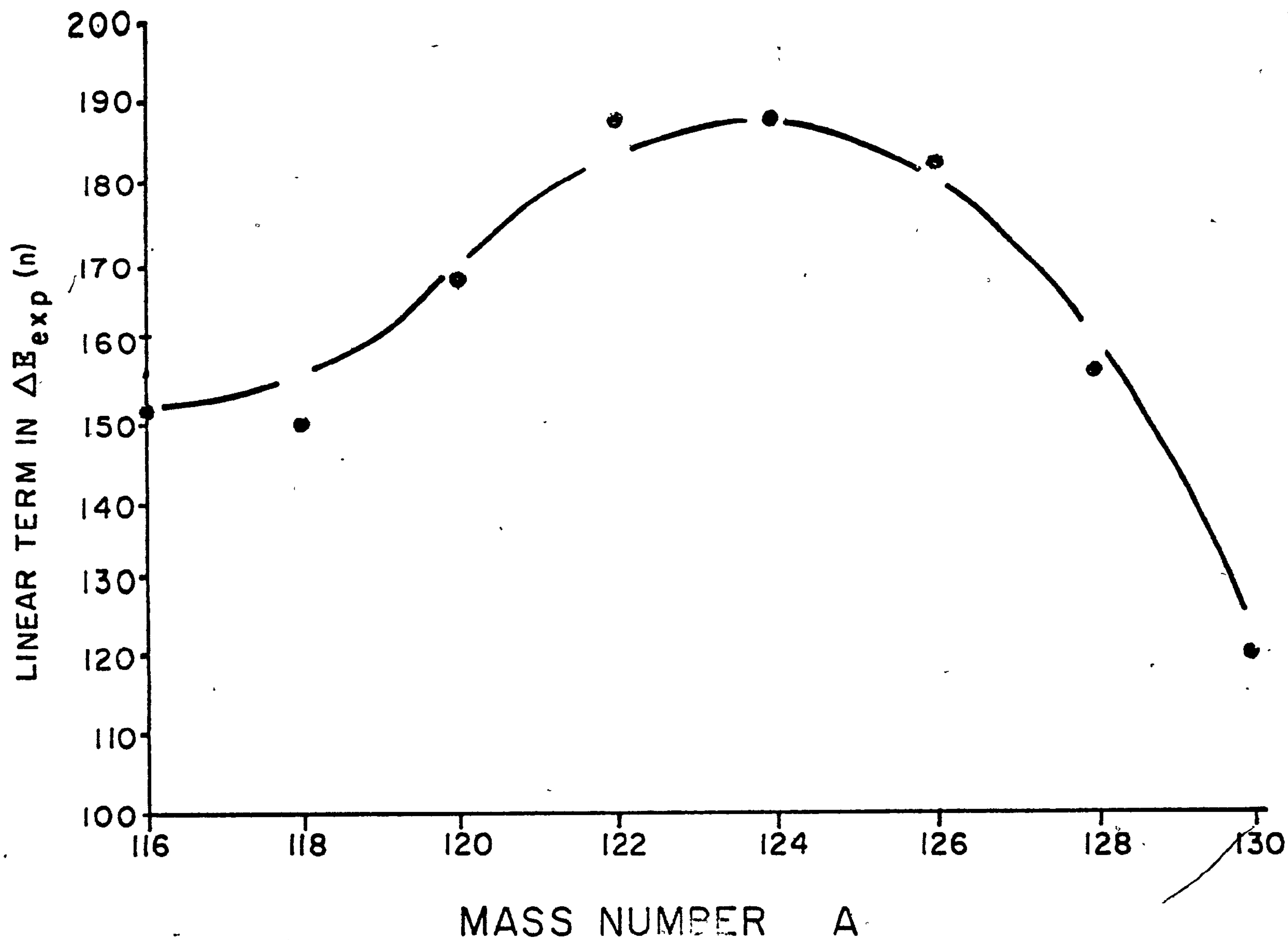

LINEAR TERM IN ΔB_{exp} (n)
200
190
180
170
160
150
140
130
120
110
100
116
118
120
122
124
126
128
130
MASS NUMBER A

Figure 60

Variation of the quadratic term in

ΔE_{exp} as a function of the mass number.

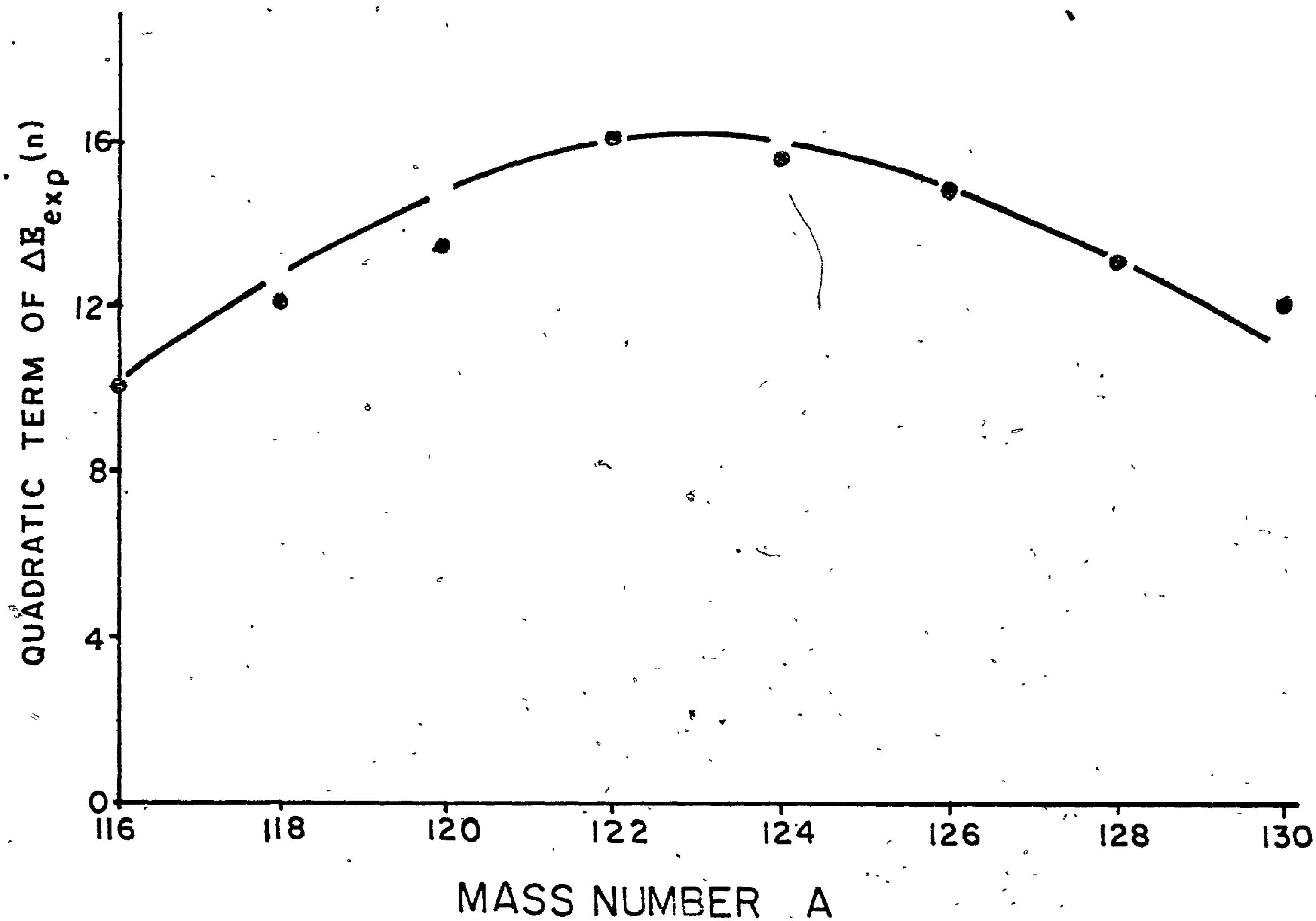
QUADRATIC TERM OF $\Delta B_{exp}(n)$
0
4
8
12
16
116
118
120
122
124
126
128
130
MASS NUMBER A

the parameters CH1 and CH2 have to be included. G, the strength of the interaction ($<d^2 0|H|s^2 0>$) which changes s- bosons into d- bosons, adds a constant linear and a quadratic term to the level spacing of the ground band. HBAR adds a constant term and C_4 ($<d^2 4|H|d^2 4>$), a d- boson - d-boson interaction adds a linear term to the level spacing. In fitting the experimental spectra, a set of HBAR, C_4 and G which would reproduce A,B, and C (eq.(5)) was determined. The calculated, constant, linear and quadratic terms are linear functions of G. Therefore from the experimental value of the quadratic term the corresponding value of G was obtained. From this value the corresponding constant and linear terms that G adds to the level spacing were determined. Finally from the experimental values of the constant and linear terms (A,B in eq.(5)) the values of HBAR and C_4 were obtained. This set of estimated parameters was adjusted slightly and CH1 was included. CH1, which depends on the number of s- bosons, adds a linear term to the level spacing of the ground band and its effect is dependent on the value of G.

In the vibrational limit, the analytic formula for the excitation energies of the Hamiltonian given in eq. (3) (Arima and Iachello 1976a) is:

$$E([N], n_d, n_\beta, n_\Delta, L) = \varepsilon \times n_d + \frac{1}{2}\alpha n_d(n_d - 1)$$

$$+ 2\beta\, n_\beta\, (2n_d - 2n_\beta + 3) + \gamma(L(L+1) - 6n_d) \qquad (6)$$

where α,β,γ can be expressed in terms of C_0, C_2 and C_4:

$\alpha = (4C_2 + 3C_4)/7$

$\beta = (7C_0 - 10C_2 + 3C_4)/70$

$\gamma = (C_4 - C_2)/14$

The inverse relations are:

$$C_4 = \alpha + 8\gamma$$
$$C_2 = \alpha - 6\gamma$$
$$C_0 = \alpha + 10\beta - 12\gamma$$

Different states obtained from this analytic formula are arranged into bands. The important bands are called Y, X, Z and β; which are defined as follows:

Y - band	$\lvert n_d, n_\beta=0, n_\Delta=0, L=2n_d, M >$	$n_d \geq 0$
X - band	$\lvert n_d, n_\beta=0, n_\Delta=0, L=2n_d-2, M >$	$n_d \geq 2$
Z - band	$\lvert n_d, n_\beta=0, n_\Delta=0, L=2n_d-3, M >$	$n_d \geq 3$
β - band	$\lvert n_d, n_\beta=1, n_\Delta=0, L=2n_d-4, M >$	$n_d \geq 2$

where the Y - band is the ground - band and the X and Z bands combine to form what is known more conventionally as the gamma band. The positions of the states in the bands can be calculated from eq. (6). In Fig. 61 the energy differences $\Delta E = E(n_d+1) - E(n_d)$ of various bands are plotted as a function of spin (number of d- bosons), where:

$$\Delta E_y = \varepsilon + C_4\, n_d \qquad n_d \geq 0$$
$$\Delta E_x = \varepsilon + C_4\, n_d - 8\gamma \qquad n_d \geq 2$$
$$\Delta E_z = \varepsilon + C_4\, n_d - 12\gamma \qquad n_d \geq 3$$
$$\Delta E_\beta = \varepsilon + C_4\, n_d + 4\beta - 16\gamma \qquad n_d \geq 2$$

The different bands are parallel, with an equal slope of C_4. Therefore for vibrational-like nuclei the y band depends only on ε (HBAR) and C_4, while the X, Z bands depend on ε, C_4, and C_2. When ε and C_4 have been determined by

Figure 61

The energy difference ΔE for the Y-, X-, Z- amd β- bands as a function of the number of d-bosons (n_d).

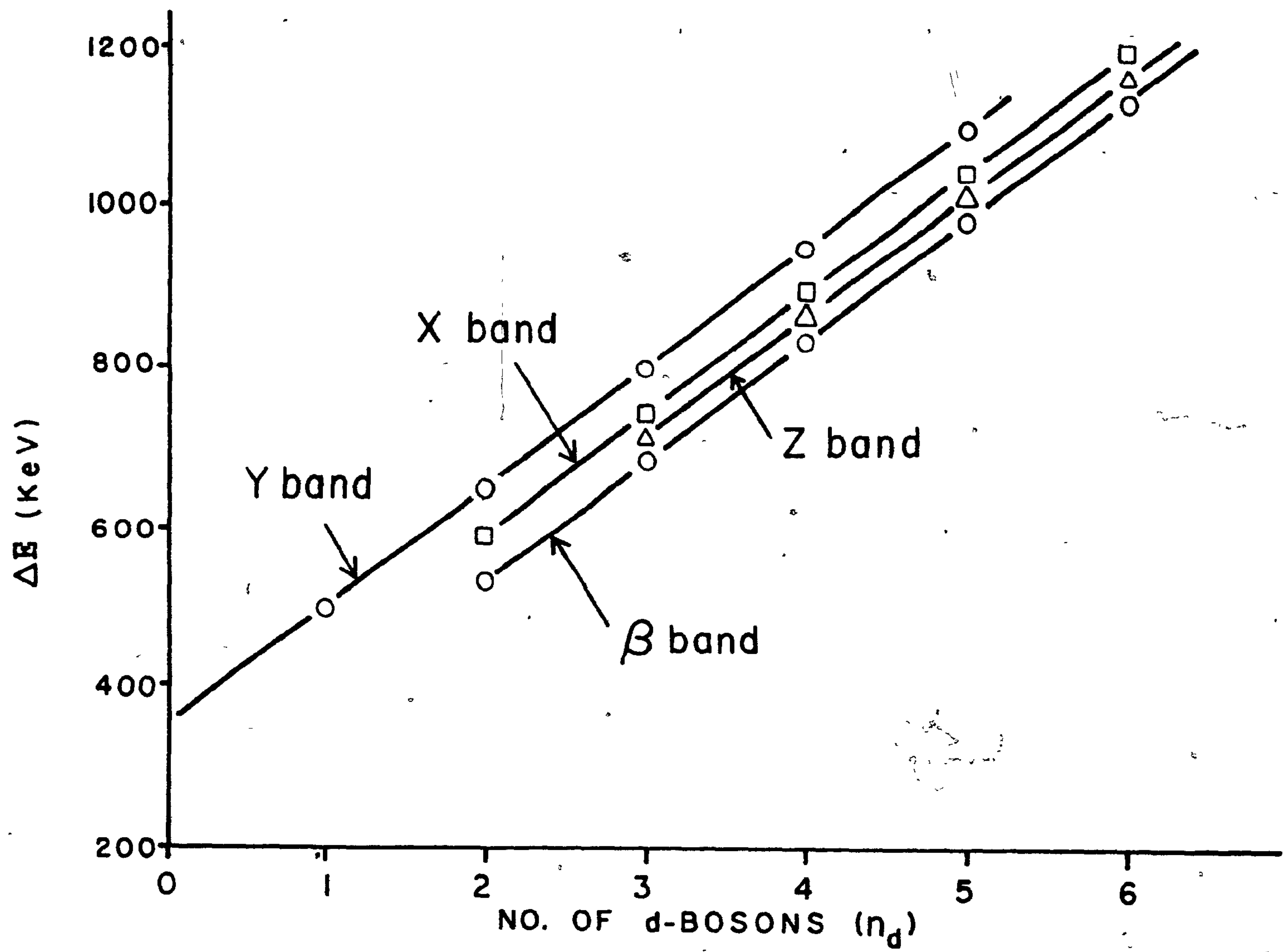

1200
1000
800
600
400
200
ΔE (KeV)
X band
Y band
Z band
β band
0
1
2
3
4
5
6
NO. OF d-BOSONS (n_d)

fitting the ground band (Y - band), the X and Z bands could be used to extract the third parameter C_2. However in the change from vibrational towards rotational nuclei the effect of the interaction which changes s-bosons into d- bosons becomes important. The most effective term in the interaction is $\langle s^2 0|H|d^2 0\rangle$ (G parameter). The effect of the interaction on the X and Z bands is shown in Fig. 62. This effect is dependent on the energy difference between single s- and d- bosons (HBAR $\equiv \varepsilon$). The parameter CH1 ($\langle s^2 0|H|s^2 0\rangle$) has the same effect on the E_x and E_z band energies as it had on the main band, adding a linear term (Fig. 63). Therefore once the ground band is fitted the calculated E_x and E_z band energies were close to the experimental ones. The ε and C_4, parameters were obtained and the E_x and E_z values were used to adjust the G and CH1 parameters. It is then possible to adjust the C_2 parameter to reproduce the experimental energies of the gamma-band. However in the present work the best fit to the gamma band was obtained with a value of zero for the C_2 parameter. The parameters used in fitting the ground and gamma-band of even xenon isotopes are listed in table 15 and their values as a function of the neutron number are shown in Fig. 64 and 65. The parameters vary in a smooth and predictable way from one nucleus to another. As the neutron number decreases nuclei change from vibrational-like structure to rotational-like structure in the middle of the region (N = 66), and again move towards vibrational structure as the neutron number decreases from N = 66. The single boson energy difference (HBAR) is maximum for nuclei close to the vibrational limit (Fig.64). Its value then decreases as the neutron number decreases and the transition from vibrational to rotational structure occurs; it increases past the middle of the region as vibrational structure is again approached. The

Figure 62

Position of the X and Z bands as a function of the Hamiltonian parameter G.

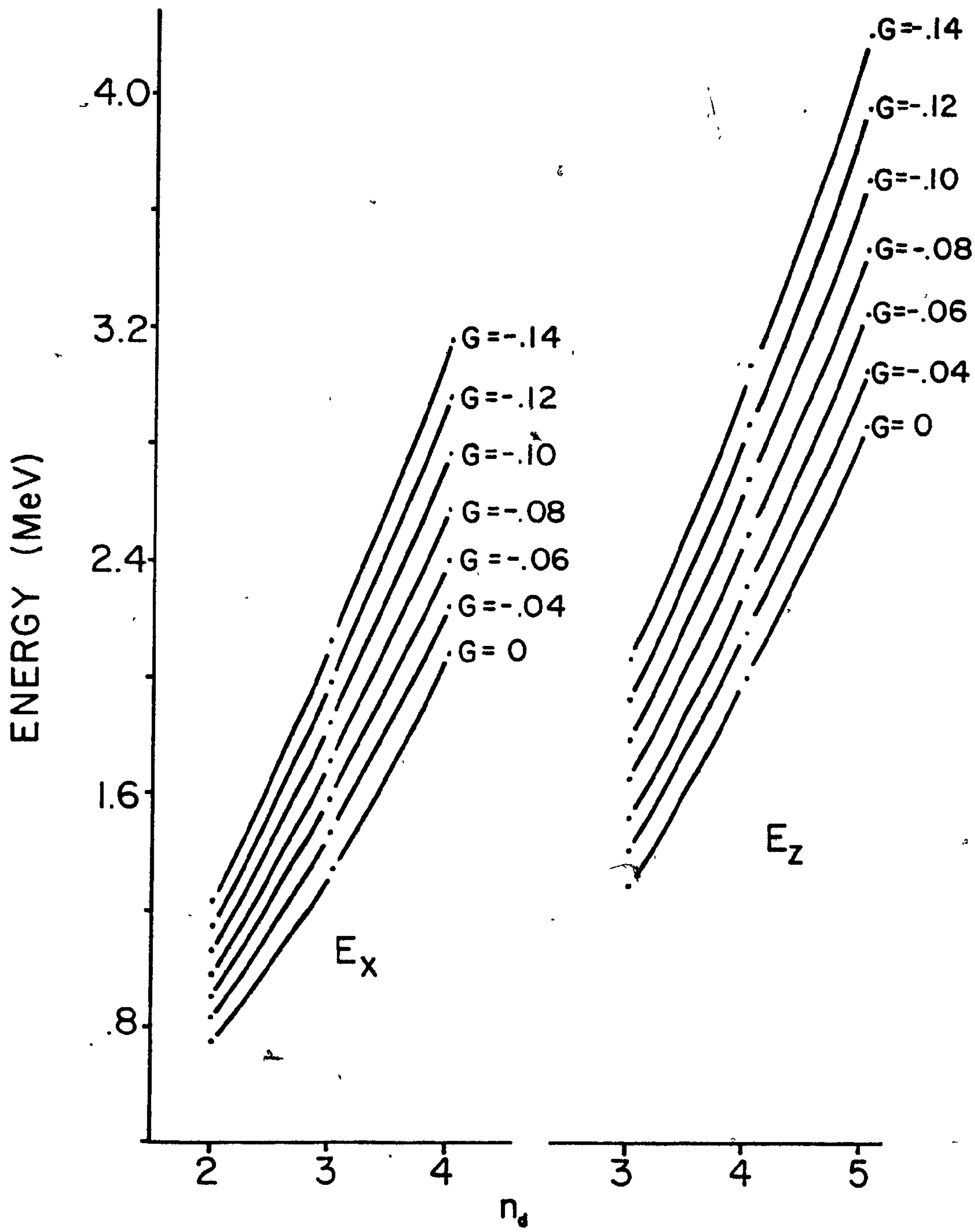

ENERGY (MeV)
4.0
3.2
2.4
1.6
.8
G=-.14
G=-.12
G=-.10
G=-.08
G=-.06
G=-.04
G=0
E_X
G=-.14
G=-.12
G=-.10
G=-.08
G=-.06
G=-.04
G=0
E_Z
2
3
4
3
4
5
n_d

Figure 63

Position of the X and Z bands as a function of the Hamiltonian parameter CH1.

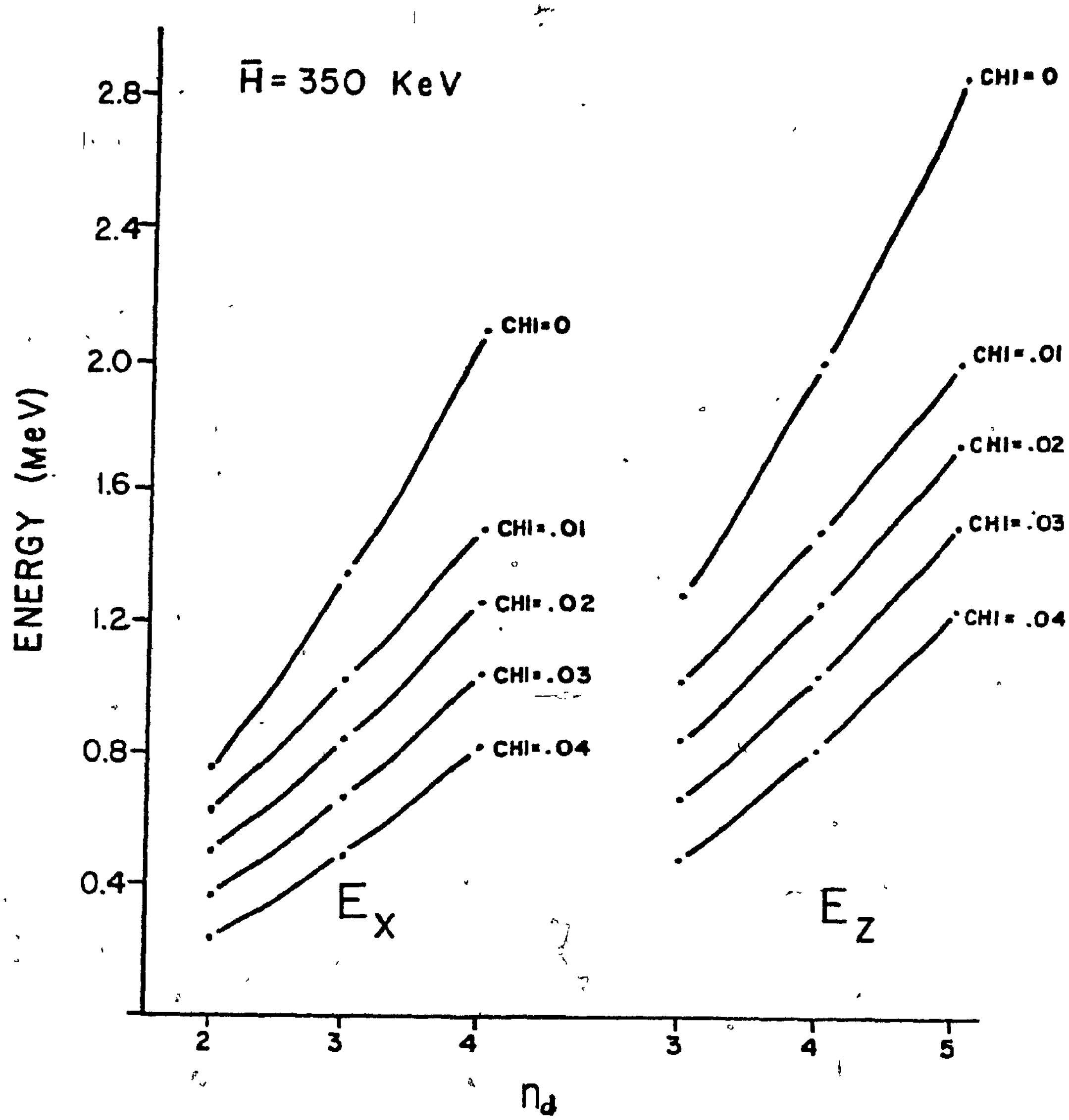
H̄ = 350 KeV
ENERGY (MeV)
2.8
2.4
2.0
1.6
1.2
0.8
0.4
CHI=0
CHI=.01
CHI=.02
CHI=.03
CHI=.04
E_x
E_z
2
3
4
3
4
5
n_d

TABLE 15. $^{116-130}$Xe Hamiltonian Parameters

A	HBAR	C_4	$-G$	CH1
116	0.22	0.07	0.12	0.015
118	0.10	0.07	0.14	0.017
120	0.04	0.08	0.15	0.02
122	0.05	0.09	0.15	0.02
124	0.14	0.108	0.14	0.02
126	0.27	0.11	0.122	0.02
128	0.40	0.105	0.096	0.013
130	0.51	0.08	0.09	0.008

In fitting the ground band the results were found to be most sensitive to the parameters HBAR, G and CH1. The best fit to the γ-band was obtained by choosing $C_0 = C_2 = 0$.

Figure 64

Variation of the HBAR and G Hamiltonian parameters as a function of neutron number.

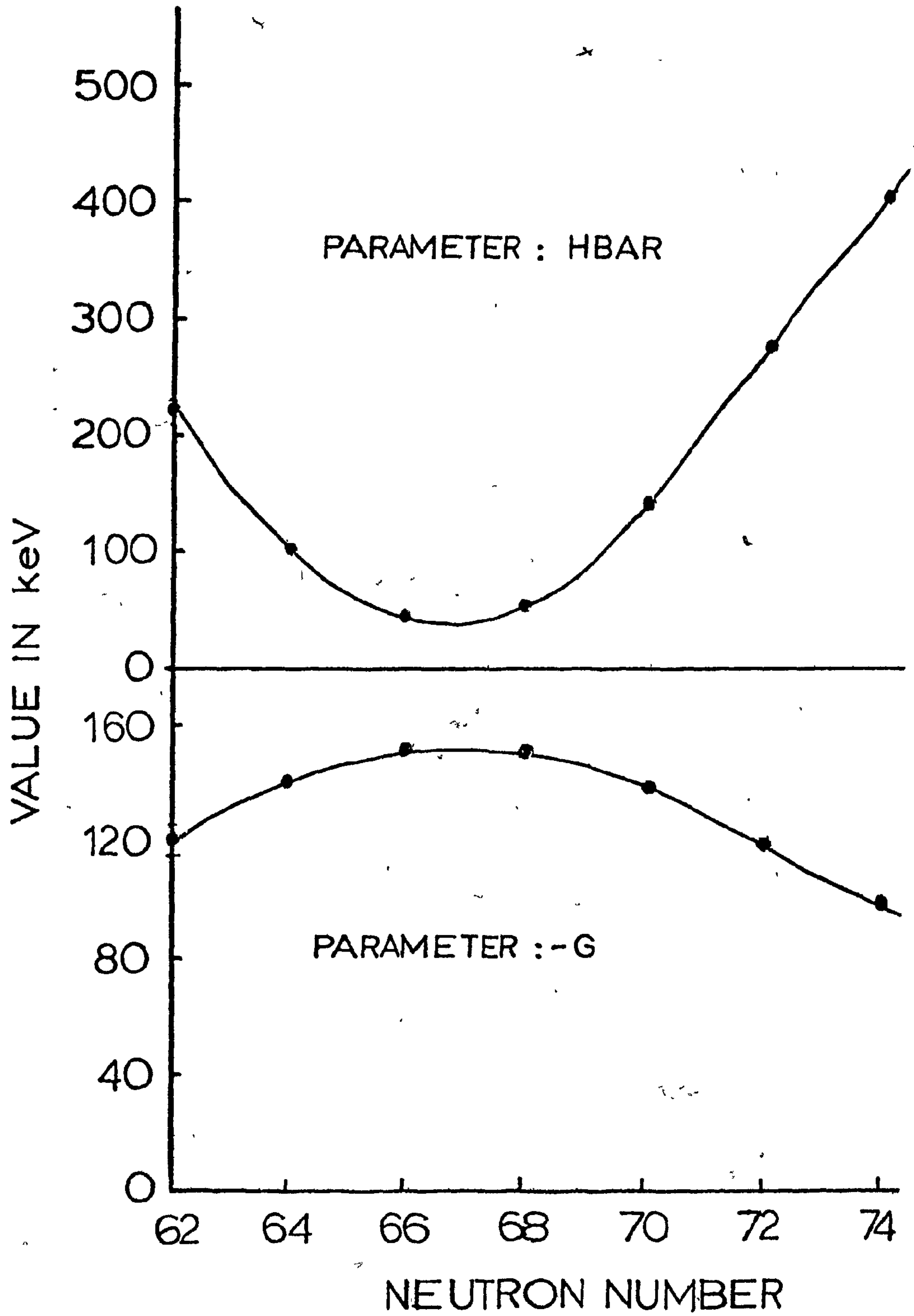

500
400
300
200
100
0
160
120
80
40
0
VALUE IN keV
PARAMETER : HBAR
PARAMETER : -G
62
64
66
68
70
72
74
NEUTRON NUMBER

Figure 65

Variation of the C_4 and CHl Hamiltonian parameters as a function of neutron number.

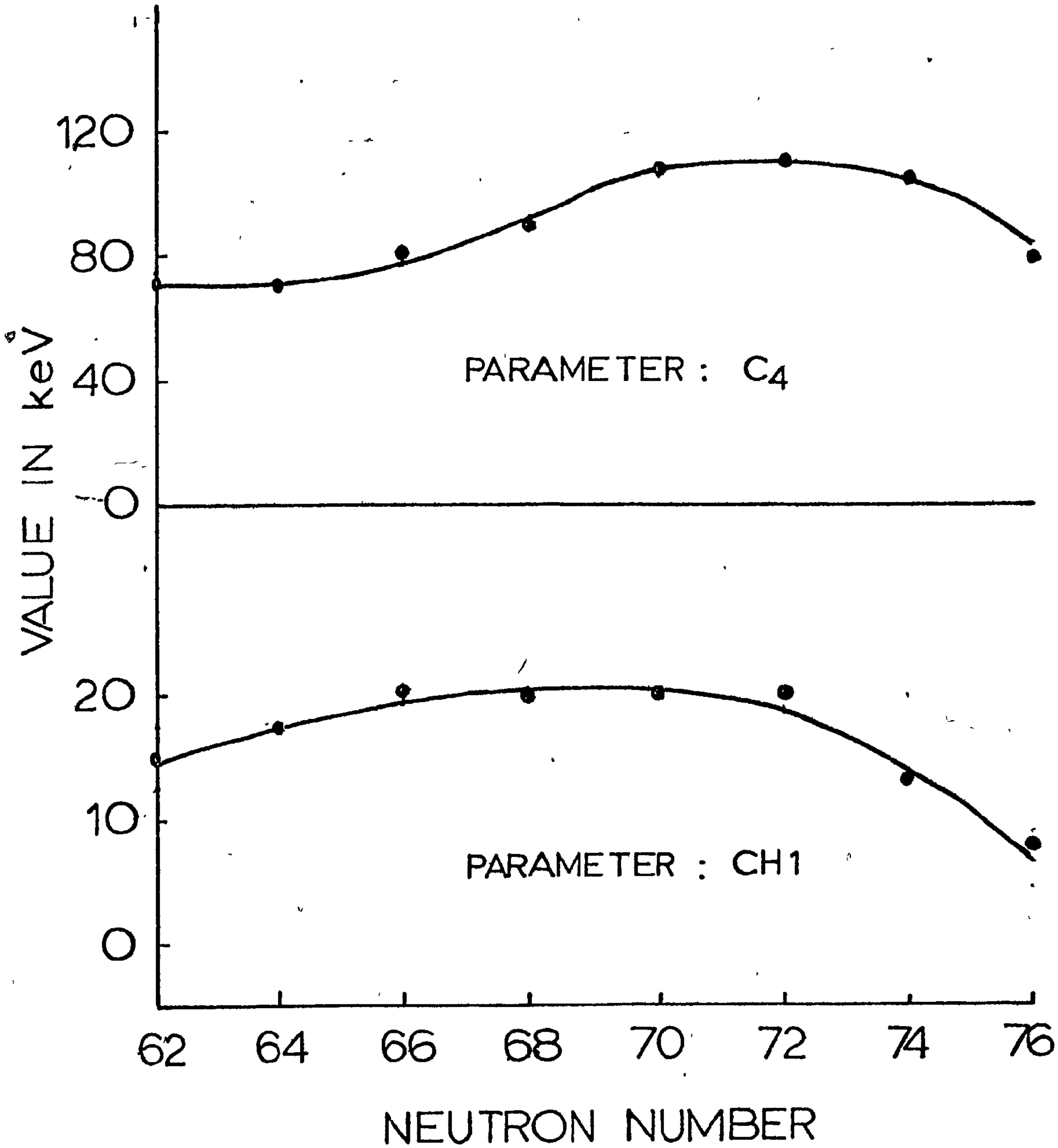
120
80
40
0
20
10
0
VALUE IN keV
PARAMETER : C4
PARAMETER : CH1
62
64
66
68
70
72
74
76
NEUTRON NUMBER

interaction which changes s- into d- bosons (G) follows the changes in the single boson energy, as the neutron number decreases from N = 76 and ε decreases. The results of the present calculation are given in Fig. 66 where the calculated energies of members of the ground band are compared with the experimental ones. In Figs 67 to 71 the calculation of the gamma-bands for $^{118-126}Xe$ are compared with the experimental ones. The experimental data of $^{122,124}Xe$ were taken from the present work. The $^{118-120}Xe$ information was obtained from the decay study of $^{118,120}Cs$ by Genevey-Rivier et al.(1977), and the information on ^{126}Xe was obtained from the work of Kusakari et al.(1975). Experimental information on $^{128,130}Xe$ was obtained from the recent study by Goettig et al.(1981).

The calculated and experimental systematics of the ground band and of the gamma-band in even xenon isotopes are shown in Fig. 72 and 73 respectively. The agreement with the experiment is very good and the changes observed from one nucleus to another are reproduced by a smooth variation of the Hamiltonian parameters (Fig. 64 and 65). In these systematics the energy of the first 2^+ level decreases with decreasing numbers of neutrons; then at N = 66, in the middle of the shell, it starts to increase as the neutron number further decreases. The position of the second 2^+ is below that of the 4_1^+ one for $^{124-130}Xe$ and above it for $^{118-122}Xe$.

Finally a comparison between the experimental levels of ^{122}Xe and ^{124}Xe obtained in the present work and the IBA predictions are presented in Fig. 74 and 75. From these figures it is clear that the IBA model does reproduce the ground band, gamma-band and the position of the first excited 0^+ state which is the head of the beta-band. However it does not reproduce the backbending observed in these nuclei. The fact that the energy levels of the xenon nuclei were reasonably reproduced by the IBA

Figure 66

Comparison between the theoretical and experimental energy levels of the ground-state band in $^{116-130}Xe$.

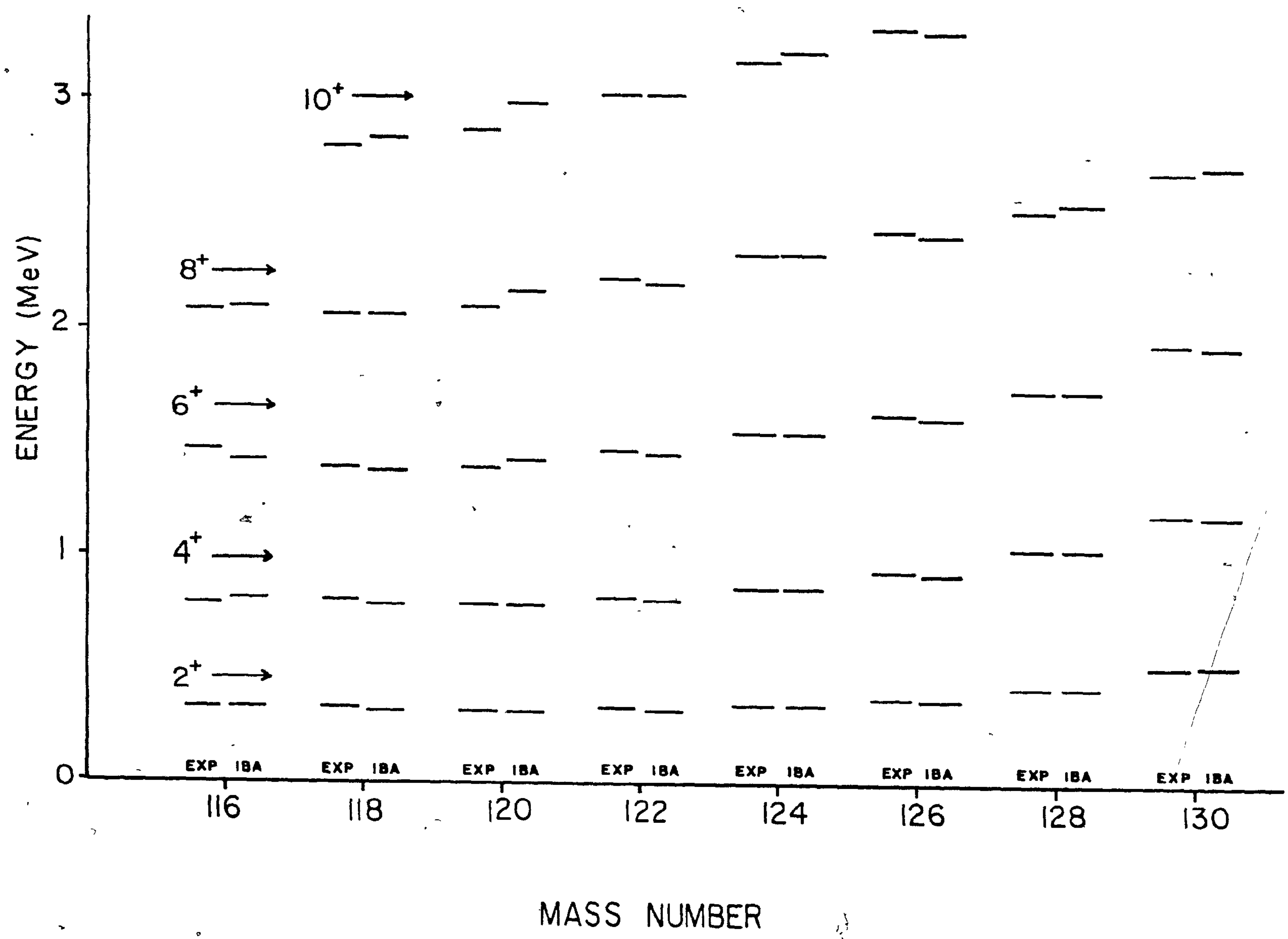
ENERGY (MeV)
0
1
2
3
2^+
4^+
6^+
8^+
10^+
EXP IBA
116
118
120
122
124
126
128
130
MASS NUMBER

<u>Figure 67</u>

Comparison of the experimental and theoretical X and Z bands in ^{118}Xe.

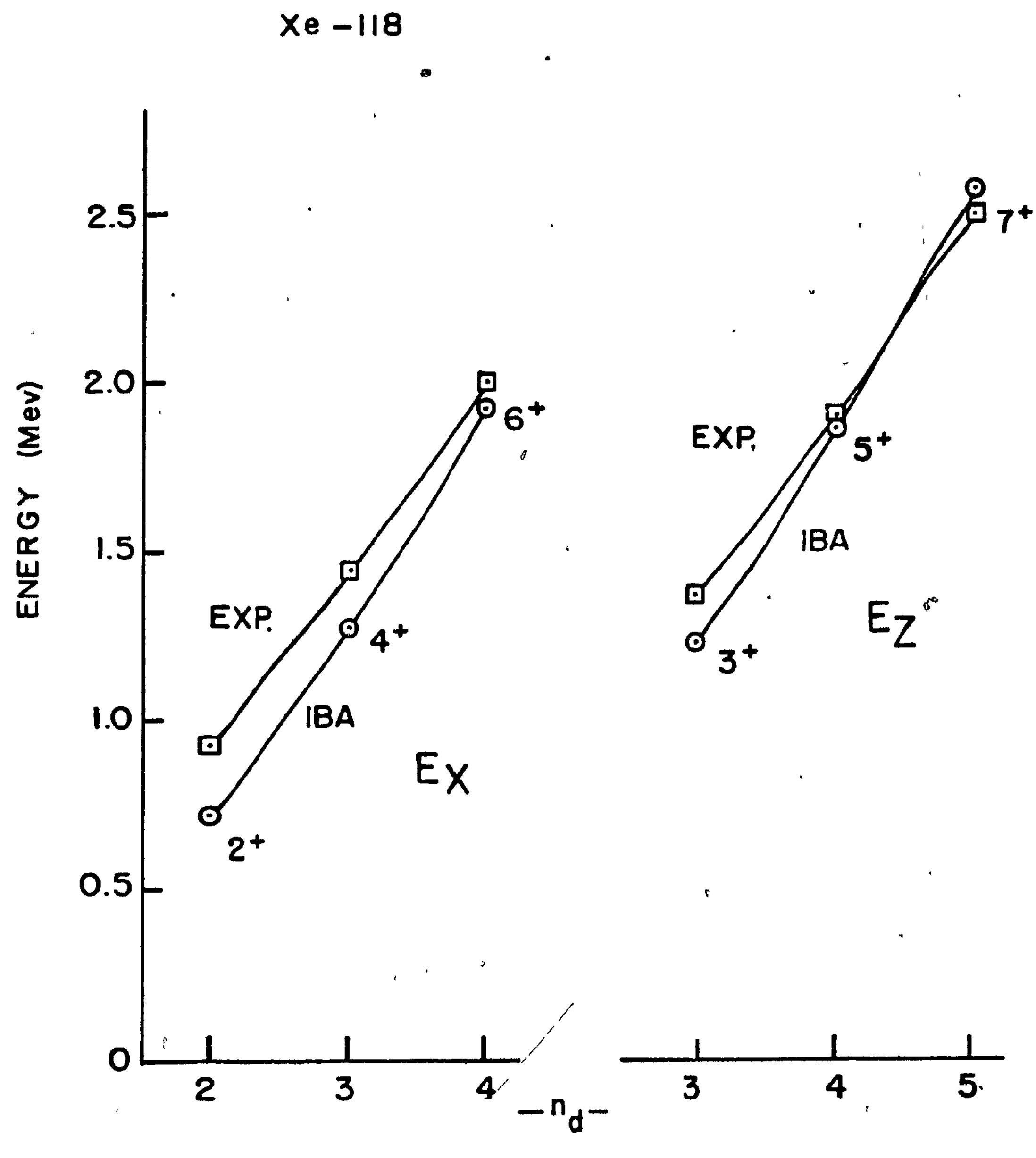

Xe -118
ENERGY (Mev)
2.5
2.0
1.5
1.0
0.5
0
EXP.
IBA
2^+
4^+
6^+
E_X
3^+
5^+
7^+
E_Z
2
3
4
$-n_d-$
3
4
5

Figure 68

Comparison of the experimental and theoretical X and Z bands in ^{120}Xe.

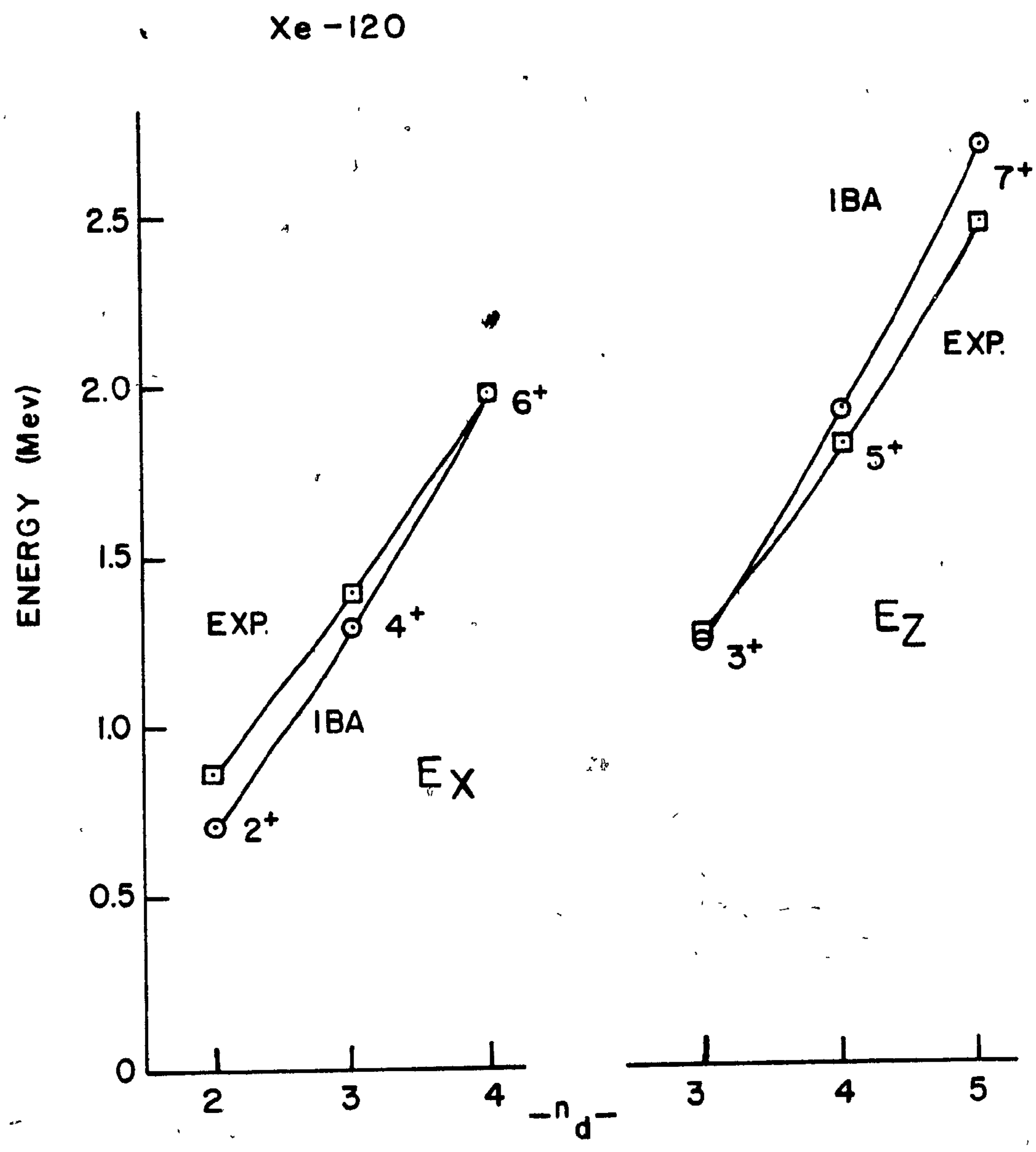

Xe -120
ENERGY (Mev)
2.5
2.0
1.5
1.0
0.5
0
EXP.
IBA
2+
4+
6+
Ex
IBA
EXP.
7+
5+
3+
Ez
2
3
4
-nd-
3
4
5

Figure 69

Comparison of the experimental and theoretical X and Z bands in ^{122}Xe.

Xe-122

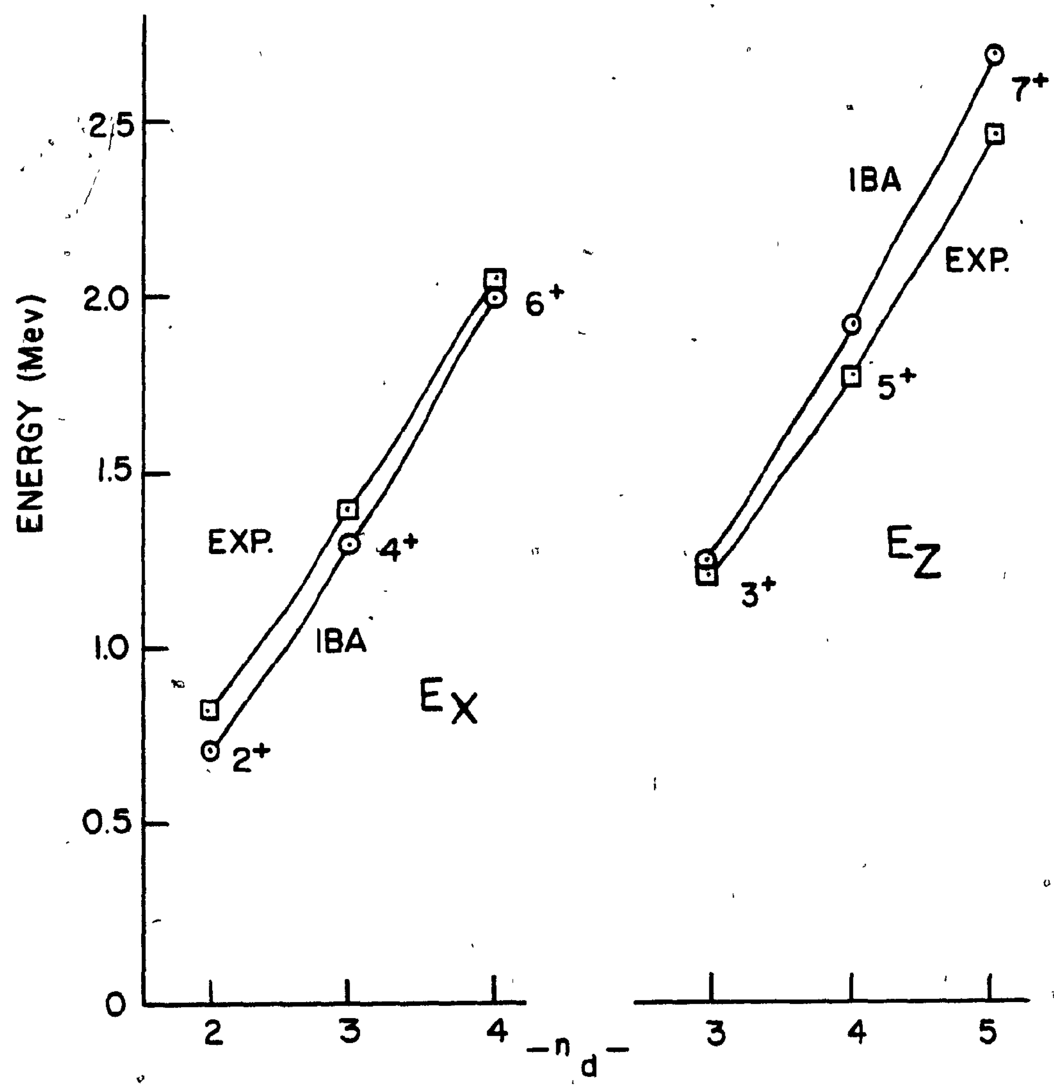

ENERGY (Mev)
2.5
2.0
1.5
1.0
0.5
0
EXP.
IBA
6+
4+
2+
EX
IBA
EXP.
7+
5+
3+
EZ
2
3
4
-nd-
3
4
5

Figure 70

Comparison of the experimental and theoretical X and Z bands in ^{124}Xe.

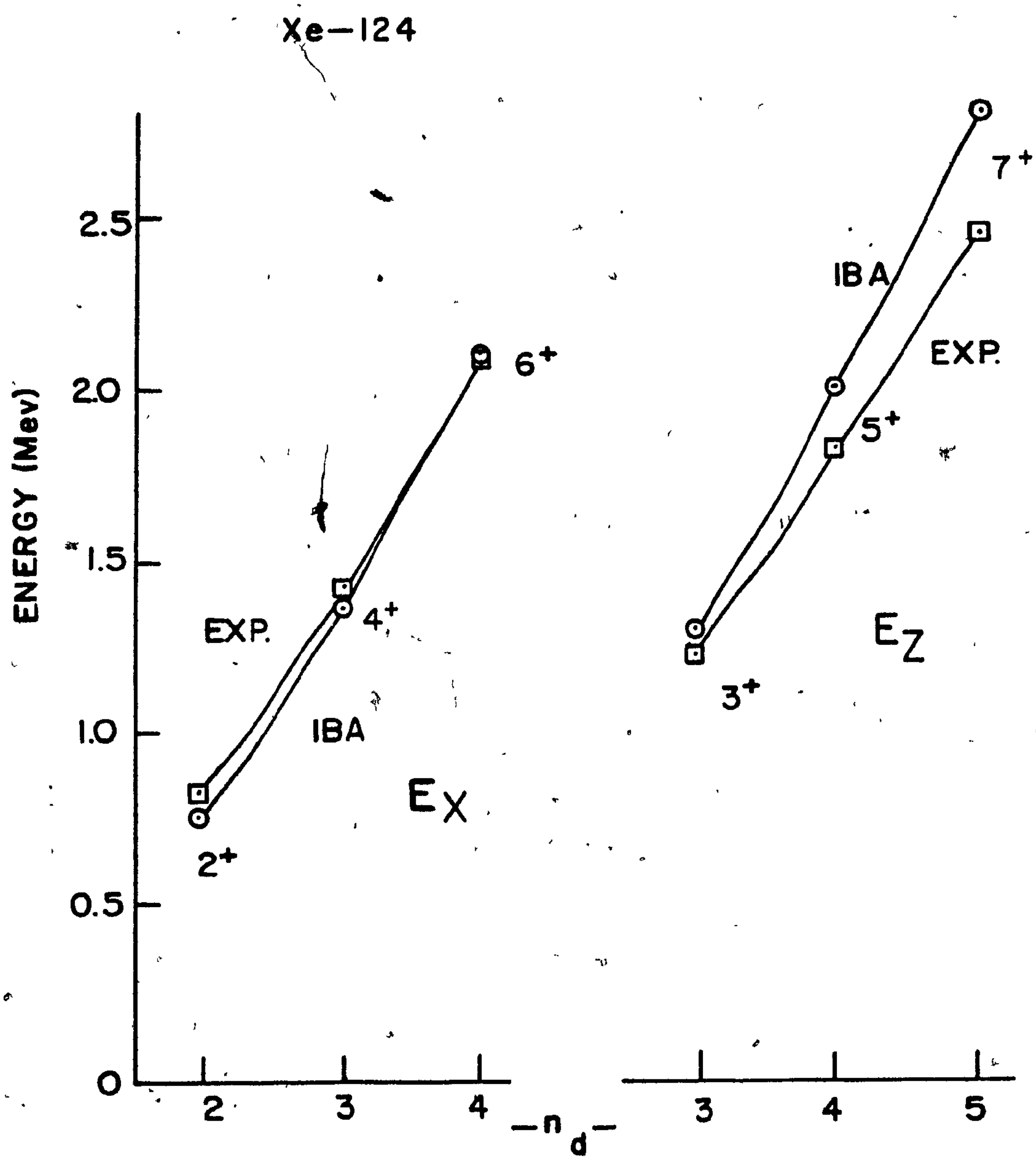
Xe—124
ENERGY (Mev)
2.5
2.0
1.5
1.0
0.5
0
6+
4+
2+
EXP.
IBA
Ex
7+
5+
3+
IBA
EXP.
Ez
2
3
4
—n d—
3
4
5

Figure 71

Comparison of the experimental and theoretical X and Z bands in ^{126}Xe.

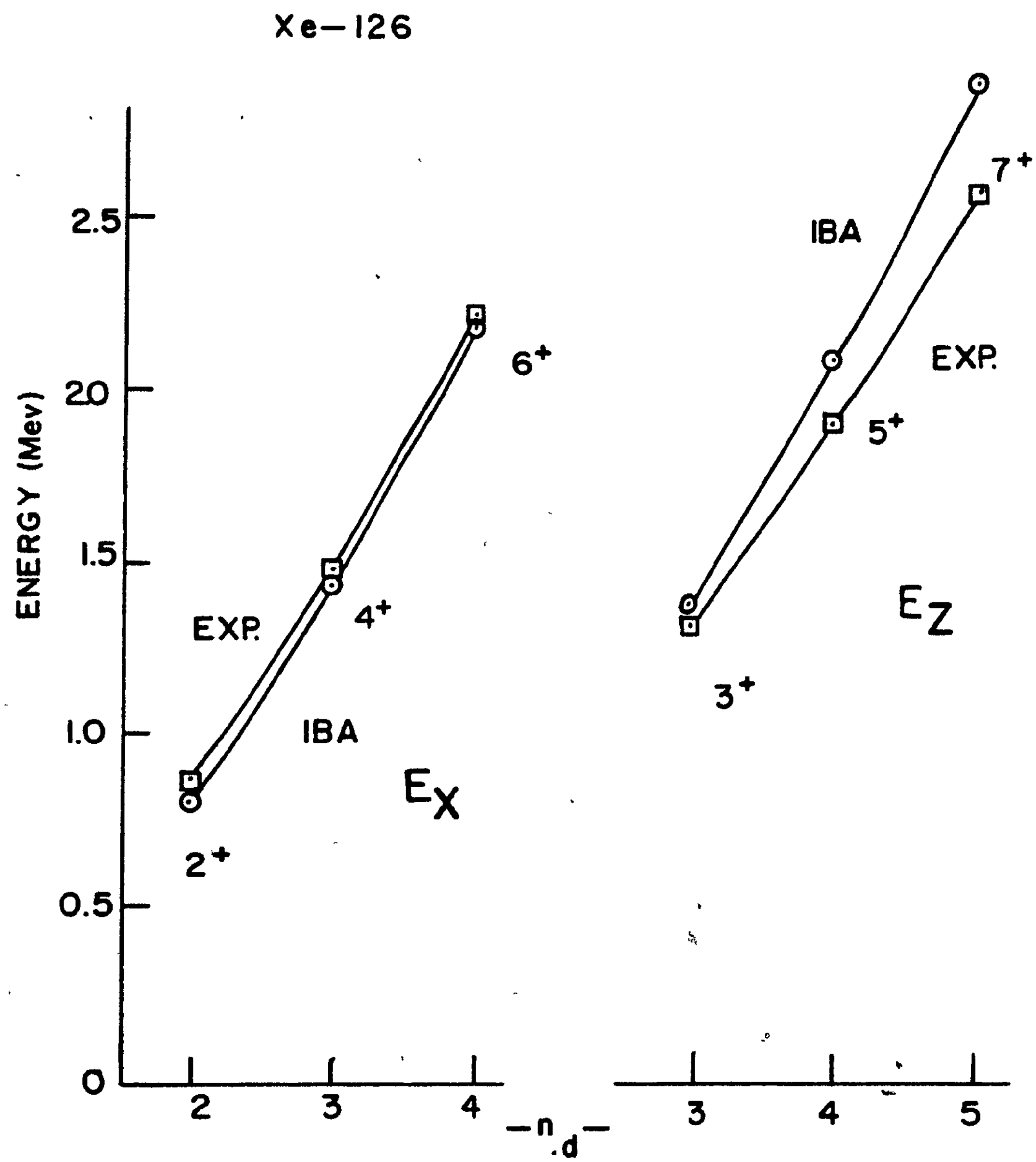

Xe-126
ENERGY (Mev)
2.5
2.0
1.5
1.0
0.5
0
6+
EXP.
4+
IBA
2+
E_X
7+
IBA
EXP.
5+
3+
E_Z
2
3
4
—n_d—
3
4
5

Figure 72

Theoretical and experimental (data points) systematics of the ground-state band in xenon nuclei.

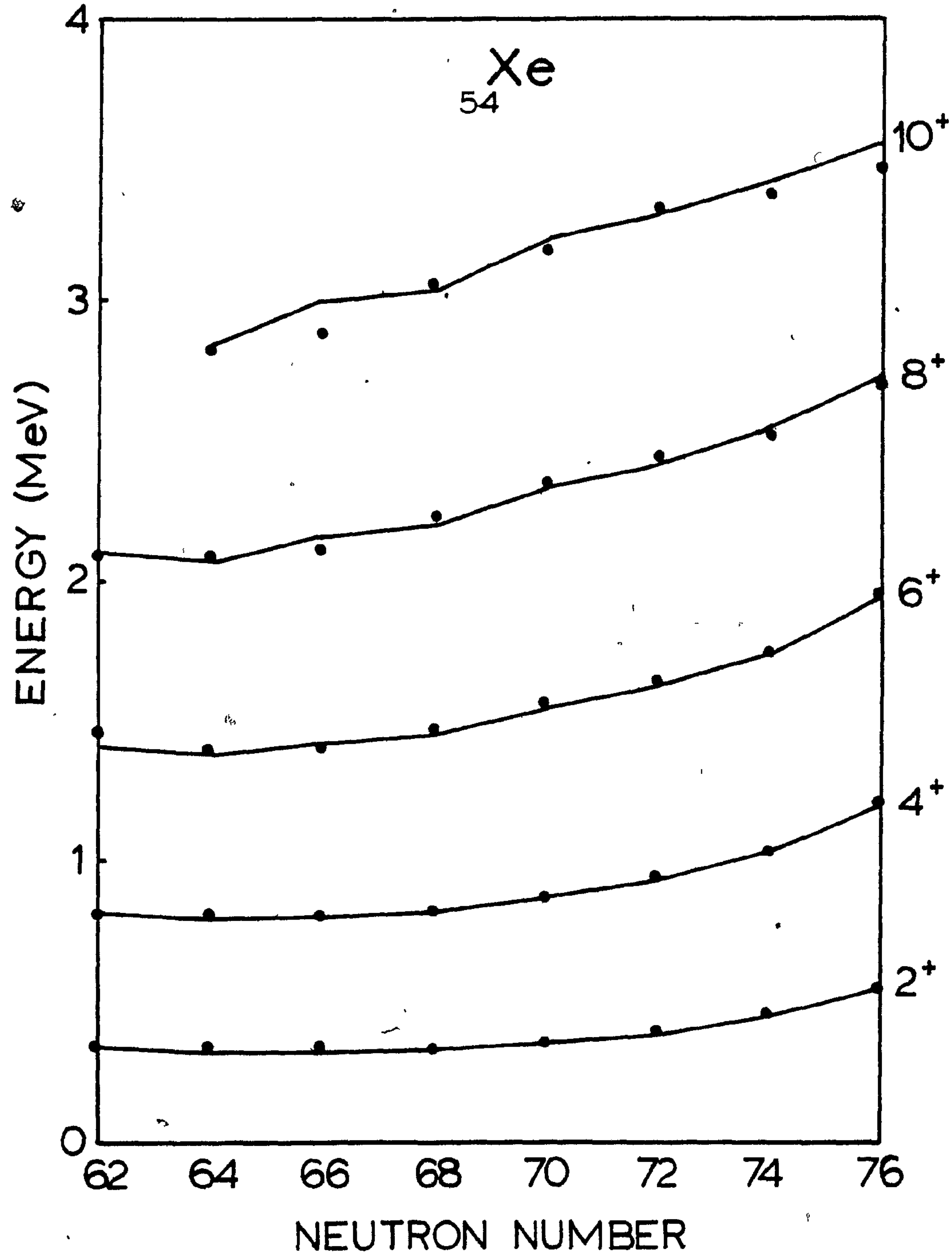

$_{54}$Xe
ENERGY (MeV)
0
1
2
3
4
10+
8+
6+
4+
2+
62
64
66
68
70
72
74
76
NEUTRON NUMBER

Figure 73

Theoretical and exerimental systematics of the gamma band in $^{116-130}Xe$.

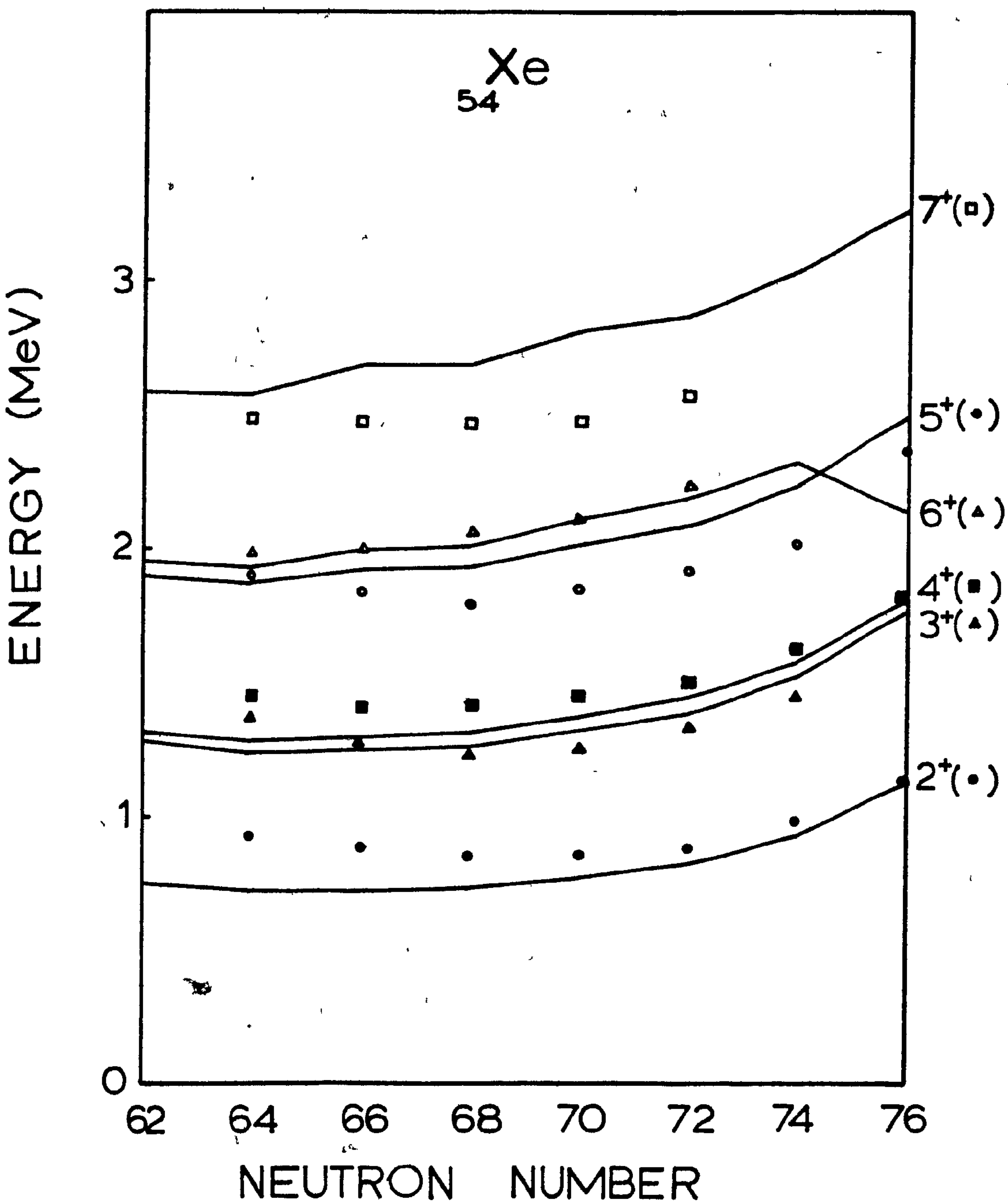

$_{54}$Xe
ENERGY (MeV)
0
1
2
3
62
64
66
68
70
72
74
76
NEUTRON NUMBER
7+(□)
5+(○)
6+(△)
4+(■)
3+(▲)
2+(●)

Figure 74

Comparison of the experimental and theoretical level schemes of ^{122}Xe.

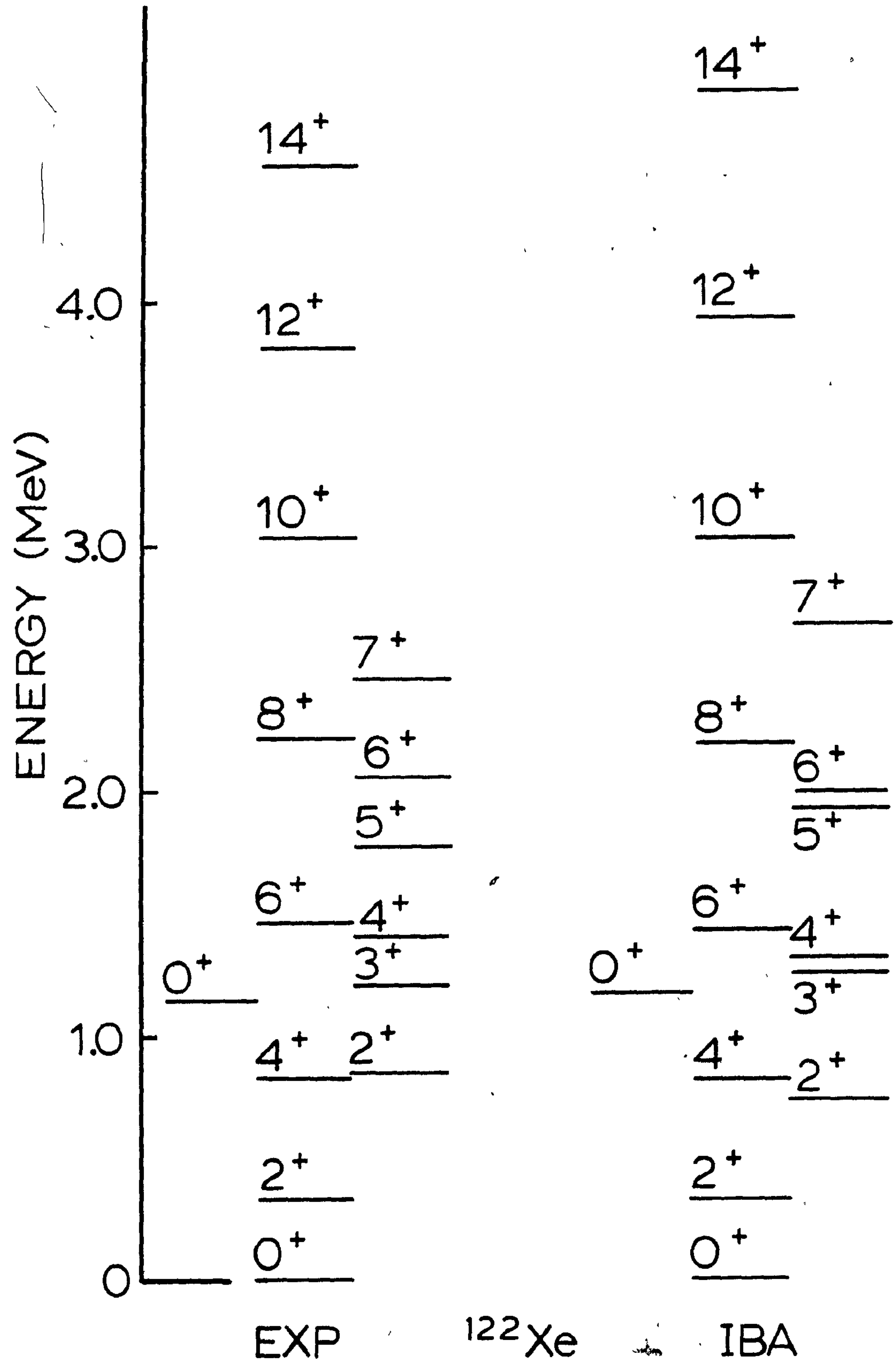
ENERGY (MeV)
4.0
3.0
2.0
1.0
0
14+
12+
10+
8+
7+
6+
5+
4+
3+
2+
0+
EXP
^{122}Xe
IBA

Figure 75

Comparison of the experimental and theoretical level schemes of ^{124}Xe.

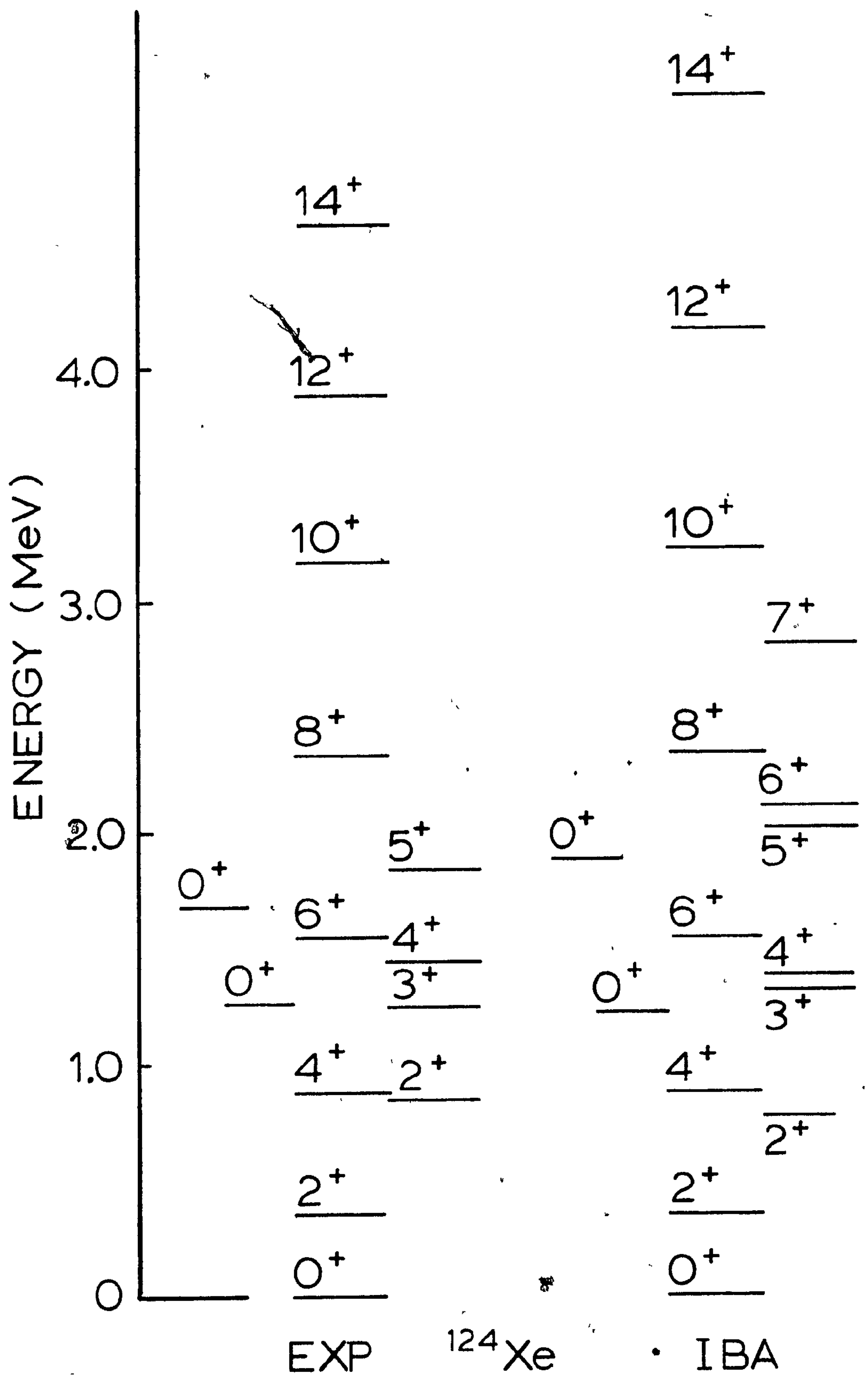

ENERGY (MeV)
4.0
3.0
2.0
1.0
0
14+
12+
10+
8+
6+
4+
2+
0+
0+
0+
5+
4+
3+
2+
7+
6+
5+
4+
3+
2+
EXP
124Xe
IBA

model indicates that the symmetries in these energy levels could be reproduced by a group theoretical approach.

2. Interpretation of the Backbending and the Side-Bands in Terms of the Rotation Alignment Model

In 1970 Newton et al. summarized the information then available on high-spin yrast states. They reached several conclusions on the population and deexciting mechanisms. In particular they pointed out that the feeding point of the ground state band was near its intersection with other bands which implies a major change in the nature of the yrast levels above this spin value. Shortly after, the backbending phenomenon was discovered by Johnson et al.(1971, 1972). This phenomenon was observed in the present work in both ^{122}Xe and ^{124}Xe (Fig. 76, 77). The name "backbending" refers to the unusual shape of the plot of the nuclear moment of inertia versus the square of the rotational frequency $(\hbar\omega)^2$. A sudden increase in the moment of inertia is accompanied by a decrease in the rotational frequency, causing the backbend in the plot around the spin $I = 10^+$. Since $\hbar\omega$ is nearly half the rotational transition energy, the backbending shape results from the fact that several transition energies around the critical spin value (10^+) are lower than those for spins just below this value. This change in the nature of the yrast levels at high spin was explained in terms of the rotational alignment picture of Stephens and Simon (1972). In their investigation of the Corolis effect, they showed that as the angular momentum of the system increases particles (particularly those in a high j shell) tend to decouple from the core and add their rotationally aligned angular momenta (2j-1) to that of the core. Enough energy is gained at about $I \geq 10$ that these states become lower in energy than those states which

<u>Figure 76</u>

Backbending plot for the ground-state band of ^{122}Xe. The dotted line indicates the position of the side-band.

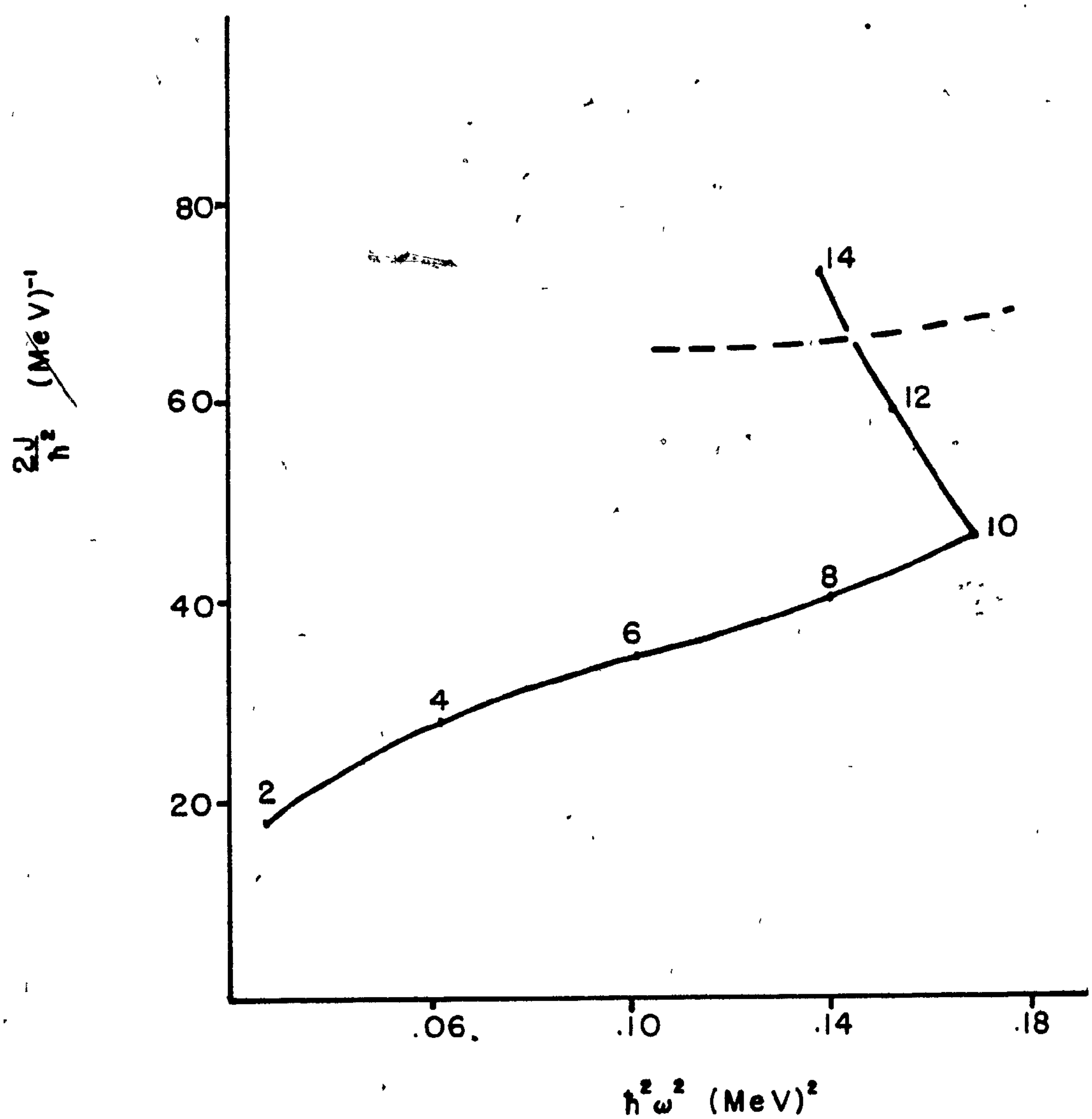

80
60
40
20
$\frac{2J}{\hbar^2}$ (MeV)$^{-1}$
2
4
6
8
10
12
14
.06
.10
.14
.18
$\hbar^2\omega^2$ (MeV)^2

Figure 77

Backbending plot for the ground-state band of ^{124}Xe. The dotted line indicates the position of the side-band.

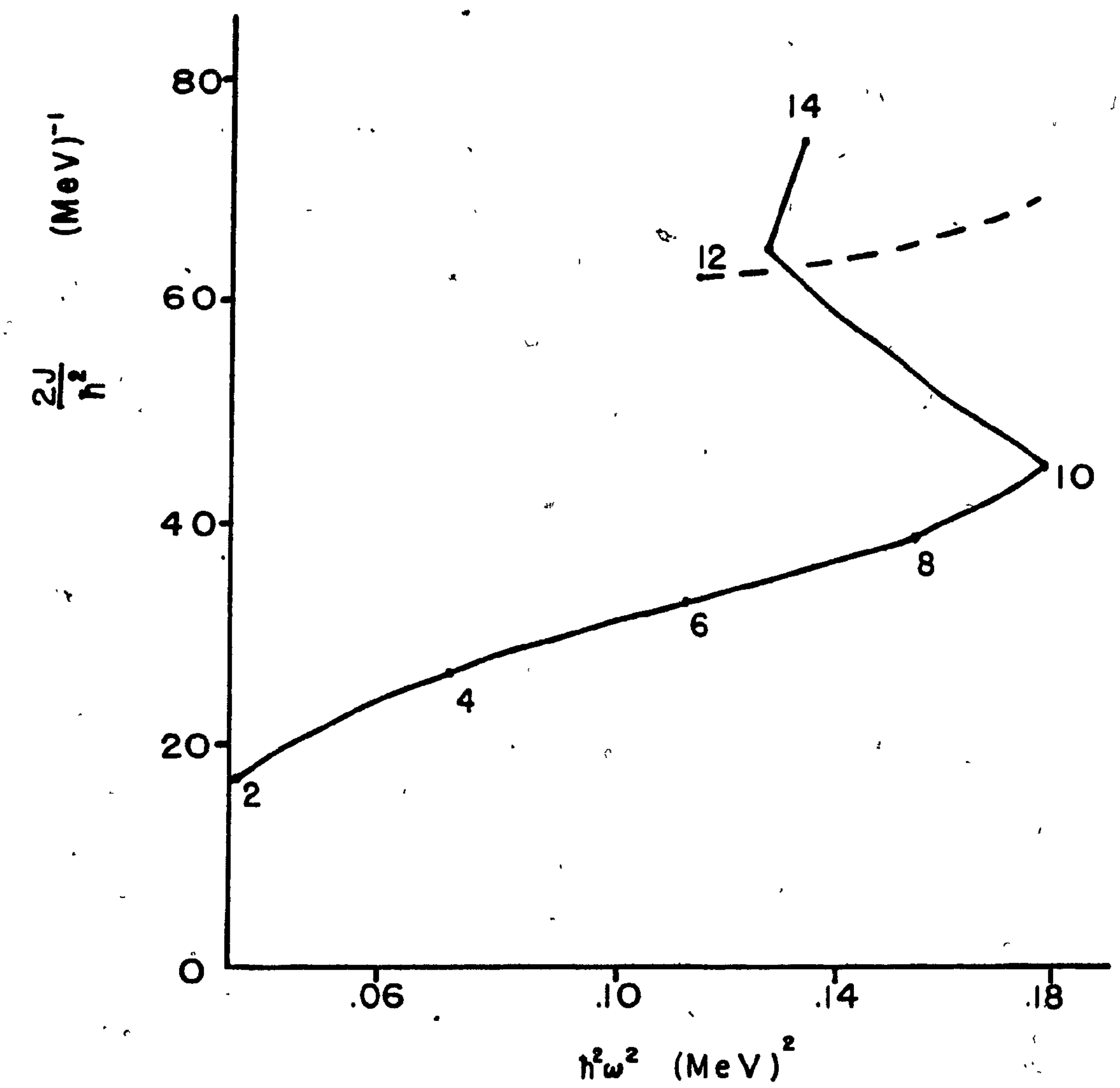

80
60
40
20
0
$\frac{2J}{\hbar^2}$ $(MeV)^{-1}$
14
12
10
8
6
4
2
.06
.10
.14
.18
$\hbar^2\omega^2$ $(MeV)^2$

involve only the rotational energy of the system. The band formed by these states intersects with the rising ground state band causing the backbending (Stephens and Simon, 1972). The effect observed in the case of ^{122}Xe and ^{124}Xe is illustrated in Fig. 78 and 79 respectively.

The investigation of high-spin states in even-mass rare earth nuclei and transitional nuclei with small deformation revealed the existence of a negative parity band which has a spin sequence $\Delta I = 2$ and deexcites by means of E1 transitions into the ground state band (Lieder and Ryde 1978). Negative parity bands of this kind have also been found in $^{126,128}Ba$ (Flaum et al. 1974 and 1976) and in ^{136}Ce (Müller-Veggian et al. 1975). These bands have been interpreted as two-quasiparticle aligned bands in the framework of the rotation alignment model (Flaum et al. 1976) and (Vogel 1976), similar to the rotation alignment of two particles discussed above which is responsible for the backbending. The side bands observed in the present work in both ^{122}Xe and ^{124}Xe (Fig. 51 and 57) have E2 interband transitions and feed the ground state band through a dipole transition.

The single particle levels $3s_{1/2}$, $2d_{3/2}$, $2d_{5/2}$, $1g_{7/2}$, and $1h_{11/2}$ make up the neutron 50 - 82 major shell. In the odd-A neighbouring nuclei decoupled bands built on the $h_{11/2}$ state were observed (Barci et al. 1981, Helppi et al. 1979, and Gizon and Gizon 1978) with the favoured and unfavoured levels only a few keV apart. These bands arise from the Coriolis effect on an $h_{11/2}$ neutron which partially aligns its angular momentum with that of the core (Stephens and Simon 1972). The energy spectrum of the bands can be calculated in the framework of the rotation-alignment model from (Stephens 1975, Stephens et al. 1973):

$$E_{rot\text{-}align} = \frac{\hbar^2}{2\mathcal{J}} (I-\alpha)(I-\alpha+1)$$

Figure 78

The intersection of the ground band of ^{122}Xe with the two-quasiparticle band.

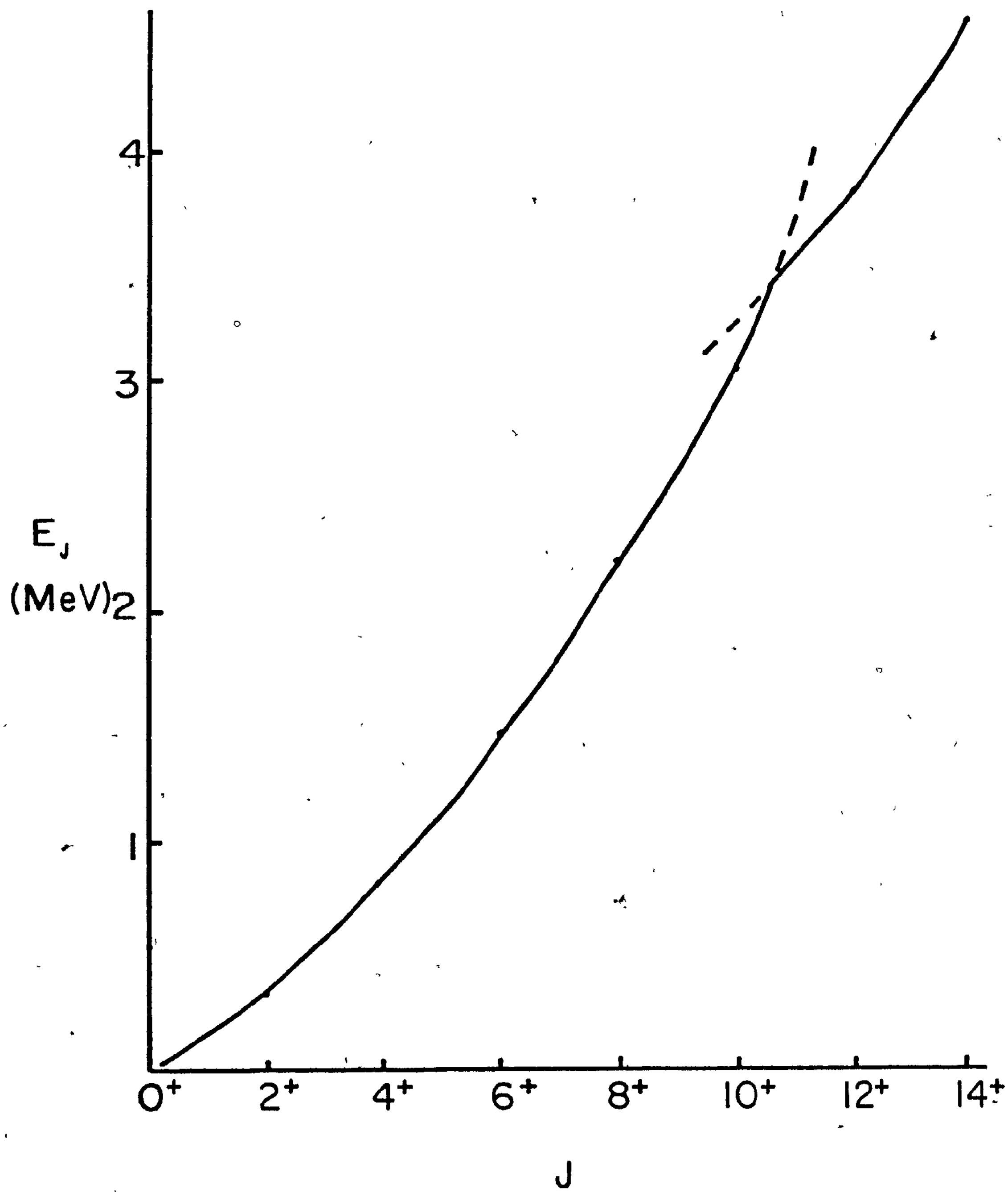

E_J
(MeV)
1
2
3
4
0^+
2^+
4^+
6^+
8^+
10^+
12^+
14^+
J

Figure 79

The intersection of the ground band of ^{124}Xe with the two-quasiparticle band.

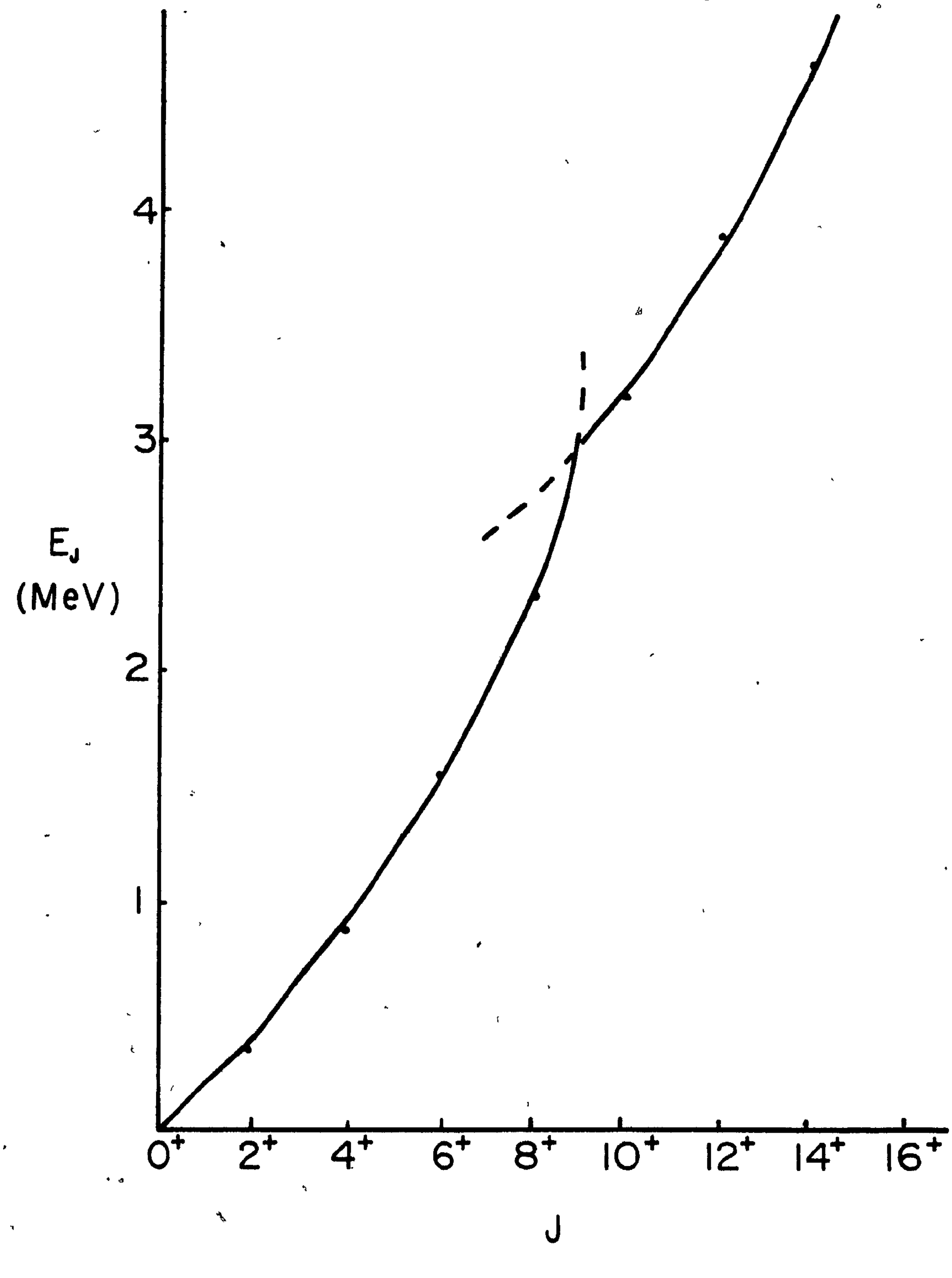

4
3
2
1
E_J
(MeV)
0⁺ 2⁺ 4⁺ 6⁺ 8⁺ 10⁺ 12⁺ 14⁺ 16⁺
J

where $I - \alpha$ must be even, and α is the projection of the particle angular momentum j on the rotation axis. The moment of inertia is that of the core. Therefore for each value of α, a $\Delta I = 2$ band occurs which has the core energy spacings and deexcites by stretched E2 transitions (Stephens 1975). The main bands are classified as the "favoured" band ($\alpha = j = \frac{11}{2}$) having spins $I = j, j + 2, j + 4 ....$ and the more weakly populated unfavoured one ($\alpha = j - 1 = \frac{9}{2}$) with $j - 1, j + 1, j + 3,....$spin sequence.

The backbending observed in the even-even adjacent nuclei is the result of the rotation-alignment of a pair of $h_{11/2}$ quasi-neutrons. This is supported by the fact that the $h_{11/2}$ decoupled bands observed in the odd-A Xe nuclei backbend at a rotation frequency much higher than the even-even nuclei (Grosse et al. 1973) where the occupation of a level by an $h_{11/2}$ quasi-neutron hinders the rotation-alignment of a further pair of quasi-neutrons derived from the same orbital.

Aligned pairs of ($h_{11/2}$, $h_{11/2}$) quasi-neutrons provide states with $I = 10^+$ (Simms et al. 1980). Therefore the backbending observed in $^{122,124}Xe$ could be explained as follows. The ground state band (vacuum state $|\tilde{0}>$) is crossed by the two quasi-neutron rotation aligned band where the first quasiparticle has the maximum angular momentum projection on the rotation axis $\alpha = j = 11/2$ and the second quasiparticle has the maximum remaining projection $\alpha = j-1 = 9/2$ ($\alpha^+_{11/2}\ \alpha^+_{9/2}\ |\tilde{0}>$) where α^+ is the quasiparticle creation operator (Stephens 1975). The aligned angular momentum could be obtained from the experimental data by subtracting the spin of the ground band (no quasiparticles) from the spin of the two quasiparticle band at the same rotational frequency ($\sim E_\gamma/2$). If data are available from the neighbouring odd-A nucleus, it is possible to verify that quasiparticles in a particular j-shell couple to form the 2-quasiparticle band; the aligned angular momentum should be the sum of the aligned angular momenta of the favoured ($\alpha = 11/2$) and unfavoured ($\alpha = 9/2$) bands. This idea is illustrated in Fig. 80 and 81, where $\Delta E/2$ ($\hbar\omega$) is plotted versus I for ^{122}Xe and ^{124}Xe respectively. The angular momentum of the two Q.P band is matched with the sum constructed from the $h_{11/2}$ decoupled bands in ^{121}Xe (Barci et al. 1981) for the case of ^{122}Xe and ^{125}Xe (Gizon and Gizon 1978) for the case of ^{124}Xe.

Similarly the side-band could be explained as a Coriolis - decoupled two quasineutron band. Simms et al. (1980) have found that the condition of high - j, unique parity orbitals in the rotation-alignment model of Stephens was unnecessary. It was also found that features of transitional nuclei with low -j and or mixed -j orbitals can be understood in a general rotational treatment (Smith et al. 1976, Samuelson et al. 1979, and Popli et al. 1979). This is in accordance with the observation of $d_{3/2}$ decoupled bands in $^{121-129}Xe$ nuclei (Barci et al. 1981, Luukko et al. 1981, Helppi et al. 1979 and Helppi et al. 1981). Therefore the side band could be the result of an aligned neutron pair of ($h_{11/2}$, $d_{3/2}$). In the case of ^{124}Xe (Fig. 81) the aligned angular momentum of the side band matches that obtained by summing the aligned angular momenta of the $h_{11/2}$ ($\alpha = 11/2$) and $d_{3/2}$ which is obtained from the decoupled bands observed in ^{125}Xe (Helppi et al. 1979) by taking the even-even nucleus ground band (no quasi-particle) as reference. This ($h_{11/2}$, $d_{3/2}$) pair alignment produces a 7^-, 9^-, 11^-, ...band, which is in agreement with the experimental predictions [IV B(b)]. In the case of ^{122}Xe (Fig. 80) the aligned angular momenta of the $h_{11/2}$ and $d_{3/2}$ do not match that of the side band. This band could be

Figure 80

The angular momentum as a function of the rotational frequency for ^{122}Xe yrast and side-bands and the $h_{11/2}$, $d_{3/2}$ decoupled bands in ^{121}Xe.

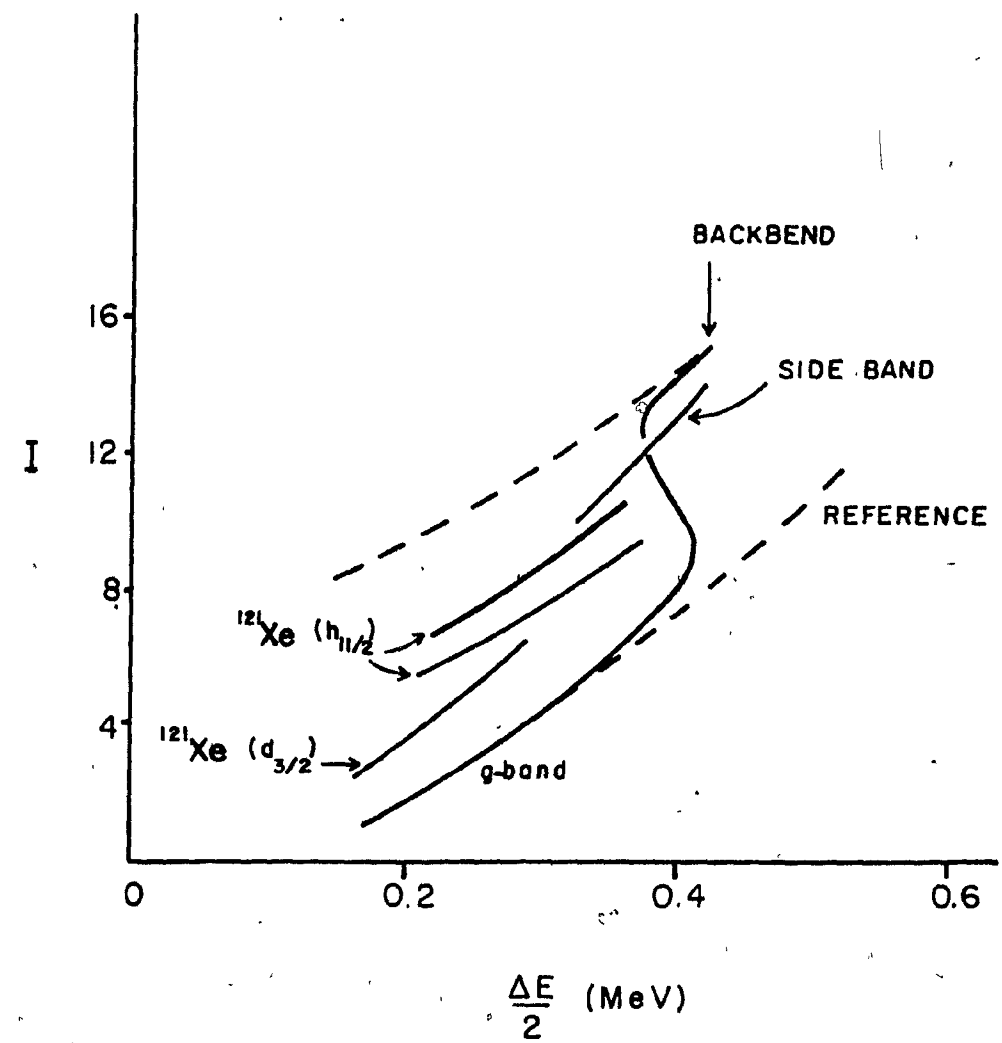

BACKBEND
SIDE BAND
REFERENCE
I
16
12
8
4
^{121}Xe ($h_{11/2}$)
^{121}Xe ($d_{3/2}$)
g-band
0
0.2
0.4
0.6
$\frac{\Delta E}{2}$ (MeV)

Figure 81

The angular momentum as a function of the rotational frequency for ^{124}Xe yrast and side-bands and the $h_{11/2}$, $d_{3/2}$ decoupled bands in ^{125}Xe.

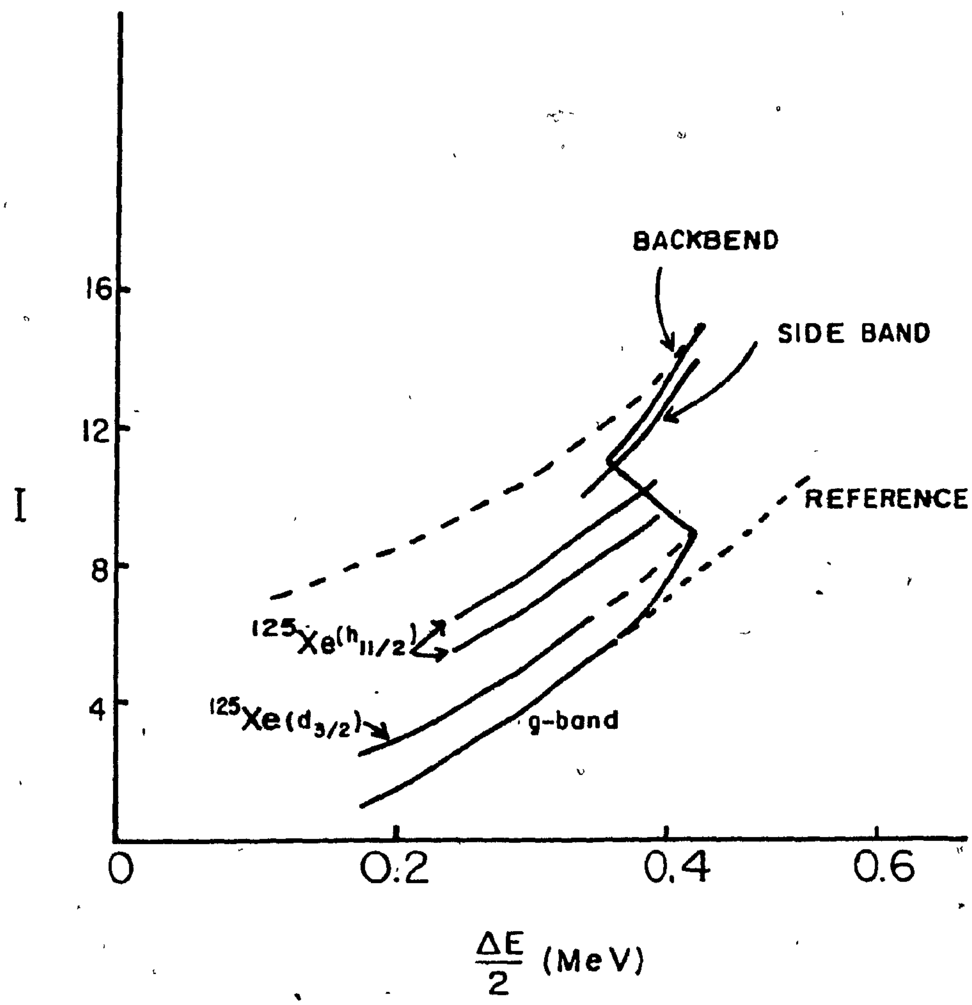

BACKBEND
SIDE BAND
REFERENCE
125Xe(h11/2)
125Xe(d3/2)
g-band
I
16
12
8
4
0
0.2
0.4
0.6
ΔE/2 (MeV)

the result of an aligned pair of neutrons in other shells, possibly an $(h_{11/2}, g_{7/2})$ pair. This, however cannot be verified since no decoupled bands built on the $g_{7/2}$ state are observed in the neighbouring ^{121}Xe nucleus.

B. ODD - A ISOTOPES

a. i. Description of the Interacting Boson-Fermion Model

The spectra of transitional odd-A nuclei are difficult to interpret since these nuclei cannot be explained with simple theoretical models such as the Nilsson model (Nilsson 1955). The triaxial rotor-plus-particle model of Meyer-ter-Vehn (1975) is very successful in describing transitional nuclei but it is restricted to dealing with one single-particle level. It would therefore be expected to be useful only in describing negative parity states of the nuclei in the N = 50-82 region which originate from the single particle in the $h_{11/2}$ orbit. The Interacting Boson-Fermion Model (IBFM) has had considerable success in describing odd-A nuclei. The collective states of $^{123-129}$Xe, for example, were reproduced by this model (Cunningham 1981b), and it was also successful in predicting low-spin states of ^{131}Xe (Cunningham 1981a). A successful prediction of the details of the low-lying structure is considered to be a good test of this model.

In the IBFM the odd-A nucleus is considered as a system of interacting bosons and fermions, where the fermions in shell model orbitals (j) are coupled to the boson structure of the even-even core. The Hamiltonian of the system is written as (Iachello and Scholten 1979)

$$H = H_B + H_F + V_{BF}$$

where H_B is the boson Hamiltonian [eq. (2)], and the fermion Hamiltonian H_F is written as:

$$H_F = \sum_{jm} \varepsilon_j \, a^+_{jm} \, a_{jm}$$

The boson-fermion interaction V_{BF} has the following form:

$$V_{BF} = \sum_j A_j[(d^+ \times \tilde{d})^{(0)} \times (a_j^+ \times \tilde{a}_j)^{(0)}]^{(0)}$$

$$+ \sum_{ij} \Gamma_{ij}[\{(s^+ \times \tilde{d} + d^+ \times \tilde{s})^{(2)} + \chi(d^+ \times \tilde{d})^{(2)}\} \times (a_i^+ \times \tilde{a}_j)^{(2)}]^{(0)}$$

$$+ \sum_{ijk} \Lambda_{ij}^{K} [(a_i^+ \times \tilde{d})^{(K)} \times (d^+ \times \tilde{a}_j)^{(K)}]^{(0)}$$

where $d^+(d)$ and $a^+(a)$ are the creation (annihilation) operators of bosons and fermions respectively. In order to reduce the number of parameters the BCS equations are solved in the fermion space and the A_j, Γ_{ij} and Λ_{ij}^K are j-dependent; where:

$$A_j = A\sqrt{2j+1}$$

$$\Gamma_{ij} = \Gamma(u_i u_j - v_i v_j) \langle i\| Y^{(2)} \| j \rangle$$

$$\Lambda_{ij}^K = \Lambda(u_i v_K + u_K v_i) \langle i\| Y^{(2)} \| K\rangle\langle K\| Y^{(2)} \| j\rangle$$

$$(u_j v_K + u_K v_j)/\sqrt{2K+1}$$

Here the parameters A, Γ and Λ denote the strength of the monopole, quadrupole and exchange terms of the boson-fermion interaction and u_i, v_i are the BCS occupation probabilities (Scholten 1979).

In the BCS calculation (de Shalit and Feshbach 1974, Eisenberg and Greiner 1972) a state of an odd number of particles corresponds to a state of one quasiparticle. The quasiparticle excitation energy E_j is:

$$E_j = \sqrt{(\varepsilon_j - \lambda)^2 + \Delta^2}$$

where:

ϵ_j = single particle energy

λ = chemical potential

Δ = pairing gap energy .

and the occupation probability is given as:

$$v_j^2 = \frac{1}{2}\,[1 - \frac{\epsilon_j - \lambda}{E_j}]$$

where:

$$\sum_j (2j+1) v_j^2 = n$$

Here n is the number of particles outside the closed shells. For more details on the BCS formalism the reader is referred to those references mentioned above.

ii. Calculation of Low-Lying Positive Parity States in ^{121}Xe

For xenon nuclei the odd fermion can occupy the $3s_{1/2}$, $2d_{3/2}$, $2d_{5/2}$, $1g_{7/2}$ and $1h_{11/2}$ single particle orbitals lying between the major shell closures at 50 and 82. In the BCS calculation the pairing energy Δ was taken to be $\Delta \simeq 12/\sqrt{A} \simeq 1.08$ MeV, and the quasiparticle energies and occupation probabilities were generated using the single particle levels in ^{131}Sn (Lederer and Shirley 1978). The BCS calculation of $s_{1/2}$, $d_{3/2}$, $d_{5/2}$, $g_{7/2}$ and $h_{11/2}$ single particle orbitals were included. However in the IBFM calculation of positive parity states of ^{121}Xe, only the quasiparticle energies of the positive parity orbitals were included. These quasiparticle energies have been modified slightly to improve the agreement with the data. The computer code ODDA written by Scholten was used

Figure 82

Comparison of the theoretical and experimental spectrum of ^{121}Xe.

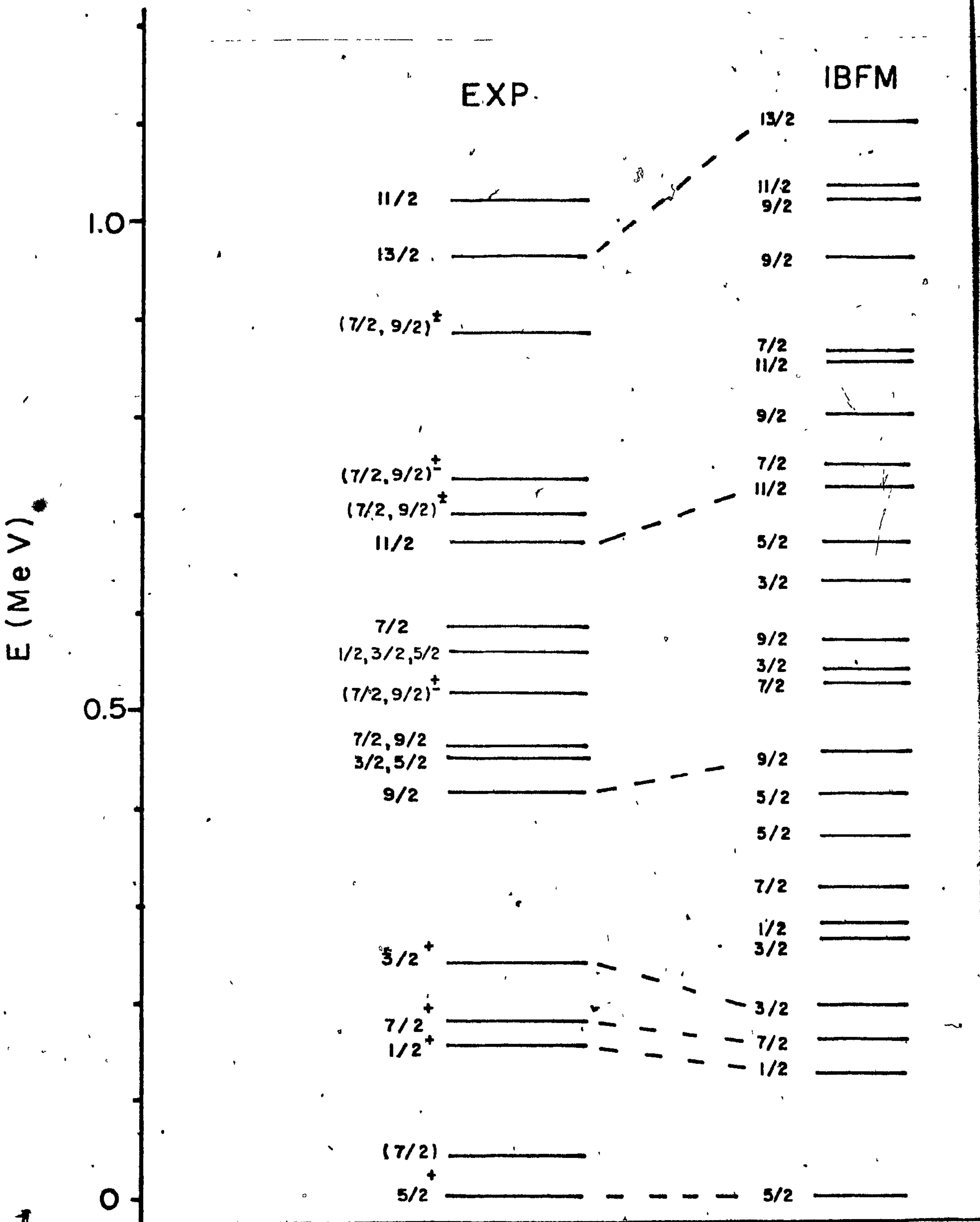

EXP
IBFM
E (MeV)
1.0
0.5
0
11/2
13/2
(7/2, 9/2)±
(7/2,9/2)±
(7/2, 9/2)±
11/2
7/2
1/2,3/2,5/2
(7/2,9/2)±
7/2,9/2
3/2,5/2
9/2
3/2+
7/2+
1/2+
(7/2)
5/2+
13/2
11/2
9/2
9/2
7/2
11/2
9/2
7/2
11/2
5/2
3/2
9/2
3/2
7/2
9/2
5/2
5/2
7/2
1/2
3/2
3/2
7/2
1/2
5/2

to perform the calculation of a neutron in the $s_{1/2}$, $d_{3/2}$, $d_{5/2}$ and $g_{7/2}$ levels coupled to the even-even ^{122}Xe core where the parameters of the latter were obtained from the calculation of even-even xenon isotopes of the present work. The parameters A, Γ and Λ were adjusted so as to produce a good fit. Their values, however, were chosen so as to vary smoothly with those used in fitting heavier odd Xe isotopes (Cunningham 1981b). The parameters used in the present fit are listed in table 16. In Fig. 82 a comparison between the experimental and theoretical levels is presented. The calculation reproduces the low-lying levels reasonably well, and also reproduces the high spin band built on the $g_{7/2}$ state (7/2, 9/2, 11/2, 13/2,...) which was observed in the in-beam study (Barci et al. 1981). Since the existence of the $7/2^+$ level at 38 keV is uncertain (chapter IV), the theoretical fit was attempted with and without the inclusion of this level. It was found that a better fit was obtained by excluding it.

b. Systematics of Odd-A Xe Isotopes

The systematics of positive parity low-lying levels in odd-A xenon nuclei are presented in Fig. 83. These systematics were established from the results of the present work and from the published results by Helppi et al. (1979, 1981) and Jha et al. (1972). The $1/2^+$ and $3/2^+$ levels are the ground state and first excited state in ^{123,125,127}Xe. The position of the $3/2^+$ state drops as the neutron number decreases from N = 73. The first excited $5/2^+$ and $7/2^+$ positions drop from ^{127}Xe to ^{125}Xe and the $5/2^+$ suddenly becomes the ground state in ^{121}Xe. This could be explained by the lowering of the Fermi level as the neutron number

TABLE 16. ^{121}Xe Hamiltonian Parameters

ODD Particle Parameters

A = -.05MeV	Γ = -.1MeV	Λ = 4MeV

	$3s_{1/2}$	$2d_{3/2}$	$2d_{5/2}$	$1g_{7/2}$
E_j (Mev)	1.2	1.34	1.25	1.4
V_j^2	.327	.220	.822	.768

Figure 83

Systematics of positive parity low-lying levels in odd-A xenon nuclei

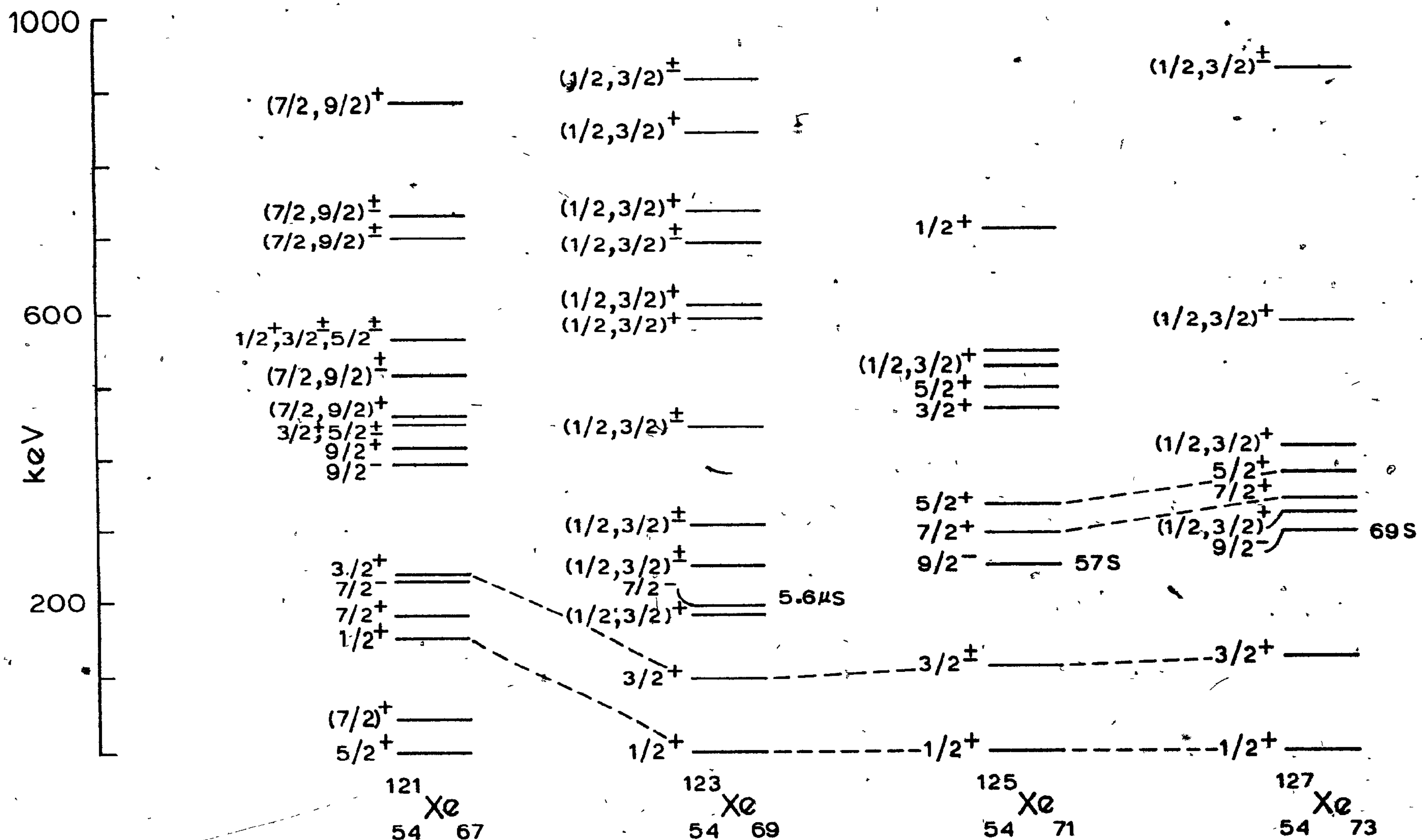
1000
600
200
keV
(7/2, 9/2)+
(7/2,9/2)±
(7/2,9/2)±
1/2+,3/2±,5/2±
(7/2,9/2)±
(7/2,9/2)+
3/2±,5/2±
9/2+
9/2−
3/2+
7/2−
7/2+
1/2+
(7/2)+
5/2+
121 Xe 54 67
(1/2,3/2)±
(1/2,3/2)+
(1/2,3/2)+
(1/2,3/2)±
(1/2,3/2)+
(1/2,3/2)+
(1/2,3/2)±
(1/2,3/2)±
(1/2,3/2)±
7/2−
5.6μs
(1/2,3/2)+
3/2+
1/2+
123 Xe 54 69
1/2+
(1/2,3/2)+
5/2+
3/2+
5/2+
7/2+
9/2−
57s
3/2±
1/2+
125 Xe 54 71
(1/2,3/2)±
(1/2,3/2)+
(1/2,3/2)+
5/2+
7/2+
(1/2,3/2)+
9/2−
69s
3/2+
1/2+
127 Xe 54 73

decreases. The fact that the Fermi level is much lower in A = 123 than in 125 and 127 is supported by the observation of many 1/2, 3/2 levels at low excitation in ^{123}Xe. The position of the first excited $3/2^+$ and $7/2^+$ states in ^{123}Xe is not known since in the present work only $J^\pi = 1/2$ and 3/2 states were populated. Unfortunately the in-beam results of Luukko et al.(1981) cannot be used with confidence since their spin assignments were based on the assumption that the 180 and 252 keV levels have $J^\pi = 5/2^+$ and $7/2^+$, and not $1/2^+$ and $3/2^+$ as the results of the present work indicate (chapter IV). Interpretation of low-lying states in ^{121,123}Xe, in terms of Nilsson model predictions, can be found in Sofia et al.(1981). An isomeric state of $9/2^-$ was observed in ^{127}Xe and ^{125}Xe with 69 sec and 55 sec lifetimes respectively (Helppi et al. 1979, Helppi et al. 1981). This isomeric state in ^{123}Xe is believed to be a $7/2^-$ (Luukko et al. 1981) which suggests that the lowest $7/2^-$ state is below the $9/2^-$. No isomeric state is observed in the case of ^{121}Xe, since positive parity high-spin states in this nucleus occur at low excitation, including a ground state of $5/2^+$.

CHAPTER VI

SUMMARY AND CONCLUSION

This section summarizes the studies carried out in this thesis project, and emphasizes the original work carried out by the author.

Both even- and odd- mass Xe nuclides are of considerable interest because a wide variety of theoretical models of the nucleus may be used to describe the observed levels. Studies of the heavier nuclei, namely $^{126,128}Cs$ and $^{129,127,125}Cs$, have been reported (Pathak et al. 1976, Droste et al. 1976) and (Jha et al. 1972, Schneider et al. 1979). Studies of lighter even isotopes of $^{118-122}Xe$ were also reported (Genevey-Rivier et al. 1977, Batsch et al. 1976). However little information was previously available on the decay of ^{124}Cs, ^{123}Cs and ^{121}Cs. Previous studies of these decays had aimed at determining their half-lives and decay energies (D'Auria and Preiss 1966, Chaumont et al. 1969, Mathur and Hyde 1954, Westgard et al. 1975) without attempting detailed nuclear spectroscopy. The present study of these nuclei was carried out in order to establish a complete systematic investigation of xenon nuclei which is essential for the interpretation of their structure.

Levels of ^{124}Xe, ^{123}Xe and ^{121}Xe were populated in the beta decay of radioactive samples of ^{124}Cs, ^{123}Cs and $^{121}Cs^{m,g}$. The cesium activity was produced by bombardment of 41% enriched ^{124}Xe targets with 15-52 MeV protons through (p,n), (p,2n) and (p,4n) reactions respectively, where xenon gas targets were used. These gas targets were encapsulated in beryllium containers with the use of a gas filling system (Bavaria 1975), which was modified for the experiments presented in this work in order to obtain a higher transfer efficiency. This higher efficiency was important, since the separated ^{124}Xe isotopes are very expensive and hence a very small amount of them was available. A fast pneumatic probe (Bavaria 1975) suitable for gas target transport was used to carry the targets to and from bombardment in the McGill synchrocyclotron.

In the investigation of low-lying levels of those nuclei, β and γ spectroscopy techniques were employed. The investigation was a challenging one due to the fact that for these nuclei most of the β- feeding is to the ground state with very little feeding to higher excited states. The spectra obtained were complex because of the mixed isotopic composition of the xenon targets, and by the production of other isotopes through open reaction channels at high bombarding energies. Gamma-ray energies and intensities were determined with the use of high-resolution germanium detectors. Gamma-gamma coincidence techniques were used in establishing decay schemes. Precise half-life measurements were carried out by observing the time decay of γ-rays depopulating excited states which were fed in the beta decay of the parent nucleus. These measurements yielded a half-life of 365 ± 4 sec for the decay of ^{123}Cs, $T_{1/2}$ = 136 ± 3 sec for the decay of the $3/2^+$ ground state of ^{121}Cs and $T_{1/2}$ = 121 ± 3 sec for the decay of the high-spin isomer ($9/2^+$). In the case of the short-lived ^{124}Cs, the use of the pneumatic fast probe allowed the counting of activity to start only a few seconds after the end of bombardment; hence a precise value of 29.7 ± 0.2 sec for the half-life was obtained. The beta end-point energies were measured for the intense positron branches through the $\beta - \gamma$ coincidence technique. In these measurements the positrons were detected with the use of the beta superconducting solenoid (Moore et al. 1976). Measurements of internal conversion coefficients by the usual technique of recording electron spectra were not possible because of the thickness of the beryllium container, which stops conversion electrons of $\leq$ 175 keV energy and causes broad lines for higher energy ones. Thus, an indirect method of determining the number of K-shell vacancies caused by the ejection of K conversion electrons per unit γ-ray intensity by determining X/γ was used. Using this method the K-internal conversion coefficients of the 38 keV transition in ^{121}Xe and the 83 and 97 keV transition in ^{123}Xe were determined to be $\alpha_K(38) = 11 \pm 1$, $\alpha_K(97) = 0.9 \pm 0.1$ and $\alpha_K(83) = 1.3 \pm 0.1$. These values suggest that the 38 KeV transition is 40% M1 + 60% E2, the 97 keV transition is 80% M1 + 20% E2 while the 83 keV transition is inferred to be 90% M1 $\pm$ 10% E2.

Precise gamma ray energies and intensities supported with the information from gamma-gamma coincidences led to the construction of decay schemes of ^{124}Cs, ^{123}Cs and $^{121}Cs^{g,m}$. Measured end- point energies as well as total beta feeding permitted the determination of percentage feeding to the ground state and the excited states and hence the calculation of log ft values. The decay schemes of both ^{124}Xe and ^{123}Xe represent the first extensive investigation of these nuclei and those of $^{121}Cs^{m,g}$ constitute the first decay schemes to be reported. The investigation of the decay of ^{123}Cs and $^{121}Cs^{m,g}$ was summarized in a publication (Sofia et al 1981) which may be found in the Appendix.

Low-lying levels in ^{121}Xe were fitted using the Interacting Boson Fermion Model of Arima and Iachello (1976B). A reasonably good fit was obtained for levels observed in the beta decay as well as high spin states observed in the in-beam study (Barci et al, 1981).

The position of the first excited 0^+ states (head of the β band) in even- xenon nuclei of mass 122 and 124 were confirmed in the present work.

These states were postulated in the present beta-decay study of ^{124}Cs and in the ^{122}Cs study of Genevey-Rivier et al. (1977) on the basis of their decay patterns. The present measurement confirms these 0^+ assignments by $\gamma - \gamma$ angular correlation techniques; in these studies the angular-correlation spectrometer consisted of a fixed Ge(Li) detector and a movable NaI(Tl) detector. For the case of ^{122}Xe another Ge(Li) detector was used in place of the NaI detector. The ^{124}Cs radioactive samples were produced as mentioned earlier in the (p,n) reaction on enriched ^{124}Xe targets. Samples of ^{122}Cs were produced in the (p,3n) reaction at 45 MeV bombarding energy. These measurements identified the levels at 1149 and 1269 keV to be the positions of the first excited 0^+ states in ^{122}Xe and ^{124}Xe respectively. The position of the second excited 0^+ position in ^{124}Xe was also identified to be the 1690 keV level. The results of the present work have been presented in a publication (Singh et al. 1979), a copy of which can be found in the Appendix. The identification of the first excited 0^+ position fits in the systematics of the position of these states in xenon nuclei where the energy increases with increasing numbers of neutrons. This is in agreement with the results of the dynamic calculations of collective states (Rohozinski et al. 1977) of even-even neutron deficient Xe and Ba isotopes. The positions determined are also in agreement with the positions predicted in the Interacting Boson Approximation calculation of even-even xenon nuclei which was carried out in the present work.

The present study also reports on high-spin states of ^{122}Xe and ^{124}Xe. These states were populated in the $(\alpha,4n\gamma)$ reaction on enriched targets of ^{122}Te (96.5%) and ^{124}Te (92.4%) respectively. The investigation of these isotopes was carried out using in-beam gamma-ray spectroscopy techniques. Contributions to the development of these techniques as well as to the construction and development of the in-beam set-up at McGill were made by the author. Precise gamma-ray energies and intensity measurements were carried out. Assignment of γ-rays were done on the basis of excitation functions, and by gamma-gamma coincidence measurements. Information on the multiplicity of gamma rays belonging to different cascades was obtained through the γ- multiplicity filter technique, which proved to be a very powerful technique in reducing beta-delayed activity as well as in enhancing γ-rays which are members of long cascades. In these measurements $\gamma - \gamma$ coincidence information of events was recorded along with the multiplicity of each event. The $\gamma - \gamma$ coincidence set-up consisted of two germanium detectors, while the multiplicity was recorded with the use of an array of six NaI detectors and one BGO. This array did not provide any information on the γ-ray energies. Another technique which was used in the investigation of these nuclei was a neutron multiplicity filter study. In these measurements γ-ray spectra were recorded in coincidence with different numbers of neutrons. Detection of neutrons was carried out by means of liquid scintillator detectors. This technique proved very useful in the assignment of γ-rays to different reaction channels having different numbers of outgoing neutrons. It also proved very effective in minimizing radioactivity lines.

Information about the mutipolarity of the emitted γ-rays and the spin-values of the levels was obtained from the angular distribution measurements, where the γ-ray yield at various angles relative to the incoming beam was obtained. These measurements were repeated in order to confirm the assignments.

In this in-beam investigation of $^{122,124}Xe$ the ground-state bands up to $J^{\pi} = 16^{+}$ were observed. Also the so-called quasi-gamma bands were observed up to $J^{\pi} = 5^{+}$ or 7^{+}. The backbending was observed in both nuclei to occur around spin $J^{\pi} = 10^{+}$, where the name refers to the unusual shape of the plot of the nuclear moment of inertia versus the square of the rotational frequency. At some critical value of the rotational frequency the sudden increase in the moment of inertia was accompanied by a decrease in the rotational frequency, causing a backbend in the plot. The present observations of this anomaly in the structure of the ground state band is the first to be reported for the xenon isotopes. In the present study, the backbending observed was interpreted in the framework of the rotational alignment model of Stephens and Simon (1972) as the result of the crossing of the ground state band and a decoupled two $h_{11/2}$ quasi-neutron band, where the quasi-neutron pair is broken by the Coriolis force and their angular momentum is aligned with that of the core. An anomalous $\Delta I = 2$ sideband was also observed in both ^{122}Xe and ^{124}Xe nuclei. These bands were found to be connected to the 8^{+} states of the ground band by pure dipole transitions. Therefore their possible spins are $(7,9)^{\pm}$, $(9,11)^{\pm}$ and $(11,13)^{\pm}$. Similar sidebands have been observed in $^{126,128}Ba$ isotopes (Flaum et al, 1976). However this is the first observation of such bands in xenon nuclei. These sidebands were interpreted as decoupled two-quasi-neutron bands. This is in accordance with the rotation alignment picture (Stephens and Simon, 1972, Simms et al, 1980).

Finally the ground-state bands observed in $^{116-130}Xe$ as well as quasi-gamma bands in these nuclei were fitted using the Interacting Boson Approximation. A good fit to the experimental spectra was obtained with a smooth variation of the parameters. This suggests that levels in the spectra of these nuclei may be reproduced with a group theoretical approach.

REFERENCES

A. Arima and F. Iachello, Ann. of Phys. 99 (1976a) 253.

A. Arima and F. Iachello, Phys. Rev. C14 (1976b) 761.

A. Arima and F. Iachello, Phys. Rev. Lett. 16 (1975) 1069.

A. Arima, T. Otsuka, F. Iachello and I. Talmi, Phys. Lett. 66B (1977) 205.

D.A. Arseniev, A. Sobiczewski and V.G. Soloviev, Nucl. Phys. A126 (1969) 15.

G. Azuelos, M. Belleau, J.E. Crawford and J.E. Kitching, Nucl. Inst. and Meth. I42 (1977) 491.

W. Bambynek, B. Crasemann, R.W. Fink, H.U. Freund, H. Mark, C.D. Swift, R.E. Price and P. Venugopala Rao, Rev. of Mod. Phys. 44 (1972) 716.

V. Barci, A. Gizon, J. Crawford, J. Genevey, J. Gizon and A. Płóchocki, Conference on Nuclei Far From Stability, Helsingor (1981) 478.

W.H. Barkas and M.J. Berger, Studies in Penetration of Charged Particles in Matter NAS-NRC Publication 1133 (1964) 187.

T. Batsch, M. Nowicki, J. Zylicz, D.D. Bogdanov, V.A. Karnaukhov, L.A. Pietrov and A. Płóchocki, 3rd Int. Conf. on Nuclei Far From Stability, Cargèse (1976) 106.

G. Bavaria, Ph.D. Thesis, McGill University, 1975.

I. Bergström, C.J. Herrlander, A. Kerek and A. Luukko, Nucl. Phys. A123 (1969) 99.

REFERENCES (cont'd.)

M. Blann, U.S. Atomic Energy Commission Report No. Coo-3494-29 (unpublished) 1978.

J.M. Blatt and V.F. Weisskopf, Theoretical Nuclear Physics, John Wiley and Sons, New York (1952) 627.

A.K. Bohr, Dan Vid. Selsk. Mat. Fys. Medd. 26 (1952) 14.

A. Charvet, J. Genevey-Rivier, L.C. Carraz, C. Richard-Serre, A. Knipper and G. Walter, Le Journal de Physique Lett. 38 (1977) L-241.

J. Chaumont, E. Roeckl, Y. NR-EL, C. Thibault-Phillippe, R. Klapisch and R. Bernas, Phys. Lett. 29B (1969) 652.

P. Chowdhury, U. Garg, T.P. Sjoreen and D.B. Fossan, Phys. Rev. C23 (1981) 733.

J.E. Clarkson, R.M. Diamond, F.S. Stephens and I. Perlman, Nucl. Phys. A93 (1967) 272.

T.W. Conlon and A.J. Elwyn, Nucl. Phys. A142 (1970) 359.

M.A. Cunninghan, to be published, 1981a.

M.A. Cunningham, Private communication, 1981b.

J.M. D'Auria and I.L. Preiss, Nucl. Phys. 84 (1966) 37.

J.M. D'Auria, J.W. Gruter, L. Westgaard, G. Nyman, P. Peuser, E. Roeckl and H. Otto, Int. Conf. on Nuclei Far From Stability, Cargèse (1976) 100.

A.S. Davydov and V.S. Rostovsky, Nucl. Phys. 12 (1959) 58.

A.W. Der Mateosian and A.W. Sunyar, Nucl. Data 13 (1974) 391.

A. De Shalit and H. Feshbach, Theoretical Nuclear Physics, J. Wiley and Sons, New York., Vol. 1 (1974) 552.

N. de Takacsy and S. Das Gupta, Phys. Rev. C13 (1976) 399.

R.M. Diamond, E. Matthias, J.O. Newton and F.S. Stephens, Phys. Rev. Lett. 16 (1966) 1205.

R.M. Diamond and F.S. Stephens, Ann. Rev. Nucl. Part. Sci. (1980) 85.

J. Dobaczewski, S.G. Rohozinski and J.Srebrny, Z. Phys. A282 (1977) 203.

J.E. Draper and R.M. Lieder, Nucl. Phys. A141 (1970) 211.

Ch. Droste, K.J. Blinowska, L. Goettig, T. Morek, J. Srebrny and A. Turowiecki, Z. Physik A277 (1976) 167.

Ch. Droste, L. Goettig, T. Morek, J. Srebrny, J. Bucka, J. Dobaczewski and S.G. Rohozinski, Z. Physik A284 (1978) 297.

Ch. Droste, W. Neubert, S. Chojnacki, T. Morek, K.F. Alexander and Z. Wilhelmi, Nucl. Phys. A192 (1972) 595.

H. Ejiri, T. Itahashi, Y. Nagai, T. Shibata, S. Nakayama, T. Kishimato, K. Maeda, H. Sakai and M. Hoshi, Nucl. Phys. A305 (1978) 167.

H. Ejiri, M. Ishihara, M. Sakai, K. Katori and T. Inamura, Phys. Lett. 18 (1965) 314; Nucl. Phys. 89 (1966) 641.

H. Ejiri, T. Shibata, A. Shimizu and K. Yagi, J. Phys. Soc. Japan, 33 (1972) 1515.

M. Eisenberg and W. Greiner, Nuclear Theory, North Holland Publ., American Elsevier Publ., Vol. 3 (1972) 133.

C. Ekstrom, S. Ingelman, G. Wannberg and M. Skarestad, Nucl. Phys. A292 (1977) 144.

W. Fischer, H. Huhnermann, G. Kromer and H.J. Shafer, Z. Phys. A270 (1974) 113.

C. Flaum, D. Cline, A.W. Sunyar and O.C. Kistner, Phys. Rev. Lett. 33 (1974) 973.

C. Flaum, D. Cline, A.W. Sunyar, O.C. Kistner, Y.K. Lee and J. S. Kim, Nucl. Phys. A264 (1976) 291.

W. Gelletly, B.J. Varley and J.C. Cunnane, J. Phys. G: Nucl. Phys. 2 (1976) 811.

J. Genevey-Rivier, A. Charvet, G. Marguier, C. Richard-Serre, J. D'Auria, A. Huck, G. Kotz, A. Knipper, G. Walter, Nucl. Phys. A283 (1977) 45.

J. Gizon and A. Gizon, Z. Phys. A285 (1978) 259.

L. Goettig, Ch. Droste, A. Dygo, T. Morek, J. Srebrny, R. Broda, J. Styczen, J. Hattula, H. Helppi and M. Jääskeläinen, Nucl. Phys. A357 (1981) 109.

E. Grosse, F.S. Stephens and R.M. Diamond, Phys. Rev. Lett. 31 (1973) 840.

D. Habs, H. Klewe-Nebenius, K. Wisshak, R. Löhken, G. Nowicki and H. Rebel, Z. Phys. 267 (1974) 149.

U. Hagemann, H.J. Keller, Ch. Protochristow and F. Stary, Z. Phys. A290 (1979) 399.

R.S. Hager and E.C. Seltzer, Nucl. Data Sec. A4 (1968) 1.

I. Halpern, B.J. Shepherd and C.F. Williamson, Phys. Rev. 169 (1968) 805.

H. Helppi, J. Hattula and A. Luukko, Nucl. Phys. A332 (1979) 183.

H. Helppi, J. Hattula, A. Luukko, M. Jääskeläinen and F. Dönau, Nucl. Phys. A357 (1981) 333.

D. Hetherington, private communication, 1981.

F. Iachello and A. Arima, Phys. Lett. 53B (1974) 309.

F. Iachello and O. Scholten, Phys. Rev. Lett. 43 (1979) 679.

S. Jha, N.F. Peck, W.J. Knox and E.C. May, Phys. Rev. C6 (1972) 2193.

A. Johnson, H. Ryde and J. Sztarkier, Phys. Lett. 34B (1971) 605.

A. Johnson, H. Ryde and S.A. Hjorth, Nucl. Phys. A179 (1972) 753.

A. Johnson and Z. Szymanski, Phys. Rep. C7 (1973) 181.

A. Kerek, C.J. Herrlander, A. Luukko and M. Grecescu, Phys. Lett. 31B (1970) 10.

J.E. Kitching, private communication, 1981.

K.S. Krane, Nucl. Inst. Meth. 98 (1972) 205.

H.W. Kraner, C. Chasman and K.W. Jones, Nucl. Inst. and Meth. 62 (1968) 173.

K. Kumar and M. Baranger, Phys. Rev. Lett. 12 (1964) 73.

K. Kumar, Proceedings of the International Conferences on the Properties of Nuclei Far From the Region of Beta Stability, Leysin, Switzerland, 1970, Vol. 2, p.779.

H. Kusakari, N. Yoshikawa, H. Kawakami, M. Ishihara, Y. Shida and M. Sakai, Nucl. Phys. A242 (1975) 13.

W. Kutschera, W. Dehnhardt, O.C. Kistner, P. Kump, B. Povh and H.J. Sann, Phys. Rev. C5 (1972) 1658.

R.M. Lieder and H. Ryde, Advances in Nuclear Physics, Vol. 10, Ed. M. Baranger and E. Vogt, Plenum Press, New York (1978) 1.

C.M. Lederer and V.S. Shirley, Table of Isotopes, 7th ed., John Wiley and Sons, New York (1978).

A. Luukko, J. Hattula, H. Helppi, O. Knuuttila and F. Dönau, Nucl. Phys. A357 (1981) 319.

G. Marguier, A. Charvet, J. Genevey, C. Richard-Serre, A. Knipper and G. Walter, J. Phys. G. Nucl. Phys. 7 (1981) 101.

H.B. Mathur and E.K. Hyde, Phys. Rev. 95 (1954) 708.

J. Meyer-Ter-Vehn, Nucl. Phys. A249 (1975) 111; A249 (1975) 141.

R.B. Moore, S.I. Hayakawa and D.M. Rehfield, Nucl. Inst. and Meth. 133 (1976) 457.

H. Morinaga and P.C. Gugelot, Nucl. Phys. 46 (1963) 210.

H. Morinaga and N.L. Lark, Nucl. Phys. 67 (1965) 315.

H. Morinaga and T. Yamazaki, In-Beam Gamma-Ray Spectroscopy, North Holland Publ., New York (1976).

S.A. Moszkowski, in Alpha, Beta and Gamma-Ray Spectroscopy, ed. by K. Siegbahn, North Holland Publ., Amsterdam (1965) Chapter XV.

M. Müller-Veggian, R.M. Lieder, A. Neskakis, Y. Gono and C. Mayer-Böricke, Proceedings of the International Symposium on High Excited States in Nuclei, Julich (1975) Vol. 1, p.50.

F. Münnich, H. Kugler, H. Schrader and R. Stippler, Nucl. Phys. A179 (1972) 205.

O. Nathan, Nucl. Phys. 4 (1957) 125.

J.O. Newton, F.S. Stephens, R.M. Diamond, W.H. Kelly and D. Ward, Nucl. Phys. A141 (1970) 631.

S.G. Nilsson, Mat. Fys. Medd. Dan-Vid. Selsk. 29 No. 16 (1955).

T. Otsuka, A. Arima, F. Iachello and I. Talmi, Phys. Lett. 76B (1978) 139.

B.P. Pathak, L. Lessard, L. Nikkinen and I.L. Preiss, Phys. Rev. C14 (1976) 1573.

R.H. Pehl, N.W. Madden, J.H. Elliott, T.W. Raudorf, R.C. Trammell and L.S. Darken, IEEE Transactions on Nuclear Science, Vol. NS-26, No. 1 (1979) 321.

R.K. Popli, J.A. Grau, S.I. Popik, L.E. Samuelson, F.A. Rickey and P.C. Simms, Phys. Rev. C20 (1979) 1350.

I. Rezanka, A. Kerek, A. Luukko and C.J. Herrlander, Nucl. Ph. A141 (1970) 130.

S.G. Rohozinski, J. Srenbrny, and K. Horbaczewsk, Z. Phys. 268 (1974) 401.

S.G. Rohozinski, J. Dobaczewski, B. Nerlo-Pomorska, K. Pomorski and J. Srebrny, Nucl. Phys. A292 (1977) 66.

J.T. Routti and S.G. Prussin, Nucl. Inst. and Meth. 72 (1969) 125.

H. Sakai, E. Ejiri, T. Shibata, Y. Nagai and K. Okada, Phys. Rev. C20 (1979) 464.

M. Sakai, Proceedings of the International Conference on Nuclear Structure, Tokyo (1967) 576.

M. Sakai and A.C. Rester, Atomic Data and Nuclear Data Tables 20 (1977) 441.

L.E. Samuelson, J.A. Grau, S.I. Popik, F.A. Rickey and P.C. Simms, Phys. Rev. C19 (1979) 73.

D.G. Sarantites, L. Westerberg, R.A. Dayras, M.L. Halbert, D.C. Hensley and J.H. Barker, Phys. Rev. C17 (1978) 601.

R.O. Sayer, J.S. Smith and W.T. Milner, Atomic and Nuclear Data Tables 15 (1975) 85.

E.W. Schneider, M.D. Glascock, W.B. Walters and R.A. Meyer, Phys. Rev. C19 (1979) 1025.

O. Scholten, Ph.D. Thesis, University of Groningen, unpublished (1979).

R.K. Sheline, T. Sikkeland and R.N. Chanda, Phys. Rev. Lett. 7 (1961) 446.

P.C. Simms, F.A. Rickey and R.K. Popli, Nucl. Phys. A347 (1980) 205.

B. Singh, R. Iafigliola, K. Sofia, J.E. Crawford and J.K.P. Lee, Phys. Rev. C19 (1979) 2409.

K. Sofia, B.N. Subba Rao and J.E. Crawford, Phys. Rev. C24 (1981) 1615.

H.A. Smith and F.A. Rickey, Phys. Rev. C14 (1976) 1946.

R.A. Sorenson, Rev. Mod. Phys. 45 (1973) 353.

F.S. Stephens and R.S. Simon, Nucl. Phys. A183 (1972) 257.

F.S. Stephens, R.M. Diamond and S.G. Nilsson, Phys. Lett. 44B (1973) 429.

F.S. Stephens, Rev. Mod. Phys. 47 (1975) 43.

R. Tacik, M.Sc. Thesis, McGill University, 1980.

T. Tamura et al, Nucl. Data Sheets 29 (1980) 453.

H.W. Taylor, B. Singh, F.S. Prato and R. McPherson, Nuclear Data Tables 9 (1971) 1.

H. Toki and A. Faessler, Z. Phys. A276 (1976) 35; Nucl. Phys. A253 (1975) 231.

P. Vogel, Phys. Lett. 60B (1976) 431.

A.H. Wapstra, G.J. Nijgh and R. Van-Lieshout, Nuclear Spectroscopy Tables, North Holland Publ., Amsterdam (1959).

A.H. Wapstra and K. Bos, Atomic and Nuclear Data Tables 19 (1977) 177.

D. Ward, H. Bertschat, P.A. Butler, P. Colombani, R.M. Diamond and F.S. Stephens, Phys. Lett. 56B (1975) 139.

L. Westgaard, K. Aleklett, G. Nyman and E. Roeckl, Z. Phys. A275 (1975) 127.

C.F. Williamson, S.M. Ferguson, B.J. Shepherd and I. Halpern, Phys. Rev. 174 (1968) 1544.

C.S. Wu and S.A. Moszkowski, Beta Decay, Interscience Publ., New York (1966).

T. Yamazaki, Nuclear Data A3 (1967) 1.

APPENDIX A

Decay of $^{121}Cs^{m,g}$ and ^{123}Cs

Physical Review C 1981

PHYSICAL REVIEW C VOLUME 24, NUMBER 4 OCTOBER 1981

Decay of $^{121}Cs^{m,g}$ and ^{123}Cs

K. Sofia, B. N. Subba Rao, and J. E. Crawford*
Foster Radiation Laboratory, McGill University, Montreal, Quebec, Canada
(Received 16 March 1981)

Radiations from $^{121}Cs^{m,g}$ and ^{123}Cs, produced by bombarding 41% enriched ^{124}Xe gas targets with protons, have been investigated with several Ge detectors in singles, two parameter γ-γ and β-γ coincidence, and multispectrum modes. Two groups of gamma rays with slightly different half-lives are observed in $^{121}Cs^m(\frac{9}{2}^+)$ to decay to high spin levels with a half-life of 121 ± 3 sec, and $^{121}Cs^g(\frac{3}{2}^+)$ to low spin levels with 136 ± 3 sec half-life. The decay energy of $^{121}Cs^g \to {}^{121}Xe^g$ was measured to be 5.40 ± 0.02 MeV and that of ^{123}Cs (365 ± 4 sec) to be 4.0 ± 0.1 MeV. K-conversion coefficients determined by the x/γ method are 11 ± 1 for the 38.38 keV transition of $^{121}Cs^m$, and 1.3 ± 0.1 and 0.9 ± 0.1 for the 83.38 and 97.39 keV transitions of ^{123}Cs, requiring these transitions to be 40% $M1$ + 60% $E2$, 90% $M1$ + 10% $E2$, and 80% $M1$ + 20% $E2$, respectively. The $\log ft$ values, the above multipolarities, and the branchings of electromagnetic transitions enable a few spin and parity assignments to levels in ^{121}Xe and ^{123}Xe. Decay schemes of $^{121}Cs^m(\frac{9}{2}^+)$, $^{121}Cs^g(\frac{3}{2}^+)$, and $^{123}Cs(\frac{1}{2}^+)$ are deduced from these observations. Some of the levels of ^{121}Xe and ^{123}Xe can be identified with low lying excitations of intrinsic states of the Nilsson model with deformation parameter $\beta = +0.16$ to $+0.19$.

[RADIOACTIVITY $^{124}Xe(p,2n)^{123}Cs$, $E_p = 33$ MeV; $^{124}Xe(p,4n)^{121}Cs$, $E_p = 52$ MeV; measured E_γ, I_γ, γ-γ coincidence, ICC, Q_{EC}; deduced ^{121}Xe, ^{123}Xe levels, $\log ft$, I, π; enriched Xe gas targets. In-beam $^{122}Te(\alpha,5n\gamma)^{121}Xe$, $E_\alpha = 69$ MeV, γ-γ coincidence, enriched Te targets.]

I. INTRODUCTION

The aim of this investigation is to obtain further knowledge of the structure of nuclei in the transitional region. Isotope shift and Coulomb excitation studies[1] of even-even stable Te, Xe, and Ba nuclei have demonstrated that the deformation parameter is about $|\beta| \leq 0.1$ at $N = 80$ and increases with decreasing neutron number N to $|\beta| = 0.22$ at $N = 68$. Some theoretical unified model calculations[2] preceded the experimental evidence and had speculated on the existence of shape isomerism while predicting for odd-A Xe nuclei a deformation parameter β increasing from $+0.15$ or -0.16 at $N = 73$ to $+0.26$ or -0.30 at $N = 61$. Odd-A Xe nuclei with $N \leq 69$ so far have not been the subject of sufficient research, while even-even Xe nuclei down to $A = 114$ have been extensively and intensively investigated. Spin and parity measurements[3] of the Cs isotopes have revealed that Cs nuclei with $N \leq 68$ require a Nilsson model description with a deformation parameter $\beta \simeq +0.28$ to explain[2] $^{121}Cs^m(\frac{9}{2}^+[404\uparrow])$, $^{121}Cs^g(\frac{3}{2}^+[422\downarrow])$, and $^{123}Cs(\frac{1}{2}^+[420\uparrow])$ levels. These developments indicate that the daughters ^{121}Xe and ^{123}Xe may exhibit characteristic Nilsson level structure of moderate deformations, as well as the Cs parents.

The present work is aimed at experimentally investigating the nuclear structure of ^{121}Xe and ^{123}Xe, using 41% enriched ^{124}Xe gas targets bombarded by protons to produce $^{121}Cs^{m,g}$ and ^{123}Cs through $(p,4n)$ and $(p,2n)$ reactions. Previous studies of these decays had aimed at determining their half-lives[4–7] and decay energies[4,8] without attempting detailed nuclear spectroscopy. In the following experimental procedure, results and decay schemes of

$^{121}Cs^{m}$, $^{121}Cs^{g}$, and ^{123}Cs are presented along with relevant discussion of the nuclear structure of ^{121}Xe and ^{123}Xe in terms of Nilsson model intrinsic states.

II. EXPERIMENTAL PROCEDURE

Target material of 100.0 mole % Xe gas consisted, in terms of mole % abundances in parenthesis, enriched to ^{124}Xe (40.5), ^{126}Xe (9.7), ^{128}Xe (12.5), ^{129}Xe (34.9), ^{130}Xe (1.0), ^{131}Xe (1.1), ^{132}Xe (0.3), ^{134}Xe, and ^{136}Xe (<0.1). This target gas was transferred into a beryllium target container in a vacuum. This target container had a tapered head of about 0.25 mm wall thickness and 0.8 mm side wall. After sealing, it was mounted in a 2.50 cm outer diameter Delrin holder.[9] In order to reduce radioactive buildup, several such targets were used in rotation. These targets were blown down penumatically to the predetermined proton orbit radius of the internal circulating beam of the McGill synchrocyclotron. After bombardment for a time period of the order of a fraction of the half-life of the isotope to be produced, the target was blown back pneumatically. Cooling these activated targets for about a half minute reduced the short-lived activities of ^{124}Cs (30 sec) and ^{126}Cs (98 sec) significantly. Beryllium (99.88% pure) was chosen for target container material since it is a nonporous material and does not produce short-lived γ activity when bombarded by protons.[9] Because of the isotopic composition of Xe target material, several (p,xn)Cs, (p,pxn)Xe, and $(p,\alpha xn)$I isotopes were produced along with ^{121}Cs or ^{123}Cs of concern here. High resolution Ge detector γ-ray spectra together with half-life data from multispectra were usually sufficient to identify γ rays of an isotope.

Singles γ-ray spectra and multispectra were recorded with an x-ray detector of 250 eV FWHM, and three large volume Ge detectors of 2 keV FWHM, by means of a state of the art modular electronic system interfaced to the on-line computer (PDP-15). A γ-ray multispectrum was observed over four half-lives, consisting of several time bins, with and without the positron annihilators. This annihilator was a 4.267 g/cm^2 Cu jacket around the source. The multispectrum with this annihilator yielded the total positron count relative to the prominent γ ray of the isotope, so that a ground to ground positron branch could be deduced. γ-ray spectra were analyzed for energy and intensity and the multispectra data were used to sort them according to half-life.

Four Ge detectors were used in two pairs to record two parameter γ-γ coincidence data by means of the on-line computer. Data were recorded on magnetic tape event by event. In these coincidence experiments the two detectors were placed nearly 90° relative to each other with the source at the center to avoid collinear or 180° coincidence events from annihilation quanta. The interscattering between the two detectors was minimized with radiation intercepting graded absorbers. Such coincidence data were analyzed by setting digital gates on either detector spectrum.

The decay energy of ^{123}Cs was measured by means of two parameter β-γ coincidences. For this purpose a vertical superconducting solenoid was used to minimize γ-ray background in the intrinsic Ge detector which determined the energy resolution of the positron spectrum.[10] A vertical 8% Ge(Li) detector below the source was the γ-ray spectrometer with 2.4 keV FWHM. Data analysis was similar to the two parameter γ-γ coincidence experiments using digital gates on the γ-ray spectrum to obtain coincident positron spectra. Fermi-Kurie (FK) plots of such coincident spectra gave the positron end-point energy, from which the decay energy of ^{123}Cs was deduced.

The larger decay energy of ^{121}Cs was manifest in γ-ray multispectra with Ge detectors, in that the positron spectrum, with over-riding γ rays, was clearly visible from 1 MeV upward in the γ-ray spectra. The γ-ray count beyond 3.5 MeV was negligible so that a Fermi-Kurie plot analysis of the 3.5 to 4.0 MeV region of these multispectra gave both the half-life and end-point energy of the highest energy positron group. While these multispectra were without the annihilator, the γ-ray multispectrum with positron annihilator had shown that the $^{121}Cs^{g} \rightarrow {}^{121}Xe^{g}$ positron spectrum (83% of ^{121}Cs decay) dominates all other positron components in this energy region. Therefore, the end-point energy from this Fermi-Kurie plot was used to deduce the decay energy of $^{121}Cs^{g}$.

The Be container of the Xe gas target, 47 mg/cm^2 thick in the tapered end and 140 mg/cm^2 thick on the sides, stops internal conversion electrons of 175 keV and less. Energy loss and straggling persists up to 500 keV resulting in broad lines and large low energy tails, riding on a Compton continuum of γ rays. The most highly internally converted transitions of interest are the 38.38, 83.38, and 97.39 keV ones. An indirect method of determining the number of K-shell vacancies caused by the ejection of K conversion electrons per unit γ-ray intensity by determining X/γ was used. The two-parameter γ-γ coincidence data was sufficient to obtain the K conversion coefficients (α_K) of the 83.38 and 97.39 keV transitions of ^{123}Cs. However, to determine the α_K of the 38.38 keV transition ^{121}Cs and to ensure that this transition does appear in high spin band structure, an auxiliary experiment ^{122}Te(69 MeV $\alpha,5n\gamma$)^{121}Xe was performed with the external α beam of the McGill synchrocyclotron. In this experiment a ^{122}Te target isotopically enriched to 96.45% and containing 0.14% ^{123}Te, 0.34% ^{124}Te, 0.45% ^{125}Te, 0.88% ^{126}Te, 0.97% ^{128}Te, and 0.77% ^{130}Te was used. One x-ray detector and one large volume Ge detector were used for two parameter γ-γ coincidence in-beam experiment. From the two parameter coincidence data analysis, the X/γ ratio of the 38.38 keV transitions, which was found as intensely as in ^{121}Cs decay, was determined and used to deduce its α_K.

III. EXPERIMENTAL RESULTS

A. $^{121}Cs^m$ and $^{121}Cs^g$

Energies and relative intensities of γ rays were determined with γ-ray spectra obtained by means of a 250 eV FWHM x-ray detector [Fig. 1(a)] and a 2 keV FWHM large volume Ge detector [Fig. 1(b)]. γ-ray multispectrum data obtained with a large volume Ge detector and with an x-ray detector suggest the existence of two distinct groups of γ rays of ^{121}Cs decay: the group of γ rays of energy 179.4, 196.1, and 234.5 keV having 121 ± 3 sec half-life (Fig. 2), which are known to belong to the high spin band structure of positive and negative parities of ^{121}Xe,[11] and a second group of γ rays of energy 85.85, 153.75, and 239.6 keV with 136 ± 3 sec half-life (Fig. 2), which are not associated with this high spin band structure.[11] The first group of γ rays is due to $^{121}Cs^m(\frac{9}{2}^+)$ decay and the second one is due to $^{121}Cs^g(\frac{3}{2}^+)$ decay. Previous half-life determination had resulted in 125.6 ± 1.4 sec (Ref. 5) for ^{121}Cs, without $^{121}Cs^m$ and $^{121}Cs^g$ distinction. The existence of a γ decay branch for $^{121}Cs^m$ is confirmed by the observation of Cs $K_{\beta1}$ and Cs $K_{\beta2}$ x rays of about 2 min half-life [$\times 13$ magnified region in Fig. 1(a)]. The Cs K_β x-ray intensity is 3.0 ± 0.5 relative to the 38.38 keV γ ray. Based on the Weisskopf estimate an isomeric $\frac{9}{2}^+ \rightarrow \frac{3}{2}^+$ $M3$ transition with a half-life of about 2 min has an en-

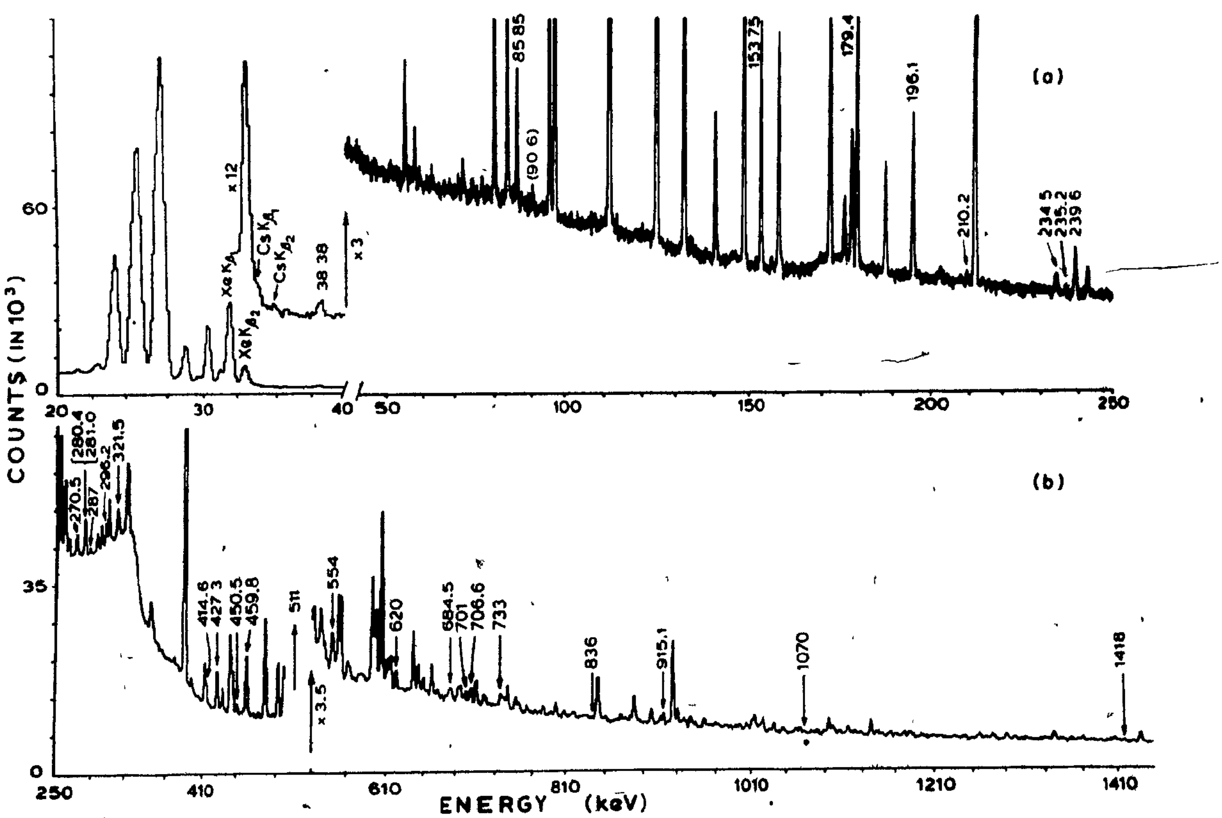

FIG. 1. ^{121}Cs γ-ray spectrum recorded with (a) low energy photon detector, and (b) a large volume Ge(Li) detector. Cs $K_{\beta1}$ and $K_{\beta2}$ x rays and 38.38 keV γ ray are shown magnified.

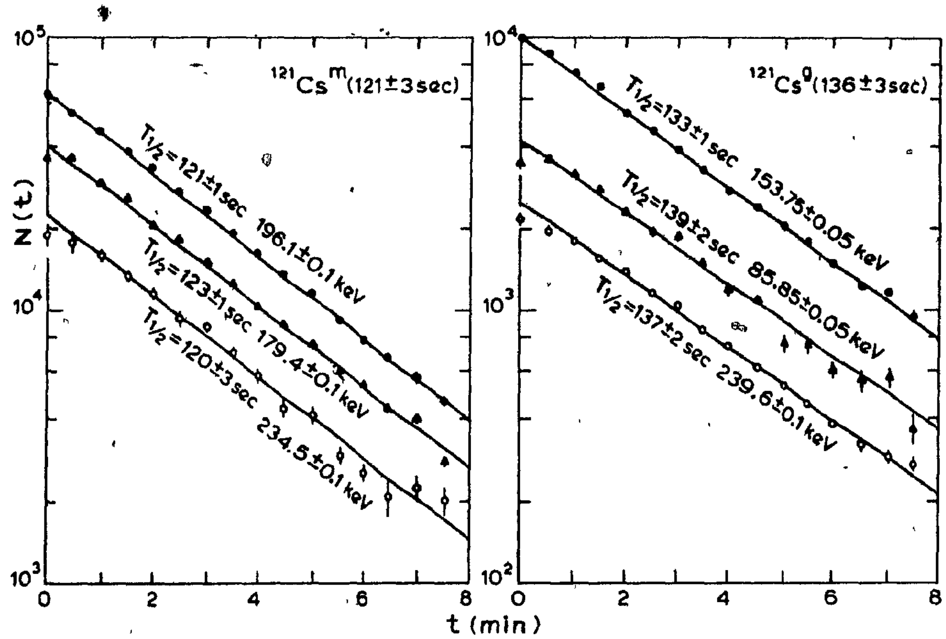

FIG. 2. Two distinct groups of γ rays of ^{121}Cs with 121 ± 3 and 136 ± 3 sec half-life.

ergy of about 36 keV, $\alpha_T \simeq 11\,100$.[12] Therefore, the isomeric γ-ray intensity of 0.0065, relative to the Cs $K_{\beta1}$ x ray [Fig. 1(a)] is below the limits of observation. These results, together with the fluorescence yield[13] for Cs, $\omega_K = 0.895$, and K x ray to K_β x-ray intensity ratio of 5.257,[13] require $^{121}Cs^m$ to have (60 ± 4)% isomeric transition to $^{121}Cs^g$, and (40 ± 4)% positron emission and electron capture to ^{121}Xe. There are more than 25 other γ rays with about 2 min half-life identified from multispectrum analysis as belonging to ^{121}Cs decay.

γ-γ coincidence results (Fig. 3, Table I) obtained with the $^{121}Cs^{m,g}$ source and analyzed by setting digital gates on either the x-ray detector or the large volume detector require mutual coincidences between the 196.1 and 38.38 keV γ rays, and no coincidences between the most intense γ rays of energy 153.75, 179.4, and 196.1 keV in any pairwise combination. The γ rays of 196.1 and 38.38 keV are in coincidence (Fig. 3), but which one of them directly feeds the ground state of ^{121}Xe can be determined only by knowing the total transition intensity of these two transitions. This requires the internal conversion coefficient (ICC) and multipolarity, in particular, of the low energy highly converted transition of 38.38 keV. The spectrum of Xe K x rays and the 38.38 keV γ ray in the 196.1 keV γ gate (Fig. 3) gives through the X/γ ratio only an upper limit of $\alpha_K < 27$, because Xe K x rays arise both due to K conversion and K capture processes. The auxiliary $^{122}Te(69\text{ MeV }\alpha5n\gamma)^{121}Xe$ in-beam two parameter γ-γ coincidence experiment does not generate any K capture x rays and the region of the 38.38 keV γ ray also shows the well resolved Xe $K_{\beta1}$ and $K_{\beta2}$ x rays due to the dominant internal conversion of this transition (Fig. 4), recorded with the x-ray detector. From this γ/X ratio, the K conversion coefficient $\alpha_K = 11 \pm 1$ is deduced for this 38.38 keV transition, using the fluorescence yield[13] for the K shell of Xe, $\omega_K = 0.889$, and the K_β x ray to total K x-ray intensity ratio of 0.155.[13] Theoretical[12] α_K values for various multipolarities of this 38.38 keV transition in ^{121}Xe are 10.4($E2$), 11.51($M1$), 2.44($E1$), 263($M2$), 18.2($E3$), and 0.1230($M3$). From a comparison of the experimental and theoretical $\alpha_K S$, the 38.38 keV transition is inferred to be 40% $M1$ + 60% $E2$. This α_K and multipolarity require a total ICC[12] of $\alpha_T = 43$, so that although the 38.38 keV γ-ray has only 3.8 ± 0.5% intensity relative to the 196.1 keV γ ray, the 38.38 keV transition intensity is 167% of the 196.1 keV transition. Therefore, the 38.38 keV transition is below the 196.1 keV transition in the coincident cascade and these two are at the bottom of the negative parity band structure.[11]

The standard deviation on the α_K does not rule out pure $M1$ or pure $E2$ multipolarities. Pure $E2$ multipolarity requires a total ICC of $\alpha_T = 62.6$, which would make the 38.38 keV transition intensity 242% of the 196.1 keV transition, which would

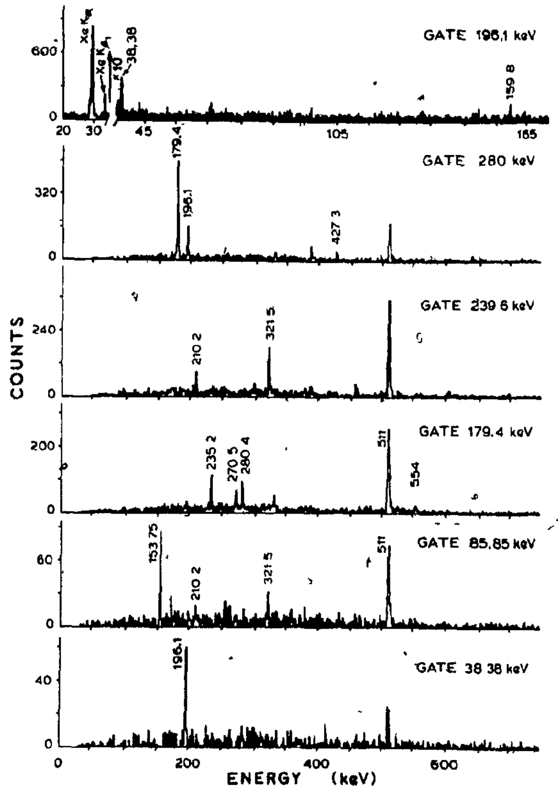

FIG. 3. γ-γ coincidence spectra of ^{121}Cs for γ gates in keV shown therein.

mean more feeding and a lower logft value for the 38.38 keV level. Pure $M1$ multipolarity would mean an ICC of $\alpha_T = 13.4$, so that the 38.38 keV transition intensity is 51% of the 196.1 keV transition; in this case the 196.1 keV would be below the

TABLE I. $^{121}Cs^{m,g}$ gamma-gamma coincidence results.

Gate E_γ (keV)	Coincident gamma rays, E_γ (keV).
38.38	196.1
85.85	153.75, 210.2, 321.5
153.75	85.85, 296, 915
179.4	235.2, 270.5, 280.4, 554
196.1	38.38, 159.9, 281
235.2	179.4
239.6	210.2, 321.5
270.5	179.4
280.4 } 281 }	179.4, 196.1, 427.3
321.5	85.85
554.0	179.4

38.38 keV. Without extremely precise values no certitude can be associated with the ordering of these transitions.

After separating the decay of ^{121}Cs into $^{121}Cs^m(\frac{9}{2}^+)$ and $^{121}Cs^g(\frac{3}{2}^+)$ decay schemes based on the 121 ± 3 and 136 ± 3 sec half-lives, respectively, and using the coincidence results in Fig. 3 and Table I, and the Ritz combination principle, the transitions belonging to the two separate decay modes were deduced in terms of their energies and intensities (Tables II and III). There are a few other low intensity γ rays, such as the 90.6 keV γ rays in Fig. 1, which have about 2 min half-life but which could not be definitely placed in either of the decay modes. They are not included in Table II or III. A 69 keV transition was observed in an in-beam study by Chowdhury *et al.*[11] and assigned to the negative parity high spin band. In our γ-γ coincidence in-beam measurement we did not observe that transition (Fig. 4). From these data one concludes that if the 69 keV γ ray does exist it would be very weak, $< 3\%$ of the 38.38 keV γ-ray intensity.

The annihilation quantum intensity due to all positrons of $^{121}Cs^m + {}^{121}Cs^g$ relative to 100 γ rays of 196.1 keV was determined from the γ-ray multispectrum with the 4.267 g/cm^2 positron annihilation of Cu by extracting the 2 min component through least squares analysis to overcome contributions from other Cs, Xe, and I positron emitters in

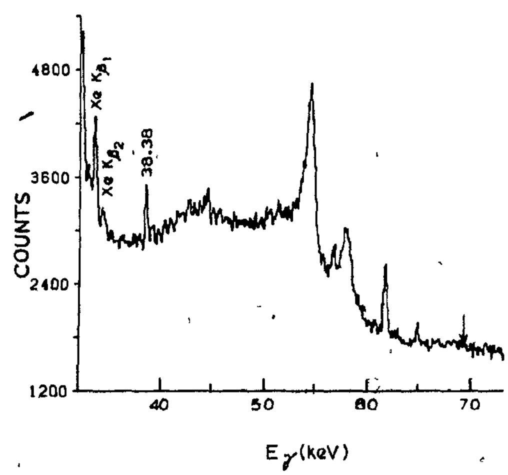

FIG. 4. $^{122}Te(69$ MeV $\alpha,5n\gamma)^{121}Xe$ in-beam γ-γ coincidence gating spectrum recorded with 250 eV FWHM low energy photon detector to determine α_K of the 38.38 keV transition. The arrow points at the position of a proposed 69 keV transition.

TABLE II. $^{121}Cs^{m}$(121 ± 3 sec) gamma-ray energy and intensity.

E_γ (keV)	I_γ%	E_γ (keV)	I_γ%
38.38 ± 0.02	3.8 ± 0.5	414.6 ± 0.2	19 ± 5
159.8 ± 0.3	4 ± 1	427.3 ± 0.1	39 ± 4
179.4 ± 0.1	96 ± 5	459.8 ± 0.1	51 ± 3
196.1 ± 0.1	100	554.0 ± 0.2	8 ± 1
234.5 ± 0.1	20 ± 1	684.5 ± 0.3	1.9 ± 0.5
235.2 ± 0.1	6 ± 1	701.0 ± 0.5	1.5 ± 0.5
280.4 ± 0.5	16 ± 1	706.6 ± 0.3	3 ± 1
281.0 ± 0.5	6 ± 1	733 ± 1	2 ± 1
287 ± 1	2 ± 1	1418 ± 1	1.0 ± 0.5

the ^{121}Cs source to be 12 363 ± 776, corresponding to 6182 ± 388 positrons of $^{121}Cs^{m}$ + $^{121}Cs^{g}$. Earlier decay energy measurement[8] through the β-γ coincidence method had obtained 1263 ± 282 annihilation quanta of ^{121}Cs per 100 γ rays of 195 ± 1 keV. The present positron intensity and transition intensity balance require 98 ± 7 % of the $^{121}Cs^{g}$ (136 ± 3 sec) decay to feed $^{121}Xe^{g}$, corresponding to 89% positron branching. This is the most intense positron group in the decay of ^{121}Cs. $^{121}Cs^{m}$ activity of positron emission plus electron capture was only 5.7 ± 0.5% of the corresponding activity of $^{121}Cs^{g}$ in the source of ^{121}Cs from the (p,4n) reaction. This result, together with the Cs K_β x-ray intensity, suggest that the activation cross sections of ^{124}Xe(52 MeV p,4n)$^{121}Cs^{m,g}$ are in the ratio of $(\sigma^{g}_{3/2^+}/\sigma^{m}_{9/2^+})\simeq 6$.

With the large volume Ge detector x-ray multispectrum without the positron annihilator of Cu, a very conspicuous β continuum following a half-life of 2 min was noticed in the 1 to 4 MeV energy region. The 3.5 to 4 MeV region of this continuum was free from γ-ray disturbance. In view of the above inference that 98% of all positrons of $^{121}Cs^{g}$ or 92% of all positrons of $^{121}Cs^{m}$ + $^{121}Cs^{g}$ is the ground to ground positron component of ^{121}Cs decay, this continuum in this region is considered to be due to this component. A Fermi-Kurie plot analysis (Fig. 5) of this positron component from the 2 and 5 min bins of the γ-ray multispectrum through the least square method resulted in 4.37 ± 0.02 and 4.42 ± 0.06 MeV, and a weighted mean value of 4.38 ± 0.02 MeV, for the end-point energy of the highest energy and highest intensity positron component. Only the standard deviation from the least squares analyses are shown in these numbers. This result corresponds to a decay energy of $^{121}Cs^{g}$ to $^{121}Xe^{g}$ of Q_{EC} = 5.40 ± 0.02 MeV, to be compared to the earlier result[8] of $Q_{EC} \geq 5.65 \pm 0.49$ MeV (where EC represents electron capture). If the mass excess of ^{121}Xe is taken as −82.33 ± 0.11 MeV, then the mass excess of $^{121}Cs^{g}$ is −76.93 ± 0.11 MeV from the present result, while the earlier tabulation[13] was −77.13

TABLE III. $^{121}Cs^{g}$(136 ± 3 sec) gamma-ray energy and intensity.

E_γ (keV)	I_γ%	E_γ (keV)	I_γ%
38.38 ± 0.02	0.009 ± 0.005	296.2 ± 0.1	10.6 ± 0.5
85.85 ± 0.05	11.4 ± 0.6	321.5 ± 0.1	10 ± 1
153.7 ± 0.05	73 ± 2	450.5 ± 5	9 ± 1
179.4 ± 0.1	10.3 ± 0.3	563 ± 1	13 ± 2
196.1 ± 0.1	0.33 ± 0.16	620.0 ± 0.5	3 ± 1
210.2 ± 0.5	10 ± 2	836 ± 1	0.4 ± 0.2
234.5 ± 0.1	0.07 ± 0.04	915.1 ± 0.2	1.8 ± 0.8
239.6 ± 0.1	50 ± 1	1070 ± 1	0.7 ± 0.4
270.5 ± 0.5	11.3 ± 0.3		

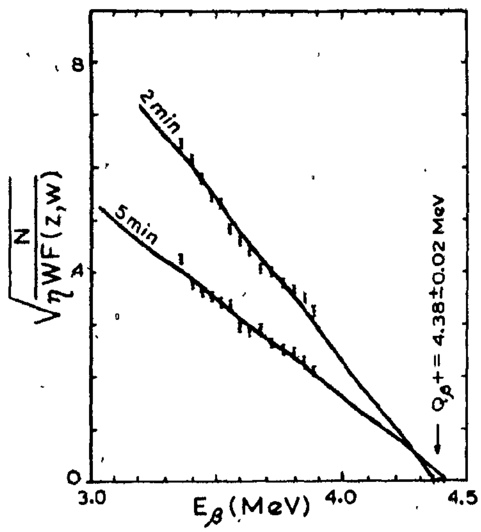

FIG. 5. FK plots of β spectrum of $^{121}Cs^g \rightarrow {}^{121}Xe^g$ observed in 2 and 5 min bins of a large volume Ge(Li) multispectrum. Solid lines are the least squares fit to data points. The end-point energy shown is the weighted mean of the two results.

MeV from mass systematics. The isomeric $^{121}Cs^m(\frac{9}{2}^+$, 121 ± 3 sec) state, being ≃36 keV above the $^{121}Cs^g(\frac{3}{2}^+$, 136 ± 3 sec) state, has a mass excess of −76.89 ± 0.11 MeV.

B. ^{123}Cs

The γ-ray spectrum of the $(p,2n)$ reaction product ^{123}Cs recorded with an x-ray detector [Fig. 6(a)], and a 2.2 keV FWHM Ge(Li) with a positron annihilator of Cu [Fig. 6(b)] and without the annihilator [Fig. 6(c)] indicates that the number of impurity γ rays is less with ^{123}Cs than with ^{121}Cs (Fig. 1). This is due to the fewer exit channels of (p,xn), (p,pxn), and $(p,\alpha xn)$ reactions at 33 MeV than at 52 MeV proton energy. The γ-ray multispectrum with x-ray and Ge(Li) detectors yields the half-life of ^{123}Cs to be 365 ± 4 sec, for the most intense 83.38 and 97.39 keV γ rays. This result is to be compared to 336 ± 6 sec,[4] 352 ± 3 sec,[5] 360 sec,[6] and 480 ± 30 sec.[7] The other γ rays nearly following this half-life were identified as belonging to ^{123}Cs decay. Their energies and relative intensities are given in Table IV.

Digitized γ-γ coincidence events were recorded on magnetic tape event by event. A sample of coincident γ-ray spectra for a few significant gates is shown in Fig. 7, and most of the coincidence results are given in Table V. Coincidence results require the 610 keV γ-ray peak to be a doublet consisting of 610.3 ± 0.2 and 610.9 ± 0.2 keV components, whose relative intensities were deduced to be as given in Table IV.

TABLE IV. $^{123}Cs(365 \pm 4$ sec) gamma-ray energy and intensity.

E_γ (keV)	I_γ%	E_γ (keV)	I_γ%
71.26 ± 0.03	1.2 ± 0.1	596.4 ± 0.2	57 ± 3
83.38 ± 0.02	21 ± 1	610.3 ± 0.2	1.3 ± 0.4
97.39 ± 0.03	100	610.9 ± 0.2	16.7 ± 1.9
180.77 ± 0.03	3.1 ± 0.3	644.1 ± 0.1	15 ± 2
209.7 ± 0.2	0.7 ± 0.2	667.6 ± 0.4	7 ± 1
238.0 ± 0.5	2.2 ± 0.6	693.6 ± 0.4	8 ± 2
252.0 ± 0.5	2.2 ± 0.6	711.0 ± 0.2	4 ± 1
261.9 ± 0.1	13 ± 1	725.0 ± 0.5	1.3 ± 0.3
278.0 ± 0.5	1.1 ± 0.4	741.5 ± 0.1	17 ± 2
294.5 ± 0.5[a]	1.6 ± 0.4	750.7 ± 0.2	4.8 ± 0.7
304.0 ± 0.1	5 ± 1	819.0 ± 0.5	1.2 ± 0.6
307.1 ± 0.1	21 ± 1	841.8 ± 0.2	1.8 ± 0.5
344.5 ± 0.5	3.4 ± 0.9	849.0 ± 0.5	0.7 ± 0.4
405.0 ± 0.5	1.1 ± 0.2	945.0 ± 0.3	1.9 ± 0.5
422.0 ± 0.5	0.7 ± 0.3	1125.3 ± 0.3	3.7 ± 0.3
430.0 ± 0.5	0.8 ± 0.2	1176.2 ± 0.4	9 ± 4
434.3 ± 0.2	4.7 ± 0.7	1255.8 ± 0.4[a]	1.6 ± 0.5
498.9 ± 0.2	6 ± 2	1273.2 ± 0.2	14 ± 2
511 ($\gamma^\pm$)	1300 ± 200	1355.6 ± 0.5	5 ± 2
540.5 ± 0.5	4 ± 1	1453.0 ± 0.5	1.1 ± 0.5

[a]Not placed in the decay scheme.

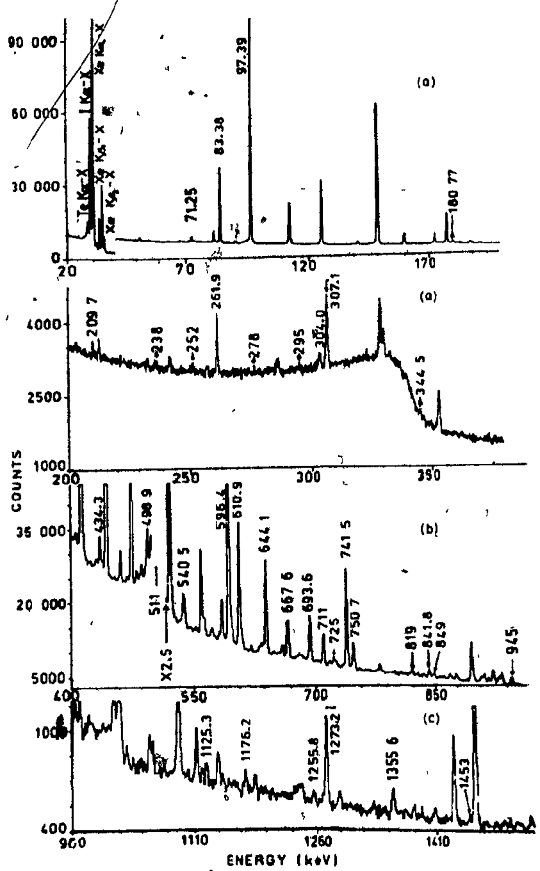

FIG. 6. [123]Cs γ-ray spectrum recorded with (a) 250 eV FWHM low energy detector, (b) 2.2 keV FWHM Ge(Li) detector with positron annihilator, and (c) without this annihilator.

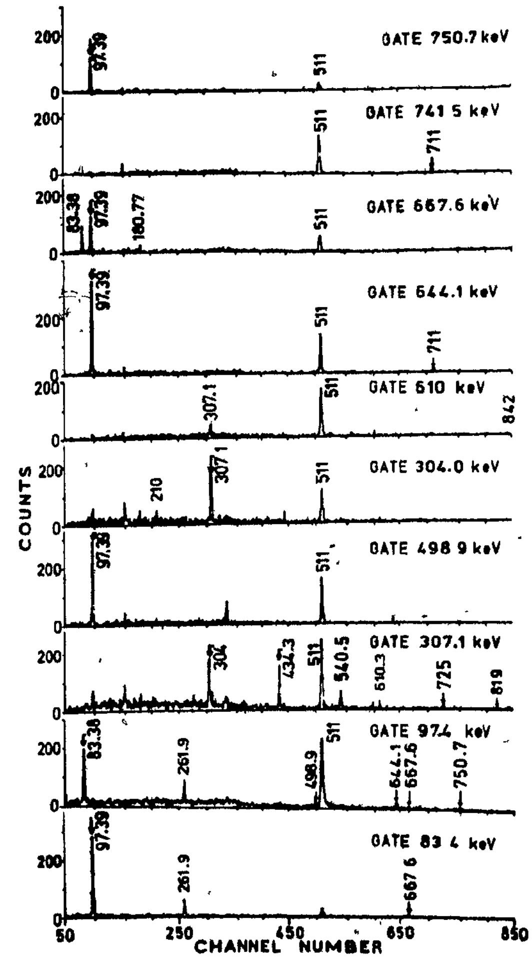

FIG. 7. [123]Cs γ-γ coincidence spectra for the gates shown as γ-ray energy in keV.

TABLE V. [123]Cs gamma-gamma coincidence results.

Gate E_γ (keV)	Coincident gamma rays, E_γ (keV).
83.38	71.26, 97.39, 261.9, 430.3, 667.6, 945.0
97.39	83.38, 209.7, 261.9, 498.9, 644.1, 667.6, 750.7, 1355.6
261.9	83.38, 97.39, 180.77, 405
304.0	209.7, 307.1
307.1	304, 434.3, 540.5, 610.3, 725, 819
498.9	97.39
610.3 } 610.9 }	307.1, 841.9
644.1	97.39, 711
667.6	83.38, 97.39, 180.77
741.5	711
750.7	97.39

Because gas targets are enclosed in 175 keV electron energy equivalent Be containers, the ICC of the highly converted high intensity 83.38 and 97.39 keV transitions were determined by the X/γ ratio method. X rays in coincidence with any γ ray are due to internal conversion and electron capture; the annihilation quantum (511 keV) gate was used to bypass capture x rays. The resulting x-ray detector spectrum [Fig. 8(a)] shows Xe $K_{\alpha 1}$, $K_{\beta 1}$, and $K_{\beta 2}$ x rays and both 83.38 and 97.39 keV γ rays. If the intensity ratio of the 83.38 and 97.39 keV γ rays in the 511 keV gate is C_1 and that of the Xe K x ray and the 97.39 keV γ ray in the same spectrum is C_2 (0.085 ± 0.005 and 0.86 ± 0.02, respectively), and if $\alpha_K(83)$ and $\alpha_K(97)$ are the K-conversion coefficients of the 83 and 97 keV transitions, then

$$C_1 \alpha_K(83) + \alpha_K(97) = \frac{C_2}{\omega_K}\,, \tag{1}$$

where ω_K is the K shell fluorescence yield of the Xe atom ($\omega_K = 0.889$).[13] At least one more coincidence relation between the 83 and 97 keV transitions is required in order to solve for their α_K's. The 261.9 keV γ gate provides [Fig. 8(b)] this needed relation. If C_4 is the ratio of observed relative intensities of the 83.38 and 97.39 keV γ rays in this gate and since the transition intensities of the 83 and 97 keV transitions should be equal in the 261.9 keV gate, then

$$C_4 \alpha_K(83) - \alpha_K(97) = R(1 - C_4)\,, \tag{2}$$

where R is the α_K to total ICC, α_T ratio, which is the same for both the 83.38 and 97.39 keV transitions, being 0.86 in the $M1$ limit.[12] A contour plot of these two coincidence relations gives $R = 0.80 \pm 0.01$ for both transitions. Using C_4, which was deduced to be $C_4 = 0.79 \pm 0.03$, it is possible to solve these coincidence relations with the results $\alpha_K(83) = 1.3 \pm 0.1$ and $\alpha_K(97) = 0.9 \pm 0.1$. Theoretical[12] α_K's of 1.20($M1$) and 2.12($E2$) for the 83.38 keV transition suggests that it is probably 90% $M1$ + 10% $E2$ multipolarity, and those of 0.77($M1$) and 1.32($E2$) for the 97.39 keV transition suggest a 80% $M1$ + 20% $E2$ multipolarity.

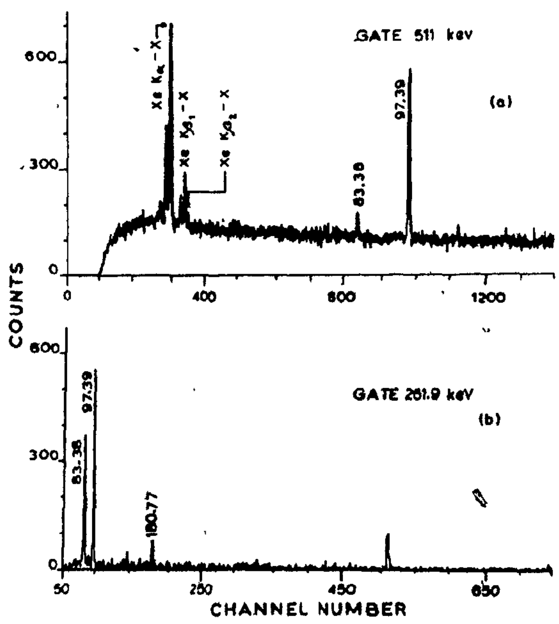

FIG. 8. Low energy γ spectra in coincidence with (a) 511 keV annihilation quanta, and (b) 261.9 keV γ rays, used in determining α_K's of the 83.38 and 97.39 keV transitions.

The Ge(Li) multispectrum with a positron annihilator of Cu yields the total positron intensity of ^{123}Cs to be 650 ± 100 per 100 γ rays of the 97.39 keV transition. A Fermi-Kurie plot of the positron spectrum observed in coincidence with the 596.4 keV γ ray, in the two parameter β-γ coincidence measurement, using an intrinsic Ge detector and a superconducting solenoid,[10] is shown in Fig. 9. To obtain this, the positron spectrum in the neighboring background gate was subtracted and the spectrum was folded to improve the count rate per datum point. The solid line in Fig. 9 is the least squares fit to data points resulting in the end-point energy of the positron group to the 596.4 keV level of $Q_\beta^*(596.4) = 2.37 \pm 0.14$ MeV. This corresponds to a decay energy of ^{123}Cs of $Q_{EC} = 4.0 \pm 0.1$ MeV, and a mass excess of ^{123}Cs of -81.29 ± 0.14 MeV, if the mass excess of ^{123}Xe is -85.29 ± 0.10 MeV.[13] Earlier results on the mass excess of ^{123}Cs were -81.19 ± 0.32 MeV,[13] and on the decay energy of ^{123}Cs were 3.6 ± 0.5 MeV,[4] and 4.1 ± 0.3 MeV.[8]

IV. DECAY SCHEMES

A. $^{121}Cs^m$ and $^{121}Cs^g$

The isomeric, $^{121}Cs^m(\frac{9}{2}^+)$, and the ground, $^{121}Cs^g(\frac{3}{2}^+)$, states which were identified in spin and parity measurements with $\frac{9}{2}^+[404\uparrow]$ and $\frac{3}{2}^+[422\downarrow]$ Nilsson states at a deformation parameter $\beta \simeq +0.28$ were found by Ekstrom *et al.*[3] to emit positrons with nearly the same half-life of 2 min. Unified model calculations[2] had earlier predicted

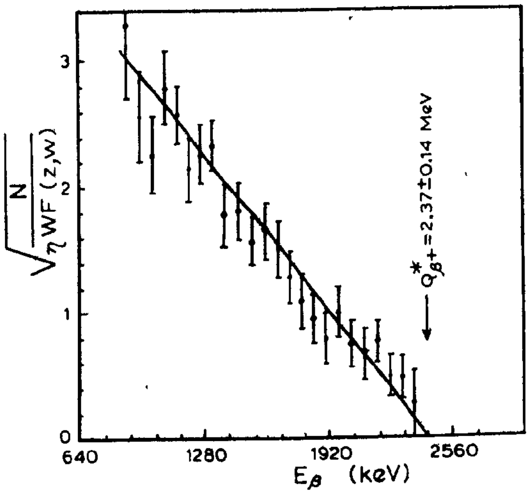

FIG. 9. FK plot of the ^{123}Cs positron spectrum in the 596.4 keV γ gate. The solid line is the least squares fit to data points. Q^*_β shown is the result for the end-point energy of positron spectrum to the 596.5 keV level from this least squares fit.

$\beta = +0.27$ or -0.26 for the $\frac{3}{2}^+[422\downarrow]$ ground state of ^{121}Cs. The ground state of ^{121}Xe has been inferred to be $\frac{5}{2}^+$ from its 40.1 ± 2.0 min β decay predominantly to $\frac{7}{2}^+$, $\frac{5}{2}^+$, and $\frac{3}{2}^+$ states and very little to $\frac{9}{2}^+$ and $\frac{1}{2}^+$ states of ^{121}I. The half-life of 61.9 ± 5.6 psec (Ref. 13) of the first excited 2^+ state of ^{122}Xe suggests $\beta(^{122}\mathrm{Xe}) = \pm(0.22 \pm 0.01)$, so that odd-even staggering[1] of β requires $\beta(^{121}\mathrm{Xe}) \simeq +0.22$. The unified model[2] predicts $\beta = +0.26$ or -0.25. Based on the present experimental results on the half-life of isomeric and ground states of ^{121}Cs, γ-ray energy and relative intensity coincidence relations, the Ritz combination principle, decay energy and multipolarity of the 38.38 keV transition from its ICC, transition intensity balance and annihilation quantum intensity, and also Cs K_β x-ray intensity to determine isomeric branching, the decay schemes of $^{121}\mathrm{Cs}^m(121 \pm 3$ sec) and $^{121}\mathrm{Cs}^g(136 \pm 3$ sec) in Fig. 10 are proposed. In the decay scheme of $\frac{9}{2}^+$ $^{121}\mathrm{Cs}^m(121 \pm 3$ sec), while there is no decay branch to $^{121}\mathrm{Xe}^g(\frac{5}{2}^+)$, the branching ratio of positron and capture mode to isomeric mode of the parent state has been included in obtaining the logft values in Fig. 10(a).

The first excited 38.38 keV state, now self-evident from both ^{121}Cs β decay and the ^{122}Te(69 MeV $\alpha,5n\gamma)^{121}$Xe in-beam γ-ray spectrum, is fed by a 7.2% β^+ + EC branch with a logft of 6.3 ± 0.3. This allowed or first forbidden β transition, and the multipolarity of 40% $M1$ + 60% $E2$ of the 38.38 keV transition, require this first excited state at 38.38 keV to be $\frac{7}{2}^+$. If the negative parity band head[11] is above the 196.1 keV γ ray, then the 234.5 and 196.1 keV transitions from this 234.5 keV level, which is now identifiable as this band head, are both of $E1$ multipolarity and therefore this 234.5 keV level could be a $\frac{5}{2}^-$ or $\frac{7}{2}^-$ state. The β transition from the $\frac{9}{2}^+$ parent state to this 234.5 keV level has a logft of 6.16 ± 0.03 and corresponds to an allowed or first forbidden transition. It appears that this 234.5 keV level is a $\frac{7}{2}^-$ state and is possibly the head of the negative parity band.[11] This agrees with the systematic observation of a negative parity band head in odd-A Ba nuclei[14] that it is $\frac{11}{2}^-$ at $N = 77$, $\frac{9}{2}^-$ at $N = 71$, 73, and 75, and $\frac{7}{2}^-$ at $N = 69$, so that this band head is also possibly $\frac{7}{2}^-$ at $N = 67$ in Ba and Xe nuclei. $^{121}\mathrm{Cs}^m(\frac{9}{2}^+)$ decays to the 179.4 keV level with a logft of 6.17 ± 0.08, so that this level is possibly $\frac{7}{2}^+$, $\frac{9}{2}^+$, or $\frac{11}{2}^+$. The 179.4 and 414.6 keV levels are observed in the positive parity band structure[11] connected by $\Delta I = 1$ transitions, so that these two levels may be assigned $\frac{7}{2}^+$ and $\frac{9}{2}^+$, respectively. The logft of 6.6 ± 0.2 for the β transition from the $\frac{9}{2}^+$ parent to the 414.6 keV level does not contradict such a $\frac{9}{2}^+$ assignment. The level at 394.3 keV, fed by a β transition of logft 7.2 ± 0.1 and connected by the 159.8 keV transition to the $(\frac{7}{2}^-)$ 234.5 keV level and by the 356 keV transition to the $(\frac{7}{2}^+)$ level, has $\frac{7}{2}^-$ or $\frac{9}{2}^-$ spin and parity assignment. The other levels at 459.8, 515.5, 701, 733, 886.6, and 1418 keV are assigned $\frac{7}{2}^\pm$ or $\frac{9}{2}^\pm$ on the basis of the logft of β transitions from $^{121}\mathrm{Cs}^m(\frac{9}{2}^+)$.

The decay scheme of $^{121}\mathrm{Cs}^g(\frac{3}{2}^+)$ in Fig. 1 has the highest branching of 98% to the ground state of ^{121}Xe with a logft of 5.20 ± 0.07 for an allowed β transition, supporting the $\frac{5}{2}^+$ assignment to this ground state of ^{121}Xe. The 153.75 keV level is fed by a β transition with a logft of 7.37 ± 0.09 and deexcites through only the 153.75 keV transition with no branching to the $\frac{7}{2}^+$ state of 38.38 keV, so that it appears to be a $\frac{1}{2}^+$ state. The 239.6 keV level is a $\frac{1}{2}^+$ or $\frac{3}{2}^\pm$ state on the basis of the logft of 7.12 ± 0.06 for the β transition, and the observation of the 85.85 keV γ ray in coincidence with the 153.75 keV γ ray and a crossover of 239.6 keV to the $(\frac{1}{2}^+)$ and $(\frac{5}{2}^+)$ states. The levels at 450, 562, and 1070 keV are assigned $(\frac{3}{2}^+, \frac{5}{2}^\pm)$, $(\frac{1}{2}^+, \frac{3}{2}^\pm, \frac{5}{2}^\pm)$, and $(\frac{3}{2}^-, \frac{5}{2}^\pm)$ on the basis of logft values and deexciting γ rays.

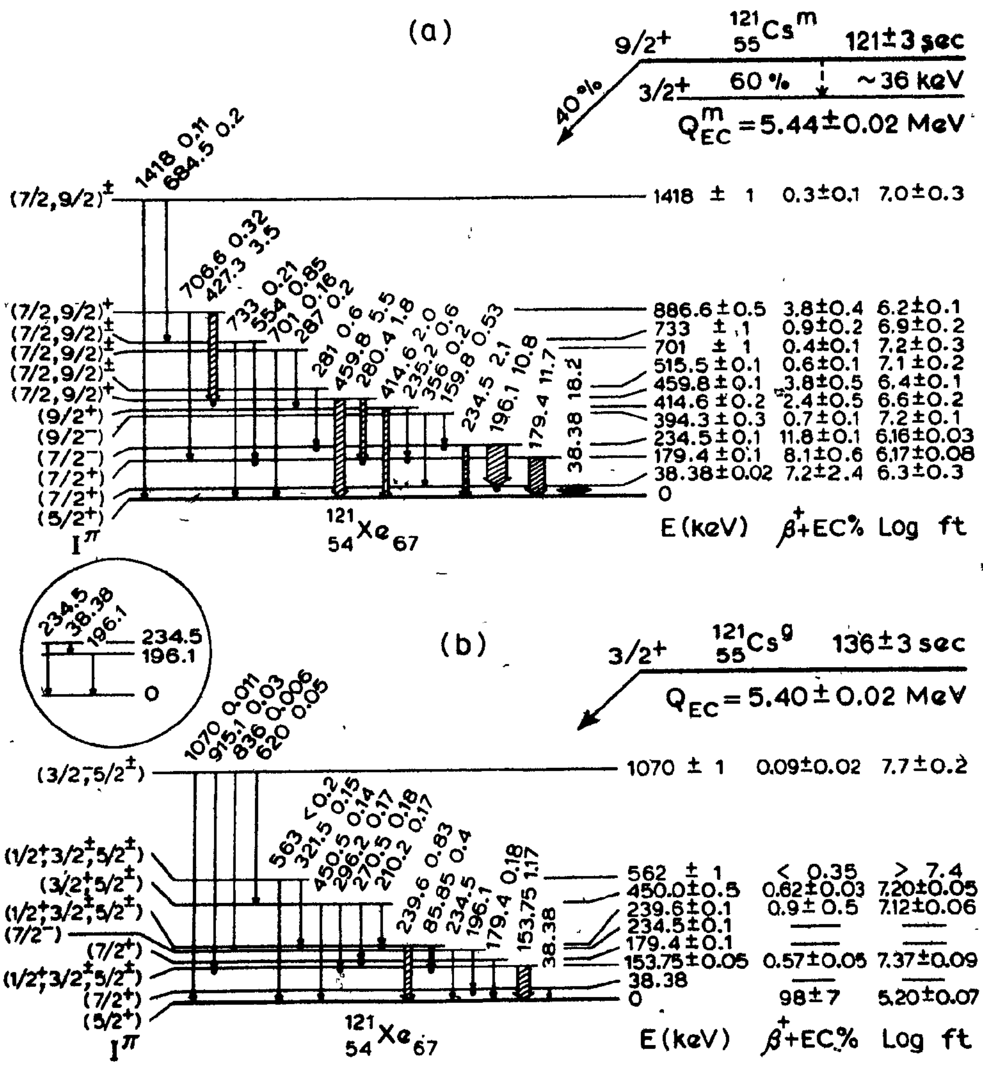

FIG. 10. Decay schemes of (a) $^{121}Cs^m(\frac{9}{2}^+$; 121 ± 3 sec) and (b) $^{121}Cs^g(\frac{3}{2}^+$; 136 ± 3 sec.) Transition intensities shown after energy in keV are per 100 decays of parent. The circular insert for the ground state transitions reflect the uncertainty in the intensity of the 38 keV transition and thus the lowest level ordering.

Nilsson model predictions for neutrons with parameters $\mu = 0.45$, $x = 0.0637$, and $\beta = +0.16$ to $+0.19$ predict a $\frac{5}{2}^+[413\downarrow]$ ground state and low-lying intrinsic excitations of $\frac{7}{2}^+[404\downarrow]$, $\frac{1}{2}^+[411\downarrow]$, $\frac{7}{2}^-[523\uparrow]$, and $\frac{9}{2}^-[514\uparrow]$. The decay schemes in Fig. 10 permit the identification of the above Nilsson states with the $\frac{5}{2}^+$ ground state, 38.38 keV ($\frac{7}{2}^+$), 153.75 keV ($\frac{1}{2}^+$), 234.5 keV ($\frac{7}{2}^-$), and 394.3 keV ($\frac{9}{2}^-$) levels. The 179.4 keV $\frac{7}{2}^+$ and 414.6 keV $\frac{9}{2}^+$ levels are the quasirotational levels based on the $\frac{5}{2}^+[413\downarrow]$ ground state, with the inertial parameter $(\hbar^2/2I) = 25.83 \pm 0.01$ keV characteristic of transitional nuclei where intermediate coupling in the unified model is applicable. These comparisons with the predictions of the Nilsson model[2,3] suggest that ^{121}Xe is probably associated with a deformation parameter of $\beta \simeq +0.16$ to $+0.19$. This $\frac{5}{2}^+[413\downarrow]$ state, which is the positive parity band head in ^{121}Xe, is also the positive parity band head[15] in $^{117,119}Te$ with 65 and 67 neutrons.

B. ^{123}Cs

The spin of $\frac{1}{2}$ and magnetic moment of 1.389 ± 0.016 mm have resulted from an atomic beam magnetic resonance[3] studies for ^{123}Cs. This ground state of ^{123}Cs has been identified in this context[3] to be the Nilsson $\frac{1}{2}^+[420\uparrow]$ proton state at a deformation parameter comparable to that of ^{121}Cs, $\beta \sim +0.28$. The ground state[16] of ^{123}Xe has been inferred to be $\frac{1}{2}^+$ from its β decay with a half-life of 2.08 h to the 148.91 keV $\frac{1}{2}^+$ level of ^{123}I having $\log ft = 5.59$ and the absence of a β branch to the $\frac{5}{2}^+$ ground state of ^{123}I. The present experimental results on the 365 ± 4 sec decay of ^{123}Cs($\frac{1}{2}^+$) with a decay energy of 4.0 ± 0.1 MeV, γ-ray energy and intensity measurements, and γ-γ coincidences lead to the decay scheme of ^{123}Cs in Fig. 11.

The β transition to the ground state of ^{123}Xe has a $\log ft$ of 5.2 ± 0.2 which supports a $\frac{1}{2}^+ \to \frac{1}{2}^+$ nature of this transition. The $\log ft$ of the transition to the 97.39 keV level is 5.82 ± 0.05, requiring a ($\Delta I = 0,1; \Delta\pi = +$) allowed nature of this β transition, so that the 97.39 keV level may be assigned $\frac{1}{2}^+$ or $\frac{3}{2}^+$. The K-shell conversion coefficient of the 97.39 keV transition, measured here to be 0.9 ± 0.1, requiring a multipolarity of 80% $M1 + 20\%\ E2$, also supports these spin and parity assignments. The $\log ft$ of 6.3 ± 0.1 for the β transition to the 180.77 keV level and the 90% $M1 + 10\%\ E2$ multipolarity of the 83.38 keV transition from its K shell conversion coefficient, measured here to be 1.30 ± 0.06, require a $\frac{1}{2}^+$ or $\frac{3}{2}^+$ assignment to this level. In the context[17] of a 6.3 μsec isomer with $\frac{9}{2}^-$ assignment, this 180.77 keV level had been assigned $\frac{5}{2}^+$ and the 97.39 keV level had been assigned $\frac{3}{2}^+$. The 252.03 keV level was considered by these authors[13,16,17] to be the $\frac{9}{2}^-$ isomeric state since 1970. A thorough search of all possible very low intensity transitions has been made here to seek justification for earlier results.[13,16,17] However, the best that can be inferred about the 252.03 keV level is that it may not be the $\frac{9}{2}^-$ isomeric state because it is fed by a β transition from the $\frac{1}{2}^+$ parent with a $\log ft$ of 7.4 ± 0.6, which requires a $\frac{1}{2}^\pm$ or $\frac{3}{2}^\pm$ assignment to the level. The present observation of a 252.03 keV gamma ray to the $\frac{1}{2}^+$ ground state of ^{123}Xe also forbids a $\frac{9}{2}^-$ assignment to this 252.03 keV level. It is proposed from the present results that this level has spin and parity of $\frac{1}{2}^+$ or $\frac{3}{2}^+$, but not $\frac{9}{2}^-$. The $\log ft$ deduced for the other levels requires the allowed classification of β transitions to 596.4, 611.1, 741.5, 848.5, 1125.8, 1273.4, and 1452.8 keV levels which may be assigned spin and parity of $\frac{1}{2}^+$ or $\frac{3}{2}^+$, while the other β transitions to 307.1, 442.7, 693.6, 917, and 1032.6 keV levels are of allowed or first forbidden nonunique classification, requiring these five levels to have spin and parity of $\frac{1}{2}^\pm$ or $\frac{3}{2}^\pm$.

Unlike the level structure of ^{121}Xe, in the decay of a high spin ^{121}Cs^m($\frac{9}{2}^+$) and a lower spin ^{121}Cs^g($\frac{3}{2}^+$) to $\frac{9}{2}^+$ states being observable, this ^{123}Cs($\frac{1}{2}^+$) decay populates ^{123}Xe levels with just $\frac{1}{2}^\pm$ or $\frac{3}{2}^\pm$. The Nilsson model with the same neutron parameters[3] as ^{121}Xe can account for the change from the $\frac{5}{2}^+[413\downarrow]$ ground state at $N = 67$

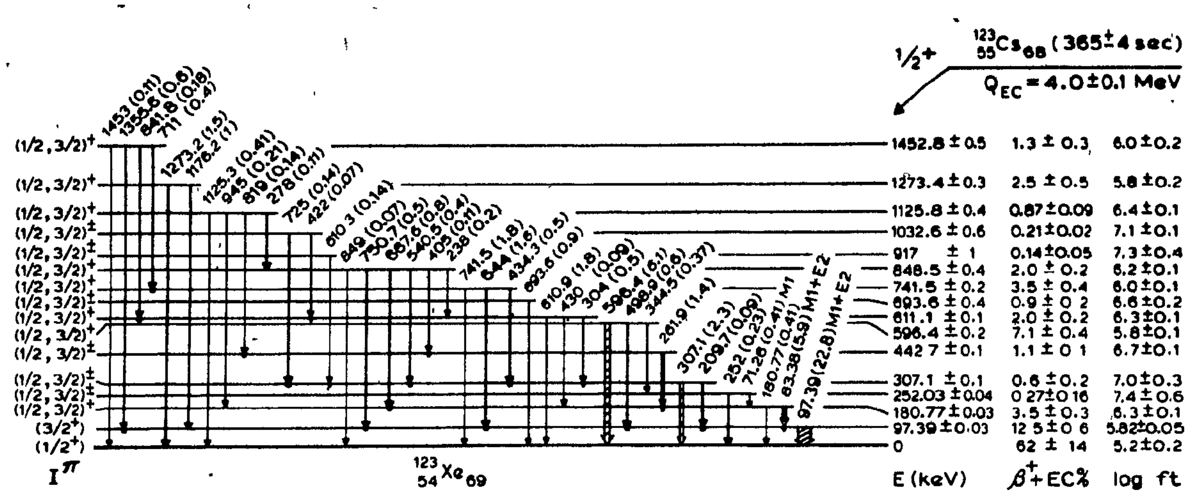

FIG. 11. Decay scheme of ^{123}Cs($\frac{1}{2}^+$, 365 ± 4 sec) with the same notations as in Fig. 10.

^{121}Xe to the $\frac{1}{2}^{+}[411\downarrow]$ ^{123}Xe ground state, at the same deformation parameter $\beta = +0.16$ to $+0.19$ as ^{121}Xe. The 6.3 μsec isomeric state[13,16,17] of ^{123}Xe is possibly the $\frac{7}{2}^{-}[523\uparrow]$ Nilsson state as in 69 neutron ^{125}Ba,[14] rather than the higher lying $\frac{9}{2}^{-}[514\uparrow]$ state.

V. CONCLUSIONS

Decay schemes of $^{121}Cs^{m}(\frac{9}{2}^{+})$, $^{121}Cs^{g}(\frac{3}{2}^{+})$, and $^{123}Cs(\frac{1}{2}^{+})$ deduced from γ-ray spectroscopy here suggest that ^{121}Xe and ^{123}Xe are moderately deformed with $\beta = +0.16$ to $+0.19$, which is less than the β value for the parent states. The ground and low-lying excitations of ^{121}Xe can be identified with some of the intrinsic states of the Nilsson model, while only the ground state of ^{123}Xe is identified with the corresponding intrinsic state in the model.

ACKNOWLEDGMENTS

The authors wish to thank Prof. J. E. Kitching and Dr. B. Varley for their help with the in-beam experiments. This work was supported by a grant from the Natural Sciences and Engineering Research Council of Canada.

*On leave at Institut des Sciences Nucléaires, Université de Grenoble, France.

[1]W. Fischer, H. Huhnermann, G. Kromer, and H. J. Schafer, Z. Phys. A 270, 113 (1974).
[2]D. A. Arseniev, A. Sobiczewski, and V. G. Soloviev, Nucl. Phys. A126, 15 (1969).
[3]C. Ekstrom, S. Ingelman, G. Wannberg, and M. Skarestad, Nucl. Phys. A292, 144 (1977).
[4]J. M. d'Auria and I. L. Preiss, Nucl. Phys. 84, 37 (1966).
[5]J. Chaumont *et al.*, Phys. Lett. 29B, 652 (1969).
[6]H. B. Mathur and E. K. Hyde, Phys. Rev. 95, 708 (1954).
[7]I. L. Preiss and P. M. Strudler, I. Inorg. Nucl. Chem. 24, 589 (1962).
[8]L. Westgaard, K. Aleklett, G. Nyman, and E. Roeckl, Z. Phys. A 275, 127 (1975).
[9]G. Bavaria, Ph.D. thesis, McGill University, 1975 (unpublished).
[10]R. B. Moore, S. I. Hayakawa, and D. M. Rehfield, Nucl. Instrum. Methods 133, 457 (1976).
[11]P. Chowdhury, U. Garg, T. P. Sjoreen, and D. B. Fossan, Phys. Rev. C 23, 733 (1981).
[12]R. S. Hager and E. C. Seltzer, Nucl. Data Sec. A 4, 1 (1968).
[13]*Table of Isotopes*, 7th ed., edited by C. M. Lederer and V. S. Shirley (Wiley, New York, 1978).
[14]J. Gizon and A. Gizon, Z. Phys. A 285, 259 (1978).
[15]U. Hagemann, H.-J. Keller, Ch. Protochristow, and F. Stary, Z. Phys. A 290, 399 (1979).
[16]T. Tamura *et al.*, Nucl. Data Sheets 29, 453 (1980).
[17]A. Kerek *et al.*, Phys. Lett. 31B, 10 (1970).

APPENDIX B

0^+ Excited States in $^{122,124,126,128}Xe$

Physical Review C 1979

0^+ excited states in ^{122,124,126,128}Xe

B. Singh, R. Iafigliola, K. Sofia, J. E. Crawford, and J. K. P. Lee
Foster Radiation Laboratory, McGill University, Montreal, Quebec, Canada
(Received 28 November 1978)

γ-γ directional correlation measurements have been carried out and the following 0^+ spin assignments have been made. ^{122}Xe: 1149 keV level, ^{124}Xe: 1269 and 1690 keV, ^{126}Xe: 1313 keV, ^{128}Xe: 1583 and 2599 keV. In addition, value of δ for the 493 keV $(2_2^+ \to 2_1^+)$ transition in ^{124}Xe has been measured to be 8_{-3}^{+7}.

[RADIOACTIVITY ^{122,124}Cs [from ^{124}Xe (p,xn), enriched ^{124}Xe]; ^{126,128}Cs [from ^{126,128}Ba, ^{133}Cs (p,xn)]; measured $\gamma\gamma(\theta)$, ^{122,124,126,128}Xe levels. Deduced J, γ-mixing, Ge(Li), and NaI(Tl) detectors.]

In each of the even-even Xe nuclei from $A=118$ to 128, at least one excited 0^+ state has been postulated from β-decay studies on Cs isotopes.[1-4] In the case of ^{118}Xe and ^{120}Xe, first excited 0^+ states were identified[1] through the observation of $E0$ transitions. For the other nuclei, the 0^+ states were postulated mainly on the basis of their decay patterns. The purpose of the present investigation is to confirm these 0^+ assignments by γ-γ directional correlation measurements. During the course of our measurements, results of a similar study for ^{128}Xe were reported in a conference proceeding.[5]

The angular correlation spectrometer consisted of a fixed Ge(Li) detector of 18% relative efficiency and a movable 7.5 cm × 7.5 cm NaI(Tl) detector placed at distances of 7 cm and the 10 cm respectively from the center of the source. For the ^{122}Xe study, another 15% Ge(Li) detector was used in place of the NaI detector. In each case the coincidence resolving time was about 15 ns. The random rate was kept at a negligible level. Coincidence data were recorded as pairs of addresses on a magnetic tape and were later sorted by selecting appropriate windows "on" and "off" the γ-ray peaks of interest. Normalization of data at various angles was carried out with a singles spectrum accumulated simultaneously with the coincidence spectrum. Source sizes were kept reasonably small so that corrections were negligible.

The 20 s ^{122}Cs and 30 s ^{124}Cs activities were produced by $(p,3n)$ and (p,n) reactions, respectively, by irradiating targets of isotopically enriched Xe gas containing 41% of ^{124}Xe by 45 MeV and 15 MeV protons, respectively, from the McGill synchrocyclotron. A total of about 2000 samples were used for each of the experiments. The irradiation time was about 10 s and the counting period was about 1 m.

The 1.6 m ^{126}Cs and 4 m ^{128}Cs were obtained as daughter products of 97 m ^{126}Ba and 2.4 d ^{128}Ba, which were produced by $(p,8n)$ and $(p,6n)$ reactions, respectively, on natural Cs. Energies of the proton beam were 85 MeV and 65 MeV, respectively. After a waiting period of about 30 m, barium isotopes were separated chemically by the following procedure. Irradiated cesium nitrate was disolved in water, and a few drops of barium chloride and ammonium hydroxide were added. Barium precipitate was separated and washed twice with water. This procedure gave fairly clean samples of barium isotopes. Seven samples were prepared for ^{126}Xe and only one for the ^{128}Xe studies.

Normalized peak areas were plotted as a function of the angle between the two detectors. Figure 1 shows such curves for all cases which were of interest in the present investigation. Solid lines are the result of a least squares fit of data points to the function

$$W(\theta)=A_0+A_2'P_2(\cos\theta)+A_4'P_4(\cos\theta)$$
$$=A_0(1+A_2P_2(\cos\theta)+A_4P_2(\cos\theta)),$$

where

$$A_2=\frac{A_2'}{A_0} \quad\text{and}\quad A_4=\frac{A_4'}{A_0}.$$

With the given geometry, the solid angle correction factors were 0.86 for A_2 and 0.59 for A_4. The values of the coefficients A_2 and A_4, after the correction for solid angles, are listed in Table I, together with the spin assignments of the corresponding levels. All the curves shown in Fig. 1 are characteristic of a $0^+ \to 2^+ \to 0^+$ directional correlation pattern. Although the errors are fairly large in a few cases, a large A_4 value uniquely describes a zero spin assignment to the levels quoted in

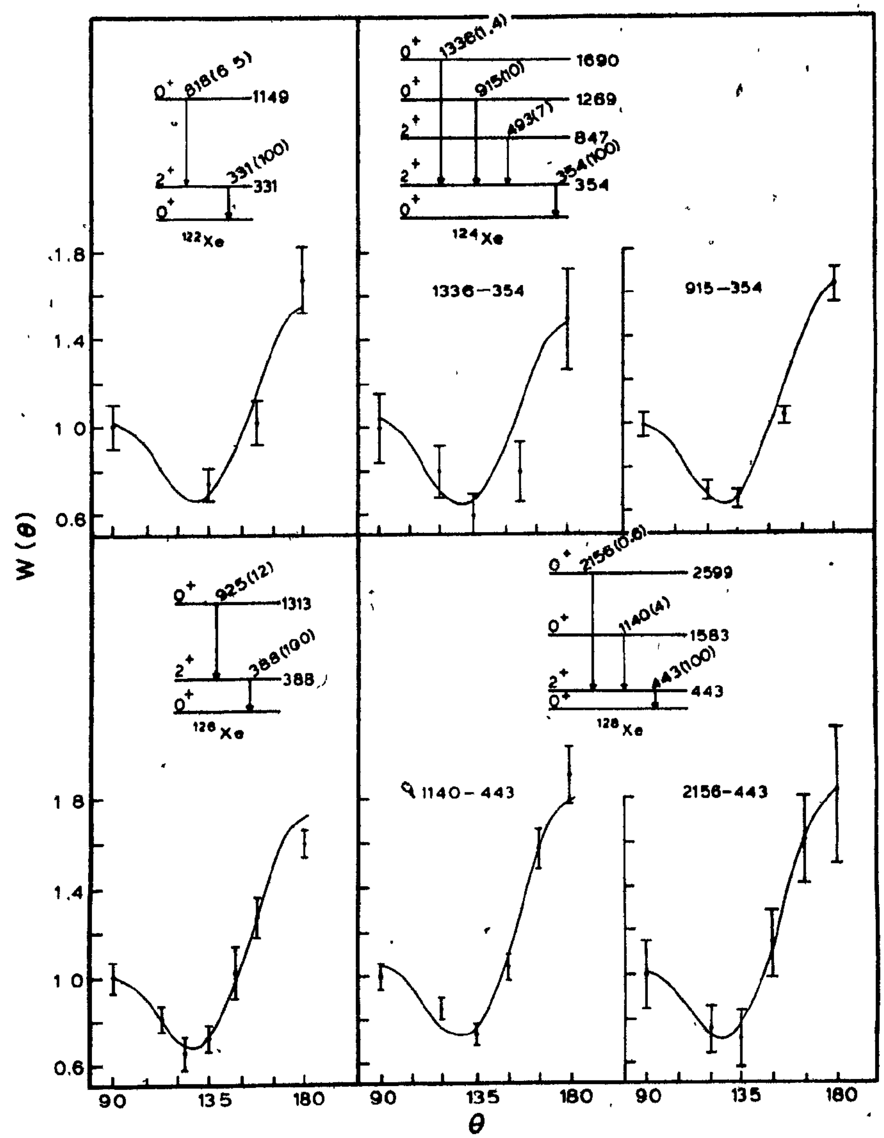

FIG. 1. Angular correlation measurements of the cascade γ rays shown in the insets. Solid lines represent least squares fitted to the experimental results.

TABLE I. Summary of angular correlation measurements in ^{122,124,126,128}Xe.

Nucleus	Level (keV)	Cascade γ-ray energies (keV)	A_2[a]	A_4[a]	Spin sequence
^{122}Xe	1149	818–331	0.2 ± 0.2	1.1 ± 0.4	$0^+ - 2^+ - 0^+$
^{124}Xe	847	493–354	-0.16 ± 0.04	0.32 ± 0.05	$2^+ - 2^+ - 0^+$ ($\delta = 8^{+7}_{-3}$)
	1269	915–354	0.23 ± 0.12	1.14 ± 0.18	$0^+ - 2^+ - 0^+$
	1690	1336–354	0.10 ± 0.20	1.0 ± 0.3	$0^+ - 2^+ - 0^+$
^{126}Xe	1313	925–388	0.30 ± 0.14	1.10 ± 0.20	$0^+ - 2^+ - 0^+$
^{128}Xe	1583	1140–443	0.29 ± 0.10	1.05 ± 0.16	$0^+ - 2^+ - 0^+$
	2599	2156–443	0.36 ± 0.16	1.10 ± 0.23	$0^+ - 2^+ - 0^+$

[a] The values quoted include solid angle corrections.

Table I. Other possible spin values of 1, 2, 3 or 4 will not satisfy these correlation coefficients.[6] Theoretical coefficients for a $0 \to 2 \to 0$ cascade are $A_2 = 0.357$, $A_4 = 1.108$. As a byproduct of this measurement, the correlation of the 493–354 keV cascade in ^{124}Xe has been obtained. Values of the coefficients are $A_2 = -0.16 \pm 0.04$, $A_4 = 0.32 \pm 0.05$, which give a value of $\delta = 8^{+7}_{-3}$ for the 493 keV transition.

These 0^+ assignments in Xe nuclei are in agreement with postulations of the earlier works.

[1]J. Genevey-Rivier, A. Charvet, G. Marguien, C. Richard-Serre, J. D'Auria, A. Huck, G. Kotz, A. Knipper, G. Walter, and Isolde Collaboration, Nucl. Phys. A283, 45 (1977).
[2]A. Charvet, J. Genevey-Rivier, L. C. Carrez, C. Richard-Serre, A. Knipper, and G. Walter, J. Phys. Lett. 38, 241 (1977).
[3]B. P. Pathak, L. Lessard, L. Nikkinen, and I. L. Preiss, Phys. Rev. 146, 1573 (1976).
[4]R. G. Helmer, C. W. Reich, R. J. Gehrke, R. C. Greenwood, and R. A. Anderl, Phys. Rev. C 15, 1453 (1977).
[5]E. W. Schneider, M. D. Glascock, B. W. Gallagher, W. B. Walters, R. A. Meyer, and S. V. Jackson, in *Proceedings of the International Conference on Nuclear Structure, Tokyo, 1977*, edited by T. Marumori (Physical Society of Japan, Tokyo, 1978), p. 364.
[6]H. W. Taylor, B. Singh, F. S. Prato, and R. McPherson, Nucl. Data Tables 9, 1 (1971).